UNIVERSITAT DE BARCELONA

Temporal Variability of Nepheloid Layer Structures on Continental Slope Environments: Natural and Anthropogenic Processes

Marta Arjona Camas

UNIVERSITAT DE BARCELONA

Marta Arjona Camas, 2021

Temporal Varibility of Nepheloid Layer Structures on Continental Slope Environments: Natural and Anthropogenic Processes

Temporal Variability of Nepheloid Layer Structures on Continental Slope Environments: Natural and Anthropogenic Processes

Marta Arjona Camas

PhD Thesis in Marine Sciences
Barcelona, 2021

UNIVERSITAT DE BARCELONA
Institut de Ciències del Mar
CSIC
CONSEJO SUPERIOR DE INVESTIGACIONES CIENTÍFICAS

TESI DOCTORAL

Facultat de Ciències de la Terra, Departament de Dinàmica de la Terra i de l'Oceà

Temporal Variability of Nepheloid Layer Structures on Continental Slope Environments: Natural and Anthropogenic Processes

Memòria de Tesi Doctoral presentada per Marta Arjona Camas per a optar al grau de Doctora, dins el programa de Doctorat de Ciències del Mar, sota la direcció del Dr. Pere Puig Alenyà i del Dr. Albert Palanques Monteys

Marta Arjona Camas

Institut de Ciències del Mar, Consejo Superior de Investigaciones Científicas (ICM-CSIC)

Barcelona, Novembre de 2021

Dr. Pere Puig Alenyà	Dr. Albert Palanques Monteys	Dr. Antoni M. Calafat Frau
ICM-CSIC	ICM-CSIC	Universitat de Barcelona
Director	Director	Tutor

This PhD thesis has been funded by the fellowship *Ayudas Predoctorales para la Formación del Personal Investigador* (FPI, ref. BES-2016-076983) granted by the *Spanish Ministerio de Economía y Competitividad* from April 2017 to September 2021. The results included in this thesis were collected in the framework of the following projects:

- Formas de fondo y su dinámica actual en el margen continental mediterráneo español (FORMED). 2013-2015. Ministerio de Economía y Competitividad (CGL2012-33989).
- Assessment of Bottom-trawling Impacts in Deep-sea Sediments (ABIDES). 2016-2018. Ministerio de Economía y Competitividad (CTM 2015-65142-R)
- Assessment of Bottom-trawling Resuspension Impacts in deep benthic Communities (ABRIC). 2019-2021. Ministerio de Ciencia, Investigación y Universidades (RTI2018-096434-B-100).
- Ocean Networks Canada (ONC) through Canada Foundation for Innovation-Major Initiative (CFI-MSI) (30199).

Funding was also provided by the Consolidated Research groups of *Oceanografia Física i Tecnològica* (2017 SGR-1241) and *Grup de Processos Litorals i Oceànics* (2017 SGR-863), awarded by the *Generalitat de Catalunya.*

What we know is a drop,

what we ignore is an ocean

Isaac Newton

Acknowledgements – Agradecimientos – Agraïments

“Hacerse una pregunta, conseguir encontrar la respuesta, y cuestionársela es lo que ha hecho avanzar la Ciencia. ¡Qué siempre te hagas muchas preguntas!”. Éstas fueron las palabras que me dedicó mi maestra de Ciencias Naturales al acabar primaria, en 2004, y que me han acompañado desde entonces. Éste siempre ha sido mi *motto* y el que, sin duda alguna, me llevó a emprender la aventura hacia el Doctorado en 2016. Recuerdo que empezó con un “vale, pese a las dudas”, y ahora hace ya más de 5 años de ese sí a la aventura de hacer esta Tesis, ahora sin duda alguna de que es una de las mejores decisiones que he tomado. Después de estos años llenos de trabajo, nervios, alegrías (y algunas penas), viajes, y nuevas emociones, llega el momento de poner fin a esta etapa. Un camino movidito que he tenido el placer y la suerte de compartir con personas estupendas, personas que han estado incondicionalmente ahí desde el principio, y que me han ayudado a crecer personal y profesionalmente. Esta aventura no hubiera sido ni lo mismo ni posible sin vosotros, así que estas líneas y esta Tesis también son vuestras.

Primero de todo, quiero dar las gracias a mis supervisores: Pere y Albert. Gràcies per donar-me l’oportunitat de viure aquesta experiència amb vosaltres. A tu Pere, per ser el meu guia durant tota la Tesi, sempre disposat a ajudar-me, i a fer la feina ben feta. També per la teva implicació, pel teu detallisme corregint els meus treballs, per escoltar les meves idees i recolzar-me, i per sempre motivar-me a buscar el “per què” de les coses. En fi, gràcies per animar-me i per donar-me les eines per a arribar on soc avui. A tu Albert, gràcies per la teva implicació i ajuda, per les hores que hem passat discutint dades i resultats, i sobretot per la teva confiança en mi en aquesta Tesi i en futurs projectes. Ha sigut un vertader plaer compartir amb vosaltres congressos, grans viatges com ara a Estats Units o a la Xina, però sobretot campanyes, que ja en van 10! Gràcies pel vostre mentoratge, i per endinsar-me al món dels *moorings*. Espero que puguem compartir moltes més!

També vull agrair al meu tutor de la Universitat de Barcelona, en Toni Calafat, la seva ajuda, disponibilitat, i predisposició a ajudar-me sempre que ho he necessitat.

Esta Tesis tampoco hubiera sido posible sin mis compañeros y amigos del ICM. A mis chicas del B-38: Ruth y Sarah. Ruth, gracias por todos tus consejos, por tu disposición a ayudarme siempre que lo he necesitado, por los tés en el despacho cuando el día se nos estaba haciendo eterno, y por tu calidez. Sarah, mi compañera de batalla. Aunque no nos conocimos hasta un tiempo después de empezar la Tesis, no podía haberme tocado mejor compañera para hacer este camino. Siempre he admirado tus ganas y tu *hard-work*. He aprendido muchísimo contigo, y espero poder hacer más ciencia juntas. Lo he pasado genial: desde nuestro primer congreso hasta todas las campañas que hemos hecho juntas, mi eterna compañera de camarote. Siempre recordaré las largas horas en el laboratorio filtrando agua, cortando *cores*

(con buena y no tan buena mar), las batallas de fango de mil metros, y el buen equipo que hemos hecho. Aunque hemos compartido menos tiempo juntas, a mis compañeras de proyecto: Meri y Cecilia. Meri, it was awesome to meet you, to work with you, and to share such an awesome cruise. It was hard, but it was really worth it. Now, I cannot wait to see your results! I wish you all the best in your PhD. Cecilia, ahora te toca a ti vivir esta aventura. Aunque a veces se haga cuesta arriba, vale mucho la pena, así que siempre con buena actitud. Gracias por estos ratitos que hemos compartido, en tierra y en el mar. No puedo olvidarme de las chicas del lab: Sílvia, Neus y Elena. Moltes gràcies per crear tant bon caliu sempre que hem compartit moments juntes. Gràcies per la vostra companyia i bona energia tant al laboratori com a les campanyes. A los compañeros: Jose y Maribel. Gracias por vuestra implicación conmigo, gran parte de lo que sé sobre instrumentación oceanográfica es gracias a vosotros. No todo el mundo tiene la suerte de aprender y trabajar con vosotros, pasar horas y horas en el laboratorio montando y desmostando instrumentos, y todo acompañado de risas y muy buen rollo. ¡Sin duda las campañas no hubieran sido lo mismo sin vosotros, desde la primera hasta la última!

También me gustaría hacer una mención especial a todo el equipo de técnicos y técnicas de la UTM, y a las diferentes tripulaciones con las que he tenido el placer de trabajar a bordo del B/O *García del Cid*, B/O *Sarmiento de Gamboa,* B/O *SOCIB,* y el B/O *Pelagia*.

Sin duda, esta Tesis tampoco hubiera sido lo mismo sin Mikhail, Claudio y Fabio. Me ha encantado coincidir con vosotros en el ICM, de campaña, o de congreso. Estoy segura de que con algunos de vosotros aun podremos hacer más Ciencia. Mikhail, mis primeros pasos con el *Aqualog* los di contigo. Gracias por tu tiempo, por la paciencia, y por estar siempre dispuesto a echarme un cable con el procesado de perfiles hidrográficos. Tienes dos capítulos de la Tesis dedicados. Claudio, gracias por tu ayuda en tantos momentos de la Tesis, por tus consejos y por el buen ambiente que creas, tanto en el ICM como en las campañas. ¡Qué ganas de seguir trabajando en los nuevos datos! Fabio, I had the delight of sharing with you a cruise and two conferences, as well as working with you during the last year of my PhD. Thank you very much for introducing me to the NEPTUNE observatory, for the skypes discussing the results despite the time difference, for your professionality, and for your willingness to help. I really learned a lot with you, and I cannot wait for working with you again in the future. The last chapter of results is for you! *Muito obrigada!*

No puedo olvidarme de los grandes momentos que he vivido en la coral del ICM, la Coral del Mar. Ha sido una gran suerte la de hacer algo que me apasiona, como es cantar, y compartirlo con mis compañeros de trabajo. Anna y Carlos, mis coraleros, pero también mis amigos, me ha encantado compartir tan buenos momentos con vosotros, tanto en el ICM como fuera, y estoy segura de que nos quedan muchas aventuras por compartir. De mis compañeros del departamento de Geociencias Marinas (Queralt, Gonzalo, Jorge, Jaume, Enrique) y de mis amigos (Sergio, Slaven, Davide, Miquel, Alba, Carla, Anaïs, Gaia, Shray, Maria, Ana… y más),

me llevo todos los momentos que hemos vivido juntos, el buen ambiente que hemos creado, y todo lo que nos hemos reído juntos. Y por encima de todo, me llevo a mis *girlies*: Claudia, Estela, Irene y Cris. Hemos pasado nervios, llorado y reído juntas, pero sobretodo hemos compartido y celebrado (de largo y de corto) todos los momentos importantes juntas. Lo más guay de ir al ICM era saber que en algún momento del día nos íbamos a ver. Chicas, lo mejor está por llegar, y aún tenemos mucho por vivir y celebrar juntas. *I'll be there for you, like you're there for me too…*

During my Thesis, I had the delight and opportunity to do two stays abroad, in Galway (at the NUIG) and in Texel (at the NIOZ).

I would like to thank the very warm welcoming that my stay supervisor Martin White gave me right after arriving to Galway, and for touring me around Ireland showing me the nice landscapes of the island, from mountains to amazing fjords! Thank you very much for your guidance, for your interest in my work, for the long discussions about nepheloid layers, for introducing me to the "crazy" world of microturbulence processes in the ocean, and for encouraging me to find the answer to all my questions about nepheloid layers. The long days at the NUIG would have not been the same without my colleague back then, and friend now, Eoghan Daly. Thank you very much for your time, for the spent hours processing CTDs together, for the nice chats (with a pint in a pub, or online during the pandemic), and for being a key piece of my PhD. I am very happy to have met you! I also had the pleasure to share my stay with the guys from the EOS department: Aoife, Aisling, Jess, Martin, Séan, Oisin, Bébhinn, and Megan. Thank you very much for the lunches, for the parties and pints, for taking me out to get to know the island, for introducing me to the Irish culture, and for the unforgettable memories. You have made my stay so much more enjoyable and made me feel such a true Galwegian! To my awesome flatmates: thanks for being there in the evenings, for our nice conversations, and for your caring. It was very nice to share this experience with you. *Go raibh maith agat!*

I would also like to express my appreciation to Furu Mienis and everyone in Texel. Furu, thank you very much for the opportunity of doing a research stay at the NIOZ, for your advice, and your support to my research. I would also like to thank you for taking me in to the *Bypass Cruise* with you and your research team. It was my first cruise in the Atlantic Ocean and I really learned a lot about sampling techniques. I have never filtered so much water in my life, but it was such a great cruise. I enjoyed every second of it! *Dank je wel!* It certainly would have not been the same without my fabulous friend Sofia. Thank you very much for your warm welcoming to Texel, for the hours spent together (in the middle of the ocean and on land), and for the nice memories. As we say, we have seen half of the world together. You are awesome, and I cannot wait to have you back in Barcelona, or to reunite somewhere else! To Stanley and Uli, you also made my stay in Texel so much more enjoyable, and I am really grateful to have met you and have spent such nice days with you!

També m'agradaria agrair el suport i ànims dels meus amics de la uni, els ambientòlegs. Gràcies per ser una part fonamental d'aquests darrers 10 anys, per tots els moments que hem compartit junts, i per no deixar perdre les nostres tradicions! A la Laura i la Meri, per mantenir-nos juntes malgrat la distància i estar sempre allà. A Carme por tenernos siempre, por cuidarnos, por animarnos mutuamente, por saber entendernos y apoyarnos en cada uno de los aspectos de nuestras vidas. Gracias por estos 10 años, que seguro que son la punta del iceberg ¡Tenerte como amiga es un tesoro, eres imprescindible! ¡Ahora viene lo mejor! Gracias por todo. También quiero dar las gracias a mis amigos de Sant Joan, los de siempre, que, pese a no entender a veces qué es y qué implica hacer un doctorado, me han dado todo su apoyo y ánimo siempre, y se han preocupado por mí. En especial, a mis *rayitos* y mis *terrícolas* ¡Sois una parte esencial en mi vida! También a las chicas de coro, por nuestras cenas en el Diamant, por hacer que los jueves fueran "menos jueves", y hacer las semanas de más trabajo mucho más llevaderas.

A Manu, por reaparecer. No sabemos si fue destino o casualidad, pero brindo por el día del reencuentro. Gracias por tu apoyo durante este último (y más duro) año de Tesis, por querer contagiarme tu *xino-xano*, por tu buen humor, por escucharme, por tu paciencia, por creer en mí, y por tu amor. Gracias por conseguir que desconectara cuando más lo necesitaba, por motivarme siempre, y por haberme demostrado que "cuando se quiere, se puede". Ahora nos toca volar a nosotros… ¿a dónde vamos?

Una cosa que aprecias más cuando estás un tiempo fuera es el cariño de los de siempre, en especial el de mi familia. A mis yayos, gracias por confiar en vuestra "chiquita", por animarme siempre, por escucharme cuando os cuento "cosas del mar" y hacerme mil preguntas, y por preocuparos cada vez que me iba al mar, de viaje o de estancia. ¡Nunca tendré palabras suficientes para agradeceros todo lo que hacéis por mí! También a mi segunda familia (Manolo, Elena, Àlex y David). Os estaré siempre agradecida por todo vuestro apoyo, por el viaje a Galway y todos los buenos momentos a lo largo de estos años, y por vuestro amor incondicional.

Y mi gracias más especial es para mis dos superhéroes, mis padres ¡Lo que no hayan hecho ellos por mí no lo ha hecho nadie! Gracias por vuestro apoyo incondicional, por vuestro amor, por vuestra dedicación, por hacerme de guía durante esta etapa (¡y durante toda mi vida!). Gracias por ser los promotores de mis sueños, por creer en mí y en mis expectativas, y por ser los mejores compañeros de viaje durante mis estancias. ¡Qué bien nos lo hemos pasado! Gracias por confiar cada día en mí y animarme a conseguir todo esto, por querer aprender cada día conmigo (y juntos), por todos los consejos y por no dejar que me rinda nunca. ¡Os quiero mucho! Nosotros tenemos un lema, "todo esfuerzo tiene su recompensa", ¡Y menuda recompensa ha sido ésta!

Summary

The transport of matter and energy from the continent and upper ocean to deep-sea environments is especially important in continental margins due to the large inputs of suspended particulate matter from both terrestrial sources and high-productivity coastal waters. High-energy hydrodynamic processes, such as storms, ocean currents, or internal waves and tides, as well as anthropogenic processes, such as bottom trawling, contribute to the resuspension and remobilization of particulate matter, aiding its transference from continental shelves to continental slope environments and maintaining high concentrations of resuspended sediments at certain levels of the water column forming nepheloid layers.

The majority of investigations combining the study of both natural and anthropogenic resuspension processes, which are scarce, have been mainly carried out in coastal and continental shelf settings, disregarding the effects of anthropogenic activities at deep-sea environments beyond the continental shelf-break. Further to that, there is a lack of studies that assess the temporal and spatial variability of nepheloid layers in the water column related to trawling activities, as well as a lack of studies examining the extent to which the effects of anthropogenic activities are comparable to those of natural processes in deep-sea environments.

To fill in these gaps, at least partially, this Thesis aims to investigate the contribution of the deep-sea trawling activities, besides that of natural processes, to the sediment dynamics in different continental slope areas, particularly in the NW Mediterranean and the NE Pacific basins. To do so, the experimental techniques used in this Thesis consist of continuous measurements of variable duration of water column properties by different oceanographic sensors equipped in autonomous vertical profilers, either installed on instrumented mooring arrays or in a seafloor cabled observatory, both at depths of the continental slope.

Chapter 1 consists of a general introduction designed to focus the reader on the conceptual and geographical framework in which the present Thesis is framed. Here, an introduction to the main nepheloid layer generation processes is provided, as well as classical methods and instrumentation used to describe them. Chapter 2 provides a description of the study sites covered in this Thesis, and Chapter 3 covers the methodologies used to acquire and analyse the data employed in this Thesis dissertation.

In Chapter 4, the structure and the time-evolution of the water column turbidity in the Foix submarine canyon (Central Catalan margin, NW Mediterranean) are studied by analysing two months of hydrographic profiles collected by an autonomous vertical profiler. This device was installed in a mooring array deployed at the canyon axis, at 870 m depth. The results illustrate a well-defined water turbidity structure, consisting in intermediate nepheloid layers (INLs), developed between 300 and 500 m water depth and above the canyon rims, and INLs and

near-bottom nepheloid layers (BNLs) confined inside the canyon between 650 and 800 m water depth. Data from fishing vessels positioning obtained from *Vessel Monitoring System* (VMS) during the deployment reveals that the presence and water column levels of the observed INLs and BNLs depend on the operating depths of bottom trawlers and on the specific fishing grounds being exploited by the local trawling fleet. This data strongly suggests that bottom trawling activities in the study area are the main driver of the turbidity increases observed in the water column.

Additionally, the hydrodynamic conditions within the canyon also seem to favour sediment particle retention and to increase water turbidity in thick BNLs when water circulation is directed up-canyon. Although bottom trawling seems to be the main sediment resuspension mechanism, natural processes and ambient currents also contribute to the advection and/or retention of resuspended particles, transporting them along and across the margin as nepheloid layers.

In Chapter 5, the spatial and temporal variations on the water turbidity structure and near-bottom suspended sediment transport associated to both natural processes (storms, river floods, and dense shelf water cascading, DSWC) and bottom trawling activities are analysed in the Palamós Canyon (Catalan margin, NW Mediterranean). Data for this study have been collected by means of an autonomous vertical profiler, as well as near-bottom instrumentation deployed in the axis of the canyon (929 m depth), for about three months, covering a trawling closure period and also an active trawling period. Results from this study show that periods of enhanced water turbidity during the trawling closure period are associated with storms and DSWC events, transporting turbid dense waters into the canyon. In absence of such energetic events, the water column remains unchanged, displaying the lowest suspended sediment concentrations of the recording period, until the trawling season began. Observations from this study illustrate that INLs (250 and 350 m depth) and BNLs (> 500 m depth) are found at the water depths where trawling grounds from the Palamós Canyon are located. In this case, data from fishing vessels positioning during the recording period were obtained through Automatic Identification System (AIS). Moreover, high near-bottom suspended sediment fluxes were sporadically registered during the trawling closure period associated with a major wet eastern storm and a DSWC event, whereas smaller but more frequent increases in near-bottom suspended sediment fluxes are recorded during trawling activities. However, the continued bottom trawling activity, at least for 30 days of monitoring, produced an accumulated suspended sediment transport similar to that generated by a major DSWC event. Taking into account that bottom trawling in Palamós Canyon is practised on a daily basis throughout the year, except for the 2-month trawling closure period, a much larger contribution of anthropogenically derived suspended sediment transport can be expected.

The temporal evolution of the hydrographic and nepheloid layer structure in the upper slope of Vancouver Island (British Columbia, Cascadia margin, NE Canadian Pacific) is studied in

Chapter 6, and assessed by analysing four months of sensor data from Ocean Networks Canada's NEPTUNE cabled seafloor observatory. The distribution of suspended particulate matter during the study period illustrates a well-defined water turbidity structure, consisting in surface nepheloid layers (SNLs) (<100 m depth) associated to primary and secondary productivity, INLs between 150 and 300 m depth at the shelf-break and upper slope domain, and BNLs developed at deeper continental slope regions (~400 m depth). Strong fall storms occurring during the monitored months seem to generate the more intense INLs found at shelf-break depths. However, not all the recorded INLs coincide with the more intense storms, indicating that other sediment resuspension mechanisms might be modulating these INL detachments. This decoupling between the atmospheric conditions and water turbidity indicates that the advection of shelf sediments is not entirely dependent on the magnitude of the storm, but also on the duration of prevailing currents delivering resuspended sediments to the shelf-edge and deeper areas.

Analysis of fishing vessel's activity, through the use of AIS data, also reveal that the depths of the observed INLs coincide with the operating depths of trawlers. Although the most intense fishing activity is attributed to pelagic trawling, the presence of demersal trawling at certain time spans when INLs and BNLs were observed highlights the role of bottom trawling activities in enhancing water turbidity at the study site. Results from this study suggest that, in combination with the regional currents, the presence of continuous fishing along the continental slope off Vancouver Island, contributes to the advection of suspended sediment particles, playing a major role in their transference along the margin as nepheloid layers. This region presents great complexity in terms of studying its sedimentary and oceanographic dynamics, thereby making it difficult to determine the source of particulate matter and the processes being involved in the formation and generation of nepheloid layers.

In Chapter 7, a joint discussion of the main outcomes of this Thesis is presented, offering an integrated vision of the temporal distribution of nepheloid layer structures and the main generation mechanisms in continental slope environments. In Chapter 8, the most relevant conclusions derived from this Thesis is presented, and, in Chapter 9, future research areas, open issues, and recommendations for future work are outlined.

Resum

El transport de matèria i energia des del continent i les zones someres de l'oceà fins a ambients més profunds és especialment important en els marges continentals, a causa de les grans aportacions de partícules en suspensió procedents tant del continent com de zones costaneres altament productives. Els processos hidrodinàmics energètics, com les tempestes, les corrents oceàniques, les ones i les marees internes, així com els processos antropogènics com la pesca d'arrossegament de fons, contribueixen a la resuspensió i remobilització de la matèria particulada, d'una banda ajudant a la seva transferència des de la plataforma fins a ambients de talús continental, i d'una altra mantenint altes concentracions de sediments resuspesos a certs nivells de la columna d'aigua formant capes nefeloids.

Són escasses les investigacions que combinen l'estudi dels processos de resuspensió tant naturals com antropogènics. La majoria d'aquestes investigacions s'han dut a terme principalment a entorns costaners i de plataforma continental, ignorant els efectes de les activitats antropogèniques en ambients d'aigües profundes més enllà de la vora de la plataforma continental. D'altra banda, hi ha una falta d'estudis que avaluïn la variabilitat temporal i espacial de les capes nefeloids a la columna d'aigua relacionades amb les activitats de pesca d'arrossegament, així com una falta d'estudis que examinin fins a quin punt els efectes de les activitats antropogèniques són comparables als dels processos naturals en ambients d'aigües profundes.

Per a comprendre aquest buit de coneixement, o almenys parcialment, aquesta Tesi té com a objectiu principal investigar la contribució que exerceixen les activitats de pesca d'arrossegament a aigües profundes, a més dels processos naturals, a la dinàmica sedimentària en diferents àrees del talús continental, particularment a la Mediterrània nord-occidental i al Pacífic nord-est. Per a dur-ho a terme, les tècniques experimentals utilitzades en aquesta Tesi consisteixen en mesures contínues de durada variable de les propietats de la columna d'aigua, realitzades amb diferents sensors oceanogràfics allotjats en perfiladors verticals autònoms, instal·lats a línies de fondeig instrumentades, o bé a un observatori submarí cablejat, totes elles obtingudes a profunditats del talús continental.

El Capítol 1 consisteix en una introducció general destinada a centrar al lector al marc conceptual i geogràfic en què s'emmarca la present Tesi Doctoral. S'ofereix una introducció als principals processos de generació de capes nefeloids, així com als mètodes i instrumentació clàssica utilitzats per a descriure-les. El Capítol 2 descriu les àrees d'estudi cobertes en aquesta Tesi i, finalment, el Capítol 3 cobreix les metodologies utilitzades per a adquirir i analitzar les dades d'aquesta Tesi.

Al Capítol 4 d'aquesta Tesi s'examina l'evolució temporal de la terbolesa de la columna d'aigua al canyó submarí del Foix (marge Català central, mar Mediterrània nord-occidental). S'estudia

l'estructura hidrogràfica i nefeloid mitjançant l'anàlisi de dos mesos de perfils hidrogràfics recollits per un perfilador vertical autònom instal·lat en una línia de fondeig desplegada a l'eix del canyó, a 870 m de profunditat. Els resultats il·lustren una estructura de terbolesa de la columna d'aigua ben definida, la qual consisteix en capes nefeloids intermèdies (INLs), desenvolupades entre 300 i 500 m de profunditat i sobre els flancs del canyó, i INLs i capes nefeloids pròximes als fons (BNLs) confinades dins del canyó entre 650 i 800 m de profunditat. Les dades de posicionament dels vaixells de pesca obtingudes mitjançant el sistema *Vessel Monitoring System (*VMS*)* durant el període d'enregistrament revelen que la presència i els nivells de la columna d'aigua on s'observen les INLs i les BNLs depenen de les profunditats d'operació dels vaixells d'arrossegament i dels caladors específics explotats per aquesta flota. Aquestes dades suggereixen que les activitats d'arrossegament de fons a la zona d'estudi són el principal causant dels increments de terbolesa observats a la columna d'aigua.

Per altra banda, les condicions hidrodinàmiques dins del canyó també semblen afavorir la retenció de partícules de sediment i incrementar la terbolesa de l'aigua, particularment a les BNLs pròximes al fons, quan la circulació de l'aigua es dirigeix canyó amunt. Encara que la pesca d'arrossegament de fons sembla ser el principal mecanisme de resuspensió de sediments, els processos naturals i les corrents marines ambientals contribueixen a l'advecció i/o retenció de les partícules resuspeses, transportant-les a través i al llarg del marge en forma de capes nefeloids.

Al Capítol 5 d'aquesta Tesi, s'analitzen les variacions espacials i temporals de l'estructura nefeloid de la columna d'aigua i del transport de sediments a prop del fons, associades tant a processos naturals (tempestes, riuades, i cascades d'aigua densa de plataforma, DSWC) així com a activitats de pesca d'arrossegament de fons al Canyó de Palamós (marge continental Català, mar Mediterrània nord-occidental). Les dades per a aquest estudi s'han obtingut mitjançant un perfilador vertical autònom i instruments oceanogràfics instal·lats prop del fons en una línia instrumentada desplegada a l'eix del canyó, a 929 m de profunditat, durant aproximadament tres mesos, cobrint un període de veda i també un període de pesca d'arrossegament activa. Els resultats d'aquest estudi mostren que els increments de la terbolesa de l'aigua durant el període de veda estan associats a tempestes i a esdeveniments de *DSWC*, els quals transporten aigües denses i tèrboles cap a l'interior del canyó. En absència de tals esdeveniments energètics, la columna d'aigua roman sense canvis, mostrant les concentracions de sediments en suspensió més baixes del període d'enregistrament, fins que aquestes tornen a incrementar-se en començar la temporada de pesca d'arrossegament. Les observacions d'aquest estudi il·lustren que les INLs (250-350 m de profunditat) i les BNLs (> 500 m de profunditat) es localitzen en els nivells de la columna d'aigua on es troben els caladors de pesca d'arrossegament del Canyó de Palamós. En aquest cas, les dades de posicionament dels vaixells de pesca en el moment de l'estudi s'han obtingut a través del sistema *Automatic Identification System (*AIS*)*. Prop del fons al punt del mostreig, també es van enregistrar esporàdicament elevats fluxos de sediment en suspensió durant el període de

veda associats a una gran tempesta de llevant i a un esdeveniment de DSWC, mentre que durant les activitats de pesca d'arrossegament es registren augments menors però més freqüents en els fluxos de sediment en suspensió prop del fons. No obstant això, l'activitat continuada d'arrossegament de fons, almenys durant els 30 dies de seguiment de l'estudi, produeix un transport de sediments en suspensió acumulat similar al generat per l'esdeveniment de DSWC més important. Tenint en compte que l'arrossegament de fons en el Canyó de Palamós es practica diàriament durant tot l'any, exceptuant els 2 mesos de veda, cal esperar una contribució molt major al transport de sediments en suspensió d'origen antropogènic.

Al Capítol 6 d'aquesta Tesi s'estudia l'evolució temporal de l'estructura hidrogràfica i nefeloid en el talús superior de l'Illa de Vancouver (British Columbia, marge Cascadia, Pacífic Canadenc nord-est), i s'avalua mitjançant l'anàlisi de 4 mesos de dades obtingudes mitjançant sensors instal·lats a l'observatori submarí cablejat NEPTUNE, del *Ocean Networks Canada.* La distribució de les partícules en suspensió durant el període d'estudi il·lustra una estructura de la terbolesa de la columna d'aigua ben definida què consisteix en capes nefeloids superficials (SNLs) (<100 m de profunditat) associades a productivitat primària i secundària, INLs entre 150 i 300 m a profunditats de la plataforma continental i el talús superior, i BNLs desenvolupades a les zones més profundes del talús continental (~400 m de profunditat). Les fortes tempestes de tardor que es produeixen durant els mesos monitorejats semblen generar les INLs més intenses que es troben a les profunditats de la vora de la plataforma continental. No obstant això, no totes les INLs registrades coincideixen amb les tempestes de més intensitat, la qual cosa indica que altres mecanismes de resuspensió de sediments podrien estar modulant la generació d'aquestes capes. Aquesta discordança entre les condicions atmosfèriques i la terbolesa de l'aigua indica que l'advecció de sediments de la plataforma no depèn totalment de la magnitud de la tempesta, sinó també de la durada de les corrents predominants que transporten els sediments resuspensos cap a la vora de la plataforma i cap a zones més profundes del talús.

L'anàlisi de l'activitat dels vaixells d'arrossegament, mitjançant la utilització de dades AIS, revela que les profunditats a les quals es troben aquestes INLs coincideixen també amb les profunditats d'operació dels vaixells d'arrossegament. Encara que l'activitat pesquera més intensa s'atribueix a l'activitat de pesca d'arrossegament pelàgica, la presència d'activitats de pesca d'arrossegament de fons en determinats períodes de temps en els quals també s'observen INLs i BNLs, posa de manifest el possible paper de les activitats d'arrossegament de fons en l'augment de la terbolesa de l'aigua en aquesta regió. Els resultats d'aquest estudi suggereixen que, en combinació amb la circulació regional, la presència contínua de pesca d'arrossegament al llarg del talús continental davant l'Illa de Vancouver contribueix a l'advecció de sediment en suspensió, exercint un paper important en la seva transferència al llarg del marge en capes nefeloids. Aquesta regió presenta una gran complexitat en quant a l'estudi de la dinàmica sedimentària i oceanogràfica, fet que dificulta la determinació de

l'origen de les partícules i dels processos que intervenen en la formació i generació de capes nefeloids.

Al Capítol 7 es presenta una discussió conjunta dels principals resultats d'aquesta Tesi, oferint una visió integradora de la distribució temporal de l'estructura nefeloid i dels principals mecanismes de generació en ambients de talús continental. Finalment, al Capítol 8, es presenten les conclusions més rellevants derivades d'aquesta Tesi i, al Capítol 9, s'assenyalen les possibles àrees d'investigació futures, les qüestions que romanen obertes i les recomanacions per a futurs treballs.

Resumen

El transporte de materia y energía desde el continente y las zonas someras del océano hasta ambientes más profundos es especialmente importante en los márgenes continentales, debido a los grandes aportes de partículas en suspensión procedentes tanto del continente como de zonas costeras altamente productivas. Los procesos hidrodinámicos energéticos, como las tormentas, las corrientes oceánicas, las ondas y mareas internas, así como los procesos antropogénicos como la pesca de arrastre de fondo, contribuyen a la resuspensión y removilización de la materia particulada, por una parte, ayudando a su transferencia desde la plataforma hasta ambientes de talud continental, y por otra manteniendo altas concentraciones de sedimentos resuspendidos a ciertos niveles de la columna de agua formando capas nefeloides.

Son escasas las investigaciones que combinan el estudio de procesos de resuspensión tanto naturales como antropogénicos. La mayoría de estas investigaciones se han llevado a cabo principalmente en entornos costeros y de plataforma continental, ignorando los efectos de las actividades antropogénicas en ambientes de aguas profundas más allá del borde de plataforma continental. Por otro lado, hay una falta de estudios que evalúen la variabilidad temporal y espacial de las capas nefeloides en la columna de agua relacionadas con las actividades de pesca de arrastre, así como una falta de estudios que examinen hasta qué punto los efectos de las actividades antropogénicas son comparables a los de los procesos naturales en ambientes de aguas profundas.

Para comprender este vacío de conocimiento, o al menos parcialmente, esta Tesis tiene como objetivo principal investigar la contribución que ejercen las actividades de pesca de arrastre en aguas profundas, además de los procesos naturales, a la dinámica sedimentaria en diferentes áreas del talud continental, particularmente en el Mediterráneo noroccidental y en el noreste del Pacífico. Para ello, las técnicas experimentales utilizadas en esta Tesis consisten en mediciones continuas de duración variable de las propiedades de la columna de agua, realizadas con diferentes sensores oceanográficos alojados en perfiladores verticales autónomos, bien instalados en líneas de fondeo instrumentadas, o bien en un observatorio submarino cableado, ambos a profundidades del talud continental.

El Capítulo 1 consiste en una introducción general destinada a centrar al lector en el marco conceptual y geográfico en el que se enmarca la presente Tesis Doctoral. Se ofrece una introducción a los principales procesos de generación de capas nefeloides, así como a los métodos e instrumentación clásica utilizados para describirlas. El Capítulo 2 describe las áreas de estudio cubiertas en esta Tesis y el Capítulo 3 cubre las metodologías utilizadas para adquirir y analizar los datos de esta Tesis.

En el Capítulo 4 de esta Tesis se examina la evolución temporal de la turbidez de la columna de agua en el cañón submarino de Foix (margen catalán central, mar Mediterráneo noroccidental). Se estudia la estructura hidrográfica y nefeloide mediante el análisis de dos meses de perfiles hidrográficos recogidos por un perfilador vertical autónomo instalado en una línea de fondeo desplegada en el eje del cañón, a 870 m de profundidad. Los resultados ilustran una estructura de turbidez de la columna de agua bien definida, que consiste en capas nefeloides intermedias (INLs), desarrolladas entre 300 y 500 m de profundidad y sobre los flancos del cañón, e INLs y capas nefeloides cercanas al fondo (BNLs) confinadas dentro del cañón entre 650 y 800 m de profundidad. Los datos de posicionamiento de los buques de pesca obtenidos mediante el sistema *Vessel Monitoring System (*VMS*)* durante el periodo de registro revelan que la presencia y los niveles de la columna de agua donde se observan las INLs y las BNLs dependen de las profundidades de operación de los barcos de arrastre y de los caladeros específicos que son explotados por dicha flota. Estos datos sugieren que las actividades de pesca de arrastre de fondo fueron el principal causante de los incrementos de turbidez observados en la columna de agua.

No obstante, las condiciones hidrodinámicas dentro del cañón también parecen favorecer la retención de partículas de sedimento y aumentar la turbidez del agua, particularmente en las BNL cercanas al fondo, cuando la circulación del agua se dirige cañón arriba. Aunque la pesca de arrastre de fondo parece ser el principal mecanismo de resuspensión de sedimentos, los procesos naturales y las corrientes marinas ambientales también contribuyen a la advección y/o retención de las partículas resuspendidas, transportándolas a lo largo y ancho del margen en forma de capas nefeloides.

En el Capítulo 5 de esta Tesis, se analizan las variaciones espaciales y temporales de la estructura nefeloide de la columna de agua y del transporte de sedimentos cerca del fondo, asociadas tanto a procesos naturales (tormentas, riadas y cascadas de agua densa de plataforma, DSWC) como a actividades de pesca de arrastre de fondo en el Cañón de Palamós (margen continental catalán, mar Mediterráneo noroccidental). Los datos para este estudio se han obtenido mediante un perfilador vertical autónomo y mediante instrumentos oceanográficos instalados cerca del fondo en una línea instrumentada desplegada en el eje del cañón, a 929 m de profundidad, durante aproximadamente tres meses, cubriendo un periodo de veda y también un periodo de pesca de arrastre activa. Los resultados de este estudio muestran que los aumentos de la turbidez del agua durante el periodo de veda están asociados a tormentas y a eventos de DSWC, los cuales transportan aguas densas y turbias hacia el interior del cañón. En ausencia de tales eventos energéticos, la columna de agua permanece sin cambios, mostrando las concentraciones de sedimentos en suspensión más bajas del periodo de registro, hasta que estos aumentan de nuevo justo en el comienzo de la temporada de pesca de arrastre. Las observaciones de este estudio ilustran que las INLs (250-350 m de profundidad) y las BNLs (> 500 m de profundidad) se localizan en los niveles de la columna de agua donde se encuentran los caladeros de pesca de arrastre del Cañón de

Palamós. En este caso, los datos de posicionamiento de los barcos de pesca en el momento del estudio se han obtenido a través del sistema *Automatic Identification System (*AIS*)*. Cerca del fondo en el punto de fondeo, también se registraron esporádicamente elevados flujos de sedimento en suspensión cerca del fondo durante el periodo de veda asociados a un gran temporal de levante y al mayor evento de DSWC, mientras que durante las actividades de pesca de arrastre se registran aumentos menores, pero más frecuentes en los flujos de sedimento en suspensión cerca del fondo. No obstante, la actividad continuada de arrastre de fondo, al menos durante los 30 días de seguimiento del estudio, produce un transporte de sedimentos en suspensión acumulado similar al generado por el evento de DSWC. Teniendo en cuenta que la pesca de arrastre de fondo en el Cañón de Palamós se practica diariamente durante todo el año, exceptuando los 2 meses de veda, cabe esperar una contribución mucho mayor a la turbidez del agua y al transporte de sedimentos en suspensión de origen antropogénico.

En el Capítulo 6 de esta Tesis se estudia la evolución temporal de la estructura hidrográfica y nefeloide en el talud superior de la Isla de Vancouver (British Columbia, margen de Cascadia, Pacífico Canadiese noreste), y se evalúa mediante el análisis de cuatro meses de datos obtenidos mediante sensores instalados en el observatorio submarino cableado NEPTUNE, del *Ocean Networks Canada*. La distribución de las partículas en suspensión durante el periodo de estudio ilustra una estructura de turbidez de la columna de agua bien definida que consiste en capas nefeloides superficiales (SNL) (<100 m de profundidad) asociadas a productividad primaria y secundaria, INLs entre 150 y 300 m a profundidades de la plataforma continental y el talud superior, y BNLs desarrolladas en las zonas más profundas del talud continental (~400 m de profundidad). Las fuertes tormentas de otoño que se producen durante los meses monitoreados parecen generar las INLs más intensas que se encuentran a las profundidades del borde de la plataforma continental. Sin embargo, no todas las INLs registradas coinciden con las tormentas de más intensidad, lo que indica que otros mecanismos de resuspensión de sedimentos podrían estar modulando la generación de estas capas. Esta discordancia entre las condiciones atmosféricas y la turbidez del agua indica que la advección de sedimentos de la plataforma no depende totalmente de la magnitud de la tormenta, sino también de la duración de las corrientes predominantes que llevan los sedimentos resuspendidos hacia el borde de la plataforma y a zonas más profundas del talud.

El análisis de la actividad de los buques de arrastre, mediante el uso de datos AIS, revela que las profundidades a las que se encuentran estas INLs coinciden con las profundidades de operación de los arrastreros. Aunque la actividad pesquera más intensa se atribuye a la actividad de pesca de arrastre pelágica, la presencia de actividades de pesca de arrastre de fondo en determinados periodos de tiempo en los que también se observan INLs y BNLs, pone de manifiesto el posible papel de las actividades de arrastre de fondo en el aumento de la turbidez del agua en esta región. Los resultados de este estudio sugieren que, en combinación con la circulación regional, la presencia continua de pesca de arrastre a lo largo del talud

continental frente a la Isla de Vancouver contribuye a la advección de sedimento en suspensión, desempeñando un papel importante en su transferencia a lo largo del margen en capas nefeloides. Esta región presenta una gran complejidad en cuanto al estudio de su dinámica sedimentaria y oceanográfica, lo que dificulta la determinación del origen de las partículas y de los procesos que intervienen en la formación y generación de capas nefeloides.

En el Capítulo 7 se presenta una discusión conjunta de los principales resultados de esta Tesis, ofreciendo una visión integradora de la distribución temporal de la estructura nefeloide y de los principales mecanismos de generación en ambientes de talud continental. Finalmente, en el Capítulo 8, se presentan las conclusiones más relevantes derivadas de esta Tesis y, en el Capítulo 9, se señalan las posibles áreas de investigación futuras, las cuestiones que permanecen abiertas y las recomendaciones para futuros trabajos.

Table of contents

Part III. Results

Thesis Presentation

I. Motivation and Innovation of this research

Fine sediment particles (settling and suspended) are responsible for much of the particulate matter fluxes in the marine environment, playing an important role in the global oceanic geochemical cycles and in the marine ecosystems (Asper et al., 1992). Sedimentary processes control the transport of most suspended particulate matter generated in or introduced to the oceans, being particularly important in continental margins because of the large inputs of organic and inorganic particles from both terrestrial and high-productivity coastal waters (e.g., Blair and Aller, 2012; Milliman and Farnsworth, 2013; Liu et al., 2016). However, the transport and fate of sediment particles are influenced by the action of both natural processes and anthropogenic activities, which occur both in the sea and on the land. Particularly, recent studies assessing the impact of anthropogenic activities in the marine environment have highlighted the effects of bottom trawling, where its spatial extent has been estimated to be an order of magnitude greater than all other anthropogenic activities (Benn et al., 2010). Aside from the direct effects on benthic fauna and its habitats, the dragging of the trawling gears over the seafloor causes the loss of surface seabed morphology (Puig et al., 2012; Martín et al., 2014c; Oberle et al., 2018). Additionally, bottom trawling can also resuspend large volumes of surface sediments and inject them into the water column, particularly when trawling is carried out over soft bottoms (Jones, 1992; Pilskaln et al., 1998). Therefore, the combined action of natural processes and bottom trawling in the marine environments supposes a high complexity in studying the sedimentary dynamics on continental margins. Only a few studies have brought this aspect into focus, proposing that bottom trawling activities are able to rival natural processes as the main agent for sediment resuspension and transport in middle and outer shelf environments (Churchill, 1989; Ferré et al., 2008). However, the body of literature assessing this subject is still scarce and mainly devoted to coastal and continental shelf settings, leaving a big gap of knowledge on the effects of this human practice at depths beyond the shelf-break.

This Thesis aims to investigate the contribution to the sedimentary dynamics that deep trawling activities, besides natural processes, exert in different continental slope areas of the NW Mediterranean and NE Pacific margins. This PhD dissertation was initially inspired by precedent studies conducted in continental slope areas affected by trawling activities, where it was observed that bottom trawling introduced sediment particles into the water column, contributing to the formation of nepheloid layers (e.g., Chronis et al., 2000; Martín et al., 2014a; Wilson et al., 2015b; Daly et al., 2018). However, these studies were limited to punctual observations of nepheloid layers in hydrographic vertical profiles, and whether these trawling-induced nepheloid layers lasted for a prolonged time in the water column, and to which degree they were comparable to the effect of natural processes in deep-sea environments was still unknown. This Thesis will try to envisage the effects of bottom trawling in the water column over continental slope environments during longer study periods, and to compare them with the natural processes that characterize each of the studied regions.

The methodology employed in this Thesis is typical of studies on hydrography and sedimentary dynamics. However, it includes data from automated hydrographic profiling technologies to measure and detect nepheloid layers in continental slope environments, and to assess the temporal evolution of these features in the water column. The results presented in the following chapters of this PhD dissertation can be translated into an improvement of the detection and measurement of nepheloid layers in deep-sea environments, and to a better understanding of their distribution and temporal variability.

II. Aims and Thesis structure

The general aim of this Thesis is to study the temporal and spatial variability of the nepheloid layer structure in continental slope environments, including submarine canyons, and to identify the contribution of deep bottom trawling as a sediment resuspension mechanism to the natural sedimentary dynamics of these deep-sea environments. This research focuses on the Catalan margin (NW Mediterranean Basin) and the Cascadia margin off Vancouver Island (Canadian NE Pacific), where deep bottom trawling has been practiced for several decades and where the distribution of the fishing effort is known in detail. In particular, this investigation combines high-resolution fishing vessel positioning data and different field observational and sampling techniques to shed light on the impacts of this anthropogenic activity to the contemporary sedimentary processes that occur within continental slope regions.

This Thesis envisages defining the natural and anthropogenic contribution affecting the formation of nepheloid layers in these continental slope regions, under the assumption that these features are the means of lateral suspended sediment transport. In order to assess the spatial and temporal variability of nepheloid layers in the Catalan and the Cascadia margins, and to examine, besides natural resuspension mechanisms, the contribution of deep bottom trawling to the sedimentary dynamics, the specific aims of this Thesis are to:

- Identify the oceanographic regimes and sediment transport processes that influence nepheloid layer dynamics within submarine canyons incising the Catalan margin
- Identify the oceanographic regimes and sediment transport processes that dominate at the Cascadia margin off Vancouver Island (Canadian NE Pacific), and that exert an influence on the nepheloid layer dynamics in this area
- Assess the spatial and temporal patterns of the local trawling fleets and establish the relationship with the presence of nepheloid layers in the study areas
- Describe the hydrographic structure and temporal evolution of the distribution of nepheloid layers in the water column as indicators of trawling-induced resuspension processes in the study sites
- Prove the usefulness of autonomous hydrographic profiling systems to study the temporal evolution of nepheloid layers in the water column

This Thesis is primarily structured into five parts. The first part gives an introduction to the main nepheloid layer generation processes and describes the study sites covered in this Thesis. The second part describes the methodologies used to acquire and analyse the data employed in this Thesis dissertation. The third part corresponds to the Results obtained during the development of this Thesis to study the hydrographic and nepheloid layer structure in the study sites. The fourth part includes a general discussion of the results obtained in this Thesis and their contextualization in the current knowledge of contemporary sedimentary processes contributing to nepheloid layer formation, and the fifth and last part comprises a summary of the main outcomes of the Thesis and future perspectives.

Part I. Introduction

i. **Chapter 1** provides a description of the deep-sea and the role of lateral advection in continental margins. In this chapter it is provided a broad literature overview and background of nepheloid layer formation processes, and history of instrumentation and methods that have been classically used to described them.

ii. **Chapter 2** presents a description of the hydrology and general circulation, as well as the dominant sediment transport processes of the two main study sites covered in this Thesis: the Catalan margin (NW Mediterranean) and Cascadia Margin off Vancouver Island (Canadian NE Pacific). This chapter also provides information of the trawling activities practiced at both study sites.

Part II. Methodology

iii. **Chapter 3** provides the details of the research surveys, and describes the methodology employed in this Thesis, including: the retrieval of hydrographic and turbidity vertical profiles acquired from hydrographic transects, moored instruments installed in autonomous hydrographic vehicles and submarine cabled observatories, the acquisition of currents' data, and the processing that has been applied to assess the nepheloid layer structure within the water column. A brief description of a laboratory calibration carried out for the Catalan margin is also provided here. Finally, this chapter also includes the procedures used to identify bottom trawling grounds. Specific details of the methodology used in this Thesis are given at the corresponding section of methods in each chapter of Results.

Part III. Results

Chapter 4 and **Chapter 5** present the results obtained from oceanographic deployments with an autonomous hydrographic profiler (Aqualog), as a tool for assessing the spatial and temporal evolution of the hydrographic and nepheloid structure within two submarine canyons incising the Catalan margin (NW Mediterranean).

iv. **Chapter 4** focuses on the hydrographic structure and the distribution of intermediate and bottom nepheloid layers in the Foix Canyon, a sinuous submarine canyon incising the Central Catalan margin, analysing 2 months of profiling data. The chapter examines the contribution of deep-bottom trawling activities carried out within and around the canyon to the water turbidity structure, using the spatial information of the local trawling fleet provided by the Vessel Monitoring System (VMS). This study was published in *Journal of Marine Systems* in 2019[1].

v. **Chapter 5** covers the spatial and temporal variations on the hydrographic and nepheloid layer structure linked to natural processes (storms and dense shelf water cascading events) and deep-bottom trawling activities in the Palamós (La Fonera) Canyon, one of the most prominent submarine canyons incising the Catalan margin. This deployment lasted for 3 months and covered part of a 2-month trawling closure and the recommencement of trawling activities along the canyon flanks, allowing to capture the natural sedimentary dynamics during the fishing closure and the transition to the trawling season. The contribution of natural and trawling-induced mechanisms to the near-bottom sediment fluxes and transport is also assessed in this chapter through the analysis of the near-bottom instrumentation deployed in the same oceanographic mooring. Results presented in this study have been accepted in *Marine Geophysical Research*[2].

vi. **Chapter 6** addresses the hydrographic and nepheloid layer structure in the upper slope region off Vancouver Island (Cascadia margin, Canadian NE Pacific) by analysing 4 months of hydrographic and turbidity profiles collected by a vertical profiling system (VPS) combined with currents' data from an instrumented platform installed on a seafloor cabled observatory. This chapter also analyses the physical generation of nepheloid layers and examines the possibility of bottom trawling activities influencing the water column turbidity structure. The outcomes of this study have been submitted for publication and under review in *Frontiers in Marine Science*[3].

Part IV. General discussion

vii. **Chapter 7** discusses the main outcomes of this Thesis and contextualize them in the global scale. In this chapter, the main advantages of using new technologies for assessing the nepheloid layer structure in these deep-sea regions are also included.

[1] **Arjona-Camas, M., Puig, P., Palanques, A., Emelianov, M., Durán, R. (2019)** Evidence of trawling-induced resuspension events in the generation of nepheloid layers in the Foix submarine canyon (NW Mediterranean). Journal of Marine Systems 196, 86-96; doi: 10.1016/j.jmarsys.2019.05.003.

[2] **Arjona-Camas, M., Puig, P., Palanques, A., Durán, R., White, M., Paradis, S., Emelianov, M. (2021).** Natural vs. trawling-induced water turbidity and sediment transport variability within the Palamós Canyon (NW Mediterranean). Marine Geophysical Research (*in press*), doi: https://doi.org/10.1007/s11001-021-09457-7.

[3] **Arjona-Camas, M., Puig, P., De Leo, F. C., Garner, G., Paradis, S., Durán, R., Palanques, A. (2021).** Influence of natural processes and bottom trawling in the nepheloid layer structure off Vancouver Island (British Columbia, Canada, NE Pacific). Frontiers in Marine Science (*under review*).

Part V. Conclusions and future perspectives

viii. **Chapter 8** synthetises the most relevant conclusions of the distribution of nepheloid layers and linked formation mechanisms in continental slope environments (including submarine canyons) and the role of trawling activities, besides natural processes, in the resuspension of sediments and generation of nepheloid layers in these deep-sea environments.

ix. **Chapter 9** outlines the future research areas that can be derived from this Thesis dissertation.

Introduction

Part I

Chapter 1. Introduction

1.1. The deep-sea environment

The deep-sea is one of the largest, most diverse, and poorly understood ecosystems on the Earth's surface. The deep-sea is traditionally defined below the shelf break (~200 m depth) because this physiographic feature coincides with the transition from the basically shallow-water fauna on the shelf to the deep-sea fauna (Thistle, 2003). The deep-sea occupies approximately 50 % of the Earth's surface and covers an area of approximately 360 million km^2 (Glover and Smith, 2003; Ramirez-Llodra et al., 2011).

The deep-sea floor had always been perceived as a species-poor environment due to its extreme characteristics. However, the idea that the deep-sea was barren, with increasing pressures and decreasing temperatures, and darkness inhibiting any organisms from living there has changed dramatically during the 19^{th} and 20^{th} centuries. Early expeditions, such as the British *HMS Challenger* (1872-1876) and the Danish *Galathea*, conclusively demonstrated the presence of abundant life in all depths and areas of the deep ocean, dispelling myths of archaic fauna (Glover and Smith, 2003; Ramirez-Llodra et al., 2011). One of the early paradigms of marine ecology was the "slow, steady sate" of the deep-sea floor (Smith, 1994) that viewed the deep as an environment remote and deliberate, where nutrient fluxes from surface waters were attenuated and buffered by the enormous water column above. However, this view began to change in the 1970s and 1980s, when several studies gave rise to many exciting discoveries in the deep-sea, including unique habitats such as chemosynthetic ecosystems created on whale falls (Smith et al., 1989), benthic storms (Hollister and McCave, 1984), and physical heterogeneity and seasonality (Deuser and Ross, 1980; Tyler and Gage, 1982; Billett et al., 1983; Thiel et al., 1989).

In recent years, there has been an increasing turning to the deep-sea for commercial uses and commodities. Potential human impacts in the deep-sea (Fig. 1.1) include those from past activities (for example, waste disposal), current undertaking impacts (for example, deep-sea fisheries, oil and gas exploration, polymetallic nodule mining and methane hydrate extraction, communication cables, and pharmaceuticals), and future potential influences (for example, ocean acidification, climate change, and CO_2 sequestration) (Glover and Smith, 2003; Ramirez-Llodra et al., 2011 and references therein).

To date, little information is available on the direct and long-term effects of human activities in the bathyal and abyssal ecosystems. The vast diversity of the deep-sea creates conservational challenges and, therefore, research on sediment and production pathways to the deep ocean can help our understanding on how the deep-sea ecosystems function.

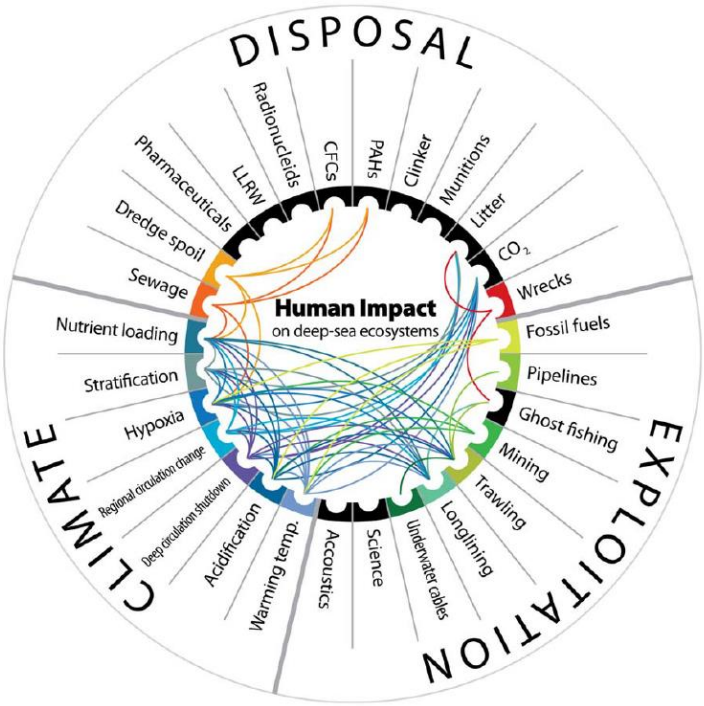

Figure 1.1. Synergies amongst anthropogenic impacts (climate-related, disposal-related, and exploitation-related) on deep-sea habitats. The lines link impacts that, when found together, have a synergic effect on habitats or faunal communities. The lines are colour-coded and indicate the direction of the synergy. LLRW: low-level radioactive waste, CFCs: chlorofluorocarbons, PAHs: polycyclic aromatic hydrocarbons. **Source:** Ramirez-Llodra et al., 2011.

1.2. The flux of energy and matter from the shallow sea to the deep abyss

Deep-sea habitats are generally considered food limited because biotic production depends on the sinking flux of particles from the euphotic zone thousands of meters up in the water column (Smith, 2006). Although this organic matter flux is very low (constituting a small percent of primary productivity), many organisms have adapted to such conditions. The energy for the deep-sea fauna is ultimately derived from high-productive remote surface waters, where autotrophic organisms such as algae, diatoms and coccolithophorids form the base of the ocean food chain. These microscopic organisms globally produce ~45-50 $Gt \cdot y^{-1}$ (Longhurst et al., 1995).

The biological pump (Fig. 1.2) describes the collection of biogeochemical processes associated with production, sinking and remineralization of organic carbon in the ocean (Giering and Humphreys, 2018). Briefly, photosynthetic organisms in surface waters fix inorganic carbon into biomass that sinks to the deep ocean, fuelling the metabolism of the organisms living there (Fig. 1.2) (Volk and Hoffert, 1985; Giering and Humphreys, 2018). Zooplankton may also play a critical role in the dynamics of particles fluxes through ingestion and fragmentation of particles, production of fast-sinking faecal material, and active vertical migration (Fig. 1.2) (Giering et al.,

2014; Svensen et al., 2014; Iversen et al., 2017; Kiko et al., 2017). The biological pump also provides valuable ecosystem function, transporting an estimate of 5-20 Gt C_{org} each year to the deep (Henson et al., 2011), where some of it (~0.2-0.5 Gt) is sequestered in marine sediments for several millennia (Guidi et al., 2015).

Sinking particles can be phytoplankton or zooplankton cells, detritus, faecal pellets, or whale falls. They range in size from a few micrometres to several meters, including particles of a diameter > 0.5 mm being referred to as "marine snow" (Alldredge and Silver, 1988). Marine snow contributes to higher sinking velocities due to its larger size and, as it escapes from surface waters, it can rapidly transport rich organic matter, triggering an awakening response of benthic organisms (Alldredge and Silver, 1988; Turner, 2002; Iversen et al., 2017). The density of pure organic matter is generally lower than water, although it has been observed that silica and other lithogenic material serve as ballast to achieve particle densities high enough to allow sinking (Iversen and Ploug, 2010). Sinking velocities for ocean particles generally range between 10 and 150 $m \cdot d^{-1}$ (McDonell and Buesseler, 2010), although particle flux events dominated by zooplankton faecal pellets can exceed sinking velocities of 1000 $m \cdot d^{-1}$ (Turner, 2015).

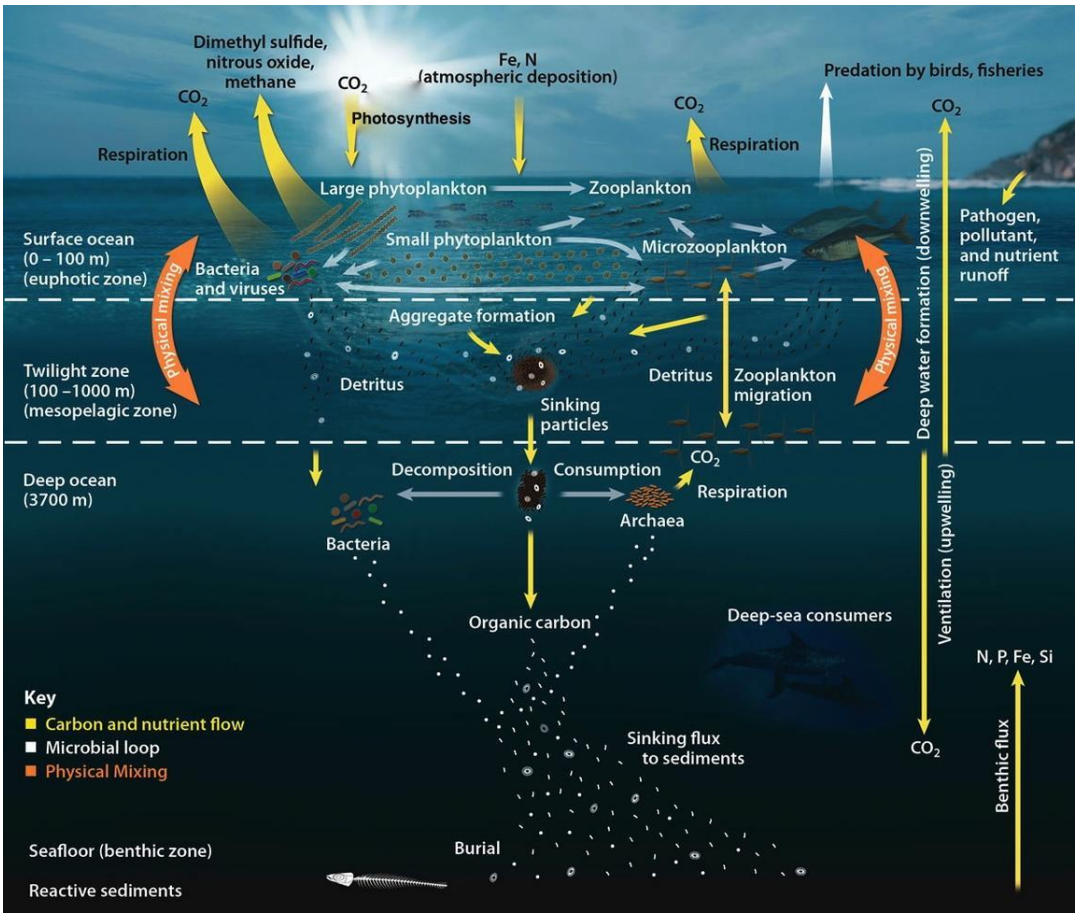

Figure 1.2. Sources of particles in the open ocean and the ocean carbon cycle. **Source:** Oak Ridge National Laboratory, https://serc.carleton.edu/eslabs/carbon/6a.html.

1.3. The continental margins: interfaces between the land and the ocean

Continental margins mark the transition between the ocean and the continents and are traditionally defined as the region between the upper limit of the tidal range and the base of the continental slope. They can be classified in two types: passive continental margins, which are those that ride passively within the interior of a lithosphere plate, and active continental margins, which are those that lie along boundaries between plates and are affected by the plate movement, formed along convergent boundaries, or transform plates (Kennett, 1982).

Passive continental margins, where the oceanic crust and the continental crust move in concert, contain a coastal plain, a transition zone, that in turns contains the continental shelf, slope and rise, and an abyssal plain (Fig. 1.3). Closest to the shore, the continental shelf is a relatively flat surface with a gentle slope (~0.05 º) extending from the shoreline to the shelf-break, and it is generally located at less than 200 m depth. Depending on the regional geological setting, the shelf will extend from a few kilometres to several hundreds of kilometres away from the shore. The continental slope extends from the shelf-break to water depths ranging between 1000 m and 2000 m. Seafloor gradients on the continental slope are variable, averaging ~4 º (Pratson et al., 2007). Deeper than 2000 m depth, the continental rise can reach depths greater than 6000 m (Fig. 1.3) (Blondel, 2009).

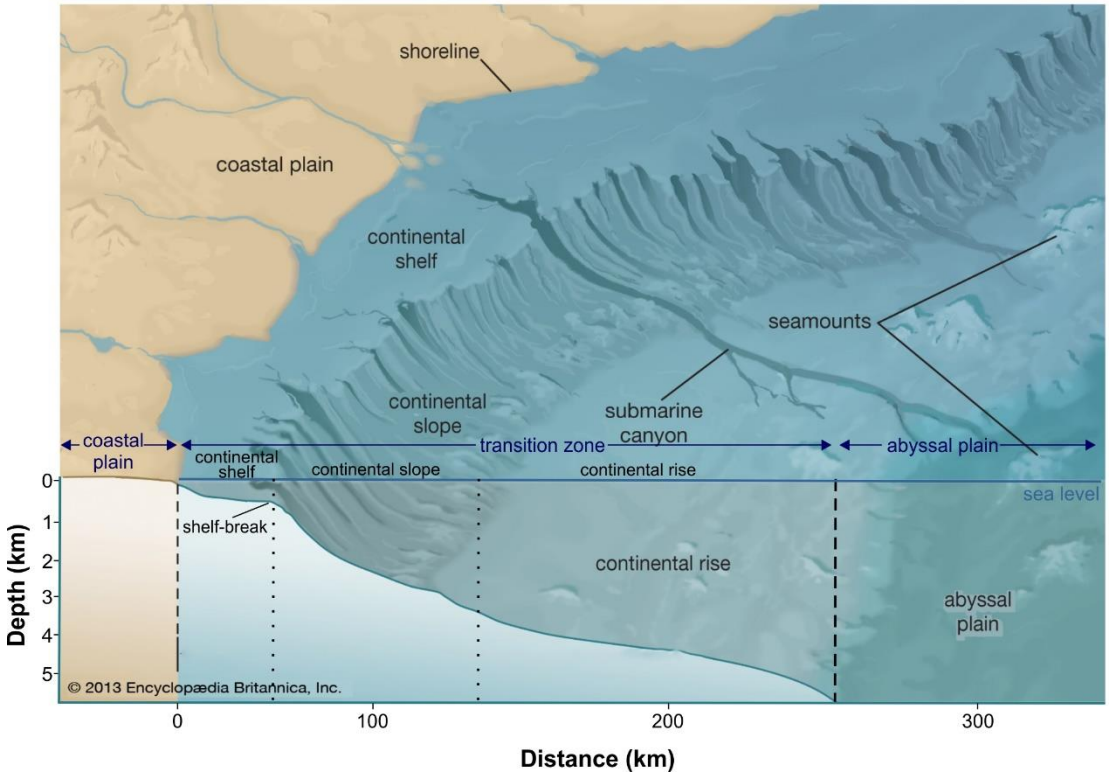

Figure 1.3. Realistic representation and schematic section of a passive continental margin. **Source:** Modified from Encyclopaedia Britannica Inc, 2013.

Part of the sediments that are submitted to the shelf can be rapidly deposited, while the less dense fraction can spread towards the open ocean forming a nepheloid layer (Biscaye and Eittreim, 1977). Nevertheless, large volumes of sediments are transported towards greater depths, following the bathymetry gradients down the continental slope (Fig. 1.3). This rapidly descent area ranges in depth between ~250 and 2000 m, and sediments are transported mainly through channels and submarine canyons until reaching the abyssal regions. Because of their steep slopes, some of the sedimentary structures may be unstable, and earthquakes or minor sea level changes can create their collapse, creating landslides. Then sediments are transported down-slope to the continental rise (Fig. 1.3), which marks the limit between the continental margins and the abyssal plains. Deeper than 2000 m depth, the continental rise can reach depths greater than 6000 m (Blondel, 2009).

1.3.1. Sediment transport in continental margins

The continental margins are submitted to the constant input of sediment particles from both fluvial and high-productivity coastal waters (Blair and Aller, 2012; Milliman and Farnsworth, 2013; Liu et al., 2016; Kwon et al., 2021), but they are also affected by pelagic rain (Fig. 1.4). Fine particles (settling and suspended) are responsible for much of the flux of matter and energy in the marine environment, having great importance in the global biogeochemical cycles and in the marine ecosystems (Walsh, 1991; Wollast, 1998). However, the study of sediment dynamics on continental margins is complex because in these areas coexist anthropogenic activities and oceanographic processes that combine their action to influence sediment particles transport and deposition. Generally, up to 90 % of the sediments moved by rivers are carried out in the water column as sediment loads, part of them depositing on the continental shelf, and part being exported in suspension in nepheloid layers seawards (Biscaye and Eitreim, 1977; Syvitski et al., 2003). High energetic processes such as internal waves, bottom currents, and tides contribute to the remobilization of ephemerally deposited sediments on the shelf, favouring their transference to the continental slope and deeper areas of the ocean (Fig. 1.4) (Walsh and Nittrouer, 2009).

Both vertical export and lateral advection of particulate matter represent relevant sources of nutrients for deep-sea ecosystems (Thunell et al., 2000; Honjo et al., 2008). In the last decades, sinking particles have received large interest from the scientific community resulting in numerous international programs (e.g., VERTEX, CARIACO Ocean TimeSeries, MedFlux) focused on the processes governing vertical particle fluxes in the water column. However, the study of lateral advection is more complex, although it occurs globally in continental slope environments. Nevertheless, a holistic approach including both vertical and lateral sediment transport processes would be necessary to understand these high complex settings that are moulded by the interplay between biology, physics, biogeochemistry, oceanography, and sedimentology.

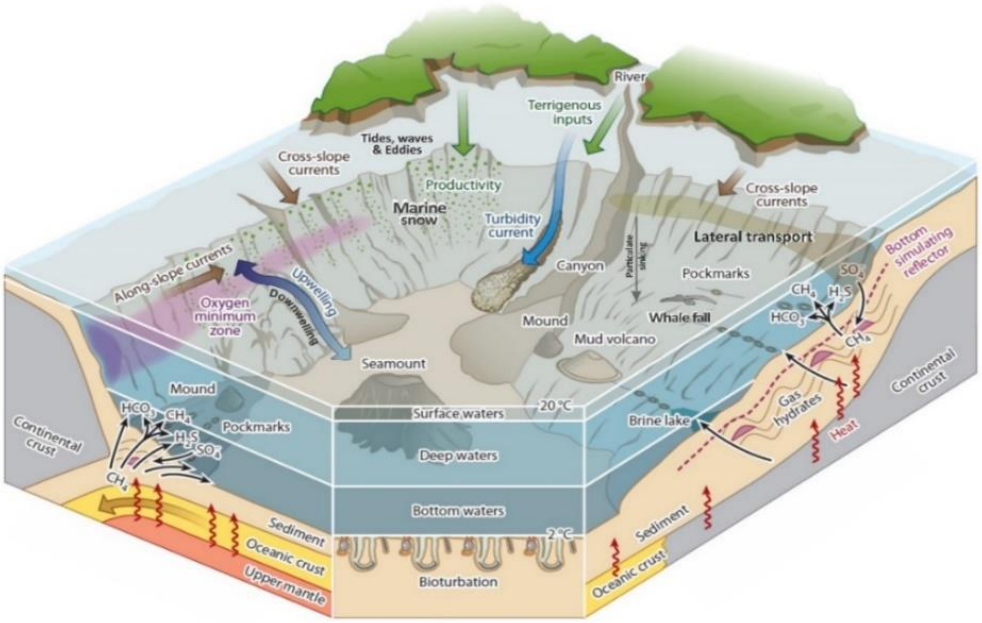

Figure 1.4. Schematic illustration of the geological, chemical, hydrological, and biological sources of particles on continental margins. Strong depth-related and geographic variations in water masses, productivity and hydrodynamic processes superimposed on typical continental margin habitats such as submarine canyons, chemosynthetic communities linked to cold methane seep structures (pockmarks and mud volcanoes) and whale falls are illustrated. Major exchange processes (such as downwelling/upwelling, along- and cross-slope currents, tides, waves and eddies) and factors affecting energy and particle fluxes at continental margins are also represented. **Source:** Modified from Levin and Sibuet, 2012 and Menot et al., 2010.

A first tentative global marine carbon cycle was published by Walsh et al. (1981), but lateral particle fluxes between the shelf, the slope and the open ocean could only be indicated by question marks. Up to now, lateral transport has been investigated by many large international projects, for example SEEP I and SEEP II on the outer margin of the Mid Atlantic Bight (Biscaye et al., 1994; Walsh et al., 1988), OMEX I in the northern Bay of Biscay and OMEX II at the NW Iberian Margin (van Weering and McCave, 2002), and STRATAFORM off northern California and New Jersey (Nittrouer, 1999), which demonstrated the relative role of continental margins in lateral transport. The ECOMARGE project conducted in the Gulf of Lions (NW Mediterranean) emphasized the importance of seaward flux of particles of coastal origin, especially in submarine canyon systems (e.g., Lacaze Duthiers Canyon) (Monaco et al., 1990). The second ECOMARGE experiment (ECOFER), which took place in the Cap Ferret Canyon (southern part of the Biscay margin), also showed preferential focusing of particulate matter in a submarine canyon incising the slope (Monaco et al., 1999). The ECOMARGE project, as well as the SEEP-I and the SEEP-II projects (Etcheber et al., 1996) or subsequently the OMEX project (Wollast and Chou, 2001a) concluded that particle fluxes to the slope are mainly supplied by lateral transport from the shelf and upper slope rather than by pelagic settling. Other authors reached the same conclusion from deficit found between the vertical flux of particulate matter and the energy and organic matter requirements of the benthos (e.g., Thomsen, 1999; Druffel and Robinson, 1999). Wollast and

Chou (2001b) added to these conclusions the possible role and importance of submarine canyons in the transference of organic carbon to slope depths, which was not included in OMEX-I project. This point was further confirmed in OMEX-II, namely in the Nazaré Canyon (W Iberian Margin) (van Weering and McCave, 2002; van Weering et al., 2002).

1.3.2. Relevance of submarine canyons in the across-margin transport of particulate matter

Submarine canyons are morphological features incising continental margins around the world (Shepard and Dill, 1966). Recent technological developments including imaging, underwater acoustic mapping, sampling technologies, and long-term moorings or seafloor observatories have contributed to our understanding of the diverse and complex hydrodynamics and geomorphology of canyons during the last two decades (Xu, 2011; Puig et al., 2014; Quattrini et al., 2015; Robert et al., 2015). As a result of these studies, it is known that there are over 9477 submarine canyons covering 11.2 % of continental slopes worldwide (Harris et al., 2014a), with an estimated accumulated axis length over 25000 km (Huang et al., 2014).

Submarine canyons are characterised by steep and complex topography (Shepard and Dill, 1966; Lastras et al., 2007; Harris and Whiteway, 2011) that support the channelling and downward transport of particles (Allen and Durrieu de Madron, 2009; Puig et al., 2014; Porter et al., 2016), and that influence current patterns (Xu, 2011) and provide a heterogeneous set of habitats to deep-sea fauna, from rocky walls and outcrops to soft sediments (De Leo et al., 2014). These topographic features also serve the marine ecosystem by enhancing biodiversity and biomass (Leduc et al., 2014; Fernandez-Arcaya et al., 2017), and play an important role in carbon storage (Masson et al., 2010). They also constitute fundamental spawning and nursery areas for vulnerable marine ecosystems such as cold-water corals, sponge fields, and many commercially valuable species, and canyon flanks very often support bottom trawling grounds (Farrugio, 2012; Fernandez-Arcaya et al., 2017). However, these biodiversity hotspots also serve as conduits of marine litter and pollutants from the coast to the deep ocean (Palanques et al., 2008; Mordecai et al., 2011; Pham et al., 2014; Tubau et al., 2015; van den Beld et al., 2017) and are vulnerable to anthropogenic pressures such as fishing, bottom trawling, and hydrocarbon exploitation (Puig et al., 2014).

Erosion and sediment remobilization induced by sediment-laden gravity flows (e.g., turbidity currents), which travel from the head and flanks of the canyon towards the deep oceanic basins, are the main factors in the generation and formation of submarine canyons. Temporary sediments that deposit near the canyon head and on the shelf-edge areas may become unstable due to a number of factors (e.g., oversteepening, earthquake-triggered deformation, sediment liquefaction, and dense-shelf water cascading events), and propitiate the transport of sediments down-canyon (Puig et al., 2014). Other factors, such as hyperpycnal flows (i.e., water and sediment plumes denser than the seawater), also generate erosion at the canyon head (Canals et al., 2006; Palanques et al., 2006b; Puig et al., 2014), transporting large sediment volumes along

the entire canyon (Canals et al., 2006; Company et al., 2012). In spite of their relevance and widespread distribution, the genesis and evolution of submarine canyons continues under debate (Bertoni and Cartwright, 2005). Firstly, there is a great complexity and diversity of submarine canyon topographies from different continental margins (Harris and Whiteway, 2011), and secondly, it is difficult to observe contemporary sediment transport and canyon formation processes directly on site (Puig et al., 2014).

However, there is evidence that, in the present high sea-level stand, many submarine canyons incising in the world's continental margins channel and/or accumulate substantial amounts of sediments (e.g., Puig and Palanques., 1998a). So that, some submarine canyons can act as passive depocenters for the particles entering them, while others are able to convey the particulate matter further deeper, acting as preferential conduit for the transference of water and sediments between shelf environments and adjacent basins (Allen and Durrieu de Madron, 2009; Puig et al., 2014; Porter et al., 2016).

Many studies have also highlighted the important modifications that along-canyon currents experiment when they encounter a submarine canyon (Puig et al., 2000; Petrenko, 2003). By intercepting the path of these currents, submarine canyons induce a new dynamic balance, eventually enhancing non-geostrophic motions and shelf-slope exchanges (Huthnance, 1995). The modifications of these currents may result in local upwelling (Hickey, 1997; Sobarzo et al., 2001), which pumps nutrients to the euphotic zone and thus stimulates primary production (Ryan et al., 2005).

Submarine canyons are also both effective conduits for funnelling open-ocean internal wave energy onto the inner shelf, and sites of generation of internal waves through topographic scattering of surface tides (Kunze et al., 2002). Due to the reflection behaviour of internal waves off sloping bottoms, submarine canyon geometries should deflect low-frequency waves towards the deep ocean while trapping and focusing internal waves with higher frequencies towards the head of canyons (Kunze et al., 2002). Critical reflection of internal waves amplifies internal wave energy, which can drive to elevated turbulence and mixing of surface sediments. The resuspended particles can be advected along isopycnals as intermediate nepheloid layers, settling out in deeper waters, and/or can eventually leave the canyon confinement and contribute to the sediment transport along the margin (Gardner, 1989). Periodic internal-wave resuspension has been observed in numerous submarine canyons, including Monterey (Xu et al., 2002), Guadiaro (Puig et al., 2004b), Nazaré (de Stigter et al., 2007), Gaoping (Liu et al., 2010), Lisbon and Setubal (de Stigter et al., 2011), and Halibut (Puig et al., 2013) canyons. In other submarine canyons (Puig and Palanques, 1998a; Durrieu de Madron et al., 1999), internal-wave resuspension has been inferred typically in association with the development of enhanced nepheloid layers, which contribute to focusing deposition at specific canyon regions.

1.4. Nepheloid layers as lateral transporters of sediments

Nepheloid layers are cloudy layers within the water column with high concentrations of suspended particulate matter (SPM) compared with the surrounding clear waters (McCave, 1986; Amin and Huthnance, 1999). They are considered as the diluted product of sediment transport processes and are significant contributors to the shelf-slope exchanges of material (Fig. 1.5), serving as a link between pelagic and abyssal environments (Puig et al., 2001; Gardner et al., 2018). They are formed by a balance of settling and resuspension processes and are considered as important lateral transporters of sediments and organic matter (Amin and Huthnance, 1999).

The amount of suspended particulate matter (organic and inorganic) transported in nepheloid layers is influenced by physical and biological processes, spring blooms (Lampitt et al., 1995; Kitazato et al., 2000), hydrodynamic processes, physical gradients (Gardner et al., 1990; Gardner and Walsh, 1990), short-term events (e.g., internal waves, river floods, storms, or anthropogenic activities), and microbial and benthic activity in the water column (Thomsen et al., 2001). However, particles transported in nepheloid layers also undergo repeated sedimentation, resuspension loops, and aggregation and disaggregation processes (Thomsen and van Weering, 1998).

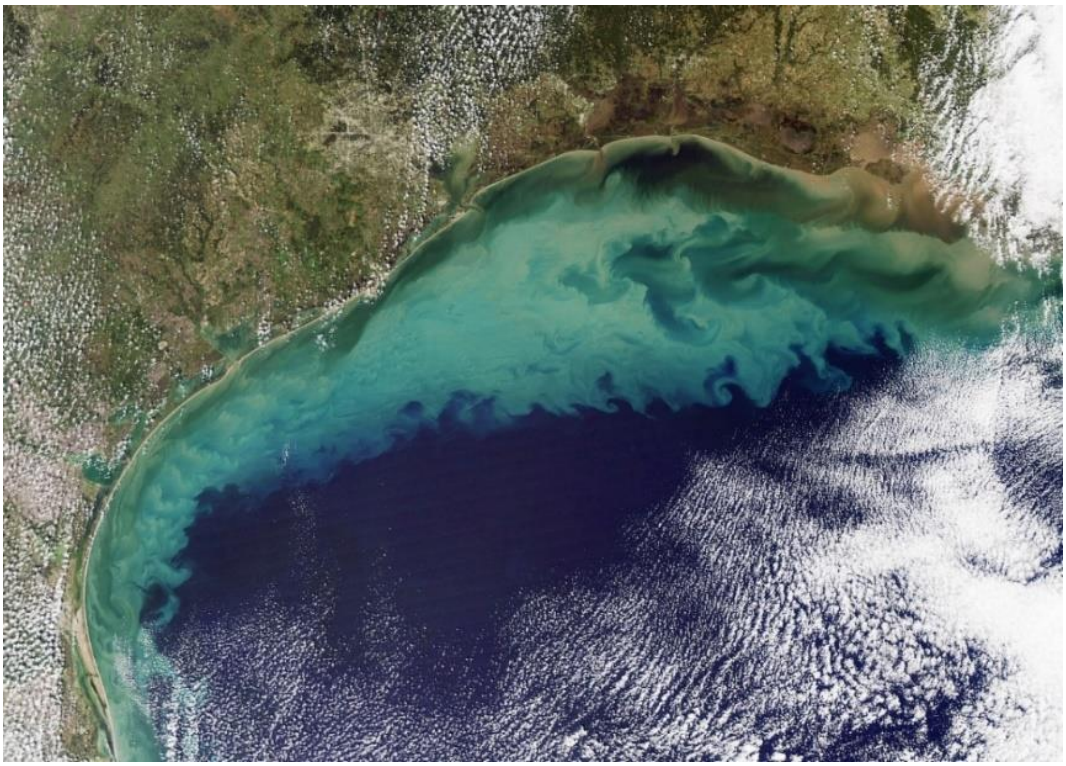

Figure 1.5. Satellite image of a strong nepheloid layer in the Gulf of Mexico. The resuspended sediment from the seafloor can be observed in the brownish and dark green waters. The ocean turbulence which likely brought the sediment to the surface is readily evident in the textured waves and eddies within the brownish and green waters. A second source of sediment is visible along the shore, where many rivers discharge sediments into the ocean, creating visible sediment plumes. The river plumes are dark brown that fade to light brown and green as the sediment is dispersed. Nutrients supplied by rivers also fuel the growth of phytoplankton, which create blooms that colour the ocean blue and green. **Source:** NASA Earth Observatory, 2009.

1.4.1. History and general description

First reports on nepheloid layers date back in the 1950s, when Jerlov (1953) reported the discovery of cloudy (turbid) layers near the seafloor using optical measurements. This author summarized that these layers might be generated by earthquakes (later seen to generate submarine slides and turbidity currents), volcanic eruptions, or seafloor erosion by strong currents. Later, Ewing and Thorndike (1965) called these turbid bottom waters "nepheloid layers" (from the Greek word *nephos*, meaning cloud) and stated that a nepheloid layer is a permanent and widespread feature, not a transitory response to an energetic phenomenon (such as a storm or an earthquake) nor restricted to the vicinity of a submarine canyon.

The first indirect data on the distribution of oceanic SPM were obtained from optical parameters or direct filtration measurements (e.g., Ewing and Thorndike, 1965; Biscaye and Eittreim, 1974). However, data from optical devices suffered the limitation that they were in units of light scattering or light attenuation, which were not directly useful for geochemistry or geological studies. Subsequently, Biscaye and Eittreim (1977) converted nephelometer data from the Atlantic Ocean into SPM concentrations. In this way, these authors were able to identify a number of distinct vertical and horizontal features in the distribution of SPM in the water. They proposed a three-layer model in which they identified three main features: (1) a surface-water turbid layer, (2) a clear water minimum, and (3) a deep-water turbid layer (Fig. 1.6).

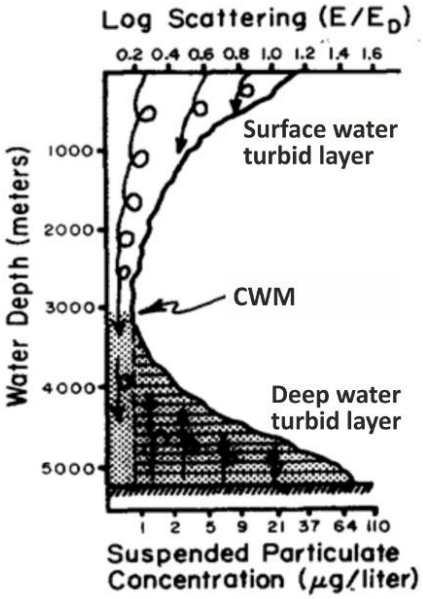

Figure 1.6. Three-layer model of SPM in the Atlantic Ocean proposed by Biscaye and Eittreim (1977). The minimum in light scattering is identified as the "clear water minimum" layer and is found at the upper limit of the nepheloid layer. This model assumes that all particles above the clear water minimum fall through the water column and feed the nepheloid layer. Also, the model assumes that particles mixed upward from abyssal depths also feed the nepheloid layer. **Source:** Adapted from Biscaye and Eittreim, 1977.

Definitions of the nepheloid layers in the 1980s and the 1990s were more quantitative and focused on the generation mechanisms. Dickson and McCave (1986) described nepheloid layers as distinct layers in the water column with reduced optical transmittance, increased light scattering and surrounding clear water. Afterwards, Naudin and Cauwet (1997) defined nepheloid layers as a vertical concentration gradient between the settling particles from the surface and the turbulent mixing velocity from seafloor.

In general, three types of nepheloid layers have been described: (1) surface nepheloid layers (SNLs), (2) benthic (or bottom) nepheloid layers (BNLs), and (3) intermediate nepheloid layers (INLs) (Fig. 1.7). SNLs tend to be found in areas of increased primary productivity, as well as close to terrestrial and riverine sources, and are a typical feature in continental shelf areas (Oliveira et al., 2002). These features are generally associated with the biologically active layer, and normally contain the highest particulate matter concentrations in the water column (e.g., Gardner et al., 1993; Oliveira et al., 2002; Lorenzoni et al., 2009). Some studies have also described sediment in these layers transported from the BNL by upwelling events (Agrawal, 2004), while others describe the possibility of INLs being transported to the surface and fuelling phytoplankton blooms under favourable conditions forming a SNL (Shatova and Branch, 2008). BNLs are found in the lower water column and are normally associated with elevated SPM near the seabed relative to surrounding waters. Driven by local hydrodynamics and energetic flows, BNLs are commonly found along slopes (McCave, 1986). Lateral transport of material from intense regions in BNLs, due to the interaction of processes that increase mixing, can result in the formation of INLs (van Weering et al., 2002). Moreover, INLs can also result from the accumulation of particles and/or detachments from BNLs along isopycnal surfaces in association with strong density gradients in the water column, particularly internal waves (Cacchione and Drake, 1986; Dickson and McCave, 1986). They are often detected near ocean boundaries (topographic and water masses) and are frequently observed in high abundance near continental shelves, offshore on the upper slope and at the depth off the shelf-break at different ocean margins (Puig and Palanques, 1998a; McCave and Hall, 2002; McPhee-Shaw et al., 2004). INLs have also been described as sub-layers within the BNL that originate in regions of strong currents, gaining material by fall-off from above (McCave, 1986). In flatter (non-sloping) environments (between 1000 and 3000 m), and away from the sides of the ocean boundaries, nepheloid layer formation is at its minimum, where a lack of primary productivity, weak stratification and strong currents limit their formation (McCave, 1986).

In the open ocean, the distribution of particulate matter in the water column present distinct turbid layers. The SNL at the photic zone is primarily associated to planktonic organisms and is highly time dependent in its thickness and intensity (Durrieu de Madron et al., 2017). Underneath this SNL, particulate matter concentrations present a decreasing gradient until reaching minimum values at intermediate depths (Biscaye and Eittreim, 1977). Below the clear water minimum (CWM), an increase of particle concentration towards the bottom has been observed in various regions of the ocean (Durrieu de Madron et al., 2017 and references there-in). These BNLs, which present concentrations that are in excess of the CWM concentrations, have been

found in areas affected by strong western boundary currents (Eittreim et al., 1976; McCave and Carter, 1997) and in regions of high bottom currents (McCave, 1986). This suggest that BNLs are generated by resuspension of the bottom sediments at the bottom boundary layer and the presence of local resuspended particles in the ocean basins at the (McCave, 1986). Other studies have also shown the broad patterns of inflowing cold bottom water in the southern Indian and Atlantic oceans are very similar to the extent of the BNL coverage, suggesting the contribution of particles coming from the Antarctic Bottom Water (AABW) (Eittreim et al., 1976; Biscaye and Eittreim, 1977).

Nepheloid layers significantly vary spatially and temporally (they can be permanent or transitory) and their intensity and thickness depend on local conditions (McPhee-Shaw et al., 2004; Inthorn et al., 2006). The shape of nepheloid layers often follows the local water column density structure, as their development is closely linked to the water column stratification and density field (Oliveira et al., 2002). The thickness of nepheloid layers varies from a few meters to frequently several tens or hundreds of meters. Thicknesses of BNLs have been reported by many authors, such as 50-200 m in the Nova Scotian continental rise (McCave, 1983) or 500-1500 m in the western Mediterranean basin (Puig et al., 2013). Greater thicknesses have been reported in trenches and passages where they can be up to 2600 m thick (McCave, 1986). In contrast, INLs are smaller, displaying thickness of ~10-50 m (Oliveira et al., 2002).

Many studies in SPM pattern dispersal have noted the presence of nepheloid layers at continental margins worldwide (Gardner et al., 2018), including the abyssal Atlantic Ocean (Biscaye and Eittreim, 1977), upwelling areas off California (Cacchione et al., 1999) and off Namibia (Inthorn et al., 2006), open continental shelves (Puig et al., 2001; McCave and Hall, 2002; Lorenzoni et al., 2019), marginal seas (Chronis et al., 2000), as well as associated with the presence of submarine canyons, for example in the NW Mediterranean (Puig and Palanques, 1998a), the Portuguese margin (Oliveira et al., 2002; Quaresma et al., 2007), the NE Atlantic (Wilson et al,. 2015a; Hall et al., 2017), and the US margin (Carson et al., 1986; Gardner, 1989).

Concentrations of SPM in nepheloid layers greatly vary amongst different locations. For instance, McCave et al. (2001) reported concentrations of 0.05-0.13 $mg \cdot L^{-1}$ off the NW Atlantic, while in the NE Mediterranean Chronis et al. (2000) reported higher concentrations of 0.2-1.5 $mg \cdot L^{-1}$. Greater concentrations in nepheloid layers are often found closer to coastal areas, in estuaries and other terrestrially influenced environments. For example, in the northern Portuguese shelf, an area that is highly influence by the Douro River, Oliveira et al. (2002) reported nepheloid layers with concentrations of 0.1-19 $mg \cdot L^{-1}$. Concentrations of SPM also depend on the local dynamics and the source of particles. Optical measurements have shown very low contrasting values in the water column deeper than about 100-200 m (5-12 $\mu g \cdot L^{-1}$), with increasing particle concentration near the seafloor (0.1-1 $mg \cdot L^{-1}$) (Hill et al., 2011; Gardner et al., 2018). Distance above the bottom will also affect SPM concentrations in the BNLs, which generally display a uniform concentration with decaying intensity from the seabed (McCave, 1986). The SPM concentration in INLs depend

on the rate of settling and aggregation, as well as on the maintenance of turbulence and shear velocity from the source in the BNL (McCave, 1986).

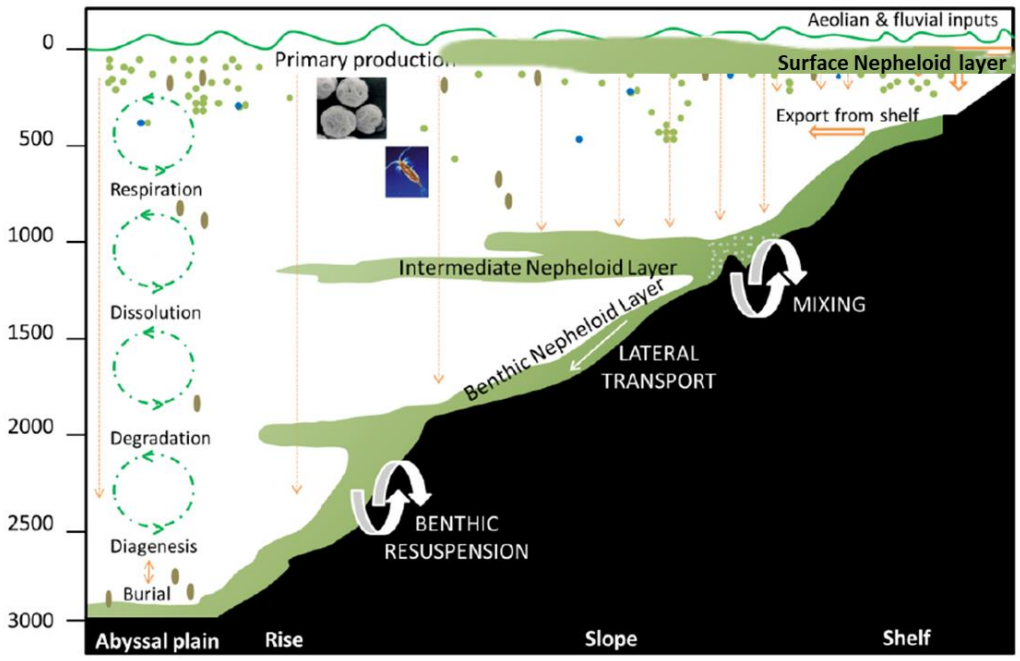

Figure 1.7. Schematic of the three types of nepheloid layers described in the literature (i.e., surface nepheloid layers, intermediate nepheloid layers, and benthic (or bottom) nepheloid layers) as lateral transporters of sediment particles along a sloping continental margin. Sources of material, transport and degradation are also shown. **Source:** Adapted from Inthorn, 2005 and Wilson, 2016.

1.4.2. Generation and formation mechanisms

The distribution of nepheloid layers often indicates an active area of resuspension, dispersal, and deposition of SPM. Hence, the primary source of particles will vary according to the geographic location, the depth in the water column and the local processes dictating the formation mechanisms of nepheloid layers (Fig. 1.8). For this reason, nepheloid layer formation cannot be easily explained by any single source and/or mechanism (McCave et al., 2001). In this section, the different mechanisms that promote nepheloid layer formation will be discussed. The generation mechanisms of nepheloid layers in the study areas covered in this Thesis will be addressed in **Chapters 4, 5** and **6**.

1.4.2.1. Natural processes

Sinking of marine snow

SNLs and shallow INLs are highly influenced by flocculation and flotation of particles derived from phytoplankton activity and primary productivity, as well as by particles introduced by

atmospheric dust and river input. Sinking velocities of algae, diatoms and coccolithophorids are generally negligible because organic matter has lower density than water. However, ballasting by lithogenic material increase particle densities to be high enough to sink through the water column (Iversen and Ploug, 2010). Marine snow constitutes a high proportion of this settling material as it has high sinking velocities, contributing to the coupling between the ocean surface and the deep-sea. To date, only a few studies contain data of these aggregates in nepheloid layers (Ransom et al., 1997; Diercks et al., 2019).

Deep energetic flows (bottom currents, eddies, and benthic storms)

Although vertical sinking plays an important role in the delivery of fresh material to the seafloor, the input of resuspended material directly related to annual variability in near-bed current regimes diminishes seasonal settling signals in the maximum flux and bulk composition of material near the seabed (Mienis et al., 2009). Resuspended sediment particles represent the largest component of nepheloid layers (Gardner et al., 2018), particularly in bottom nepheloid layers (BNLs). This suggests that the distribution of BNLs is a good proxy for the presence of local resuspension processes in the ocean basins.

In physical oceanography, deep-sea bottom currents are generally defined as the flow of water masses in the cold-water sphere beneath the base of the thermocline (Zenk, 2008). There are three different bottom currents types that operate in deep-water settings, including wind-driven bottom currents, thermohaline bottom currents, and tidal bottom currents (Shanmugan, 2008; Rebesco et al., 2014; Esentia et al., 2018). All types can be barotropic and baroclinic, and their velocity at the seafloor is correlated with the strength of their density gradients (Fig. 1.8). Normally, they flow parallel to depth contours in geostrophic equilibrium. However, when they encounter topographic features, such as seamounts or submarine canyons, the disrupted flow can have much higher velocities (Allen and Durrieu de Madron, 2009). These currents can transport sediments often through detached nepheloid layers (Rebesco et al., 2014). Bottom currents can also predispose the water column to locally overturn and generate eddies, which are now considered as a significant mechanism for long-distance transport of particles and the formation of nepheloid layers (Rebesco et al., 2014).

Closely linked to these mechanisms, benthic storms have also been related to nepheloid layer formation, and sediment transport and distribution, as it has been demonstrated in the Nova Scotia continental rise by the HEBBLE project (Hollister and Nowell, 1991). These storms are characterised by the periodic intensification of normal bottom current flow along-slope or following the isobaths (Fig. 1.8), where their mean flow velocity typically increases by two to five times (reaching ~20 $cm \cdot s^{-1}$), especially close to boundaries of strong surface currents (Rebesco et al., 2014). The water turbidity created by these benthic storms can last from a few days to a few weeks (Hollister and McCave, 1984).

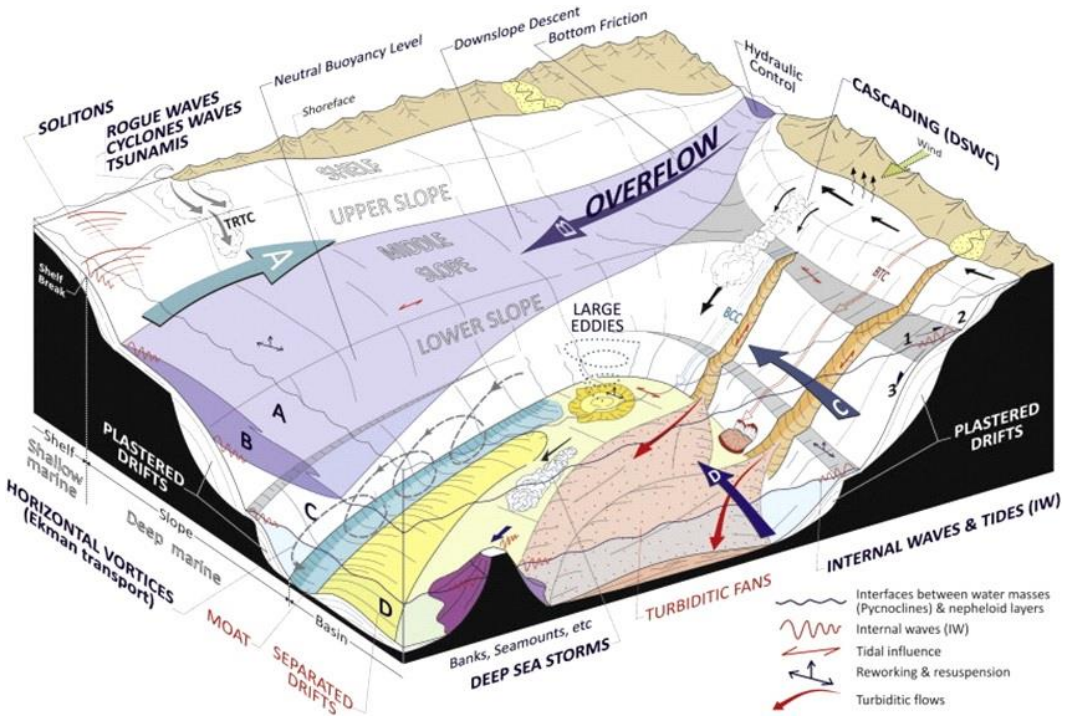

Figure 1.8. 3D sketch depicting the possible oceanographic processes in deep-sea environments that can influence the formation of nepheloid layers. The velocity at the seafloor can be affected by density currents and overflows, as well as by barotropic currents and by intermittent processes such as water cascading, eddies, deep-sea storms, internal waves, and tsunamis. **Source:** Modified from Rebesco et al., 2014.

Fluvial plumes

Much of the material entering the sea from the continent does so in the form of coastal fluvial plumes (Pratson et al., 2007) (Fig. 1.8). These plumes are usually hypopycnal (i.e., they present lower density than seawater) and spread forming a surface nepheloid layers (SNL) (Biscaye and Eittreim, 1977). This SNL can sink to the seafloor and gradually deposit the less dense portion of sediment load through flocculation processes. When these plumes are hyperpycnal (i.e., they are denser than the seawater), they propagate along the seafloor in the form of a turbulent gravity flow, following the direction of the maximum slope, and contributing to the formation of BNLs (Parsons et al., 2001).

Meteorological and oceanographic events

High-kinetic energy in the surface of the ocean can propagate downwards, causing intermittently very high speeds that can generate very high suspended sediment concentrations (SSC) in the deep sea and enhance BNLs (McCave., 1986). Storms affecting the continental shelves worldwide are considered as a major driver of off-shelf dispersal of sediments to the deep ocean, mainly through submarine canyons. In Nazaré Canyon (W Iberian margin), storm-induced currents, reaching up 0.8-1 $m \cdot s^{-1}$, have been interpreted as the means of generating INLs and BNLs (Oliveira et al., 2007; De Stigter et al., 2007; Martín et al., 2011; Masson et al., 2011). Similarly, monitoring in Quinault Canyon (off Olympic Peninsula, American NE Pacific) showed that sediment

resuspended on the shelf during storms was advected over the canyon, forming shelf-break INL detachments (Carson et al., 1986; Hickey et al., 1986) that increased particles fluxes in the upper canyon (Baker and Hickey, 1986). In the Eel submarine canyon, Puig et al. (2004a) observed strong sediment transport induced by storms into the canyon head. In the NW Mediterranean, Palanques et al. (2006b and 2008) and Ulses et al. (2008b) reported the effects of eastern storms causing downwelling and strong suspended sediment fluxes downcanyon in the Cap de Creus Canyon. Sánchez-Vidal et al. (2012) also reported the effects of a winter storm that caused strong downwelling and transported large amounts of resuspended shelf material deeper into the Cap de Creus and Blanes canyons.

The formation of nepheloid layers has also been associated with upwelling and downwelling. For instance, in the Portuguese continental shelf, Oliveira et al. (2002) observed intense BNLs under dominant downwelling conditions, where particles are transported from the nearby river or remobilised at the mid-shelf. They also reported the dispersion of particles and SNL formation with changes in the predominant circulation to upwelling combined to seasonal water stratification.

Another meteorologically driven phenomenon is dense shelf water cascading (DSWC), in which dense shelf water (DSW) is formed by cooling, evaporation or freezing of surface waters over continental shelves (Fig. 1.8). Influenced by Earth's rotation and gravity, these DSWs can propagate along-slope by the formation of spiral waves, meanders, and eddies (Shapiro et al., 2003), or move across-slope, cascading mainly through submarine canyons until they reach their neutral buoyancy (Millot, 1990; Durrieu de Madron et al., 2005a). The descent of these waters down the continental slope can create resuspension and high sediment fluxes and contribute to the formation of nepheloid layers (Fohrmann et al., 1998; Puig et al., 2013).

The Gulf of Lions (NW Mediterranean) is one of the main regions of the world where DSW are generated by cooling and evaporation, and dry winds during winter (Millot, 1990; Durrieu de Madron et al., 2005a, 2008; Canals et al., 2009). The preferential along-slope circulation towards the west, the narrowing shelf and constraining topography of the Cap de Creus promontory force most of the off-shelf DSWC events and sediment transport, which occur mainly through Lacaze-Duthiers and Cap de Creus submarine canyons, where velocities up to 80 $cm \cdot s^{-1}$ have been recorded related to DSWC events (Palanques et al., 2006b; Canals et al., 2006). Béthoux et al. (2002) first suggested the formation of a BNL attributed to a DSWC event that transported turbid shelf waters and resuspended sediment in the Gulf of Lions. Further studies showed that the BNL formed in this area is generated by the mixture of DSW formed by deep DSWC and by deep convection in the open ocean (Puig et al., 2013), transporting great amounts of material from the coastal region to the basin.

Bottom-reaching open ocean convection in the Gulf of Lions (NW Mediterranean) has been recently viewed as an effective mechanism to resuspend deep sediment, and form and feed thick BNLs (Durrieu de Madron et al., 2017; Palanques and Puig, 2018). When it consistently coincides with deep DSWC events, it is believed to add up to the impact of deep DSWC, supplying an extra

amount of fine sediments from the shelf and the slope. The synergy between the impact of both mechanisms is very important for the formation of large BNLs in the NW Mediterranean basin, but bottom-reaching open-ocean convection is able to feed and maintain BNLs in the absence of DSWC events (Durrieu de Madron et al., 2017).

Internal waves and tides

Internal waves and tides are energetic, ubiquitous, and persistent oceanographic phenomena (Fig. 1.8). The interaction of internal waves with the seafloor has been described as the main mechanism responsible for generating and maintaining high near-bottom SSC (Cacchione and Drake, 1986; Palanques and Biscaye, 1992; Puig et al., 2001, 2004a, b; McPhee-Shaw, 2006).

The concept of barotropic and baroclinic is of paramount importance in understanding currents associated with internal waves and internal tides (Shanmugan, 2014). Barotropic currents are driven by the slope of the water surface, while baroclinic currents are driven by the variations in the density of the ocean water caused by changes in temperature and salinity. Consequently, baroclinic currents are commonly associated with internal waves and internal tides that propagate along boundaries of density stratifications in the deep ocean. They can occur in mid-ocean depths and along the ocean seafloor of continental slopes and submarine canyons. The type of reflection that occurs is determined by the topographic slope (α) and the angle of internal wave energy propagation (β) which is expressed by:

$$\tan(\beta) = \left(\frac{\sigma^2 - f^2}{N^2 - \sigma^2}\right)^{1/2} \quad (equation\ 1.1)$$

The type of reflection is dependent on the Brunt-Vaisala (or buoyant) frequency (N), the internal wave frequency (σ) and the Coriolis parameter (f) (Thorpe, 2005). N is usually calculated from the vertical oceanic density gradient according to:

$$N = \left[\left(\frac{g}{p}\right)\left(\frac{\partial p}{\partial z}\right)\right]^{\frac{1}{2}} \quad (equation\ 1.2)$$

where p is the density and g is the gravitational acceleration. Typical values of N in the ocean at continental slope depths between 200 and 2000 m depth are 1 < N < 4 cycles per hour (cph).

There exist three possible scenarios (Fig. 1.9):

I. ***Subcritical reflection (transmissive conditions).*** Where the angle of propagation (β) is greater than the slope of the seafloor ($\alpha/\beta < 1$), the wave is reflected and the offshore waves and energy propagate upslope, bouncing between the mixed layer and the seafloor (Fig. 1.9A).

II. ***Supercritical reflection (reflective conditions).*** Where the angle of propagation is smaller than the slope of the seafloor ($\alpha/\beta > 1$), energy rebounds off the slope and travels

towards the seabed and back into deeper water until it is reflected (Fig. 1.9B). This scenario is the most common in submarine canyons where internal waves above canyon rims are focused on the canyon floor, and steep vertical walls focus energy on the seafloor (Cacchione et al., 2002).

III. ***Reflection (Critical conditions).*** Where the angles of propagation and the slope of the seafloor are equal ($\alpha/\beta \cong 1$), near-critical reflection occurs (Fig. 1.9C). Energy is trapped against the boundary and potentially results in non-linear effects such as solitons, internal bores, and turbulent mixing (Nash et al., 2004).

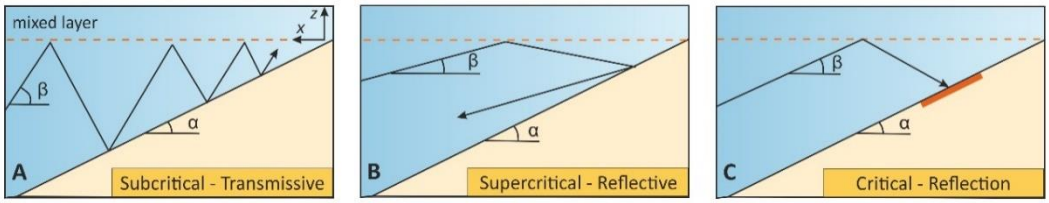

Figure 1.9. Reflection of internal wave characteristics (black line) from bottom slope (α) for A) transmissive conditions and B) reflective conditions. Energy is trapped along the bottom, and bottom velocities are intensified in C) (critical conditions). The red bar indicates velocity intensification. Bottom velocities can also increase upslope as shown in A). **Source:** Based on Cacchione et al., 2002.

In deep-sea environments, the energy associated with internal waves has been hypothesized as the main mechanism of formation and maintenance of INLs and BNLs in continental slopes and submarine canyons (McCave, 1986; Cacchione and Drake, 1986; Dickson and McCave, 1986; Cacchione et al., 2002; Puig et al., 2004a, b; McPhee-Shaw, 2006). Cacchione and Drake (1986) first suggested that high velocities caused by shoaling/breaking internal waves could explain the generation and maintenance of near-BNLs and turbid detachments at the shelf and slope off California. Similarly, McCave et al. (2001) reported intermittent INLs associated with periodic internal wave driven resuspension in the European margin.

Internal waves can be formed by the perturbation of isopycnal surfaces (density fronts) (Dickson and McCave, 1986) and, therefore, oscillate along the interface between two water masses of different densities (Cacchione et al., 2002). As early as 1989, INLs were reported moving seaward along isopycnal surfaces after internal waves and tides had caused periodic sediment resuspension (Gardner, 1989). In shelf-slope environments, resuspended material from the shelf can be advected down the slope and be retained along the density front, which is formed between low-salinity shelf waters and saline offshore waters (Puig et al., 2001). Thus, density fronts provide a path for the nepheloid layers to detach, and INLs are commonly observed in shelf-slope environments (Puig and Palanques, 1998a).

Similarly, the inflow of different water masses can cause INL detachments. For instance, in the Cretan Sea, Chronis et al. (2000) found a clear stratification between Modified Atlantic Water (MAW) and the denser Cretan Intermediate Water (CIW).

1.4.2.2. Bottom trawling

Bottom trawling consists of dragging a large net along the seafloor that is held open by two heavy doors (i.e., otter trawl boards, *OTB*) (Fig. 1.10). This fishing technique is by far the most extensive anthropogenic activity and physical disturbance in the marine environment (Eigaard et al., 2016), but also makes an important contribution to the global food supply, accounting for 23 million tons of annual catches (i.e., combined weight of reported landings, unreported and unregulated fishing, and estimated discards and landings from illegal fishing; Watson and Tidd, 2018). Hence, bottom trawling accounts approximately for 22 % of the total global fish catches (Kelleher, 2005) and up to 80 % of the high-seas benthic fish catches (Gianni, 2004). Given its importance in supplying food for a growing population, it is key to understand the impacts of this type of fishing technique. Bottom trawling increases the risk of overexploitation of many commercial species, but also increases the vulnerability of marine populations by altering food webs (Dayton et al., 1995; Jackson et al., 2001). These changes can lead to changes in community production, trophic structure, and function (e.g., Hiddink et al., 2006).

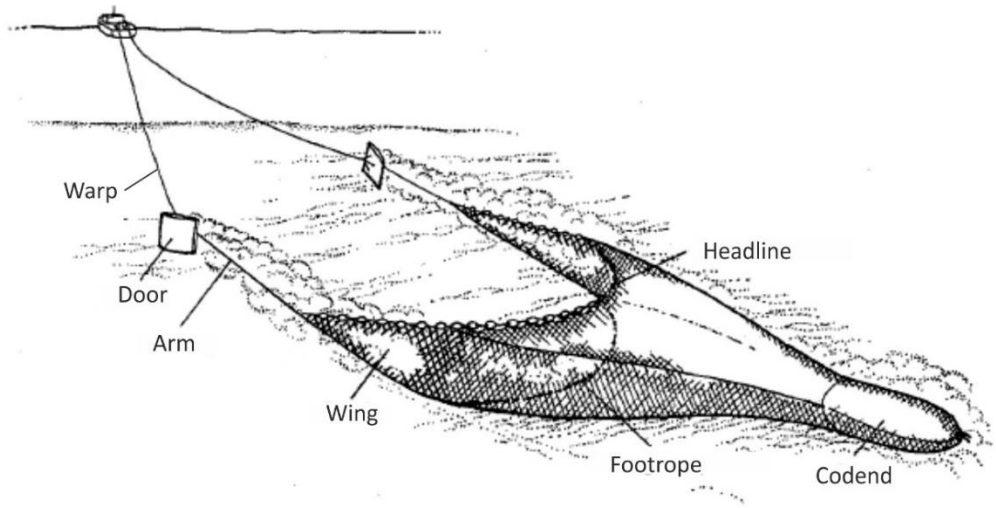

Figure 1.10. Schematic diagram of a typical bottom trawler. **Source:** Modified from Palanques et al., 2001.

Bottom trawling has global impacts on benthic communities and their habitats and is relatively non-selective (Bergman and van Santbrink, 2000). This anthropogenic disturbance can lead to reduced benthic production (e.g., Jennings et al., 2001), reduced biodiversity and habitat homogenization (e.g., Dayton et al., 1995), and changes in community composition (Hinz et al., 2009). The greatest damage occurs when animals come into contact with the hard parts of the

trawling gear. Particularly, larger body-sized organisms, such as corals or sponges, have lower natural mortalities, slower growth and lower annual reproductive output, increased longevity, and lower natural rates of intrinsic increase (Pitcher et al., 2000; Clark et al., 2016; Pitcher et al., 2016). Therefore, species with large-body sizes are less able to compensate for high mortality rates inflicted by bottom trawling than smaller-sized species that have faster life cycles and higher reproductive output (Tillin et al., 2006). Since large-body size species are often ecological engineering species, this affects their role in nutrient turnover, and the provision of highly structured habitats with host a highly rich associated fauna (Mortensen and Buhl-Mortensen, 2004). As a result, benthic communities in trawled areas are dominated by smaller species, such as deposit feeders, burrowers, and scavengers, which have higher productivity rates per unit biomass (Jennings et al., 2001; Kaiser et al., 2002).

Another noticeable effect of bottom trawling is the physical impact on the seabed, which includes the scraping and ploughing of the seafloor due to the drag of the heavy trawl doors (Fig. 1.10) (Puig et al., 2012), which can create long-lasting trawling marks consisting in deep furrows and sediment mounds (Fig. 1.11) (Smith et al., 2003; He and Winger, 2010; Eigaard et al., 2016; O'Neill and Ivanović, 2016; Buhl-Mortensen and Buhl-Mortensen, 2018).

The degree of alteration on the seafloor depends on the frequency of disturbance, sediment type, and natural hydrodynamic disturbances. Trawling in fine-grained sediments tend to form deeper trenches, and the cohesive nature of this sediments makes these impacts to last longer than in coarse-grained sedimentary environments. In a similar way, areas with weak hydrodynamic activity, usually associated to muddy environments, tend to have longer-lasting trawling-induced impacts than sandier seafloors, which are usually linked to areas that experiment high hydrodynamic activity (for example, frequent and stronger currents caused by waves and tides) (Palanques et al., 2001; Sciberras et al., 2013). Trawling impacts can vary according to the type of substrate (muddy or rocky) and the environment where these activities are practiced. Despite that sediment resuspension occurs in both sandy and muddy environments, its impact is much greater in fine-grained seafloors due to the digging action of the trawling doors and the hydrodynamic turbulence they generate (O'Neill and Summerbell, 2011; Mengual et al., 2016) (Fig. 1.11). However, the repeated towing of the net and trawl doors result in the suspension of sediments into the water column, increasing near-bottom turbidity (Fig. 1.11) (Pilskaln et al., 1998; Bradshaw et al., 2012; Palanques et al., 2014; Dellapenna et al., 2006; O'Neill and Summerbell, 2011), contributing to the formation of INLs and BNLs (Churchill, 1989; Churchill et al., 1994; Palanques et al., 2001; 2014; Dellapenna et al., 2006; Martín et al., 2014a) and sediment gravity flows that are subjected to transport away from bottom trawling grounds by local currents, waves and tides (Palanques et al., 2006a; Martín et al., 2014a), which also lead to a substantial along- and across-shelf transport of sediments and leaving behind eroded trawling grounds (Oberle et al., 2016a, 2016b; Mengual et al., 2019).

Trawling-induced resuspension also reduces the organic carbon of the surface layer (Pusceddu et al., 2014) and contributes to the advection of nutrients (Dounas et al., 2007) and contaminants

(Bradshaw et al., 2012). The nepheloid layer characteristics (i.e., lateral and horizontal extensions, SSCs, and duration) depend on multiple factors such as seabed composition (fine-particle content), trawl door type and traction speed, and local hydrodynamic forcing (Linnane et al., 2000; O'Neill and Summerbell, 2011). The heigh of the trawl-induced nepheloid layer usually reaches 2-3 times the net vertical opening and the lateral spreading ranges from a few tens to several hundred of meters depending on the distance from the source (Durrieu de Madron et al., 2005b). Nevertheless, the contact of the bottom trawling gear with the seafloor does not always cause erosion if sediment is not resuspended (Simpson and Watling, 2006). The bottom trawling gear can overturn the sediment and destroy the sedimentary structure (Watling and Norse, 1998).

Figure 1.11. Physical disturbances of bottom trawling on the seabed, which include the scraping and ploughing of the seafloor due to the drag of the trawl doors, and the resuspension of sediments into the water column. A) is an example of trawl marks observed on soft bottoms, while B) shows trawl marks on mixed bottoms. C) shows the sediment resuspended by the dragging of the doors into the seafloor (lower oval) and the generation of turbulence (upper oval). **Source:** Buhl-Mortensen and Buhl-Mortensen, 2018; O'Neill and Ivanović, 2016.

Bottom trawling grounds have been expanding to new and deeper areas since the 1950s driven by the exhaustion of shallow-water fishing stocks, technological improvements, and subsidies that encouraged the exploitation of previously inaccessible deep-sea species and resources (Morato et al., 2006; Martín et al., 2014a). Whereas prior to the 1950s, trawling grounds were generally confined in shallow-water environments, they now tend to occur up to 800 m depth and can even extend to over 1500 m (Watson and Morato, 2013). Several commercial species aggregate near topographic features such as seamounts and submarine canyons. Bottom trawling in such deep-sea environments has a greater impact on sediment resuspension that in shallow-water environments (Martín et al., 2014a), which is partly due to lower natural hydrodynamic forces capable of resuspending sediment, lower sediment fluxes arriving to the seafloor, and the heavier trawling gear required to operate at such depths (Martín et al., 2014a).

In comparison to the various studies focusing on the ecological impacts of the ecological impacts of bottom trawling in the deep-sea (Thrush and Dayton, 2002; Gage et al., 2005; Clark et al., 2016), only few studies have addressed how the expansion of trawling activities to deeper areas have affected the sediment dynamics.

The first comprehensive observations on the impacts of deep bottom trawling on the generation of nepheloid layers came from the HERMIONE Project, conducted in the Palamós Canyon (NW Mediterranean) (Fig. 2.1). In the frame of this project, it was observed that bottom trawling activities not only smoothened the complex morphology of the canyon and modified natural sediment dynamics along with resuspension of large volumes of sediment (Puig et al.,2012), but also triggered sediment gravity flows into the canyon interior and enhanced the formation of persistent INLs and BNLs at the working depth range of the trawling fleets (Palanques et al., 2006a; Martín et al., 2014a, b). Furthermore, recent studies observed that the seafloor and sediment dynamics in the Whittard Canyon (NE Atlantic) were affected by bottom trawling activities. Enhanced deep-INLs found where observed at the canyon's interior when bottom trawlers were operating in the adjacent flanks, which were attributed to the sediment advection by this human activity (Wilson et al., 2015b).

1.4.3. Classical methods of measurement and detection

The methods used to measure and detect nepheloid layers and suspended particles vary depending on the site and the type of study (Gibbs, 1974).

The pioneer studies on nepheloid layers used optical instruments (e.g., Ewing and Thorndike, 1965; Biscaye and Eittreim, 1974), which are now considered to be the standard method of mapping and detecting nepheloid layer structures worldwide (e.g., Dickson and McCave, 1986; Puig and Palanques, 1998a; Liu et al., 2010; Karageorgis et al., 2012). All optical sensors operate on the same principle, which consists of measuring the loss of light from a light emitter as it propagates through the water column to a light detector (Fig. 1.12). This light loss can be attributed to scattering and absorption from particles, which are proportional to the temporal and spatial changes in the concentration of SPM (Bloesch, 1994). In the last decades, the backscattering technique has become very popular because of the simplicity of having the emitter and the detector together (Gibbs and Wolanski, 1992).

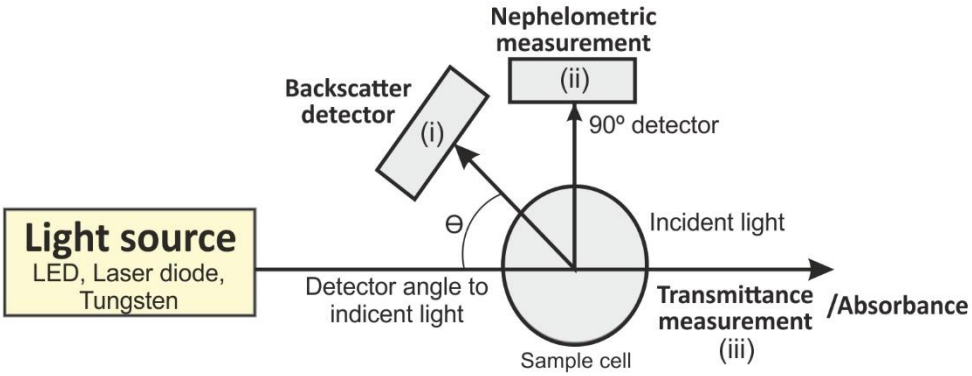

Figure 1.12. Diagram showing different set-ups of three turbidity instruments; (i) Optical backscatter sensor, (ii) nephelometer, (iii) transmissometer. **Source:** Based on Bin Omar and Bin MatJafri, 2009.

Generally, there are three main types of optical turbidity sensors, which are distinguished by the relative angular position between the light emitter and the light transmitter (Fig. 1.12):

- **Nephelometers.** There are two reference methods that mainly specify spectral and angular ranges of detected light: The US Environmental Protection Agency (EPA) Method 180.1 (USEPA, 1993) and the International Organization for Standardization (ISO) Method 7027 (ISO, 1999). Nephelometers using the EPA method measure turbidity values using Nephelometric Turbidity Units (NTU), whereas those using the ISO method report turbidity values in Formazin Turbidity Units (FTU). The two methods use main detection angles at ~90 º from the emitter to the light detector (Zheng and DiGiacomo, 2017), and were originally designed for regulatory purposes, i.e., assessing drinking water quality with turbidity values lower than 40 NTU or FTU, although they can measure to a high as 3000 NTU (Zheng and DiGiacomo, 2017).

- **Optical backscatter sensors (OBS).** OBS emit infrared light into the water column, which is reflected on contact with suspended particles. A series of light detectors positioned around the emitter detects the light reflectance (backscatter), and an empirical calibration is then used to convert sensor output voltage into SSC. They measure infrared radiation scattered by particles at an angle greater than 90º, which allows measuring turbidity values higher than 3000 FTU (Downing et al., 1981). However, the sensitivity of OBS changes with particle size by more than an order of magnitude, which can be problematic when developing calibrations (implying non-linear calibration relations). When OBS surpass their concentration limit, one can adjust the sensor gain. However, if the gain is too high, data can be lost because the sensor output is limited by the input voltage and will saturate prior to detecting sediment concentration peaks. On the contrary, if the gain is too low, the full resolution of the data logger will not be used (Curtis, 2007). Nevertheless, advantages of OBSs include wider measurement ranges, high tolerance to ranging particle sizes, and accuracy in high turbidity (Curtis, 2007).

- **Transmissometers.** Transmissometers measure the clarity of the water by measuring the fraction of light energy lost from a collimated light beam as it passes along a known pathlength (Thomson and Emery, 2014). Transmissometers use visible light, usually 650-660 nm, as they are used to determine the depth penetration of visible light through the water column. The light emitter and detector are positioned at 180º facing each other with a fixed pathlength typically ranging from 5 to 25 cm, which greatly reduces light detection by the receiver from other unwanted sources (Cochran et al., 2019). Output values for a system are provided as an attenuation coefficient that is defined by the acceptance angle of the receiver optics (0.5-1 º). Transmissometers are sensitive to low-range turbidity and are only practical in such environments.

In the past, nephelometers were the most common instruments to describe the distribution of particulate matter in the ocean (McCave, 1986). More recently, transmissometers have also been a popular choice. Modern transmissometers (e.g., WET Labs C-Star) have adopted the convention that the measure beam C is relative to the clean water calibration value, which is the beam attenuation coefficient for pure water at a given wavelength and temperature (WET Labs, 2011). However, a major disadvantage of these instruments is that some dissolved substances absorb light (e.g., organic matter), and can therefore be interpreted as increased turbidity (Gibbs, 1974).

Acoustic devices, such as ADCPS, are common instruments used to record current speed and direction, but also to record turbidity on the basis of backscattered acoustic signals from particles in the water column to visualize them (Fettweis et al., 2019). These acoustic sensors have been used to detect relative changes in water turbidity in different settings (e.g., Orr and Hess, 1978; Gruber et al., 2016). However, optical sensors have proven to be more sensitive in both high concentration environments and clear waters depending on the instrument used (Gibbs, 1974). Nowadays, optical sensors remain the most popular method for the measurement of suspended particles, providing high spatial resolution, and fast and accurate turbidity measurements.

Moreover, the quantification of turbidity so far remains complex, as the detected signal is not only dependent on the concentration of particles, but also on light and particle size, colour, concentration, and shape and surface roughness (Guillén et al., 2000; Downing, 2006; Fettweis et al., 2019). Also, the different optical instruments provide incomparable and different units (e.g., NTU, FTU, backscatter units, volts, etc), which vary on the light sources, detectors and angles of measurement for each instrument. To date, inter-comparisons of sensors have only been performed in onshore and near-shore settings, where very high particle loads are the main challenge. Open-ocean settings pose different challenges, and nearly no studies have been developed to properly quantify the output of different sensors in terms of SSC. For instance, Haallboom et al. (2021) have presented a comparative study in the Whittard Canyon (NE Atlantic) of turbidity data to assess the potential implications that different sensors have on estimating SSCs. These authors have mainly found that transmissometer data have a stronger response to material in the biologically surface layer due to higher absorption of the light signal by chlorophyll-bearing phytoplankton; OBSs and high-frequency ADCPs have corresponding backscatter records, whereas low-frequency ADCPs have remarkably different backscatter records due to different ranges in particle size sensitivity. The former devices are more sensitive for finer grained material, while the latter for coarser grained material (Haallboom et al., 2021).

High-resolution vertical measurements through the entire water column are now being used, collected primarily during CTD hydrographic casts with attached optical sensors, allowing the detection of nepheloid layers. Profiling vehicles (see **Chapter 3**) and gliders equipped with optical sensors have now increased temporal and spatial coverage, although most of them present profiling depths to 2000 m or less. In this Thesis, profiling vehicles equipped with CTDs and OBSs installed in moorings and seafloor observatories are used to assess the temporal evolution of the nepheloid layer structures in two different oceanographic settings (**Chapters 4, 5** and **6**).

1.4.4. Calibration and suspended particulate matter analysis

Various methods have been employed to analyse the suspended particulate matter (SPM) in nepheloid layers. Compared to time-series of turbidity data, water sampling provides discrete point measurements, and also allows for calibration of optical sensors to transform turbidity units into SSC units. Direct filtration of SPM dates to early studies in the 1960s (Biscaye and Eittreim, 1974), and it still remains the most frequently used method for calibration purposes (Gardner et al., 2003). Measures of weight per volume calibrations are carried out by filtration of dried filters, for instance Nucleopore and Millipore filters give satisfactory results (Gibbs, 1974). The gravimetric weight of the filters is then correlated using linear regression with the output signal of the particular sensors. However, there is not a universal calibration and therefore, studies generally apply their own calibration or one of a representative area.

Chapter 2. Study sites

2.1. The Mediterranean Sea

The Mediterranean Sea is a mid-latitude semi-enclosed basin, with limited exchanges of water, salt, heat, and other properties with the North Atlantic Ocean. It is composed of two nearly equal-size deep basins, the western basin and the eastern basin, which are separated by the Strait of Sicily and connected with the open ocean across a sill depth (290 m) at the Strait of Gibraltar. This sea is overall oligotrophic, although its waters in the eastern basin present lower nutrient concentrations in comparison to the waters in the western basin (D'Ortenzio and Ribera d'Alcalà, 2009).

Intense seasonal phytoplankton blooms occur during early-mid winter and spring due to deep convection, which brings nutrients for planktonic growth to the enlightened surface layer (Lévy et al., 1998). These periods of enhanced surface productivity can also be fed by river runoff and groundwater discharge, most of which take place in proximity to large river mouths (e.g., the Po in the North Adriatic Sea, the Rhone in the Gulf of Lions, and the Nile in the South East Levantine Sea) (Siokou-Frangou et al., 2010). Nutrients can also be supplied by episodic deposition of aerial dust, which supports a significant amount of new production especially in the southeastern part of the Mediterranean basin (Ribera d'Alcalà et al., 2003; Emeis et al., 2010). Moreover, it has been observed that individual weather systems may induce transient blooms by delivery of nitrate and other nutrients in rainfall (Malej et al., 1997). The highest density of submarine canyons within the Mediterranean margin contributes to increase its potential fertility, due to the higher nutrient fluxes within these canyons and the greater habitat complexity (Fernandez-Arcaya et al., 2017).

Of all the marine environments on Earth, the Mediterranean Sea is considered one of the most complex because of the variety and scale of physical processes occurring there (Pinardi and Masseti, 2000). The general circulation pattern is influenced by many factors, including lateral thermohaline fluxes and water exchange due to acceleration through the various straits, freshwater inputs from river flows, topographic effects of the intricate continental and insular coastlines, a Rossby deformation radius of 10-15 km, and the formation of cold, dense deep waters, which occurs in the Aegean Sea, the Adriatic Sea, and the Gulf of Lions forced by the effect of local winds (i.e., Etesian, Bora, and Mistral, respectively) (Pinardi and Masetti, 2000; Robinson et al., 2001; Durrieu de Madron et al., 2005a; Canals et al., 2009; Longhurst, 2009). The two gyral circulations of the western and eastern Mediterranean are just partially isolated, meaning that there is a general cyclonic circulation in the whole basin, with the surface waters becoming progressively saltier and the return flow progressively deeper. Notwithstanding, the principal currents are marginal, normally adjacent to the coastline and the shelf-break, so that coastal or shelf-break fronts are a typical feature that isolate these flows from the gyral and subgyral circulations (Robinson et al., 2001; Longhurst, 2009). Tides are mostly semidiurnal and

small because of the relative size of the basin (Longhurst, 2009). The wind-stress climatology is mostly dominated by northwesterly winds, although the dominant effects tend to be local and orographic, with interruptions of particularly strong, cold and dry northerly wind events, which contribute to the formation of dense waters (Durrieu de Madron et al., 2005a).

Trawling fishing activities have occurred for centuries on a large spatial scale in the entire Mediterranean Sea, and nowadays they are considered as one of the main and widespread causes of anthropogenic disturbance and habitat alteration in this marine environment. They are particularly important in the western Mediterranean margin, apparently linked to the higher nutrient concentrations in this basin. This fishery has been gaining economic importance since the 1970-80s, with increasing number of vessels targeting deep-sea commercial species using bottom trawling gears in the Mediterranean (Sartor et al., 2011). Bottom trawlers operating in this margin mostly belong to the European Union state members, principally from the Spanish, French, and Italian trawling fleets (Colloca et al., 2017).

2.1.1. The Catalan margin (NW Mediterranean)

This Thesis presents studies on the temporal and spatial variability of the hydrographic and nepheloid layer structure in submarine canyons incising the Central Catalan margin (Fig. 2.1) (**Chapters 4** and **5**). The following sections provide succinct descriptions of the general hydrodynamics and sediment transport processes in this margin, as well as descriptions of the trawling fleet operating in the study sites. A more detailed description for each specific study site is given at the beginning of each chapter.

2.1.1.1. Hydrography and general circulation

The thermohaline structure and dynamics of the water masses in this area is composed by a three-layer system (Hopkins, 1978; Salat and Cruzado, 1981; Salat et al., 2002). Within the first layer, from the surface down to 150-300 m depth, the Atlantic Water (AW) is generally found. This water mass enters from the Strait of Gibraltar and is transformed and modified while spreads and circulates cyclonically around the Western Mediterranean basin. The AW can be distinguished between “recent” and “old” according to the residence time in the Mediterranean that increases its salinity. The second layer is formed by the westward Levantine Intermediate Water (LIW), found between 300-600 m depth, which is formed in the Levantine region by intermediate convection and sporadically enriched by Cretan Intermediate Water (CIW) formed in the Aegean Sea (Font, 1987; Millot, 1999). Mainly during wintertime, cold lenses of Western Intermediate Water (WIW) can be found at around 150 m depth. The WIW is formed seasonally, and its production is related to the formation of cold and dense waters in the region of the Gulf of Lions (NW Mediterranean) (Salat and Font, 1987). The third layer is formed by the near-homogeneous Western Mediterranean Deep Water (WMDW), which is formed in the open ocean resulting from intense sea-atmosphere heat exchanges and the subsequent buoyancy loss of offshore waters induced by cold, dry and persistent N-NW winds (Salat et al., 2002; Font et al.,

2007). The typical potential temperature, salinity and density of these water masses are listed in Table 2.1.

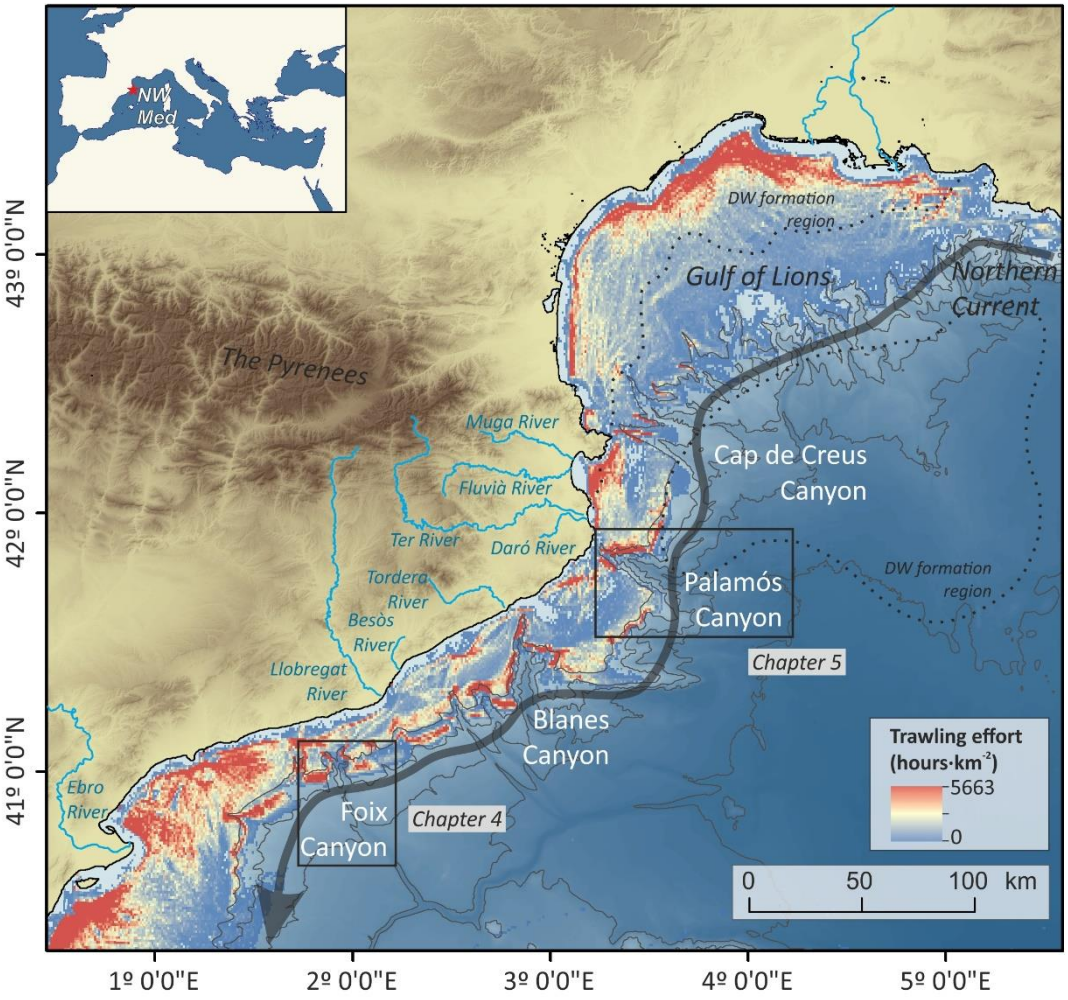

Figure 2.1. Bathymetric map of the NW Mediterranean margin, showing the cumulative fishing effort (hours·km^{-2}) between 2012-2020, annotating the regional circulation and the most important submarine canyons and rivers in this margin. Contour lines are given every 500 m. Fishing effort has been extracted from the Global Fishing Watch database (Global Fishing Watch, 2020). Dense Water (DW) formation regions are indicated with a dotted line.

Table 2.1. Acronyms and physical characteristics of the water masses found in the NW Mediterranean Basin.

Water mass	Temperature (ºC)	Salinity	σ_θ (kg·m^{-3})	Depth range (m)
"old" AW	> 13	38.0 – 38.2	< 28.9	150 – 300
WIW	12.6 – 13.0	38.1 – 38.3	28.9 – 29.0	~150
LIW	13.0 – 13.4	38.48 – 38.55	29.075	300 – 600
WMDW	12.75 – 12.82	38.43 – 38.47	29.115 – 29.120	> 600

The general circulation is cyclonic and is governed by a permanent baroclinic geostrophic current, which is formed by the presence of a shelf-slope density front (the Catalan front) that separates the fresher coastal waters from the more saline and denser open waters (Font and Miralles, 1978; Font et al., 1998; Millot, 1999). This current, which is part of the Northern Current, follows the continental slope from NE to SW parallel to the coastline (Fig. 2.1) and originates in the Ligurian Sea (Millot and Taupier-Letage, 2005). This current extends from the surface down to at least 400 m depth, with a width of 30-40 km and a mean speed at its core of ~30 cm s^{-1} (Castellón et al., 1990; García et al., 1994), and its motion is forced by the entrance of AW through the Strait of Gibraltar and its cyclonic circulation around the western basin. Eddies and meanders formed by the Northern current (Tintoré et al., 1990; Conan and Millot, 1995) can propitiate exchanges of water masses across the margin (Masó and Tintoré, 1991). Additionally, these mesoscale perturbations promoted by topographic changes can cause upwelling and downwelling events over submarine canyons, enhancing nutrient inputs and the transference of particulate matter into these canyons (Estrada, 1996; Granata et al., 1999; Palanques et al., 2005; Flexas et al., 2008).

2.1.1.2. Sediment transport processes

Particulate matter transferred into submarine canyons incising the Catalan margin can originate from sediments delivered from medium-to-small rivers and ephemeral streams. Nonetheless, riverine supply is generally low and irregular, and it is only increased in winter-spring as a result of the snowmelt in rivers draining from the Pyrenees (Liquete et al., 2009) or after increasing heavy rainfall during winter storms (Guillén et al., 2006; Sanchez-Vidal et al., 2013). Sediment delivered by these rivers to this margin form prodeltas at the mouth of the Muga, Fluvià, Ter, Tordera, Besòs and Llobregat rivers, from North to South (Fig. 2.1) (Checa et al., 1988; Díaz et al., 1993; Durán et al., 2014).

The transference of particulate matter into submarine canyons can also be enhanced by high-energy events derived from atmospheric forcing conditions, namely eastern storms and DSWC events. Eastern storms are developed when humid winds blowing from the East generate swell and high waves over the continental shelf favoured by a long fetch (Ferré et al., 2005; Guillén et al., 2006). They are normally associated with heavy rainfall that cause episodic river discharges in this margin, transporting large amounts of sediments. In addition, these storms cause wave-induced sediment resuspension and, in association with the littoral drift and the Northern Current, results in a dominant southwards along-shelf sediment transport (Puig et al., 2001; Palanques et al., 2002; Guillén et al., 2006). The large swell and intense currents associated to eastern storms along the coast can resuspend large amounts of sediment and erode the coastline and inner shelf. Ultimately, resuspended sediment during these events can be transferred into submarine canyons incising the shelf, enhancing vertical particle fluxes within these canyons (Palanques et al., 2008; Sanchez-Vidal et al., 2012; Pedrosa-Pàmies et al., 2013).

DSWC events tend to occur in the Gulf of Lions induced by dry and cold north and north-westerly winds (Tramontane and Mistral) (Fig. 2.1), which cause the cooling and heat loos of surface

coastal waters (Durrieu de Madron et al., 2005a). These shelf waters eventually get denser than the surrounding waters and sink over the shelf edge and cascade downslope, primarily through submarine canyons, until they reach their neutral buoyancy (Millot, 1990; Durrieu de Madron et al., 2005a). During mild or average winters, DSW are detached at intermediate depths, contributing to the formation of WIW found at the upper slope depths (Lapouyade and Durrieu de Madron, 2001; Dufau-Julliand et al., 2004). In very dry, cold and windy winters, DSWC events can be exceptionally intense, and DSW can affect the entire continental slope and even reach the basin floor (Canals et al., 2006; Palanques et al., 2012; Durrieu de Madron et al., 2013; Palanques and Puig, 2018). Cascades of DSW can last for several weeks and the associated strong currents can induce erosion and resuspension of sediments in the outer shelf and upper slope, sometimes detaching as nepheloid layers (Fohrmann et al., 1998; Puig et al., 2013). The intensity of these events can vary depending on the strength of winter cooling and evaporation (Canals et al., 2006), and they are mainly restricted to the submarine canyons incising on the Gulf of Lions. The strongest off-shelf sediment transport associated with DSWC events tends to occur during eastern storms, and sediment transport is then enhanced towards the western part of the Gulf of Lions because of its down-flow location and the abrupt narrowing of the shelf, being particularly intense through the Cap de Creus Canyon (Fig. 2.1) (Palanques et al., 2006b; 2012). Occasionally, DSWC can be transferred south from the Gulf of Lions, towards the central Catalan margin, and reach the Palamós (Ribó et al., 2011) and Blanes (Zúñiga et al., 2009) submarine canyons, whereas regions located farther south towards the southwest seldomly experience the effects of DSWC events (Ulses et al., 2008a) (Fig 2.1).

Beyond sediment transport, DSWC controls the off-shelf carbon fluxes and the functioning of deep-sea ecosystems (Canals et al., 2006). Sediment transport during DSWC tends to be impoverished in organic matter (Sanchez-Vidal et al., 2008; Pedrosa-Pàmies et al., 2013), but when these events coincide with spring phytoplanktonic blooms over the shelf, they can transport large fluxes of fresh and highly nutritive organic matter into submarine canyons and towards the basin (Pasqual et al., 2013; Palanques and Puig, 2018). The massive volumes of material transported downslope during these events has direct consequences to benthic communities inhabiting these canyons, as for example, increasing the amount of available food for benthic species (Company et al., 2008; Pusceddu et al., 2013). Major DSWC events reaching > 1000 m depth can affect the landings of the blue and red deep-sea shrimp *Aristeus antennatus* (Risso, 1816). Company et al. (2008) reported that strong currents associated with intense DSWC events initially caused the disappearance of this species from the vicinities of the Cap de Creus, Palamós, Blanes and Arenys canyons' fishing grounds, causing a temporary fishery collapse. Nonetheless, landings of *A. antennatus* increased between 3 to 5 years after this major DSWC event, coinciding with an increase of juveniles of this species, as a result of enhanced recruitment associated with the high transfer of organic matter to deeper regions (Company et al., 2008).

2.1.1.3. Trawling activities

The Catalan margin supports important bottom trawling grounds, that are mainly located in submarine canyons along their heads, rims and flanks, and generally extend down to 800 m water depth (Fig. 2.1). Trawling fleets mainly target the deep-sea shrimp *A. antennatus* (Sardà and Demestre, 1987), which is one of the most valuable demersal fishery resources for the bottom trawl fishery in the Mediterranean Sea (Sardà et al., 2004). In Catalonia (NE Spain), this species is an extremely important resource for the local fishermen associations, which largely depends on the incomes of this fishery (Maynou et al., 2006). Although it represents 3 % of total landings, its fishery accounts for 21 % of the annual economic income (Gorelli et al., 2016). Fishing effort (a measure of the amount of fishing, generally defined as the capacity of the fleet times days at sea) on this species was negligible until the mid-1960s, when the trawling fleet became fully industrialised and bigger trawlers were constructed, being capable of exploring deeper fishing grounds (Alegret and Garrido, 2008; Coll et al., 2014). This trend notably accelerated in the 1970s in regards to engine power and gear size and, subsequently, fishing depth and trawled area per haul also increased (Martín et al., 2008). This growth led to an overall decrease of catch per unit effort (CPUE) to minimal values, leading to an overexploitation of this fishery (Gorelli et al., 2014; 2016).

Like other commercial species, *A. antennatus* is found around submarine canyons, which host greater abundance, species richness, and biodiversity of both megafauna and meiofauna species in comparison to adjacent open slope areas (Company et al., 2012). The populations of *A. antennatus* show seasonal migrations and its lifecycle is closely related to the geomorphology of submarine canyons. The post-larval and juvenile phases occur in deep waters from 1000 to 3000 m depth, and during their adult phase they migrate up-slope, presumably following the canyon axis, to shallower depths (500-800 m), where trawling takes place (Sardà et al., 2003; 2004). In the Catalan margin, the distribution of this species tends to occur in elongate shoals concentrated at depths between 700 m and 1000 m along the continental slope through winter and spring (Sardà et al., 2003). The shoals are mainly constituted by mature adult females during spring and early summer in deep waters. From mid-summer and throughout autumn, catches in fishing grounds located on the flanks of submarine canyons increase and are made up of smaller individuals (Sardà and Cartes, 1994; Sardà et al., 2003; Tudela et al., 2003).

Other important fisheries that are conducted in the upper and middle slope ridges at the Catalan margin target the hake*, Merluccius merluccius,* the monkfish, *Lophius piscatorius*, and the Norwegian lobster, *Nephrops norvegicus* (Stefanescu et al., 1994; Tudela et al., 2003). Among this commercial species, populations of *N. norvegicus* in Catalan waters have been reported between 200 and 800 m depth, with peak abundance at 400-500 m depth, and their spatial distribution comprises high-density patches of about 7 km diameter alternating with areas of low density (Maynou et al., 1996; Bell et al., 2006). Seasonal variations in landings and catch rates of *N. norvegicus* are well known, the yield being greater in spring and summer and lower during autumn and winter (Sardà and Peired, 1998; Maynou and Sardà, 2001), and have been attributed

to the rhythmic behavior of this species at diel and seasonal scales (Aguzzi and Sardà, 2008). Along with seasonal variation, sudden variation in CPUE at short-time scales (typically within a week) have been attributed to change in the vulnerability of this species by environmental factors, such as sediment coverage, water currents, light intensity, changes in the weather, and bottom trawling (Maynou and Sardà, 2001).

The first observations of the impacts of bottom trawling in the sedimentary dynamics of submarine canyons came from an extensive study conducted in 2001 during the CANYONS Project (Palanques et al., 2005), which aimed to assess the natural sedimentary dynamics prevailing in Palamós Canyon. During these studies, several moorings located downslope from trawling grounds recorded simultaneous peaks in current speed and downward particle fluxes, indicating the occurrence of trawling-induced sediment gravity flows coming from the adjacent trawling ground. These gravity flows triggered a double-fold increase of natural sedimentation rates in a sediment core collected at 1750 m at the canyon axis, as observed in ^{210}Pb and ^{137}Cs concentration profiles and by the presence of well-preserved horizontal laminae (Martín et al., 2008). These findings led to a series of new studies aiming to understand the potential contribution of bottom trawling activities to contemporary sediment dynamics of Palamós Canyon.

Further analyses on turbidity time series during the HERMIONE project revealed that trawling-induced suspended sediment resuspension from fishing grounds was heavily dominating, both in magnitude and temporal patterns, the near-bottom water turbidity. These trawling-induced sediment gravity flows were only recorded during working days and working hours of the trawling fleet, and not during weekdays (Palanques et al., 2006; Puig et al., 2012; Martín et al., 2014a). These sediment gravity flows generated persistent nepheloid layers at the working depth range of the trawling fleets (Martín et al., 2014a), hypothesizing the possible role of trawling activities in modifying seasonal near-bottom turbidity patterns in the canyon.

Initial studies assessed the effects on the sediment resuspension by bottom trawlers using high-resolution bathymetry data and seafloor imagery from a Remoted Operated Vehicle (ROV). These results revealed that bottom trawling grounds had been ploughed and smoothened by the passage of the otter trawl boards (or otter trawl doors) during successive fishing hauls of the trawling fleet that operates in this fishing ground (Fig. 2.2), producing comparable effects on the seafloor than those generated by agricultural ploughing on emerged land (Puig et al., 2012). Subsequent analyses of sediment cores addressed the alteration of the sedimentary budget and physical properties of surface sediments, evidencing that sediments over fishing grounds showed higher degrees of mixing, erosion and sorting (Martín et al., 2014a). In comparison to the untrawled site, trawled sites had denser and coarser surface sediments due to the continuous sediment resuspension, which caused grain-size sorting through preferential advection of fine-grained sediments (Martín et al., 2014a). Also, trawled sites presented sediment impoverishment in organic carbon (~30 % loss), which also presented lower content of labile compounds (e.g., di-carboxylic acids, fatty and amino acids derived-products, cutin acids) (52-70 %) (Paradis et al.,

2021). It has also been observed that the 2-month seasonal trawling closure established was insufficient to restore the seafloor and to recover the sedimentary organic content of the sediment cover (Paradis et al., 2021).

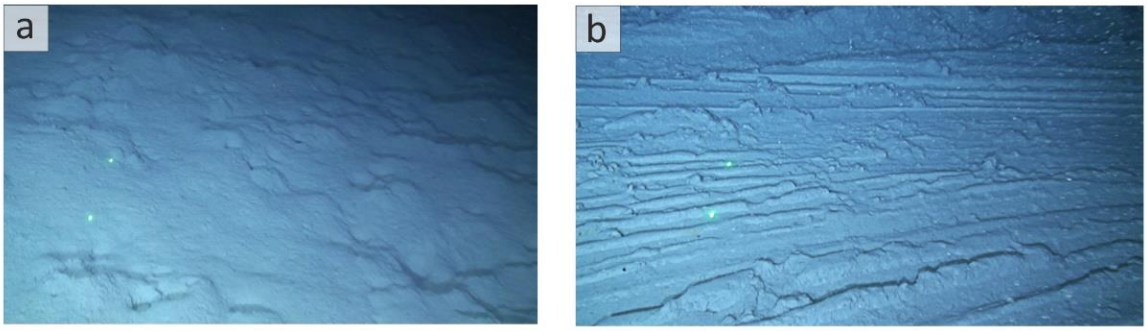

Figure 2.2. Seafloor images from the northern Flank of the Palamós Canyon during an up-slope ROV transect, showing a) an untrawled moderately steep seafloor at 963 m depth with many bioturbation mounds, and b) a flat seafloor at 770 m depth created by the passage of bottom trawlers, with high otter board marks. Distance between the ROV green laser points is 15 cm. **Source:** Puig et al., 2012.

2.2. The NE Pacific

The Pacific Ocean is by far the largest and deepest ocean on Earth's surface and extends from the Arctic Ocean in the North to the Antarctic Ocean in the South, occupying about a third of the globe. It stretches from the shores of Antarctica to the Strait of Bering along 15500 km, and its longitudinal extent measures about 19,300 km between the coasts of Colombia in South America and the Malay Peninsula in Asia (Britannica Concise, 2008).

The NE Pacific region comprises the marine waters bounded in the North by Alaska (United States of America), in the Southeast by Canada and the United States of America, and in the Northwest by the Russian Federation (eastern Gulf of Anadyr), and is associated with the American Cordilleran System. Except for its extreme northern section, which is characterized by fjords and numerous off-lying islands, and in exception of the indented Gulf of California to the South, the coastal boundary is relatively regular, and the continental shelf is narrow (Britannica Concise, 2008).

Enhanced regional nutrient supply and primary productivity depend upon several physical processes, including river discharge from the Columbia River, coastal upwelling, tidal mixing, estuarine entrainment, and mesoscale eddy formation and transport (Whitney et al., 2005). The principal riverine supply to this margin is nutrient-enriched waters with silicate and iron, which supports phytoplankton blooms. The most important source of these dissolved components to the NE Pacific Ocean is the Columbia River, which contributes iron to coastal waters in sufficient quantitities to support phytoplankton growth (Chase et al., 2002).

Variability in surface production and the eventual export of organic matter to the deep sea are partially subjected to the California Current (see 2.2.1.1 for further information). The California Current is subjected to high intra-annual variability, with seasonal upwelling influencing coastal waters as far as 500 km offshore (Whitney et al., 2005), and increasing nutrient supply and phytoplankton growth along the California to British Columbia coasts (Ianson et al., 2003). In addition, this current also experiences large-scale, non-seasonal fluctuations as noted in zooplankton biomass (Chelton et al., 1982).

Tidal mixing in estuaries and coastal straits inevitably enhances nutrient-rich, relatively fresh waters that discharge into the ocean (see 2.2.1.1). It is a common process along the NE Pacific coast, especially in regions of strong tidal currents and constricted flow (Whitney et al., 2005). Moreover, tidal mixing contributes to the advective exchange between coastal inlets and adjacent channels, resulting in periods of nutrient injections that enhance primary productivity (Gargett et al., 2003). Mackas et al. (1980) noted that estuarine outflow provides the largest supply of new nutrients to the southern Vancouver Island's shelf (British Columbia). Periods of enhanced eddy formation or recirculation may also supply iron and other nutrients into surface waters that enrich the open ocean for several decades (Foerster, 1993), which can export as much as 5000 km^3 of nutrient-rich waters from the shelf in a single eddy into deeper regions (Whitney and Robert, 2002).

Fishing activities in the NE Pacific (FAO Area 67[4]; FAO, 2019) are dominated by the fleets of the United States of America and Canada, where trawling is the most important fishing activity. Vast areas of the North Pacific have been permanently closed to bottom trawling and scallop dredging to reduce potential adverse impacts on sensitive species and to protect benthic invertebrates (Iriondo et al., 2019). Due to these restrictions, in 2013 the NE Pacific produced 3.2 million tons of fish, which roughly represents the average catches maintained since the early 1970s. Trawling activities targeting groundfish such as cod, rockfish (*Sebastes spp.*), sablefish (*Anoplopoma fimbria*) and thornyheads (*Sebastopolus spp.*) are large contributors to the regional catch (FAO, 2016). These species are mainly targeted at ~400 m depth, although trawl marks have noticed that the fishery extends to depths below 900 m depth (Friedlander et al., 1999; De Leo et al., 2017). Trawling fishing activity in the NE Pacific is mainly concentrated in the narrow Canadian continental shelf and the wider continental shelf of Alaska, where vessels mainly target pollock (Iriondo et al., 2019).

[4] Mainly for statistical purposes, the FAO (Food and Agriculture Organization of the United Nations) has established 27 major fishing areas internationally, which comprise eight major inland fishing areas and nineteen major marine fishing areas covering the waters of the Atlantic, Indian, Pacific and Southern Ocean with their adjacent seas (FAO, 2015).

2.2.1. The Cascadia margin off Vancouver Island (British Columbia, Canada)

In this Thesis, we present studies on the Cascadia margin and continental slope off Vancouver Island (British Columbia, Canadian NE Pacific) (Fig. 2.3) (**Chapter 6**). As in the previous section, the following section provides succinct descriptions of the general hydrodynamics and main sediment transport processes in this margin, as well as descriptions of bottom trawling activities carried out in this margin. A more detailed description for this study area is given at the beginning of the corresponding chapter in the results section (**Chapter 6**).

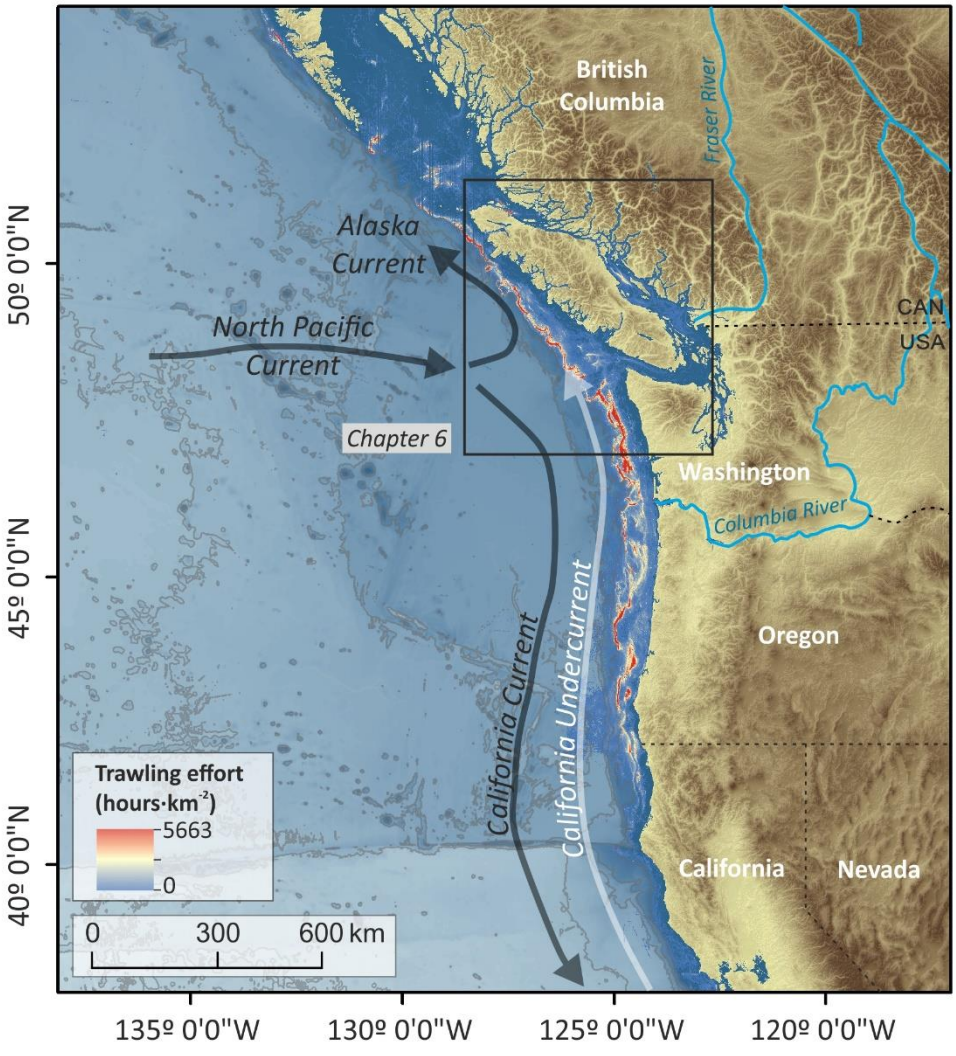

Figure 2.3. Bathymetric map of the Cascadia margin, showing the cumulative fishing effort (hours·km^{-2}) between 2012-2020, annotating the regional circulation and the most important rivers discharging in this margin. Contour lines are given every 500 m. Fishing effort has been extracted from the Global Fishing Watch database (Global Fishing Watch, 2020). The federal boundary between Canada and USA, as well as between American States, is indicated with a black dotted line.

2.2.1.1. Hydrography and general circulation

The Cascadia continental margin is located along the convergent boundary between the Explorer and Juan de Fuca Plates and the America Plate. This tectonic regime is manifested in major faults and folds which dislocate sedimentary and volcanic rocks of the Tertiary Age beneath a relatively undeformed wedge of late Neogene mudstones (Bornhold and Yorath, 1984).

The NE Pacific is the location of unique upper layer transition waters and the formation of intermediate waters along the eastern boundary (Emery and Meincke, 1986). These upper and intermediate waters are the products of subpolar waters advected equatorward along the eastern boundary and mixed with coastal waters influenced by upwelling (Sverdrup et al., 1942). In the upper layer (0-500 m depth), the NE Pacific contains the relatively fresh and cold Pacific Subarctic Upper Water (PSUW). The Eastern North Pacific Transition Water (ENPTW) is found between the fresh, cold subarctic waters and the warmer, saltier central waters. Intermediate waters (500-1500 m depth) include the Pacific Subarctic Intermediate Water (PSIW), which is formed due to the input of surface fresh waters from heavy precipitation and runoff in the North Pacific (Royer, 1982). The PSIW spreads south to latitudes of 15-20 ºN in water depths of 400-700 m depth (Talley, 1993; 1997). The NE Pacific basin is mainly fed by Circumpolar Deep Water (CDW), which is the most abundant water mass in the world's ocean (Tsuchiya and Talley, 1996; Reid, 1997). The CDW is produced by the mixing of waters entering the Antarctic region, at mid-depths, from the Indian, Pacific and Atlantic oceans with Weddell Sea bottom water (Broecker and Takashi, 1985). The typical potential temperature, salinity and density of these water masses are listed in Table 2.2.

Table 2.2. Acronyms and physical characteristics of the water masses found in the NE Pacific.

Water mass	Temperature (ºC)	Salinity	σ_θ (kg·m^{-3})	Depth range (m)
PSUW	3.0 – 15.0	32.6 – 33.6	25.8 – 27.4	0 – 500
ENPTW	11.0 – 20.0	33.8 – 34.3	< 26.0	0 – 500
PSIW	5.0 – 12.0	33.8 – 34.3	26.0 – 27.0	500 – 1500
CDW	0.1 – 2.0	34.62 – 34.73	28.0	>1500 - bottom

The general circulation of the NE Pacific is cyclonic and is driven by surface winds and coastal runoff. The region is influenced by the California Current System, which results from the bifurcation of the eastward flowing Subarctic and North Pacific currents into the northward flowing Alaska Current and the southward flowing California Current, as a result of a divergence in prevailing wind directions (Fig. 2.3) (Hickey, 1979; Lynn and Simpson, 1987; Checkley and Barth, 2009). The California Current (CC) extends ~3000 km from the north of Vancouver Island (~42 ºN; British Columbia, Canada) to approximately the southern tip of Baja California Peninsula

(23 ºN) in Mexico, flowing year-round with some seasonal patterns (Hickey, 1989; Bograd and Lynn, 2003). It reaches depths of approximately 500 m and can be intensified at the surface by wind-stress (Checkley and Barth, 2009).

Winter conditions at the CC start with a gradual completion of summer conditions after the contraction of the North Pacific high-pressure centre, while the Aleutian Low intensifies and moves to the East and South (Wooster and Hollowed, 1995). Downwelling-favourable winds result in wind-driven mixing that forces enriched surface waters towards the ocean interior at shelf-break depths (Whitney et al., 2007; Cannolly and Hickey, 2014). During the spring transition, the CC is forced by the winds blowing equatorward, and generates southward transport along the coast and offshore Ekman transport (Hollowed, 1992). The climatological summer in the CC consists in the relaxation of the Aleutian low-pressure centre and the intensification of the North Pacific high-pressure centre, which migrates westward and extends along most the North Pacific basin (Lluch-Belda et al., 2001). The CC is strongest during spring and summer months, and the regional circulation is characterized by upwelling-favourable winds and equatorward flow. Although upwelling-favourable wind stress peaks during summer, downwelling and relaxation events occur during this season (Hickey, 1979; 1989). Despite the fact that the source mechanism is not completely understood, subsurface gradients cause the California Undercurrent (CUC) to flow poleward along this margin during the late summer to early fall (Fig. 2.3). The CUC develops below the shelf-break depth over the slope (125-325 m depth, with core depths between 200 and 275 m depth; Pierce et al., 2000), also reaching its maximum strength in late summer (Hickey, 1979). During summer months, with upwelling-favourable winds, low oxygen and nutrient-enriched waters are drawn onto the shelf, leading to sustained productivity along the west coast of Vancouver Island (up to 425 g $C \cdot m^{-2} \cdot y^{-1}$; Antoine et al., 1996).

Tides in the NE Pacific present both diurnal and mixed regime. In the diurnal regime, only a single high water and a single low water occur each tidal day (which lasts 24 hours and 50 minutes). In contrast, in the mixed tide regime both diurnal and semidiurnal oscillations occur and are characterized by large inequalities in successive high (or low) water heights. This type of tide is prevalent along much of the coast of the NE Pacific (Britannica Concise, 2008).

2.2.1.2. Sediment transport processes

The sediment distribution shows a general trend from gravelly to boulder sediments inshore to sand and gravel on the mid-shelf and to muddy sands (10-40 % mud) on the outer shelf (Bornhold and Yorath, 1984; Bornhold and Barrie, 1991). The shelf-edge presents a narrow band of well-sorted sands, whereas the continental slope mainly presents glaciomarine sediments (i.e., ice-rafted dropstones and clay components) derived from the ice sheet activity during late Quaternary and early Holocene (Cosma and Hendy, 2008).

Particulate matter transferred into this margin can originate from sediments delivered from rivers. The Columbia River is the major point source of freshwater, sediments, and nutrients (e.g., silicate and iron) along the west boundary of North America (Fig. 2.3), with the peak flow in

recent years reaching 16000 $m^3 \cdot s^{-1}$ in spring. It discharges into coastal waters that flow southwards towards California during summer and northwards along the Washington and British Columbia coasts during winter, due to the changing wind field (Hickey, 1979; Freeland et al., 1984). Winter discharge then becomes part of the buoyant coastal current that is enhanced by other rivers and land runoff along the Washington, British Columbia, and Southeast Alaska coasts (Whitney et al., 2005). River discharge is at its maximum in June for the Columbia River as a consequence of snowmelt, and in November-December for the British Columbia coastal region as a result of rainfall (Freeland et al., 1984).

Waves and tides are of greater significance for the transport of sediments, particularly on the continental shelf of British Columbia. The tide floods along the shelf present near-bottom velocities that rarely exceed 50 $cm \cdot s^{-1}$, whereas in coastal constricted passages, tidal currents are intense and can exceed velocities of 150 $cm \cdot s^{-1}$ (Bornhold and Yorath, 1984; Barber, 1957). Particularly, sediment transport dynamics in this region are influenced by a meso to macrotidal environment with superimposed wave and estuarine-induced circulation (Barrie et al., 2009). Surface velocities off NW Vancouver Island related to non-tidal currents range from 10 to 30 $cm \cdot s^{-1}$ to the North in fall and winter, whereas they are less than 20 $cm \cdot s^{-1}$ to the South in summer. Long-period swell along-slope waves (i.e., coming from the Southwest, West or Northwest) accounts for most of the wave energy on the shelf in this region (Bornhold and Yorath, 1984), and are of greater significance for the transport of sediments. Reinforced by south-easterly winds, they appear to be a dominant process in the region. Waves with swell periods up to 20 s exceed significant wave heights of 4 m between 20 % and 40 % of the time during winter, and between 5 % and 15 % during summer (Bornhold and Yorath, 1984). The flood tides, reinforced by South-easterly storms, appear to be a dominant sediment transport process in the region (Crawford and Thomson, 1991; Barrie et al., 2009).

2.2.1.3. Trawling activities

In the Canadian Pacific, trawling occurs from the coastline down to depths less than 2000 m depth and occupies up to 400000 km^2 (Kulka and Pitcher, 2001), mainly targeting a mix of groundfish and shrimp. Trawling grounds form a string of partially joined patches along the shelf edge off Vancouver Island, three large patches within the southern Queen Charlotte Sound, and smaller patches surrounding Queen Charlotte Islands (Kulka and Pitcher, 2001).

Off-Vancouver Island, deep-sea bottom trawling began in the 1990s in response to the growing market demand for two groundfish species (short spine and long spine thornyheads). The depth distribution of the longspine thornyhead ranges from 500 to 1600 m, while the distribution of the shortspine thornyhead occurs over a broader range, from 90 to 1460 m (Haigh and Schnute, 2003; De Leo et al., 2017). Bottom trawling represents an important type of fishery in British Columbia despite public concerns and scientific evidence from other locations about the potential physical disturbance of seafloor habitats and associated benthic communities (Ardron et al., 2007; Finney, 2009; De Leo et al., 2017), as well as its high by-catch rates (Haigh and Schnute, 2003).

In 2012, an unprecedent agreement reached between British Columbia's Deep Sea Trawlers Association and key non-government organizations (such as Living Oceans and SeaChoice) implemented measures to reduce the impacts on deep-sea habitats, such as deep-water corals and sponge reefs. The agreement put several key fisheries management strategies into effect. First, the fishery footprint was reduced by 8000 km^2 through limiting the maximum bottom trawling depth to 800 m and banning trawling from areas where corals and sponge reefs occur in high densities. Second, a habitat quota was established for trawlers, which limited corals and sponges' catches to no more than 4500 kg annually. Third, a habitat encounter protocol was applied to trawlers that required an immediate report if they retrieve over 20 kg of corals and sponges combined. And finally, a review committee conducted ongoing evaluations of fisheries impacts on the ecosystem, with the aim of moving towards a more sustainable fishery.

Methodology

Part II

Chapter 3. Methods

3.1. Fieldwork and oceanographic surveys

The experimental techniques used in this Thesis for the study of the temporal and spatial variability of the nepheloid layer structure in the Catalan and Cascadia continental margins mainly consist of continuous measurements of variable duration collected by several underwater oceanographic sensors and sampling devices installed on mooring arrays in two submarine canyons incising the Catalan margin, and on a seafloor cabled observatory located on the Cascadia margin. In addition to the observational data, water and sediment samples were collected for calibration purposes.

The observational effort in this Thesis project was conducted during several oceanographic cruises covering the different study areas. The Catalan margin was investigated during 2014, and in the period of 2017-2018, collecting hydrographic and sedimentological data within two submarine canyons incising the margin (the Foix and the Palamós canyons). Such data collection took place in the frame of the Spanish projects FORMED (*FORmas de fondo y su dinámica actual en el margen continental MEDiterráneo español*, Ref: CGL2012-33989) and ABIDES (*Assessment of Bottom-trawling Impacts in DEep-sea Sediments*, Ref: CTM2015-65142-R). All oceanographic cruises were performed on board the R/V *García del Cid*, which has the right characteristics to carry on most of the tasks planned on each project.

The FORMED Project aimed to study the continental shelf and upper slope seafloor morphology and prevailing hydrodynamics and sediment transport processes that control large-scale (> 1 m) bottom forms in the Spanish Mediterranean continental margin. In the frame of the project, five oceanographic surveys were conducted in which several techniques (moored oceanographic instrumentation, CTD profiling, sediment sampling, and multibeam bathymetry) were used to pursue the goals of this project. Particularly during the FORMED-3 oceanographic cruise, a mooring line equipped with an autonomous hydrographic profiler (Aqualog profiler) was deployed in the Foix submarine canyon at 879 m depth to determine the evolution of the hydrographic conditions within the canyon. The same site was revisited during FORMED-4 cruise to recover the mooring line (Table 3.1).

The main goal of the ABIDES Project was to improve the knowledge on contemporary sedimentary dynamics (erosion, transport, and accumulation processes) driven by bottom trawling activities in continental slope environments, assessing the magnitude of the associated impacts in the Catalan margin. To accomplish this, during the ABIDES project's oceanographic cruises, time-series of currents, SSCs, and particle fluxes were recorded by means of several instrumented moorings deployed nearby present heavily trawled sites of the Palamós Canyon. The observational effort in this research project was conducted during three oceanographic cruises over two years, each one separated four months from the next one, which were necessary to collect high-resolution data and to perform maintenance tasks of the sensors mounted on the

moorings (i.e., to change for a similar sensor with the same configuration and new batteries). One of the moorings was equipped with the same autonomous hydrographic profiler (Aqualog profiler) used in the Foix Canyon, which was deployed in the Palamós Canyon axis at 929 m water depth, to assess the formation and evolution of BNLs and INLs in the water column, as indicators of preferential pathways for trawling-induced particle resuspension and advection. In addition, the mooring line was also equipped with near-bottom instrumentation to monitor sediment transport processes and identify the contribution of bottom trawling to the near-bottom sediment fluxes. During ABIDES-1 oceanographic cruise (February 2017), the instruments only recorded good data for two months, after the mooring line was displaced by a longline fishing vessel from a neighbouring fishing harbour. This prevented the Aqualog profiler from performing its regular up and down-casts. Nevertheless, the recorded period allowed to pursue the goals for this study (**Chapter 5**). The same mooring was successfully re-deployed during ABIDES-2 oceanographic cruise (June 2017), after repairing the damage caused during the former cruise. After successfully recovering the mooring line during ABIDES-3 cruise (October 2017), the profiler was seriously damaged, apparently due to water entering the electronic compartment of the device, that caused a short-circuit and serious damage to the battery and data storage compartment. No data could be retrieved from this cruise and, unfortunately, the Aqualog profiler could not be re-deployed in subsequent cruises. Therefore, for this Thesis, only the data retrieved during ABIDES-1 oceanographic cruise was available (Table 3.1).

This Thesis also includes data from the Ocean Networks Canada (ONC)'s NEPTUNE cabled seafloor observatory (Fig. 6.1). Particularly, data from a Vertical Profiling System (VPS) installed at the Barkley Upper Slope (BUS) Instrumented platform, located over the slope ~10 km north of the Barkley Canyon at 390 m depth, was used to study the hydrographic and nepheloid layer structure of the study site (see 3.2.2.1 for further details). The first successful deployment of the VPS was carried out in August 2012, after being extensively tested in Japan where it was originally manufactured. Since then, it has been working in different locations of the NEPTUNE observatory. In July 2018, the VPS was re-installed in the BUS Instrumented Platform, although it only recorded good data from August to November 2018. For this Thesis, it was only considered the latest recording period of the VPS (Table 3.1).

Table 3.1. Summary of the main tasks carried out during the fieldwork and oceanographic cruises during the development of this Thesis.

Study site	Project	Cruise	Period	Conducted work
Foix Canyon	FORMED	FORMED 3	1st-10th April 2014	Mooring deployment
		FORMED 4	2nd-4th June 2014	Mooring recovery
Palamós Canyon	ABIDES	ABIDES 1	5th-7th February 2017	Mooring deployment
		ABIDES 2	5th-12th June 2017	Mooring recovery, hydrographic transect
		ABIDES-ROV	5th-19th September 2017	Sediment sampling
BUS Site	Wiring the Abyss	Leg 1	19th June-3rd July 2018	VPS package deployment

3.2. Temporal characteristics of the water column

3.2.1. Instrumented moorings

Instrumented moorings are appropriate platforms when measurements are required at one single location over an extended period of time. Their design depends on the deployment location's depth, water currents, wind speed, as well as on the instrumentation for the purpose of which the mooring is deployed (Coppola et al., 2016). The basic elements of all oceanographic moorings are an anchor, a mooring line or wire, and one or more buoyancy elements that hold the mooring upright and preferably as close to the vertical as possible (Fig. 3.1). For deep-sea (> 200 m depth) experiments, the main buoyancy is placed at the top of the mooring line some 20-50 m below the ocean surface, preventing the mooring to the action of surface waves and other atmospheric/oceanographic forcings, and diminishing the risk of being damaged by ship traffic, vandalised, or stolen. Additional buoyancy is distributed along the wire to compensate for the weight of the instrumentation, and it is also arranged so that all the sections of the mooring are buoyant, enabling the recovery of the instrumentation if the mooring is damaged. At the bottom of moorings and right above the anchor, there is a remotely controllable releaser (Figs. 3.1 and 3.3a). It is normally activated through a coded acoustic signal from the ship at the time of the mooring recovery, bringing the mooring to the surface when the signal is triggered. The anchor is left at the seafloor, and can be a concrete block, a clump of disused train wheels, or a chunk of heavy chains. The weight of the mooring components and their net buoyancy are primary parameters used to calculate the mooring tension. The buoyancy is determined by the mass and displacement of the different instruments that compose the mooring (Venkatesan et al., 2018).

Conventionally, several sets of sensors are installed at fixed depths along mooring lines, collecting continuous measurements of oceanographic variables. However, this type of settings

does not allow to resolve vertical complex patterns of water masses and nepheloid layer structures. Autonomous hydrographic profiling systems have been recently used to conduct continuous measurements of water column properties over large depth ranges at high temporal and vertical resolution.

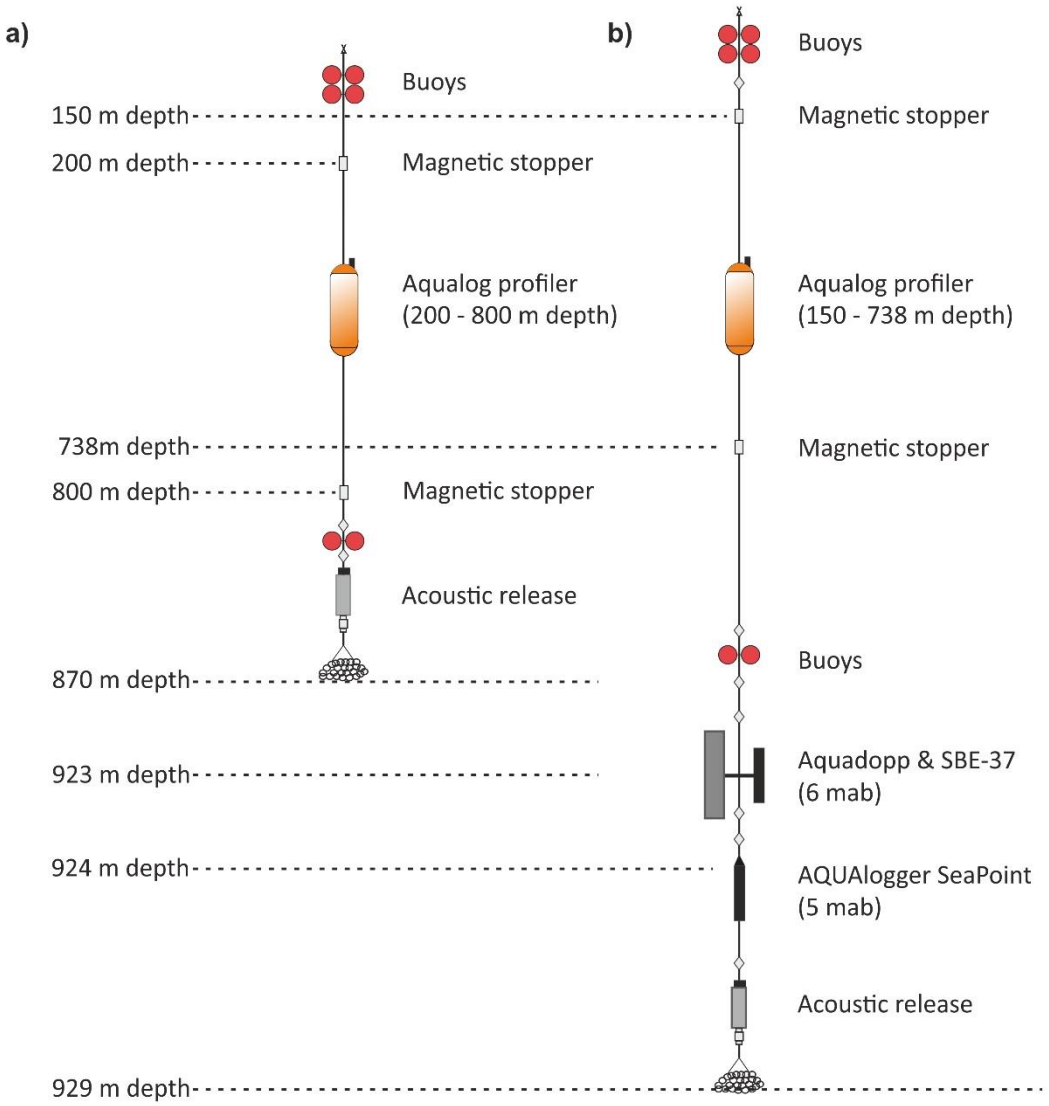

Figure 3.1. Vertical distribution of the oceanographic instruments, including the Aqualog profiler, in the mooring lines deployed in a) Foix Canyon and b) Palamós Canyon. Depths are only illustrative of the general mooring designs, but they are not scaled. For exact depths see sections 4.2.2 and 5.2.2.

3.2.1.1. Aqualog profiler

Among the profilers produced nowadays, we equipped our moorings deployed in the Catalan margin with the Aqualog profiler (hereafter referred to as “Aqualog”) (Ostrovskii et al., 2013).

Unlike conventional mooring systems, the Aqualog (Figs. 3.1 and 3.2) is designed for autonomous long-term acquisition of vertical profile time-series of oceanographic variables (e.g., current speed, temperature, conductivity, turbidity, downward fluxes, oxygen, fluorescence). It comprises a carrier equipped with convectional oceanographic probes and an optimal communication system (Carlson et al., 2013). Typical oceanographic probes integrated at the profiler are CTD probes, dissolved oxygen sensors, fluorometers and turbidity sensors, ocean current meters and acoustic backscatter sensors, and biochemical sensors for inorganic nutrient detection. The big potential for incorporating different instruments makes the Aqualog particularly flexible and tuneable for solving different problems (Ostrovskii et al., 2013). Generally, the Aqualog is mounted on mooring lines, started by a magnetic key onboard a research vessel and then deployed in the water. The profiler is streamlined and changes cross-sectional areas gradually to reduce the drag due to the effects of vortices generated around the profiler in typical ocean currents. It is constituted by modern plastic materials that enhance corrosion resistance in the ocean environment, and it has a gel-coated skin to reduce surface roughness (Carlson et al., 2013; Ostrovskii et al., 2013).

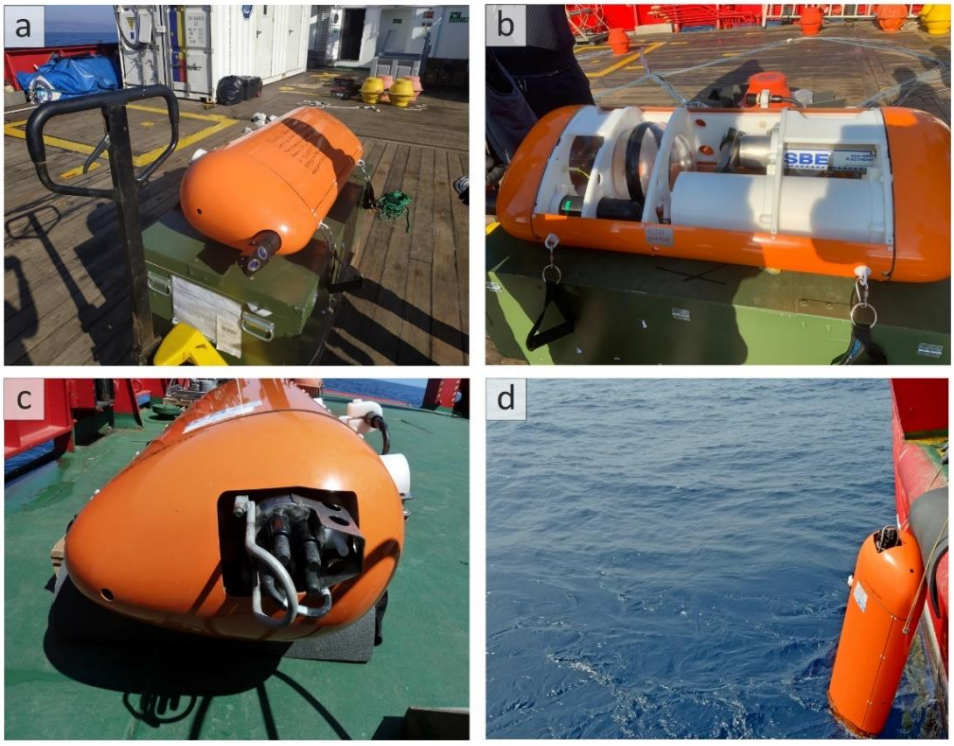

Figure 3.2. a) Preparation of the Aqualog during ABIDES-1 oceanographic cruise; b) Housing of the Aqualog profiler with the SeaBird 19 plus v2 CTD and the SeaPoint turbidity sensor, the buoyancy and the engine, and the microcontroller unit (MU); c) Detail of the CTD and turbidity sensors installed in the Aqualog profiler; d) deployment of the Aqualog profiler in the Palamós Canyon during ABIDES-1 oceanographic cruise.

The Aqualog software allows the user to develop a custom profiling schedule by setting the maximum and minimum profiling depths, and the time of each profile cycle. At the beginning of a profiling cycle, the microcontroller unit (MU) wakes up the system from “sleep mode” and

initiates the “profiling mode”. The MU evaluates the condition of the electronics by continuously monitoring electric current and voltage. It also controls all the instruments that are accommodated in the Aqualog (Fig. 3.2). After completing a cycle, the MU initiates again “sleep mode”. At this point, it is important to stress out that between profiling cycles, the Aqualog is parked in the aphotic zone to avoid extensive biofouling. The MU can host a pressure system, or alternatively, the pressure data from the CTD can be used. The former configuration provides redundancy in case of a CTD failure, while the latter allows for larger battery duration. The mooring wire has also attached two magnetic switches at the top and the bottom of the profiler, which are used to define the profiling depth range automatically. The Aqualog is equipped with a motor that propels the profiler up and down a mooring wire (made of stainless steel or Kevlar) at speeds between 0.15 and 0.25 $m \cdot s^{-1}$ and, during stops, fixes its position on the mooring wire while minimizing energy consumption (Carlson et al., 2013) (Fig. 3.2). The typical profiling depth range of the Aqualog varies from 5 to 600 m, although its titanium instrument housing allows the maximum depth of profiling to reach 3000 m. The Aqualog can work in conditions of strong horizontal currents up to 0.8 $m \cdot s^{-1}$ and at mooring inclinations of 10-15 º from the vertical.

The Aqualog was successfully used between 2010 and 2012 for scientific research in many seas around the world (i.e., the Baltic, Black, Japan/East, Kara, Mediterranean, and Red Seas). For example, in 2012, the Aqualog was deployed inside a submarine canyon, for the first time, in order to monitor the full water column. Until then, the tracking of water masses was mainly carried through extensive deployments of moorings, accompanied with hydrographic sampling, maintenance, and recovery periods, without a proper tracking of water masses’ temporal evolution. The goal of this study was to explore the temporal and vertical characteristics of the hydrographic structure inside the Besòs Canyon (Catalan margin, NW Mediterranean) (Fig. 2.1) and explore the effects of fine-scale effects on the variability of water masses in the water column, complementing previous measurements made with classical instruments (Solé et al., 2016). However, in this study the evolution of the nepheloid layer structure was not studied, even the great flexibility of this profiling device in incorporating different sensors to explore it.

For the purpose of this Thesis, the Aqualog was used to assess the temporal evolution of water masses and the nepheloid layer structure within Foix and Palamós submarine canyons, incising the Catalan margin (**Chapters 4** and **5**). In the Foix Canyon’s deployment, the Aqualog was programmed to perform one up- and down-cast per day, whereas in the Palamós Canyon’s deployment, it was programmed to perform two up- and down-casts per day. In both experiments, the Aqualog was equipped with a SeaBird 19 plus v2 CTD probe configured to measure temperature, salinity and pressure at 4 Hz (i.e., 4 scans per second). The Aqualog was also equipped with a SeaPoint turbidity sensor, programmed to measure water turbidity in Formazin Turbidity Units (FTU) by detecting scattered light from suspended particles at 0-25 FTU range, at 1 Hz (i.e., 1 scan per second) (Fig. 3.2).

3.2.1.2. Near-bottom instrumentation

In order to evaluate near-bottom sediment dynamics, the lower portion of the mooring line is often equipped with near-bottom instrumentation. In the Palamós Canyon deployment (**Chapter 5**), it mainly consisted of a single point Nortek Aquadopp current meter placed at 6 meters above the bottom (mab) that sampled at 5 min sampling interval (Fig. 3.3b). It uses the Doppler shift principle as the basis for its measurements by transmitting a short pulse of sound into the water in sequence. As the sound propagates, small particles or air bubbles in the water reflect a portion of the energy, while the backscatter energy is picked up by the transducers and further analysed. A microprocessor computer vector averages speed and direction over a sampling interval (in our case 5 min) in an area of 0.5-2 m from the instrument. The current meter was coupled with a SeaBird SBE-37 that provided pressure, temperature and salinity data, the latter using the electrical conductivity of the seawater (Fig. 3.3b). Additionally, closer to the bottom (at 5 mab), the mooring line sustained an AQUA-logger 210 TY equipped with temperature and pressure sensors, and a SeaPoint turbidity sensor that measured at 1 min sampling interval (Fig. 3.3b). The turbidity sensor uses the optical backscatter method, which relies on optical scattering of infra-red light from suspended particles and measures in FTU. The logger was set to operate in auto-gain mode (i.e., the logger goes over the different gains at the time of measuring and selects automatically the suitable turbidity range that does not saturate the signal), allowing to measure turbidity readings up to 2000 FTU.

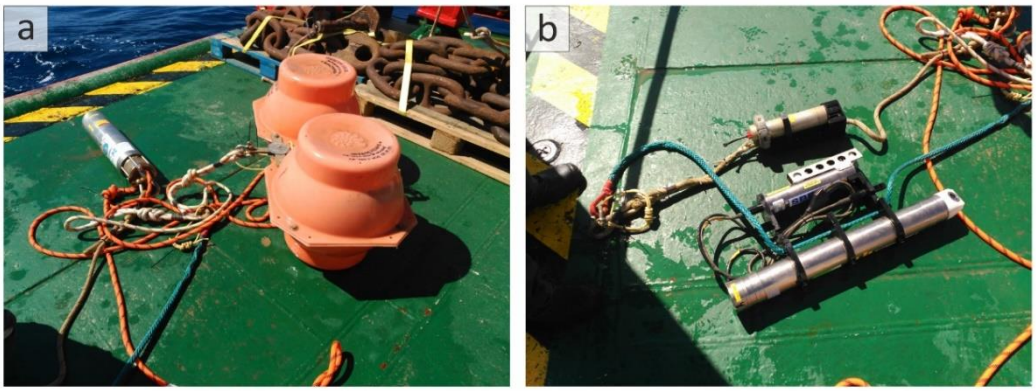

Figure 3.3. Oceanographic instrumentation installed at the bottom part of the mooring line employed in Palamós Canyon. a) Acoustic release and b) near-bottom Aquadopp current meter coupled with a SBE-37 and an AQUA-logger 210 TY equipped with a temperature and a pressure sensor, as well as a SeaPoint turbidity sensor.

3.2.2. Seafloor cabled observatories

Technically, seafloor observatories are described as unmanned stations, placed at a fixed site, capable of operating in the long-term on the seafloor, and supporting the operation of a number of instrumented packages and sensors related to various disciplines. They are connected to land either acoustically or via a seafloor node to a surface buoy or a fibre-optic cable (NRC, 2000;

Favali and Beranzoli, 2006). Seafloor observatories are characterised by the following basic elements: multiple payloads, autonomy, capability to communicate, possibility to be remotely re-configured, accurate positioning, and compatible data acquisition procedures with shore stations. Seafloor observatories can have different configurations: autonomous, acoustic linked, and cabled. **Chapter 6** focuses on the third type, exploring the capabilities of a seafloor cabled observatory to assess the nepheloid layer structure and variability off Vancouver Island.

Seafloor cabled observatory infrastructures consist of a submarine cable that provides power and real-time communication and control capabilities to instrumented nodes along a cabled system. The first observatories started in the 1950s (NRC, 2003). For instance, the Sound Surveillance System (SOSUS) was developed by the US Navy in the late 1950s to detect, track and classify submarines using hydrophone arrays that were connected to a shore station by a submarine cable, off the west coast of Washington State. During the 1960s, seafloor observatories gained importance amongst the scientific community, particularly in seismic and geomagnetic programmes (Montagner and Lancelot, 1995; Lowes, 2002). The oldest seafloor cabled observatory is the Field Research Facility off Duck, North Carolina, which was established in 1977 by the US Army Corps of Engineers to study coastal waves, tides, currents, and other meteorological phenomena. Since the 1990s, many important workshops have been organised outlining long-term scientific strategies of submarine observatories (e.g., Romanowicz et al., 2001; Beranzoli et al., 2002; Kasahara and Chave, 2003; Yada et al., 2004). Examples of the various programs found around the word can be found in Favali et al. (2010). Integrated seafloor cabled observatories equipped with biological and chemical sensors, or other sampling systems such as sediment traps or video camera structures have been recently integrated.

Some installations have been specially developed for shallow water applications to assess near-surface conditions and strong hydrodynamic forces, such as “SmartBay” in Galway (Ireland) at 22 m water depth (Cullen et al., 2015), the EMSO-Molène in the Atlantic Ocean at 18 m depth, the EMSO in the Mediterranean Sea at 20-30 m depth, the OBSEA observatory in the NW Mediterranean Sea at 20 m depth (Del-Rio et al., 2020), the LEO-15 observatory on the East coast of New Jersey in USA (Forrester et al., 1997), and the COSYNA (Coastal Observing System for Northern and Arctic Seas) at ~10 m depth (Baschek et al., 2017; Fischer et al., 2020). Other installations, such as MARS, VENUS (Dewey et al., 2007), NEPTUNE (Best et al., 2007), ALOHA (Favali et al., 2015), or LoVe (Godø et al., 2014) have been installed at relatively greater depths (Best et al., 2016) (Fig. 3.4).

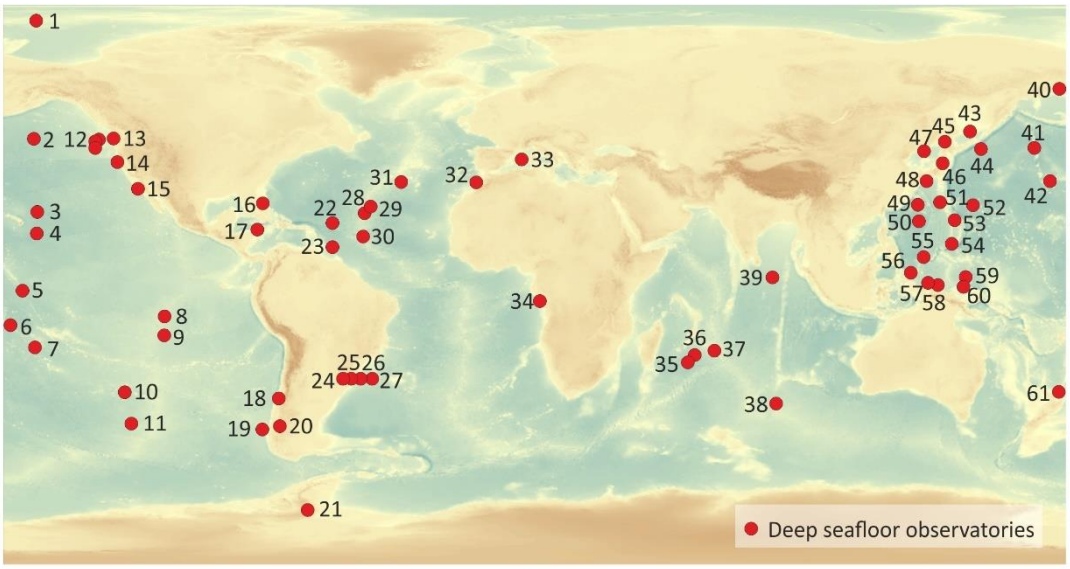

Figure 3.4. Location of some of the current seafloor observatories in the world oceans: 1) Arctic Ocean [a], 2) Aleutian Abyssal Plain [a], 3) Off Hawaii [a], 4) Hawaii [a], 5) Equatorial Pacific Ocean [a], 6) Central Pacific Ocean [a], 7) Eastern Pacific [a], 8) East Pacific Rise 14S and 15S [a], 9) East Pacific Rise 17S and 18S [a], 10) Southeast Pacific Ocean [a], 11) French Polynesia [a], 12) Cabled Axial Seamount Array [b], 13) NEPTUNE observatory [c], 14) Cabled Continental Margin Array – Oregon Slope Base [b], 15) Station M – MBARI [d], 16) Florida Cable [e], 17) Caribbean Sea [a], 18) Chilean marginal sea [a], 19) Southeast Pacific and Chilean EEZ area [a], 20) Chilean Coast [a], 21) Station B [f], 22) MOVE6 [g], 23) MOVE7 [g], 24) PIES Site A [h], 25) PIES Site B [h], 26) PIES Site C [h], 27) PIES Site D [h], 28) Mid-Atlantic Ridge 26N [a], 29) Mid-Atlantic Ridge Kane FZ [a], 30) Mid-Atlantic Ridge 15-20'FZ [a], 31) Mid-Atlantic Ridge 36N [a], 32) Iberian Margin [i], 33) ANTARES [j], 34) DELOS A [k], 35) South-west Indian Ridge Atlantis II FZ [a], 36) Southwest Indian Ridge [a], 37) Central Indian Ridge [a], 38) Antarctic Ocean [a], 39) Ninetyeast Ridge [a], 40) Bering Sea [a], 41) North Pacific Ocean [a], 42) Hess Rise [a], 43) Okhotsk Sea [a], 44) Northwest Pacific Ocean [a], 45) Off Shimokita Peninsula [a], 46) North Western Pacific [a], 47) Japan Sea [a], 48) Suruga Bay [a], 49) West Philippine Basin [a], 50) Central Basin Fault [a], 51) Sumisu Island [a], 52) Minami Torishima [a], 53) Mariana Arc [a], 54) Mariana Trench [a], 55) Kyushu-Palau Ridge [a], 56) Ayu Trough [a], 57), West Caroline Basin [a], 58) Off Papua New Guinea [a], 59) Lyra Basin [a], 60) Manus Basin [a], 61) Havre Trough [a]. ([a] JAMSTEC Data and Sample Research System for Whole Cruise information, DARWIN; [b] Ocean Observatories Initiative, OOI; [c] Ocean Networks Canada, ONC; [d] SOCCOM Project; [e] Western Boundary Time Series, WBTS; [f] FOODBANCS; [g] Meridional Overturning Variability Experiment; [h] SAM Observatory Project; [i] EMSO-ERIC Observatory; [j] Fixed-point Open Ocean Observatories, FixO3; [k] Deep-Ocean Environmental Long-term Observatory System, DELOS). **Source:** Bathymetry extracted from GEBCO 2020 Grid, GEBCO Compilation Group, 2020 (doi:10.5285/a29c5465-b138-234d-e053-6c86abc040b9); Location of the observatories extracted from Deep Ocean Observing Strategy (https://deepoceanobserving.org/deep-ocean-observations/).

Data for this Thesis were acquired from the NEPTUNE (www.neptunecanada.ca) cabled seafloor observatory (**Chapter 6**). The Ocean Networks Canada (ONC) corporation is responsible to oversee the management, development, and operation of this and the VENUS observatory (www.oceannetworks.ca). The NEPTUNE infrastructure is an 840 km optic cable with five active nodes, and ranges from 23 to 2660 m depth creating high-resolution, multiparameter platforms for the multidisciplinary study of deep-sea ecosystems of the NE Pacific, including hydrothermal vents, methane seeps and submarine canyons (Barnes et al., 2011). The cable runs from Vancouver Island across the continental shelf into the deep Cascadia Basin, Endeavour segment of the Juan de Fuca ridge and back, forming a loop (Fig. 3.5). The design using a cable loop has the advantage of redundancy, meaning that if there is a break in the cable, the data can still be

sent to the shore station and power is still available to nodes. The NEPTUNE shore station at Port Alberni on Vancouver Island provides power and communication to the five nodes and sends the collected data from the NEPTUNE observatory via fibre-optic cable to the University of Victoria Data Management and Archive Station (DMAS, also known as Oceans 2.0). Besides storing the acquired data, the DMAS enables remote interactive controls of instruments. All data are freely available to the public through web-based interfaces in near-real time (https://data.oceannetworks.ca/DataSearch) (Matabos et al., 2016).

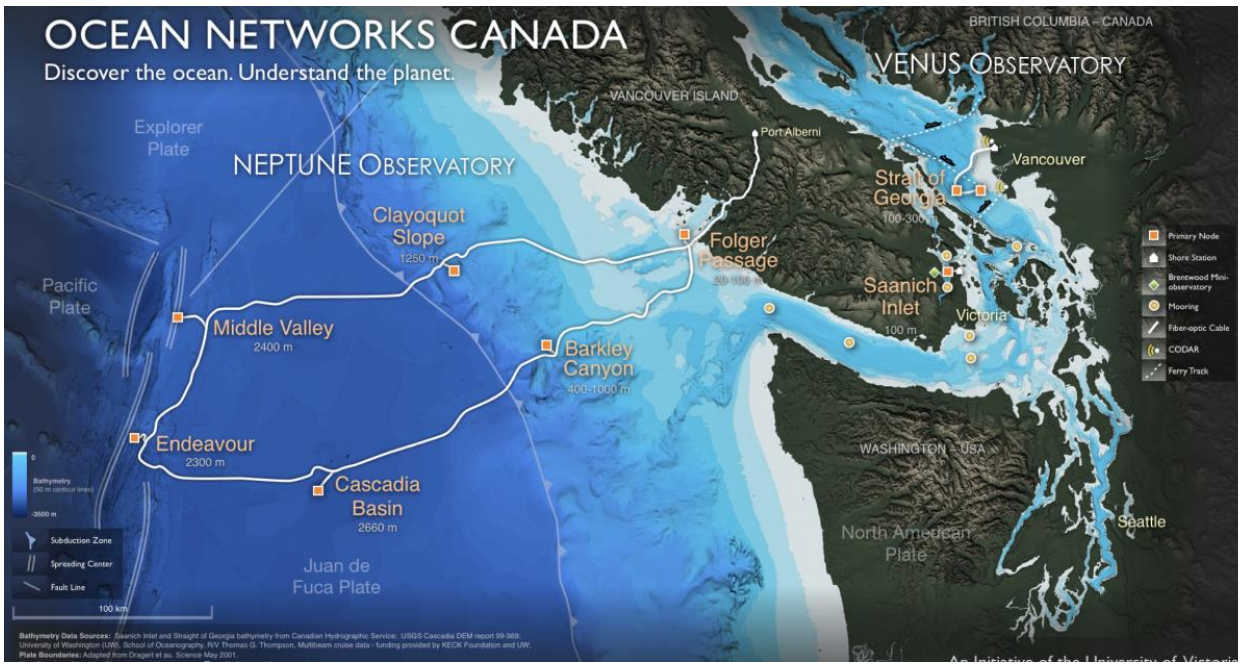

Figure 3.5. Bathymetric map showing the ONC's NEPTUNE and the coastal VENUS seafloor cabled observatories. **Source:** Ocean Networks Canada (www.oceannetworks.ca).

3.2.2.1. Vertical profiling system

For the purpose of this Thesis, data time-series were acquired from instruments on the BUS Instrumented platform. There, the Vertical Profiling System (VPS) is fixed to the seafloor at 390 m depth with a bottom-mounted winch that controls a buoyant platform to which oceanographic instruments are mounted (Fig. 3.6). The VPS is classified as a winched system, which means that it profiles by paying in/out cable from a platform. These payload systems have a large positive buoyancy that allows them to reach the surface, but they require a lot of power when working against buoyancy.

The VPS performs several profiles per day to almost the surface (25 depth), giving a temporal evolution of water masses, their dynamics and characteristics. For safety reasons, the VPS starts profiling at 375 m depth, leaving a gap of 19 m from the bottom for the docking procedure that ensures the entire package of floats and instruments safely returns to its cage on the bottom.

This docking procedure is set automatically, slowing its speed down to 1/10 the normal speed, and fully stopping in its cage after a few minutes.

The VPS is equipped with a SeaBird 19 plus v2 CTD probe to measure temperature, salinity, pressure and density at 0.25 second intervals. The profiler is also equipped with a WET Labs ECO FLNTU sensor, programmed to measure fluorescence ($\mu g \cdot L^{-1}$) and backscatter turbidity (FTU) at 1 second interval. Additionally, dissolved oxygen data was recorded by an Aandera Oxygen Optode 3830 sensor that sampled at 3 second intervals (Fig. 3.6; Table 3.2).

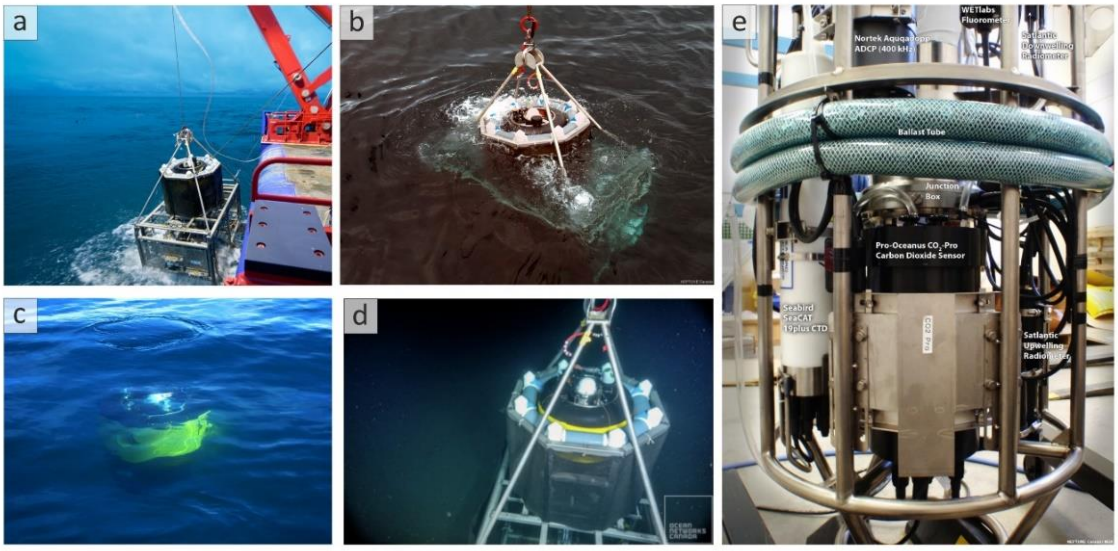

Figure 3.6. a) Deployment of the VPS platform; b) Upper vision of the instruments installed within the instrument package during a deployment; c) VPS's instrument float surfaces at the Barkley Upper Slope (BUS) site; d) Underwater photograph of the VPS; e) Some of the instruments contained within the float of the VPS. **Source:** Ocean Networks Canada.

3.2.2.2. Acoustic Doppler Current Profiler (ADCP)

In order to evaluate current dynamics potentially affecting the transport of sediments in the slope off Vancouver Island, a low-frequency upward-looking 75 kHz ADCP connected to the BUS Instrumented platform was used to measure current velocity and direction through the water column. The device is configured with vertically-stacked 8 m-thick measurement cells, with the centre of the first valid cell at 16 m above the bottom. These settings allow current velocity and direction measurements up to about 400 m above the bottom. Data are sampled at 2 sec, although the system provides valid current data at 1-min sampling interval (Table 3.2). Noise data was recorded near the seafloor due to direct vertical sidelobe reflection, and therefore these data have not been taken into account when processed.

Table 3.2. Summary of all instruments used from the Barkley Upper Slope (BUS) Instrument Platform, including the VPS and the low frequency 75 kHz ADCP dataset used in this study, spanning from August 14 to November 23, 2018.

Instrument		Coordinates		Depth (m)	Device	Property	Sampling frequency (s)
		Latitude (N)	Longitude (W)				
VPS	CTD probe	48º 25.64'	126º 10.44'	25-374	SeaCAT SBE 19plus v2	Temperature (ºC) Practical Salinity (psu) Pressure (dbar) Sigma-t ($kg \cdot m^{-3}$)	0.25
	Turbidity/ Fluorometer sensor	48º 25.64'	126º 10.44'	25-374	WET Labs ECO FLNTU	Fluorescence ($\mu g \cdot L^{-1}$) Turbidity (FTU)	1
	Dissolved oxygen sensor	48º 25.64'	126º 10.44'	25-374	Aandera Oxygen Optode 3830	Oxygen concentration corrected ($mL \cdot L^{-1}$) Oxygen concentration uncorrected ($mL \cdot L^{-1}$)	3
75 kHz ADCP	ADCP	48º 25.64'	126º 10.47'	16-416	RDI	Current velocity ($m \cdot s^{-1}$) Current direction (º) Backscatter (dB)	2

3.3. Hydrographic transect

Conductivity, Temperature, and Depth (CTD) profilers consist of a package of electronic devices used to detect how the conductivity and temperature of water bodies change relative to depth. CTD profilers are essential tools used in all disciplines of oceanography, providing information about physical and chemical properties of the water column. Basically, a CTD package comprises a temperature sensor (fast response thermistor), a conductivity cell, and a pressure sensor that can be either connected to conducting cable for real-time data or as a self-recording instrument. Additional sensors can be also attached to the CTD package, such as those to measure fluorescence (to determine chlorophyll), optical transmission (to measure turbidity), and oxygen. On a shipboard, vertically profiling CTD with real-time data transmission, the CTD package will have the electronics located at the bottom part of the package. The CTD may also include a rosette of sampling bottles attached to the frame of the CTD. These bottles open at the start of any vertical profile and can be fired from the desk command onboard a research vessel at chosen depths to allow water samples to be taken. During vertical CTD profiling, the down-casts are used for the water column measurements, whereas the up-casts are used for stopping the CTD to sample the water column using the rosette to obtain discrete water samples.$

CTD vertical profiles collected for this Thesis were acquired in June 2017 during the oceanographic cruise ABIDES-2 (**Chapter 5**). During this cruise, a ship-based hydrographic transect was conducted in the study area onboard the R/V *García del Cid*, which consisted in 15 vertical stations (Table 3.3) across the Palamós Canyon's head collected using a SeaBird 911 CTD probe, sampling at 24 Hz. The SBE 911 CTD was coupled with a SeaPoint turbidity sensor that provided data in FTU.

Table 3.3. Location, depths and dates of the CTD vertical stations acquired in June 2017 during the oceanographic cruise ABIDES-2.

Station	Date	Time	Latitude (N)	Longitude (E)	Depth
1	June 7	14:22	41º 51.07'	3º 16.44'	156.2
2	June 7	14:51	41º 51.25'	3º 16.56'	252.4
3	June 7	15:42	41º 51.51'	3º 16.63'	404.0
4	June 7	16:31	41º 51.68'	3º 16.77'	512.5
5	June 7	17:17	41º 51.88'	3º 16.88'	718.1
6	June 7	18:30	41º 52.07'	3º 16.97'	835.5
7	June 7	19:42	41º 52.29'	3º 17.10'	900.6
8	June 7	20:58	41º 52.45'	3º 17.25'	788.1
9	June 7	22:14	41º 52.70'	3º 17.36'	624.0
10	June 7	23:14	41º 52.87'	3º 17.45'	587.0
11	June 8	00:17	41º 53.10'	3º 17.519'	443.0
12	June 8	01:11	41º 53.29'	3º 17.629'	335.0
13	June 8	01:55	41º 53.48'	3º 17.699'	300.6
14	June 8	02:36	41º 53.69'	3º 17.809'	265.6
15	June 8	03:16	41º 53.89'	3º 17.920'	183.9

3.4. Hydrographic data analysis

3.4.1. Hydrographic data processing

CTD vertical profiles acquired during the hydrographic transect (conducted after ABIDES-2 oceanographic cruise), and those acquired by the Aqualog profiler during the Foix Canyon and Palamós Canyon mooring deployments, as well as by the VPS deployment on the upper slope region off Vancouver Island were analysed similarly in this Thesis. As previously mentioned, the CTD probe is normally oriented to sample on the downcast (i.e., sensors facing downward). When

the CTD is raised, there is ~100 cm of instrument and cage that block the sensors and can disturb the water column gradients during the upcast, preventing a clear up-downcast agreement. Unless specified, the down-cast data of the hydrographic profile was utilized.

During the Foix Canyon mooring deployment, the Aqualog was programmed to perform one up- and down-cast per day and acquired 58 hydrographic profiles. During the Palamós Canyon mooring deployment, the Aqualog was programmed to perform two up- and down-casts per day and acquired 118 hydrographic profiles. In both experiments, the Aqualog provided hydrographic data on temperature, salinity, pressure and turbidity within these two submarine canyons. In the Barkley Upper Slope (BUS) site, the VPS performed four up- and down-casts per day, acquiring a total of 765 hydrographic profiles for the monitoring period. Despite the differences between the two profilers, CTD and turbidity data collected by the Aqualog and the VPS were similarly processed.

First, pressure data was used to identify and evaluate the motion of both profilers, and to keep the data corresponding to profiling mode. In the case of the Aqualog, data was already pre-processed in the MU. The data flagged as “sleep mode” was removed from the Aqualog’s dataset. In the case of the VPS, pressure data was manually processed, and only those values registered when the VPS was at its cage or stopped at the surface were removed, keeping those corresponding to the up- and down-casts. Second, a MATLAB script was developed to automatically identify and remove negative values marked as “bad quality data”. In case of the Aqualog, this step was carried out manually, whereas for the VPS this data was already flagged by ONC’s data quality and assurance (QA/QC) process. Afterwards, MATLAB’s function *SpikeRemoval* (Solomon et al., 2001) was run over the entire dataset to delete undesired transients and spikes exceeding a threshold value. The threshold is defined as mean ± a number of standard deviations (std) of windowed data centred at spike locations. For the Aqualog’s dataset, the most suitable threshold was defined as 3 std and 1 pass for detection and replacement. For the VPS dataset, the most suitable threshold was defined as 1 std and 3 passes. Finally, to proceed with a homogeneous methodology for all parameters, both datasets were interpolated to 1 m of vertical resolution. The measured and calculated parameters were represented using Ocean Data View (ODV) software (Schlitzer, 2010).

During the hydrographic transect conducted after ABIDES-2 oceanographic cruise, CTD data were obtained from 15 vertical stations during a ship-based CTD transect across Palamós Canyon’s head. Post-processing of this CTD data was carried out following the methods found in White et al. (2008). CTD data was processed using SBE Data Processing’s SeaBird software. First, data was converted into engineering units using the data conversion function. The data was then filtered using two low-pass filters (0.03 s and 0.15 s, respectively) to eliminate any high-frequency fluctuations. Second, variables such as salinity, density, potential density, and potential temperature were derived from primary variables (conductivity, temperature, pressure). A loop was then applied to remove effects of the CTD moving up and down the water column with the pitch, roll and heave of the ship. Any negative pressure changes on the downcast (i.e., CTD

moving upwards) or positive pressure changes on the upcast (i.e., CTD moving downwards) were flagged as "bad quality" and were removed. The minimum CTD velocity applied was 0.15 s. Finally, data were binned to 1 m depth intervals. As the sensor package was installed on the bottom of the CTD rosette, the downcast data were converted to .txt to be further analysed using MATLAB 2017a and visualized using ODV software.

3.4.2. Visualization of hydrographic data

After a first removal of data spikes with the MATLAB software, processed hydrographic data were introduced into the ODV software. Principally, this software package works with oceanographic and other geo-referenced profile and time-series data, and produces high-quality station maps, general property-property plots of one or more stations, scatter plots of selected stations, property sections along cruise tracks, and property distributions on general 3D surfaces (Schlitzer, 2002).

First, temperature, conductivity, pressure, and turbidity geo-referenced data underwent a quality-control check procedure to eliminate any remaining spikes in the data. Afterwards, a number of derived variables (i.e., potential temperature, potential density, salinity, and 3D surfaces, such as isopycnals) were calculated from the input data. Then, interpolated maps were produced. Depending on the type of data being displayed, two different modes were used: the scatter mode and the section mode. In scatter mode, the data of all stations can be displayed and supports Z variables in addition to the X and Y variables. The value of a Z variable at a given X/Y point is displayed by ODV either by showing the actual numerical value or by filling it with a value-dependent colour. This mode was used to build the *T-S* diagrams presented in this Thesis. The section mode also supports Z variables, but the set of stations (even if it is one single station) is restricted to a section band, which usually follows the track of the given transect. This mode is useful to represent property distributions for all stations along an entire cruise or monitoring period. In particular, this mode was used to build time-series of the distribution of water properties, and to display the data from the hydrographic transect.

Finally, interpolated plots, either scatters or sections, were created using the Data Interpolating Variational Analysis (DIVA) gridding software (Troupin et al., 2012) included in ODV (DIVA parameters: scale lengths chosen automatically; quality limit = 3.0; excluding outliers).

3.4.3. Turbidity data treatment

During the Foix Canyon mooring deployment (**Chapter 4**), turbidity measurements in FTU collected with a SeaPoint turbidity sensor installed in the Aqualog profiler were converted to estimates of SSC, in $mg \cdot L^{-1}$, using the general calibration of Guillén et al. (2000) for the Western Mediterranean:

$$SSC = 0.79 \cdot (FTU - FTU_{min}) \quad (equation\ 3.1)$$

Values were adapted to the measurements made in the study site, where FTU_{min} is the lowest turbidity measured during the monitoring deployment period in the clear water minimum, which can also be attributed to the background concentration of suspended particulate matter.

During the Palamós Canyon mooring deployment (**Chapter 5**), turbidity measurements in FTU were collected with different SeaPoint turbidity sensors installed in a mooring line (installed in the Aqualog, or in a self-contained near-bottom AQUA-logger). Water and sediment samples at the Palamós Canyon area were collected during the ABIDES-ROV oceanographic cruise for calibration purposes and thus, reported FTU values could be converted into concentration units. During this cruise, seawater samples for calibration were taken with Niskin bottles coupled to a CTD. Sediment samples for calibration were obtained from a pushcore of 15 cm of length collected at the northern flank of Palamós Canyon at 898 m depth by means of a Remoted Operated Vehicle (ROV).

For the Cascadia margin (NE Pacific), turbidity measurements in FTU could not be converted into estimates of SSC since there is no turbidity calibration in the region nor at the entire Canadian NE Pacific margin. Therefore, turbidity values have been kept arbitrary and expressed in FTU.

3.4.4. Laboratory calibration

To calibrate the turbidity measurements obtained in Palamós Canyon (**Chapter 5**), a laboratory set-up with an 80 L cylindrical plastic container was used as the test tank. A manufactured structure sustaining an AQUA-logger SeaPoint turbidimeter was submerged in the water but close to the surface (Fig. 3.7). This position enables a measuring range that ideally covers the whole water column in the tank. Beforehand, the minimum required distance of the turbidity sensor was already determined. The sensor's blind side was oriented to the wall of the tank, ensuring that the whole inner volume was covered during the turbidity experiments.

To keep sediment particles in homogeneous suspension, the water of the tank was steadily mixed with a mixer. The mixing velocity was chosen carefully. With the highest possible speed, the mixer does not stay at its position and slings around, and vortices can form, whereas it has to be high enough to keep the test material in suspension and impede particle settling. Several tests were performed to determine appropriate working conditions of the mixer. Additionally, to counteract the chance of reflection created by the stirrer itself or any material, all working equipment, including the tank, was black. Before a new measuring was executed, all materials (tank, stirring device and sensors' head) were rinsed with distilled water to make sure that all particles were removed, and suspension was inhibited. The tank was filled with 30 L of seawater previously collected during ABIDES project's oceanographic cruises, and the mixing device was switched on (Fig. 3.7). The water was collected at a clear water zone in order to achieve the lowest possible initial turbidity of approximately 0 FTU before starting the actual turbidity measurements.

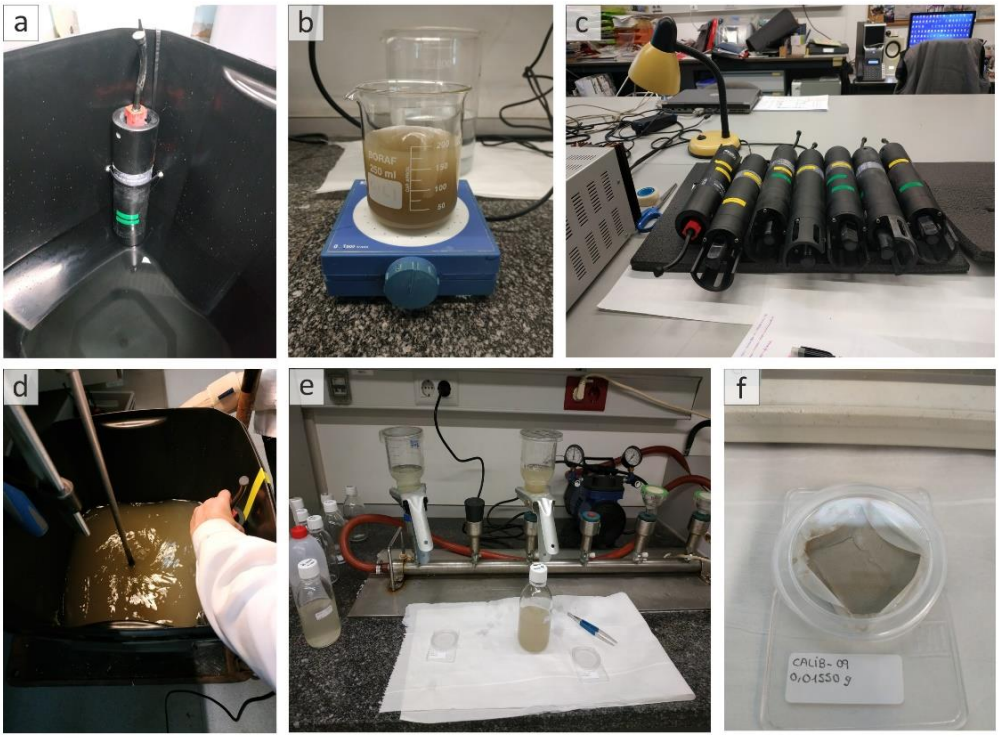

Figure 3.7. Laboratory calibration set-up. a) AQUA-logger attached to the test tank. This position allows for correct measurement that covers the whole water column in the tank; b) Dilution of sediment samples into a known volume of seawater before injection to the test tank; c) Preparation of the seven turbidimeters that were used in the calibration experiment; d) Deployment of a turbidimeter to the test tank and measuring procedure. The mixing device is also shown; e) Vacuum filtering onto pre-weighed Nucleopore membranes using a laboratory filtration system; e) Dry Nucleopore membrane after desiccation and weight.

After achieving a constant background turbidity in a time interval of 3 minutes, the experiment was initiated, and sediment samples were given in suspension. Beforehand, sediment samples were diluted in a known volume of seawater before injected to the test tank (Fig. 3.7). This ensures the correct dissolution of sediments in the water and prevents the forming of agglutinated particles. A certain quantity of this mixture was added to the test tank to set the desired turbidity, after the water was stirred for at least 2 minutes to let the particles spread out evenly. This calibration was carried out by deploying seven different AQUA-logger SeaPoint turbidity sensors to the test tank, which were introduced alternatively at each concentration interval (Fig. 3.7). For each adjusted interval, turbidity was measured every 5 seconds in a period of 2 minutes. The resulting data was averaged, and the standard deviation was determined. Detailed information on the concentration intervals is provided in Table 3.4.

Table 3.4. Detailed information of the turbidity intervals employed in the laboratory calibration and FTU values obtained from the different turbidity sensors. Averaged SSC (mg·L^{-1}) values obtained after weighing the Nucleopore membranes are also provided.

Turbidity range	FTU measured by different turbidity sensors										SSC
	024-030	024-095	024-096	024-097	024-098	024-099	024-102	024-103	Mean	Std. dev	
CWM	0.51	0.36	0.56	0.53	0.51	0.59	0.54	0.35	0.49	0.09	0.54
2 FTU	1.78	2.23	2.02	1.98	1.90	1.68	1.93	1.81	1.92	0.17	2.05
5 FTU	4.73	4.22	5.38	5.27	5.01	4.74	5.02	5.16	4.94	0.37	5.03
10 FTU	9.06	8.63	10.51	10.18	9.61	9.34	9.75	10.23	9.67	0.64	10.87
20 FTU	18.63	20.00	21.96	20.31	19.40	19.93	20.13	20.97	20.17	0.99	20.95
50 FTU	44.19	50.02	51.54	48.36	49.40	49.96	48.58	50.78	48.73	2.33	52.32
100 FTU	94.50	83.64	110.34	102.84	99.59	98.56	100.55	108.42	99.81	8.33	120.77
200 FTU	185.24	206.14	212.21	206.32	198.04	194.15	202.24	210.09	201.8	8.97	231.35
500 FTU	444.51	-	510.56	493.17	480.74	491.90	484.02	529.50	490.6	26.4	562.44

With continuous stirring, water samples were taken at given FTU readings. Afterwards, the water samples were vacuum filtered up to filter saturation onto pre-weighed Nucleopore membranes of 0.4 µm pore size (Fig. 3.7). Nucleopore membranes were dried by desiccation and weighed gravimetrically using a 10^{-5} balance with static reduction. Filters were weighed until three consecutive readings with four decimal places identical were obtained (Table A.1). The average weight of the dry residue (Table 3.4), divided by the volume of water filtered, rendered SSC in $mg \cdot L^{-1}$. Pairs of FTU/SSC data points for each turbidimeter yielded the following linear regression (Fig. 3.8).

$$SSC = 1.14 \cdot FTU - 0.37 \ (r^2 = 0.99)_{(equation\ 3.2)}$$

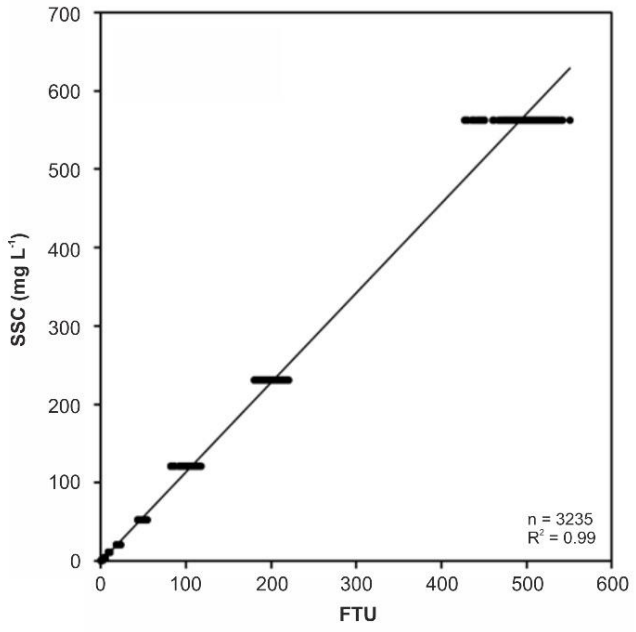

Figure 3.8. Linear regression between the turbidity signal (FTU) and the measured SSC ($mg \cdot L^{-1}$) for the eight turbidity sensors used in the laboratory calibration.

3.4.5. Calculation of the net particulate standing crop

Following Biscaye and Eittreim (1977)'s model (Fig. 1.5), the minimum in light scattering, or in SSC, found at the upper limit of the BNL is called clear water minimum (CWM), and all SPM found below is defined as the Gross Particulate Standing Crop (GPSC). This model assumes that all sediment particles above the CWM are falling through the water column, whereas the SPM below the clear water which is in excess is defined as the Net Particulate Standing Crop (NPSC), and represents particles mixed upward from the bottom (Biscaye and Eittreim, 1977).

The NPSC was originally defined by Biscaye and Eittreim (1977) in oceanic waters for BNLs as the suspended particulate matter that is found below the CWM. However, the estimation of the

NPSC approached in this Thesis (**Chapters 4** and **5**) differs from the definition of Biscaye and Eittreim (1977) because we also take into account the contribution of sediment particles contributing to INLs at various levels in the water column, instead of only considering the particles below the clear water minimum (Karageorgis and Anagnostou, 2003). To calculate the NPSC (g·cm^{-2}), the SSC at each level of the water column was integrated, thereby providing an estimation of the input of particles introduced in the water column, following:

$$NPSC = \frac{1}{h}\int_0^h SSC\ (z)\ dz \qquad (equation\ 3.3)$$

where h stands for the depth of the considered water column (in m) and $SSC\ (z)$ represents the estimated SSC (in mg·L^{-1}) (Karageorgis and Anagnostou, 2003).

3.4.6. Current data processing and determination of suspended sediment fluxes

Near-bottom currents and SSC data collected during the Palamós Canyon mooring deployment were used to calculate instantaneous suspended sediment fluxes, as well as time-integrated cumulative suspended sediment transport at each timestep (i), following:

$$Flux_i = V_i \times C_i = current_i \times SSC_i \qquad (equation\ 3.4)$$

where $current_i$, in m·s^{-1}, multiplied by SSC, in mg·L^{-1}, yielded to instantaneous suspended sediment flux in g·m^{-2}s^{-1}.

Then, the time-integrated cumulative suspended sediment transport (in kg·m^{-2}) can be calculated as following:

$$Cumulative\ transport = \sum_{i=1}^{N} Flux_i \times \Delta t\ = Sum\ of\ flux_i\ x\ timestep \qquad (equation\ 3.5)$$

where the timestep was 5 min (or 300 s), corresponding to the measuring interval of the near-bottom current meter placed at 923 m depth.

An intermediary computation prior to calculating suspended sediment fluxes and time-integrated cumulative transport is needed to estimate the current components with respect to geographic coordinates. To obtain the along- and across-canyon instantaneous suspended sediment fluxes and the along- and the across-canyon cumulative suspended sediment transport, the coordinate system was rotated by applying an angle θ with respect to the main isobath orientation at the mooring site, using the bathymetric map of the study area as a reference (Fig. 5.1).

For the purpose of this Thesis, current components were rotated 70º counterclockwise, following:

$$V_i(along-canyon) = Speed_i \times \cos(90 + Dir_i + \theta) \quad (equation\ 3.6)$$

$$V_i(across-canyon) = Speed_i \times \sin(90 + Dir_i + \theta) \quad (equation\ 3.7)$$

Current measurements were also obtained from the upward-looking ADCP connected to the BUS Instrumented platform on the slope off Vancouver Island. In this case, pre-processed data included the down-sampling of the raw data to a 1-min average ensemble, and current velocities were presented for each East, North, and vertical components, respectively. A correlation threshold of 64 counts and an error velocity of 2 $m \cdot s^{-1}$ were used to screen the data. Within each vertical bin, only pings that were within these thresholds were used in the ensemble averaging. Additionally, post-processing of the data included the rotation of the currents dataset to estimate current components with respect to geographic coordinates. For the purpose of this Thesis, an θ of 30º was applied, which corresponded to the main orientation of the isobaths at the sampling site. We used the bathymetric map of the study site as a reference to obtain this information (Fig. 6.1). The rotation of the currents was carried out by applying 3.6 and 3.7 equations.

3.4.6.1. Uncertainties and error propagation on time series

Long time series have an uncertainty associated with errors on the measurement of the different variables, which deserve to be calculated to complete sediment flux and time-integrated calculations (Durrieu de Madron, 2019). These uncertainties are derived from measurements of particle concentration derived from turbidity, as well as the propagation error along time series. Hence, for any measure on a time series, we have an uncertainty on both along- and across-canyon current components (σ_v), an uncertainty on suspended sediment concentration (σ_c), and an uncertainty on suspended sediment fluxes (σ_F) and time-integrated cumulative transport (σ^2_{NF}) (Durrieu de Madron, 2019). Estimated parameters' uncertainties derived from the measurement errors corresponding to each independent time series are shown in the corresponding chapter in Table 5.1. The uncertainty (or error propagation) in suspended sediment flux, for each time step, can be calculated following:

$$\sigma_F^2 = \left(\frac{\partial F}{\partial Speed}\right)^2 \times \sigma^2_{Speed} + \left(\frac{\partial F}{\partial Dir}\right)^2 \times \sigma^2_{Dir} + \left(\frac{\partial F}{\partial Turb}\right)^2 \times \sigma^2_{Turb} \quad (equation\ 3.8)$$

$$\sigma_F^2 = \left([A \times Turb] \times cos(90 - Dir + \theta)\right)^2 \times \sigma^2_{Speed}$$

$$+ \left(-Speed \times [A \times Turb] \times sin(90 - Dir + \theta)\right)^2 \times \sigma^2_{Dir}$$

$$+ (A \times [Speed \times cos(90 - Dir + \theta)])^2 \times \sigma^2_{Turb}$$

The uncertainty associated to time-integrated cumulative transport (NF) is calculated following:

$$\sigma_{NF}^2 = \Delta t^2 \times \sum_{i=1}^{N} \sigma_{Flux_i}^2 \ (equation\ 3.9)$$

where the sum of individual variance at each time step multiplied by the square of the timestep yields to the net flux variance (σ_{NF}^2).

3.5. Identification of spatiotemporal patterns of trawling fleets using VMS and AIS data

One of the most effective ways to understand the impacts of bottom trawling is to delimit the spatial extension of bottom trawling grounds and the trawling intensity. This was often obtained from fishermen's logbooks (i.e., records of catch and effort), but this method can be inaccurate and have poor coverage. Technological advances related to global positioning systems (GPS) allowed fishing vessels to be equipped with these technologies, mainly for safety and management reasons.

Within the European Union, GPS equipment was introduced as satellite-based Vessel Monitoring System (VMS), also referred to as "blue boxes". Blue boxes are standardized transmitters that are protected and sealed against power cuts, the marine environment, and any type of manipulation. Each blue box consists of a positioning unit and a satellite-based transmission/reception station, which contains data logging and storage devices. Blue boxes provide information on vessels' position, direction, and speed by Inmarsat-C system to the Fishing Monitoring Centre in approximately 10 min at intervals of 2 h or less, which represents the typical transmission frequency for VMS. This system is also useful to determine each vessel's activity, that is sailing, fishing or drifting. In 2005, VMS became compulsory in fishing vessels with an equal to or overall exceeding length of 15 m (European Commission, 2003). For this Thesis, the spatial distribution of the fishing activity around the Foix Canyon (**Chapter 4**) was estimated using VMS positioning of bottom trawlers navigating at sustained speeds of less than 5 knots.

VMS data has been successfully implemented for surveillance purposes, allowing the quantification of fishing intensity quite efficiently at 200 m-grid (Gerritsen et al., 2013). Despite the increasing number of applications and tools, the extensive use of VMS data for scientific purposes is hindered by the difficulty of accessing control data, often due to confidentiality and personal data protection concerns (Natale et al., 2015). The increasing need to negotiate the access to VMS data with national control centres has limited the VMS research applications to specific fisheries and areas. Also, VMS data for research and impact assessment have some limitations, preventing proper spatial management. Such limitations include incomplete coverage of vessel activities, long duration between position records, and a lack of information on whether a vessel is actually fishing when the position is reported (Lambert et al., 2012). Therefore, VMS is not useful to describe complex movements of fishing vessels, since individual

hauls cannot even be properly identified, but is useful to provide a general overview of fishing grounds (Lambert et al., 2012).

To overcome these limitations, there has been an increasing interest in the potential use of publicly available Automatic Identification System (AIS) vessel tracking data to investigate fishing activity (Natale et al., 2015; Russo et al., 2016). AIS was introduced by the International Maritime Organisation (IMO) mainly to avoid ship collisions and to improve maritime safety and was compulsory for all passenger ships and other commercial vessels that exceeded 300 of gross tonnage. Then, the EU gradually implemented this mechanism to medium-large size fishing vessels and became fully compulsory since 2014 for all fishing vessels of more than 15 m of overall length (European Commission, 2009). Differently from VMS, which is based on point-to-point satellite communications between the vessels and the ground centres, AIS messages are provided omni-directionally at intervals that can vary from 2 seconds to 3 minutes to nearby AIS-bearing ships, coastal stations, and satellites, enabling the monitoring of fine-scale vessel behaviours and movement patterns (Natale et al., 2015). However, AIS transmitters, unlike blue boxes, can be switched off by fishermen during a ship's passage or be defective, which is mainly done to hide new fishing routes or grounds, thereby not capturing the full fishing effort.

The spatial fishing effort of trawling fleets can be used as an indicator of the times that a trawler tows an area (Ragnarsson and Steingrímsson, 2003; Martín et al., 2014b). For the purpose of this Thesis, data from bottom trawlers was extracted, when possible, by filtering for fishing vessels with otter trawl boards (OTB) as main gear type by conducting a crosscheck with the AIS dataset from the Fishing Fleet Register, an online EU database that registers the full history of fishing vessels from Member States, along with their characteristics (vessel name, call sign identifier, IMO number, dimensions, and gear type, vessel position, speed over ground, course over ground and heading) (European Commission Fisheries & Maritime Affairs, 2014). This proxy was employed in this Thesis to assess the capacity of bottom trawlers to resuspend bottom sediments in Palamós Canyon and off Vancouver Island (**Chapters 5** and **6**), which can promote the generation of INLs and BNLs within continental slope and submarine canyon environments.

Results

Part III

Chapter 4. Evidence of trawling-induced resuspension events in the generation of nepheloid layers in the Foix Canyon (NW Mediterranean)

4.1. Context and objectives

On the Barcelona continental margin (NW Mediterranean), the general pattern of water column SPM distribution was described by Puig and Palanques (1998a). Their study revealed that particulate matter was consistently distributed in SNLs, INLs, and BNLs that were related to topographic and hydrographic structures. These authors suggested natural forces (i.e., internal waves' activity focused along the permanent shelf-slope density front) as the main mechanisms that could contribute to form and maintain these nepheloid layers.

Nonetheless, in the NW Mediterranean margin, deep-sea trawling activities have been identified as an important mechanism causing resuspension and erosion of sediment from fishing grounds (Puig et al., 2012; Martín et al., 2014b; Pusceddu et al., 2014). This mechanism has caused increased accumulation rates within several submarine canyon axes of this margin since the 1960s-1970s, as a result of the expansion and industrialization of the trawling fleets at that time (Martín et al., 2008; Puig et al., 2015; Paradis et al., 2017). In the Foix Canyon, Paradis et al. (2018b) reported recent sediment accumulation rates from a core collected in 2013 at the canyon axis at 860 m depth and compared them with a sediment core retrieved in 1993 at the same location (Sanchez-Cabeza et al., 1999). At this site, it was recorded an almost two-fold increase in the sedimentation rates in the 1960–70s, from 0.5 $cm \cdot y^{-1}$ to 0.9 $cm \cdot y^{-1}$, and a further increase (up to 1.8 $cm \cdot y^{-1}$) in the early 2000s, after a new renewal of the trawling fleet (Paradis et al., 2018b).

The main goal of this chapter is to assess the role of bottom trawling in resuspending bottom sediments within the Foix Canyon (Fig. 4.1) and discuss the implications in trawling-induced resuspension events in the generation of nepheloid layers in the central Catalan margin. For this purpose, we deployed a mooring line equipped with an autonomous hydrographic profiler in the canyon axis at a greater deeper location of the maximum working depth of the local trawling fleet to ensure capturing the nepheloid structure.

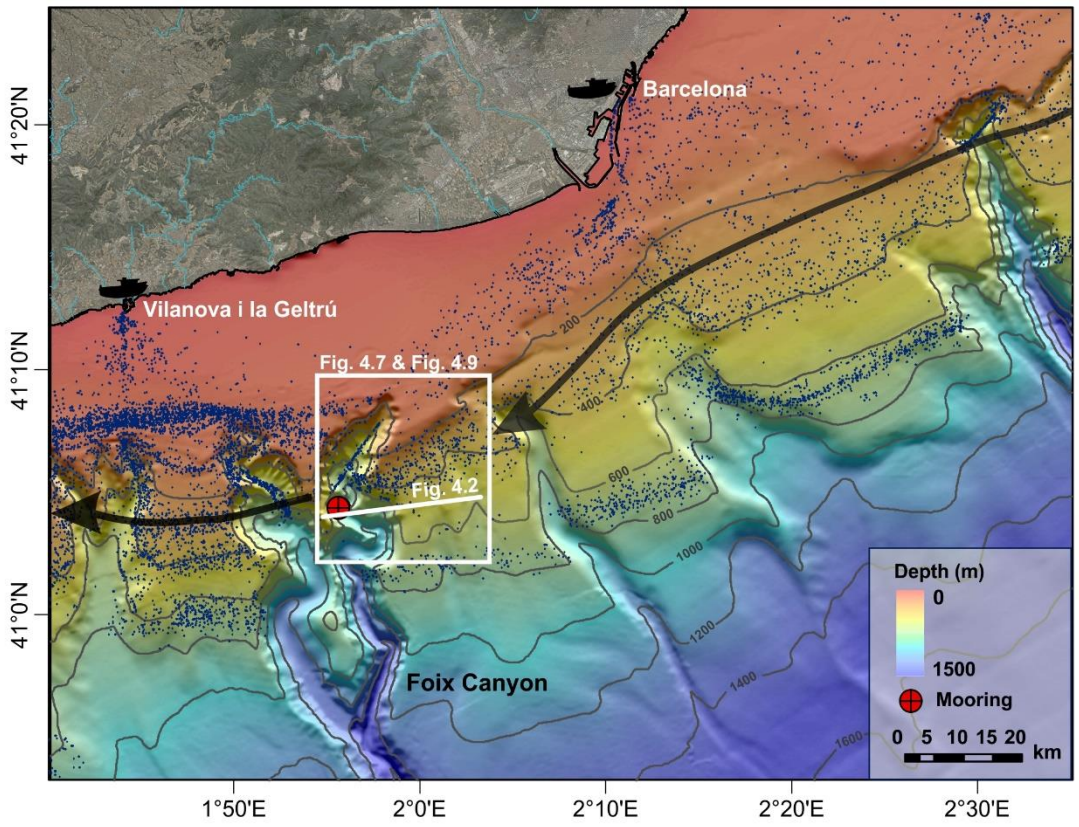

Figure 4.1. Bathymetric map of the Catalan margin (NW Mediterranean) showing the location of the Foix Canyon, and the main fishing grounds and harbours. The red dot indicates the position of the mooring used in this study. Blue dots represent Vessel Monitoring System (VMS) positions of trawlers during the monitoring period and the black arrow represents the geostrophic current. The white line depicts the transect shown in Fig. 4.2.

4.2. Methods

4.2.1. Study site

The Foix Canyon system is located in the Catalan margin a few km south of Barcelona (Fig. 4.1). This canyon incises the shelf-break at 90 m depth and molds the seafloor down to its confluence with the Valencia Channel at a water depth of 2180 m (Canals et al., 2013; Tubau et al., 2013). It consists of two sinuous branches, the eastern Foix and the western Foix branches, that conjoin at 1340 m water depth (Tubau et al., 2013). The canyon cross section at its eastern branch is V-shaped along the first 3.7 km and is defined by an axial incision, while the western branch is U-shaped, characterized by the presence of small tributaries and sedimentary instabilities (Alonso et al., 1984; Tubau et al., 2013). On the upper slope, its steep walls can reach heights of 400 m and maximum gradients of 23º at the mid canyon (Alonso et al., 1984). It also becomes narrow with depth, decreasing from 4 km at the shelf-break to 2 km at a depth of 1200 m (Fig. 4.1).

This canyon intercepts particulate matter from the continent, acting as a pathway for such sediments to the slope during sporadic events such as storms on the shelf or river discharges from the Llobregat and Besòs rivers (Puig and Palanques, 1998a). It is influenced by the geostrophic circulation of the Northern Current, which flows towards the southwest along the continental slope (Millot, 1999; Millot and Taupier-Letage, 2005). Current speed fluctuations along this margin are mainly controlled by the local inertial motion and by low-frequency oscillations (from 6 to 10 days) linked to meteorological forcing conditions (Puig et al., 2000). Near-bottom currents recorded inside the canyon are highly constrained by the canyon topography and are mainly oriented along the canyon axis both in the up- and down-canyon directions, although at the canyon head currents do not display such a clear trend of up- and down-canyon alternations. In intermediate waters at the slope depths, currents are mainly oriented along the margin towards the southwest, according to the main flow of the Northern Current (Puig et al., 2000).

The upper canyon axis and flanks of the Foix submarine canyon are heavily trawled by the fishing fleets from Vilanova i la Geltrú and Barcelona, extending to ~800 m depth (Fig. 4.1).

4.2.2. Data collection

From April to June 2014, a total of 58 hydrographic profiles were collected by an instrumented mooring array equipped with the Aqualog (Fig. 3.1a) deployed in the Foix Canyon's axis (41º 05.55820' N; 001º 55.58104' E) at 870 m depth (Fig. 4.1). The Aqualog was programmed to perform one up- and down-cast per day at 12 a.m., profiling from 800 to 200 m, and back to 800 m (parking depth), at a relative speed of 25 $cm \cdot s^{-1}$. Every cycle (up- and down-cast) took approximately 1 h to be completed. The sensors installed in the Aqualog, as well as their configuration are described in 3.2.1.1.

4.2.3. Data analyses

Hydrographic profiles acquired by the Aqualog during this experiment were analyzed following the procedures described in 3.4.1. The turbidity readings were transformed into SSC following the procedures described in 3.4.3. by applying the general calibration for the Western Mediterranean defined in equation 3.1.

According to the bathymetric section of the canyon at the mooring site and the Aqualog profiling range (Fig. 4.2) and based on the position of the canyon rims and the position of trawlers throughout the monitoring period, data were described and analyzed considering two depth ranges: 1) canyon-unconfined waters (depths between 200 and 500 m) and 2) canyon-confined waters (depths > 500 m).

The Net Particulate Standing Crop (NPSC) for each of the hydrographic profiles collected by the Aqualog was computed as described in 3.4.5 (Fig. 4.3).

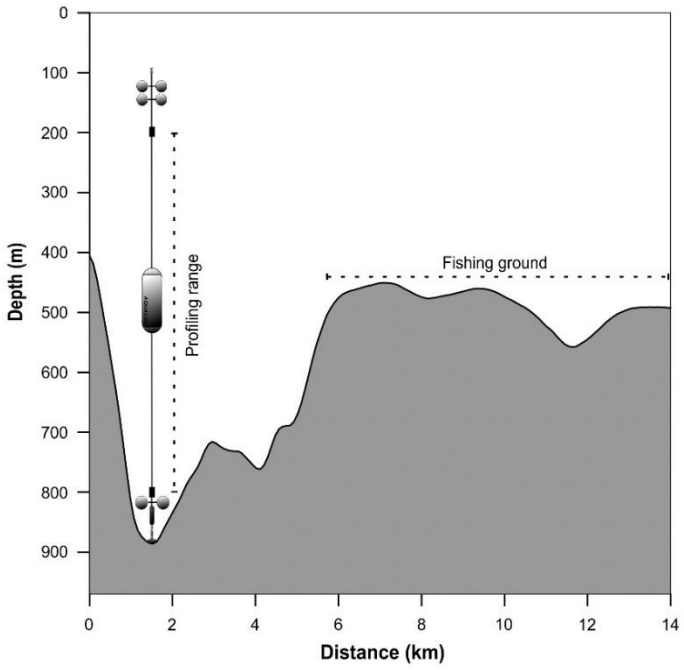

Figure 4.2. Bathymetric cross section and scheme of the mooring array deployed in the Foix canyon axis. See location in Fig. 4.1.

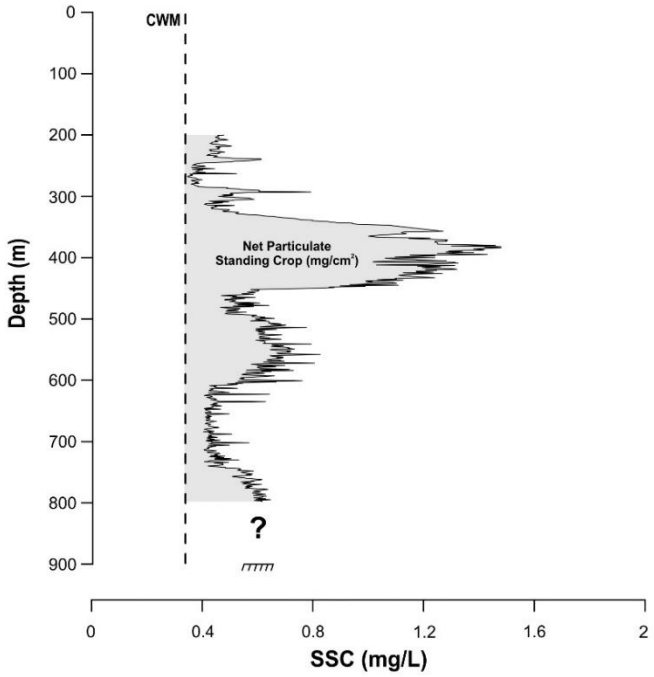

Figure 4.3. Example of a suspended sediment concentration (SSC) profile with a strong nepheloid layer. The suspended particulate matter (SPM) which is in excess of the clear water minimum (CWM) concentrations represent the net particulate standing crop (NPSC) (mg·cm^{-2}) (grey-coloured area). SSCs below 800 m depth are not shown due to the limited working range of the Aqualog (see Fig. 4.2).

4.2.4. Trawling effort from VMS data

The activity of fishing vessels in the Foix Canyon was obtained from the Fishing Monitoring Centre of the Spanish General Secretariat of Maritime Fishing (SEGEMAR) through VMS (see 3.5 for more details). The total VMS records for the period from April 6 to June 2 were filtered by speed and by working depth (> 200 m) to match the Aqualog profiling range. The total number of hauls were also considered.

4.3. Results

4.3.1. Time-series data

4.3.1.1. Hydrographic structure

Compiled data of all CTD casts revealed the presence of the three water masses permanently found in the NW Mediterranean basin, clearly distinguished by their characteristic potential temperature and salinity profiles (Fig. 4.4). The shallowest waters were occupied by relatively warm (13.6-13.7 ºC) and low salinity (38.0-38.2) old Atlantic Water (oAW) (Figs. 4.4 and 4.5a, b). Below (350-600 m water depth), the TS diagram showed the more saline Levantine Intermediate Water (LIW), characterized by both temperature and salinity relative maxima of 13.75 ºC and 38.55, respectively (Figs. 4.4 and 4.5a, b). The deepest waters (600-800 m water depth) were occupied by Western Mediterranean Deep Water (WMDW) that exhibited temperature relative minima of 13 ºC and salinity values between 38.4 and 38.55 (Figs. 4.4 and 4.5a, b). The seasonal Western Intermediate Water (WIW), occasionally found between the oAW and the LIW, was absent in the profiles. Overall, temperature and salinity showed fluctuations of a hundred meters in depth throughout the 58 days of sampling, displaying a periodicity of 4-10 days (Fig. 4.5). Several up-canyon intrusions were also observed. The most relevant was detected from April 29 to May 3, when a cold (13 ºC) and relatively less salty (38.5) pool of WMDW occupied the lowest part of the profiled water column (Fig.4.5).

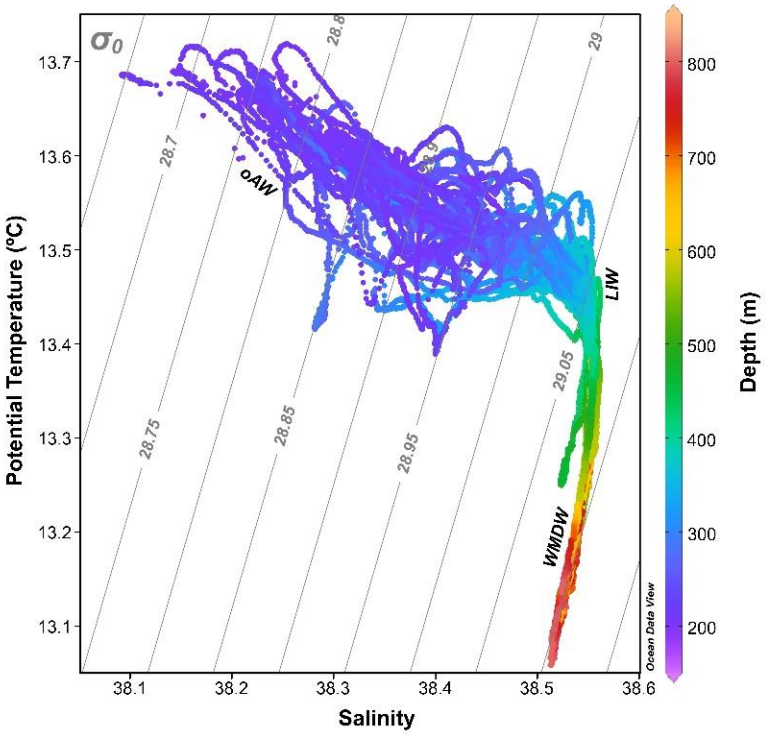

Figure 4.4. General TS diagram for all the CTD casts sampled in April-June 2014 (oAW: Old Atlantic Water; LIW: Levantine Intermediate Water; WMDW: Western Mediterranean Deep Water). Colour scale indicates the depth (m).

4.3.1.2. Suspended particulate matter distribution

From April 6 to April 17, the vertical particulate matter distribution was quite homogenous, and no SSC increases were observed in the profiled water column. From April 17, several increases of SSC (up to 1 mg·L^{-1}) were recorded at intermediate water depths (300-500 m), mainly centered at ~400 m (Fig. 4.5c). These increases corresponded to ~150 m-thick INLs developed at depths of canyon-unconfined waters (Fig. 4.5c). Deeper INLs were recorded sporadically within the canyon confined waters at ~700 m water depth, being thinner (60–90 m) than the shallower ones and reaching estimated SSC up to 1.2 mg/L, as in the case of the profiles on April 27 (cast #22) or April 30 (cast #25). On May 1, the occurrence of a relative high turbidity event was observed particularly at the lowest part of cast #26, which most probably continued below the profiling range, down to the seafloor, generating a ~150 m thick BNL. This layer displayed the highest concentrations for the whole sampling period, reaching estimated SSC of 3.8 mg·L^{-1} at 77 m above the bottom (Fig. 4.5c). Afterwards, several INLs were detected through the second half of the recording period, mainly in the profiling range corresponding to canyon-unconfined waters (Fig. 4.5c). These INLs were found at the same depth ranges (300–500 m) as observed in the first half of the sampling period, showing similar thickness, although during this part of the deployment they displayed higher estimates of SSC (1.1–1.6 mg·L^{-1}). The distribution of the suspended particulate matter depicted the presence of a turbid water mass at intermediate depths that remained in the water column at least until the end of the experiment.

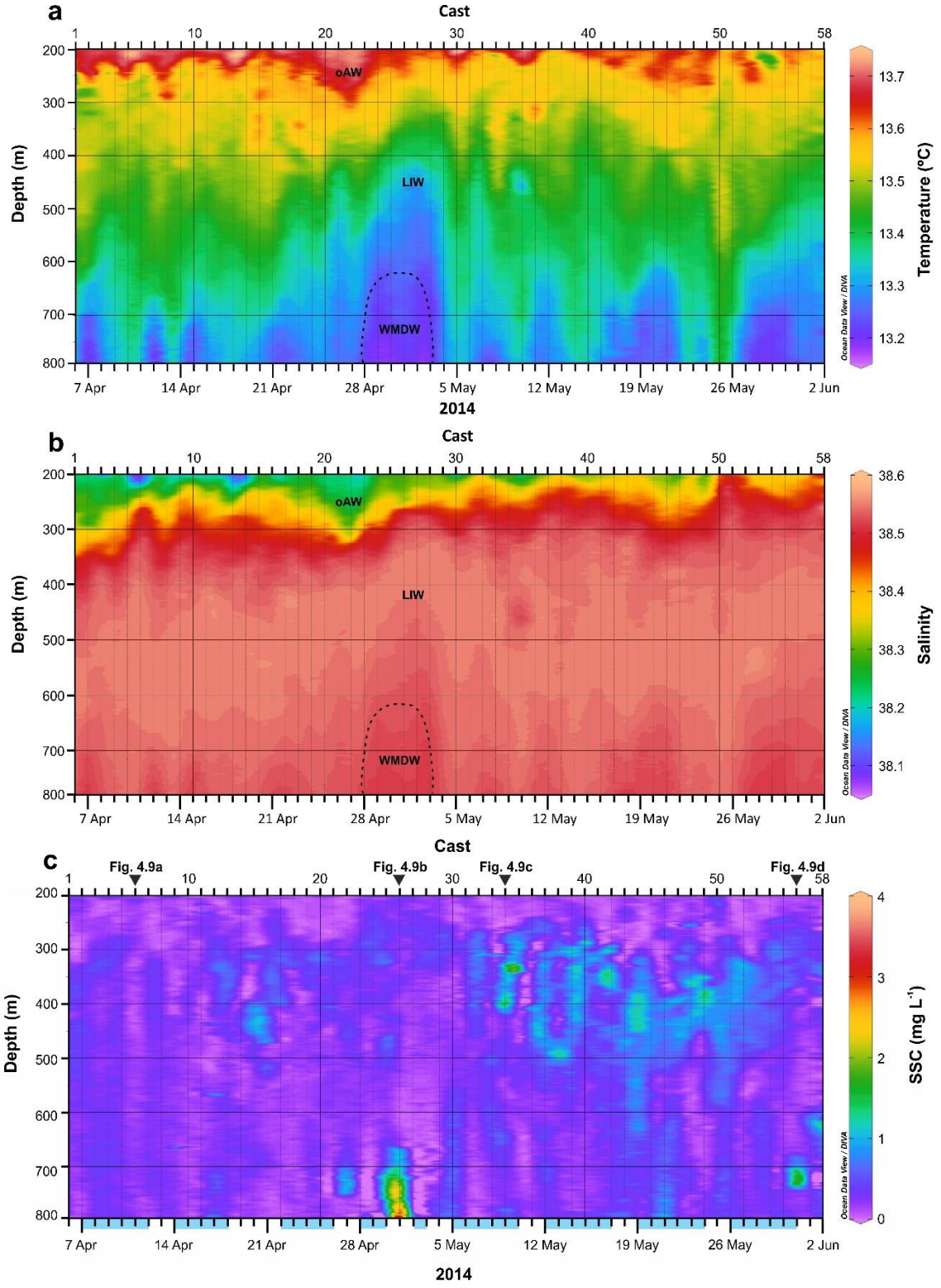

Figure 4.5. Temporal variability of the vertical distribution of a) potential temperature (ºC), b) salinity and c) suspended sediment concentration (SSC) during the monitoring period. Fishing days are indicated as blue bars on the bottom x-axis of panel c. SSC vertical profiles which were examined (Figs. 4.8a-d) are also shown in this figure.

Within the canyon confined waters, no more significant near-BNLs were detected by the end of the experiment, but an INL was clearly noticeable at ~700 m water depth on May 31 (Fig. 4.5c, cast #56). This deep INL was similar to one detected previously at the same depth range on April 27 (Fig. 4.5c, cast #22). However, it was narrower (50 m thick) and had a maximum estimated SSC of 1.9 $mg \cdot L^{-1}$ (Fig. 4.5c).

4.3.2. Trawling activity

During the experiment, VMS data showed that the fishing grounds around the Foix Canyon were exploited by 22 trawlers, mostly from Barcelona and Vilanova i la Geltrú harbors (Fig. 4.1). After speed and depth were filtered, vessel positions recorded by VMS appeared to follow the bathymetric contours and most of the trawling activity took place at 200-500 m water depth outside the canyon, along the fishing ground named *Can Pere Negre*, and at 600-800 m water depth inside the canyon, following the axis, along the fishing ground known as *San Salvador* (Fig. 4.1 and Fig. 4.6, Lleonart, 1990).

The position of fishing vessels operating near the mooring site was plotted in detail, in six consecutive period, each of them spanning 10 days of VMS data points except for the last one that lasted for 8 days (Fig. 4.6). Table 4.1 summarizes the main characteristics of each period in terms of number of hauls and number of trawlers for the identified fishing grounds. Few isolated trawlers were observed to be fishing on the slope at depths > 600 m (Fig. 4.6), but since they were far from the mooring location, they have not been taken into account in this analysis.

Time-series observation on VMS data revealed nearly no trawling activity around the mooring site during the first period (Fig. 4.6). Only 10 hauls were counted, corresponding to five active vessels that were working at the slope fishing ground (Table 4.1). No fishing activity was detected at the axis fishing ground (Table 4.1; Fig. 4.6). The remaining periods (Fig. 4.6) were characterized by the presence of trawlers both at the axis and at the slope fishing grounds. During the second period, VMS data points were mostly clustered between the 200 m and the 500 m isobaths, suggesting that the majority of trawlers were working at the slope fishing ground (Table 4.1; Fig. 4.6). Trawling activity throughout the third period remained similar to the previous period, although trawlers were concentrated at both the axis and the slope fishing grounds, but none of them were detected at depths > 400 m outside the canyon confinement (Fig. 4.6). The number of trawlers and hauls was the same for both fishing grounds during this period (Table 4.1). As far it concerns the last three periods, these were characterized by a relatively higher number of trawlers and hauls at both fishing grounds (Fig. 4.6d-f; Table 4.1). The majority of trawling activity was detected along the axis and the slope fishing grounds between the 200–500 m isobaths. Particularly, recordings for this second half of the survey showed that the highest number of hauls for both fishing grounds occurred during the fourth period (Fig. 4.6d; Table 4.1).

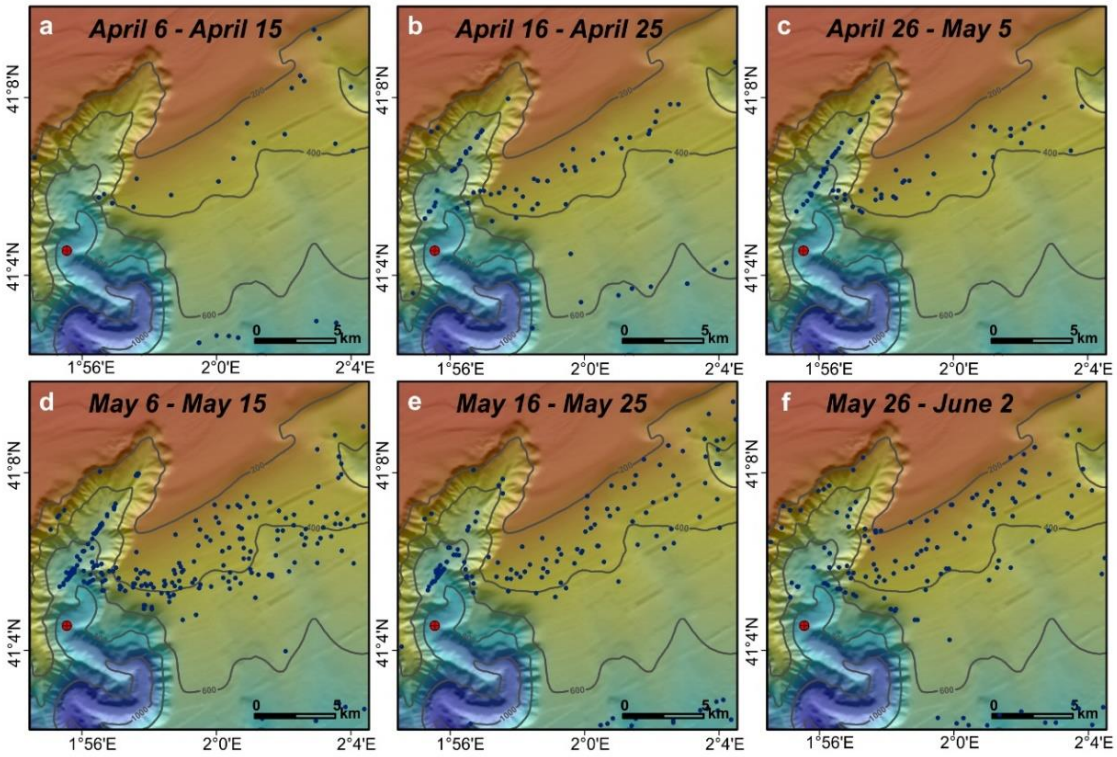

Figure 4.6. Bathymetry of the eastern branch of the Foix Canyon and the main fishing grounds. The red dot indicates the position of the mooring array used in this study. Blue dots represent Vessel Monitoring System (VMS) positions of trawlers during the monitoring period (a: first period, April 6 to April 15; b: second period, April 16 to April 25; c: third period, April 26 to May 5; d: fourth period, May 6 to May 15; e: fifth period, May 16 to May 25; f: sixth period, May 26 to June 2).

Table 4.1. Main characteristics of the defined periods. Number of hauls (#) and number of trawlers (#) are presented for the identified fishing grounds. The first column indicates the correspondence with Figure 4.6.

	Period	Date (2014)	Fishing ground			
			Slope		Axis	
			# trawlers	# hauls	# trawlers	# hauls
Fig. 4.6a	1	April 6-April 15	5	10	0	0
Fig. 4.6b	2	April 16-April 25	6	12	4	7
Fig. 4.6c	3	April 26-May 5	5	13	5	13
Fig. 4.6d	4	May 6-May 15	12	52	9	32
Fig. 4.6e	5	May 16-May 25	13	38	6	15
Fig. 4.6f	6	May 26-June 2	12	45	6	14

4.3.3. Relationship between the net particulate standing crop and the number of hauls

The number of hauls identified from the activity of trawlers operating nearby the Foix Canyon (Table 4.1) was used to infer trawlers' capacity to resuspend bottom sediments. Fig. 4.7 illustrates the relation between the NPSC for each hydrographic cast and the number of hauls identified from the activity of trawlers operating at around the Foix Canyon fishing grounds on the previous day. Two approaches were considered, first the NPSC values of the entire hydrographic profiles (200-800 m depth) were plotted against the total number of hauls on the slope and within the canyon (Fig. 4.7a), and second, the NPSC of the profiled section outside the canyon confinement (200-500 m depth) was plotted against the hauls of the slope fishing ground (Fig. 4.7b).

Despite the small number of hydrographic profiles obtained during fishing days, due to the exclusion of data during weekends and holidays, the overall fit of the two variables is fairly good. The correlation coefficients for the regression models are noticeably small, but according to the *p-values* ($p < 0.05$), both relations are statistically significant. The correlation coefficient for the relation between the NPSC at intermediate waters and the number of hauls at the slope (Fig. 4.7b), where the major fishing activity took place (Fig. 4.6, Table 4.1), is slightly bigger than for the relation between the computed NPSC for the entire profiled depth range and the total number of hauls (Fig. 4.7a).

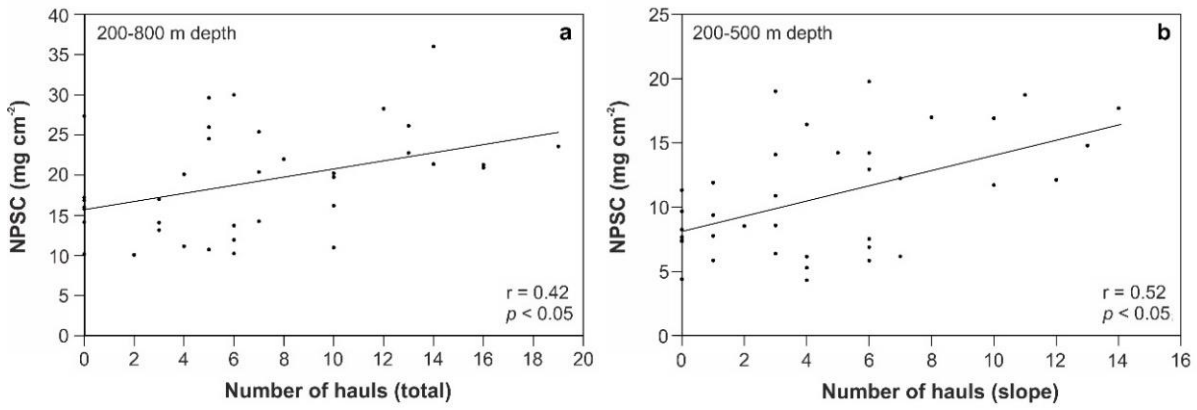

Figure 4.7. Relation between the net particulate standing crop (NPSC, mg·cm^{-2}) and the number of hauls from trawlers operating nearby the mooring location at the fishing grounds of the Foix Canyon (see Table 4.1). Linear regressions are shown for the a) total computed NPSC and the total number of hauls, considering those at the axis and at the slope fishing grounds, and for the b) computed NPSC at the slope (between the 200 and 500 m isobath) and the number of hauls counted at the slope fishing ground. Only fishing days were used to calculate the NPSC in both cases (see blue bars on the bottom x-axis of Fig. 4.5c for the exact dates).

4.4. Discussion

4.4.1. Evidence of trawling-induced nepheloid layers using VMS data

The nepheloid structure of the Barcelona continental margin was determined by Puig and Palanques (1998a) using data from three hydrographic surveys conducted in 1992-1993. These results showed that suspended particulate matter was mainly distributed at surface, intermediate and near-bottom nepheloid layers, and that nepheloid layer detachments were related to hydrographic structures. The maximum SSC observed in the area occurred at the Foix submarine canyon, more specifically at intermediate depths (between 300 and 500 m) associated with a suggested permanent INL. This layer was also observed at the adjacent continental slope (Puig and Palanques, 1998a). According to these authors, this slope INL was controlled by the shelf-slope density front and by the Northern Current and was probably re-fed by other submarine canyons incising the margin. Some authors (Cacchione and Drake, 1986; Gardner, 1989) explained that shoaling and breaking of internal waves could lead to the formation and maintenance of INLs and near-BNLs over certain slopes and continental shelves. Therefore, in the Foix submarine canyon it was also suggested that breaking of near-inertial internal waves at the upper slope could resuspend bottom sediments where the foot of the density front intersects with the seabed and, thus, feeding this slope INL (Puig and Palanques, 1998a).

During this experiment, several particulate matter detachments were found at intermediate depths within the unconfined canyon waters, mainly centered at 400 m over the slope region (Fig. 4.5c). Even though the mechanism proposed by the latter authors involving internal waves' activity could be plausible, these slope INLs were not permanent and were just observed at specific time spans throughout the sampling period (Fig. 4.5c). The results presented in this Chapter, when combined with data from fishing vessels positioning, suggest that trawling activity is likely responsible for most of the sediment resuspension that ultimately generates these INLs.

Analyses on VMS data revealed that all the observed nepheloid layers were detected during or after a period of trawling activity along the neighboring fishing grounds of the Foix submarine canyon. When no particulate matter detachments were observed at the mooring location, particularly at the beginning of the monitoring period (Fig. 4.5c) there was a low trawling activity at the neighboring fishing grounds of the canyon (Fig. 4.6a). As an example, on April 9 there were no trawlers fishing near the mooring, neither at the slope nor at the axis fishing ground. At that time, the lowest suspended sediment concentration of the entire record was observed, and VMS data identified a single trawler fishing at the 200 m depth isobath, far from the mooring location at shallower depths than the Aqualog profiling range (Fig. 4.8a). During the first 10-day period of monitoring (Fig. 4.6a), fishing activity was only detected on the slope fishing ground by 5 trawlers working at around the 400 m isobath (Table 4.1). This low trawling activity seems to be insufficient to induce any particulate matter detachments that could be subsequently detected by the Aqualog at the mooring site (Figs. 4.1, 4.6, 4.8a).

Throughout the monitoring period, the presence of a high number of trawlers on the slope fishing ground coincided with the INLs centered at 400 m water depth observed in the hydrographic profiles (Fig. 4.5c). For instance, the position of trawlers on May 8 coincided temporally and spatially with the observed INL on May 9 (Figs. 4.5c, 4.8b). Other hydrographic profiles, corresponding to the same monitoring period (Figs. 4.5c, 4.6d), showed similar SSC levels related to the presence of trawlers operating on the slope fishing ground (Fig. 4.5c). In fact, higher NPSC at this depth range (200-500 m) responded to a major number of hauls at the same bathymetric range, hence, to a higher trawling activity at the slope fishing ground (Fig. 4.5c). Therefore, it seems plausible that all observed particulate matter detachments at these depths were generated by the same mechanism. Once resuspension is generated by trawling, the presence of the geostrophic current flowing towards the southwest (Fig. 4.1) could have favored particle transport from the slope, where fishing vessels were located (Fig. 4.6d), towards the canyon-unconfined water over the mooring line (Fig. 4.2). Therefore, the Aqualog could have detected these increases in SSC as particulate matter was being detached from the slope over the canyon rims. The positive relationship between the quantification of the NPSC of the profiled section outside the canyon confinement and the number of hauls on the slope fishing ground supports this hypothesis (Fig. 4.7b). Nevertheless, previous hydrographic transects conducted along the axis of this canyon suggest that these INLs could have also been detached from the canyon head region (see Fig. 11 in Puig and Palanques, 1998a), from resuspension of trawlers operating along the canyon axis. Therefore, due to the presence of trawlers working simultaneously at both fishing grounds (Fig. 4.6d; Table 4.1), it is difficult to determine where these INLs were exactly generated, and probably both sources of resuspended particles contributed to the observed INL detachments around 400 m water depth.

Within the canyon confinement, several deep INLs were also observed at ~700 m throughout the sampling period (Fig. 4.5c). These confined INLs were recorded sporadically and displayed higher concentrations (~2 $mg \cdot L^{-1}$) than the slope unconfined INLs (Fig. 4.5c). As an example, Fig. 4.8c illustrates the confined INL observed on May 31 at the time that two trawlers were operating at the axis fishing ground. The development of these deep INLs is likely related to the presence of trawlers working along the main axis fishing ground, which can reach greater depths than the hauls on the adjacent slope. In this case, the natural conduit of the canyon and the alternation of the up- and down-canyon regime (Puig et al., 2000) could have helped retaining sediment particles in the canyon interior, as they remain outside the influence of the geostrophic flows that just affects canyon-unconfined waters (Fig. 4.2).

Within the canyon, a thick near-BNL was also detected on May 1 (Fig. 4.8d), displaying the highest SSCs on the sampling period. The high concentration and thickness of this layer seem to be related to an up-canyon of WMDW (Fig. 4.5a) that could have favored the retention at this depth range of sediment particles resuspended at the canyon axis fishing ground. The vertical oscillations of the water masses observed during the deployment had a frequency of 4-10 days, which are in agreement with the periodicity of the near-bottom along-canyon flow reversals observed by Puig et al. (2000) in this canyon. Even so, our data do not allow to determine the

concentration of this BNL at depths > 800 m due to the limited working range of the Aqualog (Fig. 4.2). Nonetheless, the SSC profile (Fig. 4.8d) suggests that the concentration tends to increase with depth. This limitation also prevented us to detect other potential BNLs developed by trawling activities along the canyon axis and that could have been extending closer to the bottom, without reaching the lower operational depths of the Aqualog.

Overall, our findings support the idea that resuspension induced by trawling activities can play a significant role in increasing SSC levels in the water column within the Foix submarine canyon, causing higher NPSC values as the number of haul increases, whether they occur at canyon-confined or unconfined waters (Fig. 4.7).

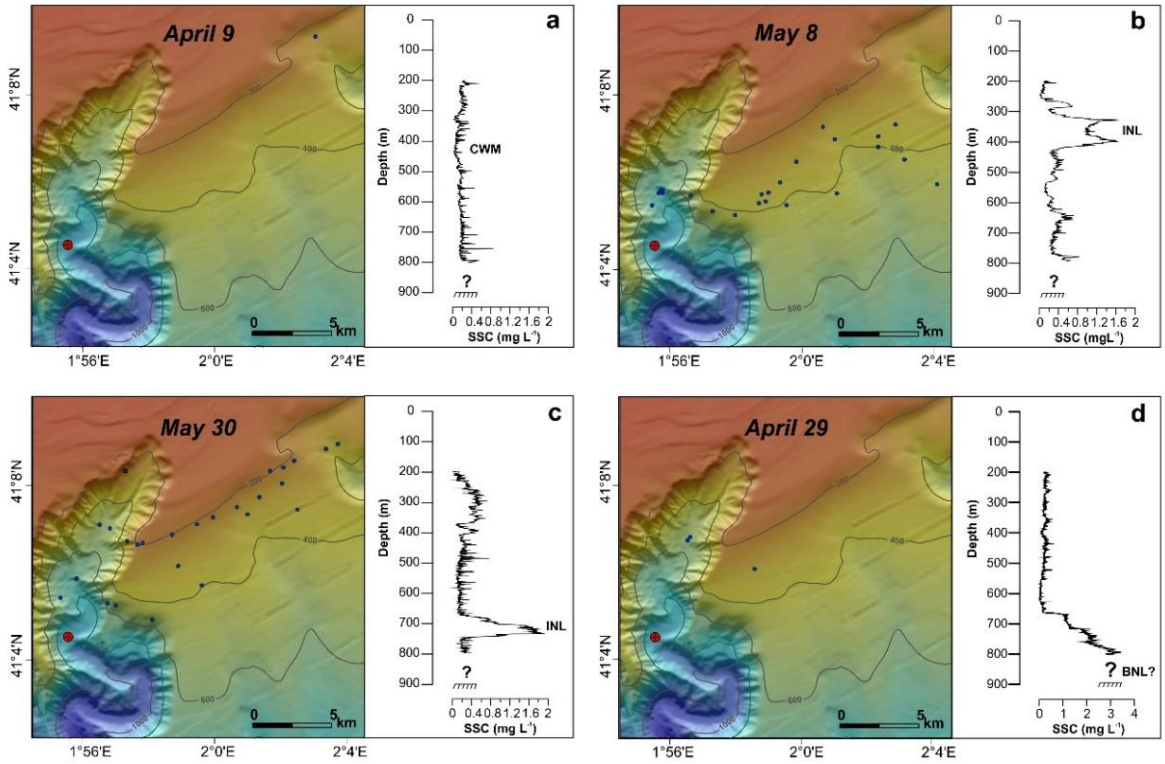

Figure 4.8. Daily VMS recordings in the study area (blue dots) when nepheloid layers were absent a) or present at different water depths: b) ~400 m, c) ~700 m and d) near the bottom. See Fig. 4.5c for profile timing throughout the entire record. Note the change of scale for the SSC axis of the d) vertical profile.

4.5. Conclusions

Daily hydrographic collected throughout this field study illustrate a well-defined water turbidity structure consisting in INLs, found between 300 and 500 m water depth and above the canyon rims at canyon-unconfined waters, and INLs and near-BNLs, confined within the canyon at depths > 650 m.

Using vessels' positioning through VMS, the temporal and spatial distribution of the local trawling fleet over the Foix Canyon at the time of the mooring deployment strongly suggests that trawling resuspension is likely the major mechanism that leads to increasing SSCs in the water column. VMS logs revealed that the presence and water column levels of the observed nepheloid layers strongly depend on the operating depths of trawlers and on the specific nearby fishing grounds being exploited.

Nonetheless, even bottom trawling appears to act as the main sediment resuspension mechanism, natural processes and ambient currents on the slope and within the Foix Canyon contribute to the advection and/or retention in suspension of resuspended particles, playing a major role in their transport along and across the margin via nepheloid layers.

The present Chapter presents, for the first time, data on the temporal evolution of water column turbidity using an autonomous hydrographic profiler deployed at the canyon axis of a trawled submarine canyon on the NW Mediterranean region. Since this study only provides a set of vertical profiles of the water column in the Foix Canyon, more extensive would be required to fully understand the turbidity structure at this or other comparable sites affected by trawling activities.

Chapter 5. Natural vs. trawling-induced water turbidity and suspended sediment transport variability within the Palamós Canyon (NW Mediterranean)

5.1. Context and objectives

As explained in section 1.4.2.1, high-energy storms and DSWC events affecting submarine canyons can increase water turbidity and sediment fluxes offshore, enhancing the transport of sediment particles towards the slope and deeper regions. The latter phenomenon is particularly relevant in the NW Mediterranean, being the Gulf of Lions one of the main regions of DSW formation (Durrieu de Madron et al., 2005a). As commented in section 2.1.1.2, DSW can be detached at intermediate depths and contribute to the formation of the seasonal WIW during mild winters (Lapouyade and Durrieu de Madron, 2001; Dufau-Julliand et al., 2004), or affect the entire continental slope (Canals et al., 2006; Palanques et al., 2012; Durrieu de Madron et al., 2013; Palanques and Puig, 2018) and be transferred south from the Gulf of Lions towards the central Catalan margin, reaching submarine canyons incising the margin (Palamós and Blanes canyons) (Zúñiga et al., 2009; Ribó et al., 2011) (Fig. 2.1).

In addition to these natural transport mechanisms, deep-sea bottom trawl fisheries mainly located on the upper continental slope of the NW Mediterranean have also been shown to contribute substantially to present-day sediment resuspension and water column turbidity (see section 2.1.1.3 for more details). The majority of studies aiming at understanding the effects of this human practice in this area have focused on the Palamós Canyon, one of the most prominent morphological features incising this margin (Serra, 1981). A previous study reported the presence of INLs and BNLs related to trawling activities in several hydrographic profiles collected at this canyon (Martín et al., 2014a). However, the continued effect of bottom trawling causing changes in the water column turbidity beyond fishing grounds is an issue that still remains unexplored in this and other submarine canyons.

In the previous chapter, the temporal evolution of turbidity increases through the water column in the Foix Canyon has been analysed, evidencing the contribution of trawling activities to the development of nepheloid layers (**Chapter 4**). However, accurate estimates of the quantity of material being introduced to the water column are still needed to better appreciate the contribution of trawling activities to sediment dynamics and the potential environmental and ecological impacts associated with it. The aims of this Chapter are to assess the spatial and temporal variations on the water turbidity structure and near-bottom suspended sediment fluxes linked to both anthropogenic (bottom trawling) activities and natural processes (storms and DSWC) in the Palamós Canyon and evaluate the contribution of each mechanism to the sediment fluxes.

5.2. Methods

5.2.1. Study site

The Palamós Canyon (Fig. 5.1) is one of the most prominent submarine canyons incising the NW Mediterranean margin (Canals et al., 2013). The canyon head is situated close to the coastline (at ~1 km) and incises the continental shelf at 90 m depth. The first ~5 km of the canyon presents a N-S direction parallel to the coastline, after which the canyon's direction turns to WNW-ESE for ~35 km, separating the Roses margin to the north, and La Planassa margin to the south (Amblas et al., 2006). This submarine canyon has a total length of 110 km, and a total maximum width of 18.4 km, and runs almost from the coastline down to 2550 m water depth. The canyon's steep walls (> 25º) present several well-developed gullies generated by sedimentary instabilities (Lastras et al., 2011), although these complex morphologies have been smoothed over the fishing grounds due to recurrent disturbance of the seafloor by the trawling gear (Puig et al., 2012).

The hydrographic structure in this area is composed by a three-layer system: the old Atlantic Water (oAW) from the surface down to 150-300 m depth, the Levantine Intermediate Water (LIW) between 300 and 600 m, and the Western Mediterranean Deep Water (WMDW) below 600 m, even covering the entire basin below 1000 m water depth (Table 2.1). The physical circulation dynamics at the area are influenced by the Northern Current (see 2.1.1.1 for more details). Although it approaches the Palamós Canyon in a south-westward direction (Font et al., 1988), the abrupt topography forces some adjustments of the Northern Current (Masó and Tintoré, 1991), which lead to significant vertical motions (Palanques et al., 2005; Jordi et al., 2005).

This submarine canyon acts as a preferential conduit for particulate matter transported during sporadic events such as storms or river discharges (Palanques et al., 2005). The most important river in the nearby coast is the Ter River, whose mouth reaches the sea at 25 km north from the canyon. It has a mean annual water discharge of 12.1 $m^3 \cdot s^{-1}$ (Liquete et al., 2009). On this margin, northern storms are very frequent and persistent, but to their reduced fetch they can only generate relatively small waves (~2 m) on the inner shelf that have limited capacity to resuspend sediment. As described in 2.1.1.2, eastern storms are rarer and brief, although they generate larger waves (> 4m), particularly during fall and winter months (Palanques et al., 2008). They are usually accompanied by heavy rains and torrential river discharges carrying large amounts of sediment to the coast (Ribó et al., 2011).

The Palamós Canyon's flanks are intensively exploited by a local trawling fleet targeting the blue and red shrimp *Aristeus antennatus*. Trawlers are active in this area on a daily basis except for weekends, holidays, and local festivities, mainly along the Sant Sebastià and Rostoll fishing grounds (Fig. 5.1). The same vessel usually carries out two hauls per day, starting typically at 7 a.m. in an offshore direction, until 6 p.m. when it heads back to port. The average length of a haul usually ranges from 10 to 20 km, with an average of 15 km. The bottom trawl gear used in this fishery consists of two heavy otter boards, each up to 1 ton in weight, spreading ~100 m

apart during the trawling operation and connected to the net opening by 60-200 m long sweeplines. The net measures 80-150 m in length and has a width of ~50 m at its ballasted mouth (Fig. 1.10) Palanques et al., 2006a; Martín et al., 2014b).

A recent fishery management established a two-month trawling closure from early-January to early-March since 2013 to allow the recruitment of juveniles and avoid the risk of overexploitation of the fishing stock (Bjørkan et al., 2020). In 2017, this seasonal trawling closure occurred from January 5 to March 8 (BOE, 2017).

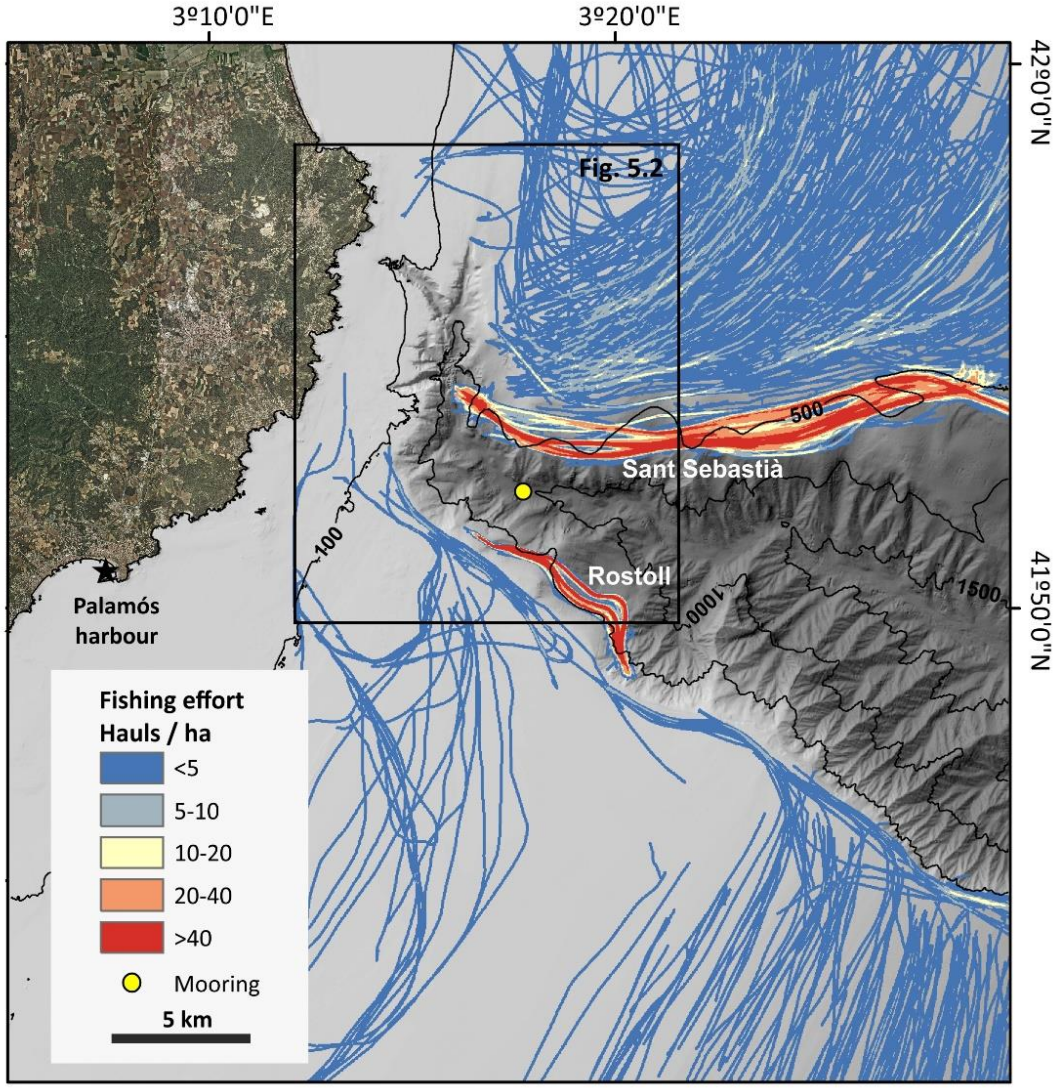

Figure 5.1. Bathymetric map of the Palamós Canyon, showing the location of the mooring line in the canyon axis (yellow dot) and the main fishing grounds along the canyon flanks (Sant Sebastià and Rostoll). The overlying density represents an estimate of the fishing effort of otter board (OTB) vessels based on the number of hauls per hectare obtained from year 2017 Automatic Identification System (AIS) data. The inset rectangle depicts the extension of Figure 5.2.

5.2.2. Data collection

From early February to early June 2017, a mooring line (Fig. 3.1b) was deployed in the axis of the Palamós Canyon at 929 m depth (41º 52.329' N; 3º 7.660' E), at a slightly deeper location than the maximum working depth of the local trawling fleet (~800 m) (Fig. 5.1). The position and deployment depth of the mooring was chosen in agreement with the Palamós fishermen guild in order to avoid interfering with their bottom trawling activities, and still be able to carry out our experimental observations in the canyon. The deployment period was originally programmed from February 7 to early June 2017, which covered a trawling closure period (February) and the continuation of the regular trawling season in the fishing grounds of the canyon (March-June). Unfortunately, the instruments recorded good data during 60 days until April 7, when the mooring line was displaced by a longline fishing vessel from a neighbouring fishing harbour. Nevertheless, the recorded period allowed to capture the transition between the fishing closure and the trawling season and to address the scientific goals pursued in this study.

The mooring line was equipped with the Aqualog, which was programmed to perform two up- and down-casts per day (at 2 a.m. and 2 p.m.), profiling from 738 to ~150 m, and back to 738 m (parking depth), at a relative speed of 25 $cm \cdot s^{-1}$. Therefore, the upper ~150 m and the lower ~200 m of the water column at the mooring location were not monitored by the Aqualog. Unfortunately, the Aqualog did not profile the entire water column at certain time spans during the study period (i.e., February 7-27), presumably caused by the tilting of the mooring line due to strong currents, which prevented the Aqualog from progressing deeper and completing the hydrographic profiles. The sensors installed in the Aqualog, as well as their configuration are described in 3.2.1.1. However, owing to technical problems during down-casts, data could only be recorded during the up-casts. The lower portion of the mooring line was also equipped with a turbidimeter, placed at 5 mab, and a current meter, placed at 6 mab (Fig. 3.1b). The configuration of these sensors is detailed in 3.2.1.2.

After the mooring recovery on June 7, 2017, a ship-based hydrographic transect was conducted across the Palamós canyon head (see location in Fig. 5.2). For more detailed information on the transect and the instrumentation used see section 3.3.

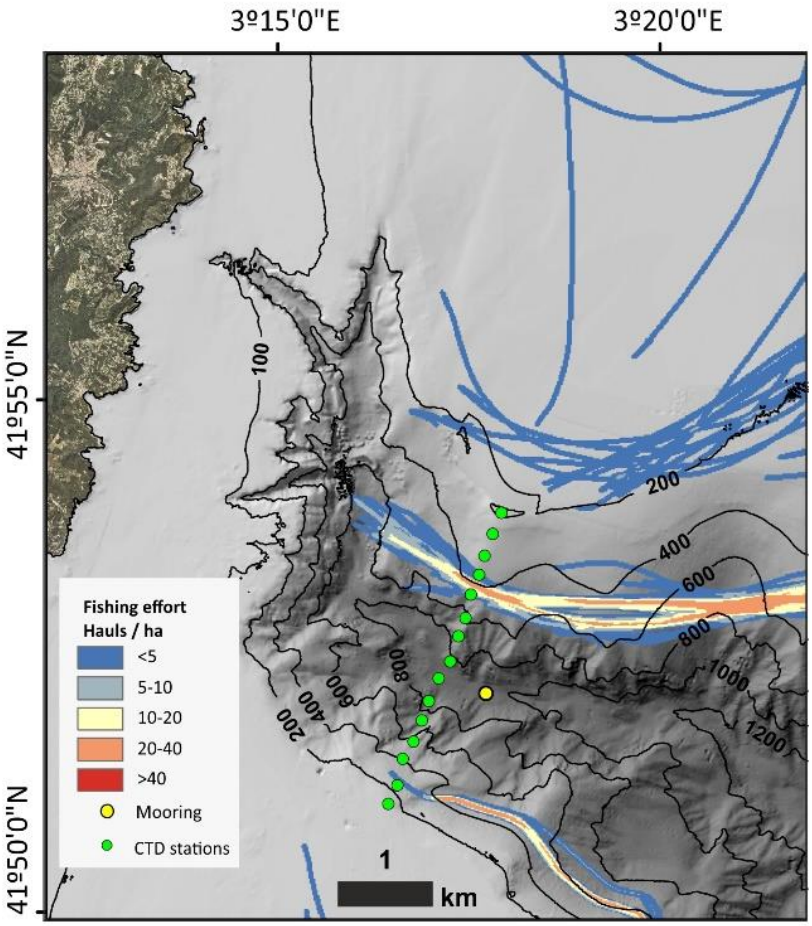

Figure 5.2. Bathymetric map of the Palamós canyon head showing the fishing effort between March 9 and April 7, 2017 (trawling season). The yellow dot depicts the location of the mooring line, while the green dots indicate the position of the hydrographic transect conducted on June 7, 2017.

5.2.3. Data analyses

Hydrographic profiles acquired by the Aqualog during this experiment were analysed following the procedures described in 3.4.1. The turbidity readings were transformed into suspended sediment concentration (SSC) using a regression equation obtained from a laboratory calibration (see section 3.4.4), by applying the equation 3.2.

The Net Particulate Standing Crop (NPSC) for each of the hydrographic profiles collected by the Aqualog was computed as described in 3.4.5, and calculated by applying the equation 3.3. As the Aqualog did not reach the same depths during the trawling closure and the trawling period, two distinct approaches were considered. In the first one, the NPSC was calculated for the 150-400 m depth interval, where data was recorded throughout the deployment period. In the second, the NPSC was computed only for the time-period when the profiler recorded data along most of the working depth range (150-738 m depth).

Near-bottom currents and SSC data acquired by the near-bottom instrumentation were used to calculate instantaneous suspended sediment fluxes and time-integrated cumulative suspended sediment transport following the procedures explained in 3.4.6. First, suspended sediment fluxes were calculated by applying equation 3.4. Then, the time-integrated cumulative suspended sediment transport was calculated following equation 3.5. To obtain the along- and the across-canyon components at the sampling location, an intermediary computation is needed. In this study, the North and the East current components were rotated 70º counterclockwise following equations 3.6 and 3.7. The uncertainty on suspended sediment fluxes (σ_F) was calculated by applying equation 3.8, while the uncertainty on time-integrated cumulative transport (σ^2_{NF}) was calculated by following equation 3.9. Estimated parameters' uncertainties derived from the measurement errors corresponding to each independent time series are shown in Table 5.1.

Table 5.1. Estimated parameters' uncertainties from the measurement errors to each independent time series. The variance of the variables, as well as constant parameters are shown. "*A*" corresponds to the constant that multiplies FTU values to yield SSCs, while *Θ* corresponds to the angle of rotation applied to obtain along- and across-canyon currents. In this case, *Θ* = 70º, with respect to the North and East components, is applied in the equations for uncertainty calculations.

Variable	Variance/constant	Value
Current Speed	σ_{Speed}	± 0.005 m·s^{-1}
Current Direction	σ_{Dir}	± 5º
Turbidity	σ_{Turb}	± 2.7 FTU
Constant of turbidity	*A*	1.14
Angle of rotation	*Θ*	70º

5.2.4. Ancillary data

The daily discharges of the Ter and the Daró rivers, located northwards of the Palamós Canyon, were supplied by the *Agència Catalana de l'Aigua* (ACA, Catalan Government Water Agency), and have been used to assess the riverine sediment supplies during the study period. This data is available online via ACA's website (http://aca-web.gencat.cat/sdim21/seleccioXarxes.do).

Wave conditions during the study period were provided by the REDEXT network of deep-water oceanographic buoys of the Spanish Ports Authority (http://www.puertos.es/es-es/oceanografia/Paginas/portus.aspx) and recorded hourly by the Cap de Begur buoy, located offshore on the northern continental slope region next to Palamós Canyon, over the 1200 m isobath (41º 55.2'N; 3º 39.0' E).

5.2.5. Trawling effort from AIS data

The activity of trawlers around the Palamós Canyon operating in the fishing grounds of Sant Sebastià (northern canyon flank) and Rostoll (southern canyon flank) (Fig. 5.1) was obtained from ShipLocus®, the main module of the Spanish Ports Authority to exploit maritime traffic data for management research purposes (Puertos del Estado, 2017), through the use of AIS data.

The spatial effort was estimated using AIS data from year 2017, which included the study period, and consisted in a combination of static data (vessel name, call sign identifier, IMO number, and vessel dimensions) and dynamic navigation sensor data (vessel position, speed over ground, course over ground, and heading). Since the large AIS dataset exceeds total computation data management capacities, the high-frequency time series (i.e., 1-2 records every 6 seconds) was reduced to the first entry per minute of each vessel, resulting in a smaller and homogenous dataset for the entire study period. Then, vessels equipped with OTB were extracted by cross-checking the AIS dataset with the data from the Community Fishing Fleet Register (European Commission Fisheries and Maritime Affairs, 2014). AIS data were then filtered according by speed to infer whether an AIS message corresponded to fishing activity, using similar criteria to those used in previous studies (e.g., Natale et al., 2015; Oberle et al., 2016a; Paradis et al., 2021). It assumes that bottom trawler speed follows a bimodal distribution corresponding to navigating (high speed) and trawling (low speed) conditions. The Expectation-Maximization (EM) algorithm (Dempster et al., 1977; Hartley, 1958) was used to obtain two gaussian distributions for each bottom trawler's speed (Fig. 5.3). Trawling speed was finally obtained as the mean of the first gaussian distribution ± 2 standard deviations (95% of the distribution) of the OTB vessel speeds, corresponding to speeds between 0.8 and 3.9 knots. However, simply filtering according to this trawling speed may lead to false-positives, when a trawler is navigating or drifting at a specified trawling speeds, and false-negatives, when a trawler is hauling at anomalous speeds for a few minutes due to piloting reasons (i.e., when trawling down-slope the vessel needs to reduce its speed to keep the gear on the seafloor). Hence, a minimum length of 10 minutes per haul per haul was assumed to correct for false-positives, whereas anomalous speeds that lasted less than 5 minutes were considered to correct for false-negatives and were converted to trawling activities. Hauls per vessel were then identified as consecutive entries that met these trawling criteria for at least 100 minutes and computed daily for the entire fleet (Fig. 5.5). Finally, bottom trawling effort was obtained on ArcGIS 10.4 by calculating the haul density per hectare (100 m x 100 m), assuming an average trawling-door spread of 100 m, which accounts for the maximum width of the trawlers' nets operating in this margin (Palanques et al., 2006a). For the purpose of this study, trawling effort was represented for the entire study period (Fig. 5.1), and for the trawling closure (spanning from February 7 to March 8) and for the trawling season (spanning from March 9 until the end of the study period on April 7) (Fig. 5.2).

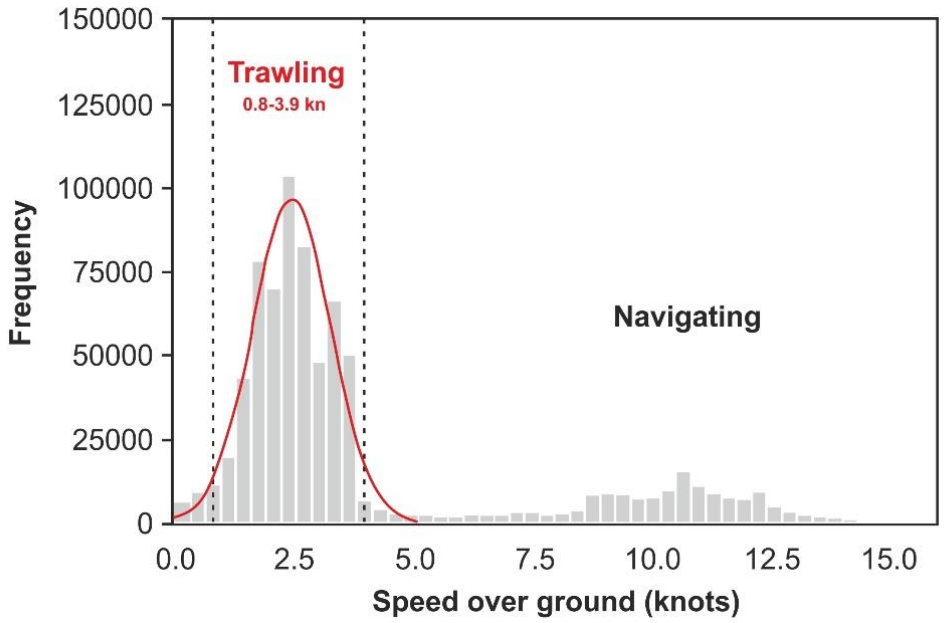

Figure 5.3. Speed over ground (SOG) histogram and fitting of the bi-modal distribution through the EM-algorithm of bottom trawler speeds. The black dashed line indicates the upper and lower limits used to classify vessels as trawling, which corresponds to operating speeds of 0.8-3.9 knots.

5.3. Results

5.3.1. Forcing conditions

During the study period, several storms, defined as sustained significant wave heights (Hs) greater than 2 m for more than 6 hours (Mendoza and Jiménez, 2009), were recorded during the monitoring in early February, and early- and late-March, the majority of them caused by strong northern winds and with Hs > 3m (Fig. 5.4a). These events were generally dry storms (Guillén et al., 2006) that did not lead to significant increases in Ter and Daró river discharges (Fig. 5.4b).

Four major storms (Hs > 4m) were recorded during the study period. A strong northern storm occurred in early February with maximum Hs of 4.9 m, which lasted more than 15 hours (Fig. 5.4a). A unique strong eastern storm with maximum Hs of 4.7 m at the peak of the storm that lasted from February 12 to February 16 (Fig. 5.4a) caused a torrential Ter River discharge that reached 30.6 $m^3 \cdot s^{-1}$ on February 15, concurrent with a small increase of 6.0 $m^3 \cdot s^{-1}$ at the Daró River (Fig. 5.4b). A stronger northern storm with a maximum Hs of 5.1 m occurred on March 4 that lasted for two days (Fig. 5.4a) and led to a Ter River discharge of 11.1 $m^3 \cdot s^{-1}$ and a Daró River discharge of 2.2 $m^3 \cdot s^{-1}$ (Fig. 5.4b). At the end of the study period, a strong southern storm with maximum Hs of 4.1 m occurred on March 25 (Fig. 5.4a), which lead to a Ter River discharge of 19.4 $m^3 \cdot s^{-1}$ and a Daró River discharge of 1.5 $m^3 \cdot s^{-1}$ (Fig. 5.4b).

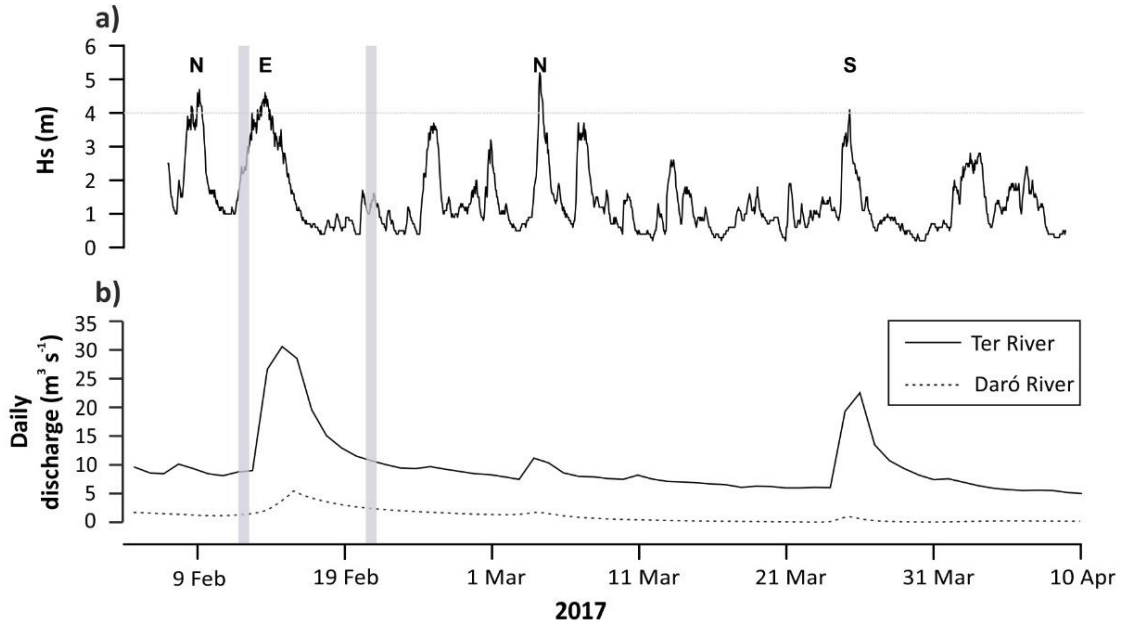

Figure 5.4. Temporal evolution of the a) significant wave height (*Hs*, m) measured at the Cap de Begur buoy and b) the Ter and the Daró river discharges ($m^3 \cdot s^{-1}$) during the study period. Major storms, with *Hs* > 4 m, are indicated with an N (northern storms), E (eastern storms) or an S (southern storms) according to their origin. The occurrence of DSWC events is indicated with a grey vertical bar.

5.3.2. Trawling activity

The fishing grounds of the Palamós Canyon were exploited by 34 OTB vessels, most of which from the Palamós harbour, but occasionally from Blanes and Roses harbours (located southwards and northwards, respectively, and not shown in Figure 5.1).

Time-series observations on OTB vessel positions, based on fishing effort, revealed no trawling activity occurred around the mooring site during the trawling closure at the flanks of the canyon, while during the trawling season, the fishing effort increased on both canyon flanks (Fig. 5.2). In the Rostoll fishing ground section located closer to the mooring and CTD transect, bottom trawling occurred at relatively shallow depths ranging from 250 and 450 m, at a predominating frequency of 5 hauls per hectare. The fishing effort in the Rostoll fishing ground increased seawards, reaching 10-30 hauls per hectare at 500-600 m depth. At the Sant Sebastià fishing ground, the predominating frequency in the canyon wall next to the mooring and the CTD transect was 20-40 hauls per hectare between 400 and 800 m depth (Fig. 5.2). The number of daily hauls was computed at both fishing grounds during the monitored trawling season, being generally higher in Sant Sebastià than in Rostoll, and accounting for a total of 74 hauls against 31 hauls, respectively (Fig. 5.5)

More scattered trawling activity was also observed on the upper continental slope at depths < 200 m (Fig. 5.2). This fishing effort was estimated to be less than 5 hauls per hectare during the monitored trawling season. The number of hauls computed at these depths was considerably

smaller in comparison to those computed at the depths of the canyon flanks' fishing grounds and accounted for a total of 18 hauls for the monitored trawling season (Fig. 5.5).

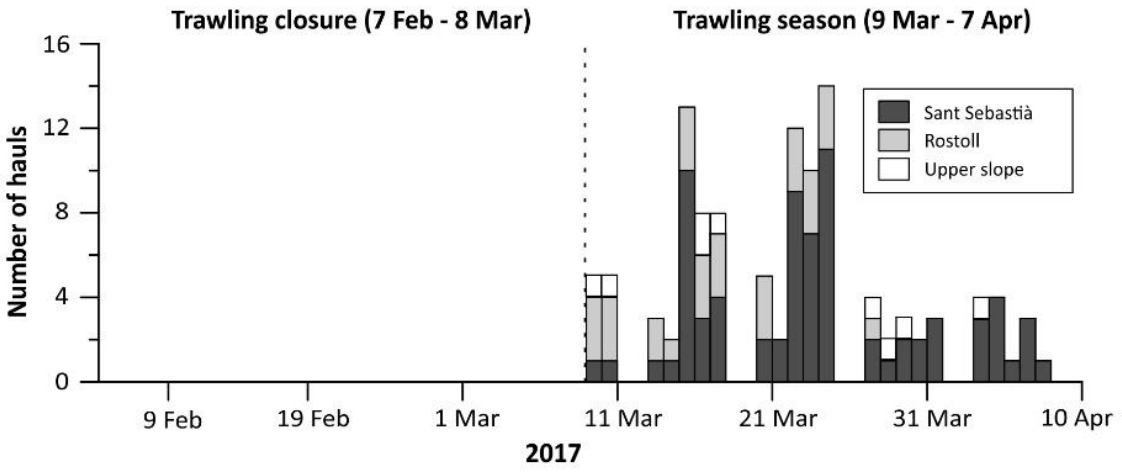

Figure 5.5. Daily hauls in the Sant Sebastià and Rostoll fishing grounds, and in the upper slope region during the study period. The dashed line separates the trawling closure from the trawling season.

5.3.3. Time-series data

5.3.3.1. Hydrographic structure

Compiled data of all hydrographic profiles during the study period revealed distinct changes in temperature and salinity throughout the water column that are ascribed to the different water masses in the study area (Fig. 5.6).

The oAW occupied the shallowest water column (150-300 m) during most of the recording period (Figs. 5.6 and 5.7). Below oAW, the temperature and salinity time series, as well as the *TS* diagram, showed the more saline LIW, mainly centered at 500-600 m water depth (Figs. 5.6 and 5.7). The WMDW was generally observed at the deepest part of the hydrographic profiles, exhibiting its characteristic temperature and salinity values (Figs. 5.6 and 5.7). In addition to these water masses, the seasonal WIW (T = 12.9-13.2 ºC; S = 38.1-38.3) and two pulses of DSW, displaying temperature minima reaching < 12.6 ºC along with salinity values < 38.2, were observed at the beginning of the recording period (Figs. 5.6 and 5.7). Particularly, the presence of DSW and WIW over the Palamós Canyon occurred from February 7 to February 24, the latter mainly ranging from 150 to ~400 m depth (Figs. 5.7a, b).

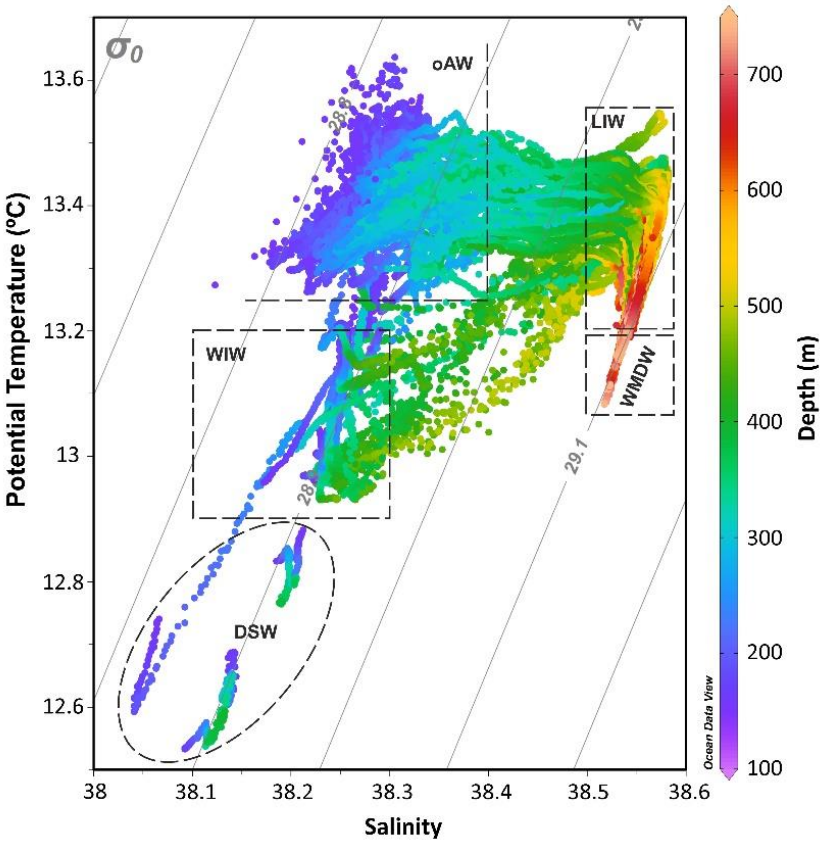

Figure 5.6. General *TS* diagram for all the hydrographic casts acquired by the Aqualog during the study period identifying the different water masses in the study area: oAW (old Atlantic Water), WIW (Western Intermediate Water), DSW (Dense Shelf Water), LIW (Levantine Intermediate Water), and WMDW (Western Mediterranean Deep Water).

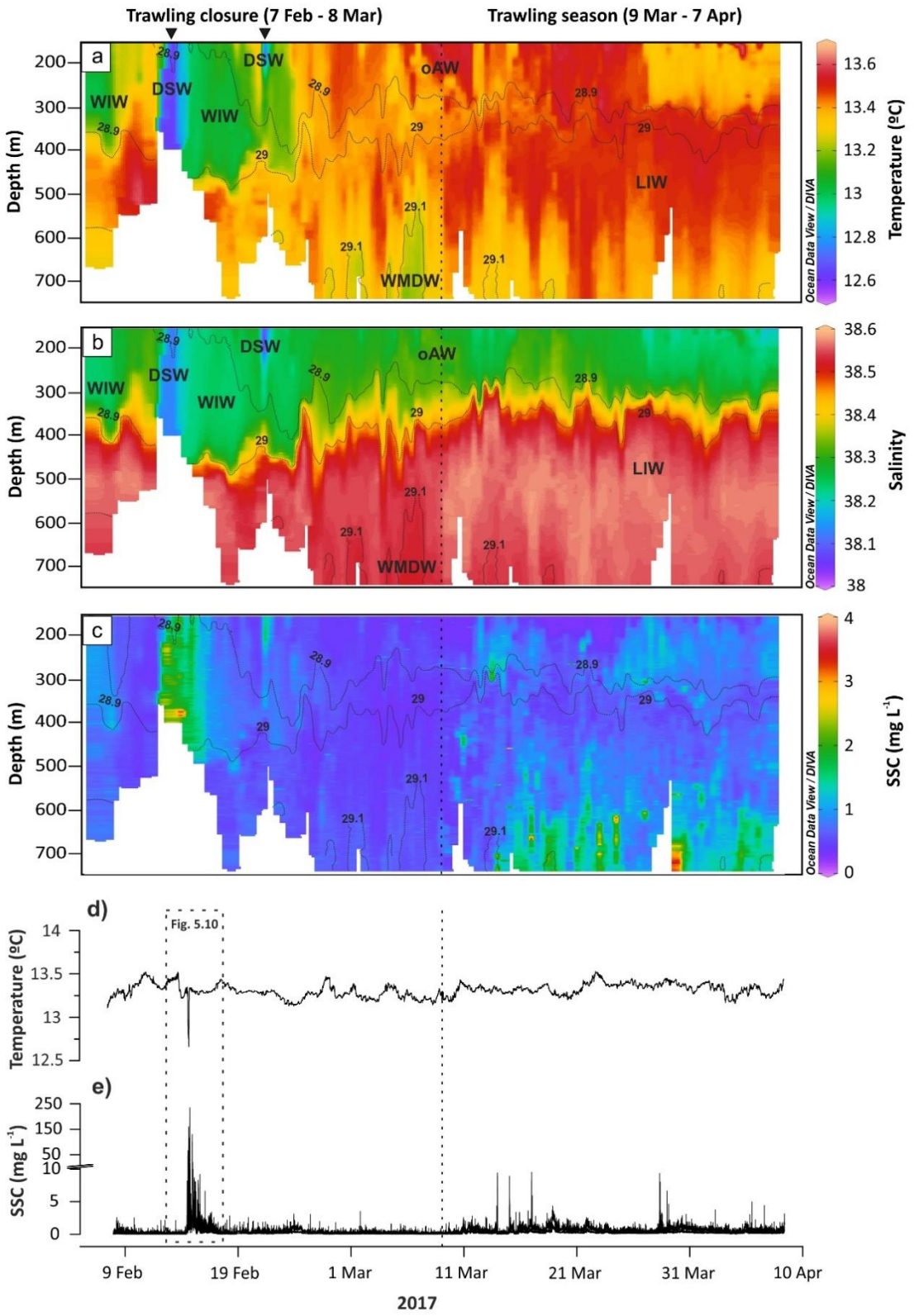

Figure 5.7. Time series of a) potential temperature (ºC), b) salinity, c) SSC (mg·L^{-1}) measured by the Aqualog, as well as d) temperature (ºC) and e) SSC (mg·L^{-1}) measured by the near-bottom instrumentation during the monitoring period. Panels a) and b) show the different water masses being present in the study area: oAW (old Atlantic Water), WIW (Western Intermediate Water), DSW (Dense Shelf Water), LIW (Levantine Intermediate Water), WMDW (Western Mediterranean Deep Water). The occurrence of two DSWC events is indicated by a black triangle. Blank spaces represent incomplete profiles. The dashed line separates the trawling closure from the trawling season.

5.3.3.2. Suspended particulate matter distribution

The vertical particulate matter distribution showed increasing SSC (up to 1 mg·L^{-1}) that lasted for the first two days of the study period, in agreement with the presence of WIW (Fig. 5.7c). Immediately afterwards, the water turbidity decreased and maintained values < 0.8 mg·L^{-1} in the profiled water column for 6 days, when water turbidity increased to between 1.1 and 3.8 mg·L^{-1} from February 13 to February 15 coinciding with the first DSW pulse into the canyon (Figs. 5.7a-c) (see the first black triangle). This DSWC event was noted by a sharp decrease in temperature (~0.5 ºC) and salinity (~0.2) values (Figs. 5.7a, b). This first pulse of DSW was detected all along the entire profiling range recorded at that time. However, it was only observed reaching depths between 370 and 400 m in the hydrographic profiles recorded by the Aqualog, without being able to capture its deeper limit in these profiles (Figs. 5.7a-c). This DSW pulse reached the canyon axis, as observed by the temperature and turbidity values recorded close to the bottom by the near-bottom instrumentation, presenting near-bottom temperatures of ~12.6 ºC (Fig. 5.7d) and maximum SSC of ~234 mg·L^{-1} (Fig. 5.7e). Afterwards, water turbidity maintained relatively high SSCs along the hydrographic profiles for three days associated with the presence of WIW, ranging from 0.4 to 1.1 mg·L^{-1} down to depths of ~500 m (Fig. 5.7c). On February 21, the shallowest part of the hydrographic profiles recorded a new decrease in temperature and salinity values, and an increase of SSC of 2.2 mg·L^{-1}, coinciding with the arrival of the second pulse of DSW into the canyon (Figs. 5.7a-c). However, it only lasted for a few hours and descended to maximum water depths of 200 m (see the second black triangle), without displacing the WIW found underneath (Figs. 5.7a, b). After this event, and until February 24, the vertical particulate matter distribution still showed events of moderate SSC elevation in the water column that ranged between 0.3 and 0.9 mg·L^{-1} from the uppermost part of the hydrographic profiles to maximum water depths of 500 m (Fig. 5.7c). From February 24 to the end of the study period, the WIW was absent and recorded temperature and salinity values that corresponded to the more general hydrographic structure of the northwestern Mediterranean, with the presence of surface oAW, the core of LIW at mid-waters and centered between 500 and 600 m and the WMDW occupying the deeper part of the profiled water column (Figs. 5.7a, b). During this period, the vertical distribution of particulate matter showed no periods of significant SSC increase in the profiled water column until the beginning of the trawling season on March 9 (Fig. 5.7c).

During the trawling season, several SSC increases were recorded at intermediate waters (from 150 to 300 m depth), reaching up to 2.5 mg·L^{-1} and at the lower part (> 500 m depth) of the profiled water column (Fig. 5.7c). A relative clear water minimum was recorded between 300 and 500 m water depth. The maximum SSC was recorded on March 30 at ~718 m depth, reaching up to 3.8 mg L^{-1} (Fig. 5.7c). Near-bottom time series (923 m depth) of temperature and turbidity values remained constant during most of the time, displaying temperature values ranging from 13.2 and 13.6 ºC (Fig. 5.7d) and SSC < 1.5 mg·L^{-1} (Fig. 5.7e). Punctual increases in SSC between 5 and 10 mg·L^{-1} were recorded during the trawling season (Fig. 5.7e), although such increases showed no relation with temperature fluctuations.

The NPSC for the upper part of the profiled water column peaked at ~40.7 mg·cm^{-2} and 23.3 mg·cm^{-2} during the two DSW pulses, respectively (see black triangles in Fig. 5.8a) and decreased to baseline NPSC values (~10 mg·cm^{-2}) at the end of the closure season. The NPSC values increased again in the trawling season, when almost a double-fold increase in the NPSC (~20 mg·cm^{-2}) was observed (Fig. 5.8a). In the second approach, considering the entire profiling range, the NPSC varied between 8.3 and 20.8 mg·cm^{-2} during the end of the closure season, whereas it was doubled and even quadrupled during the trawling period, reaching maximum values of 50.1 mg·cm^{-2} (Fig. 5.8b).

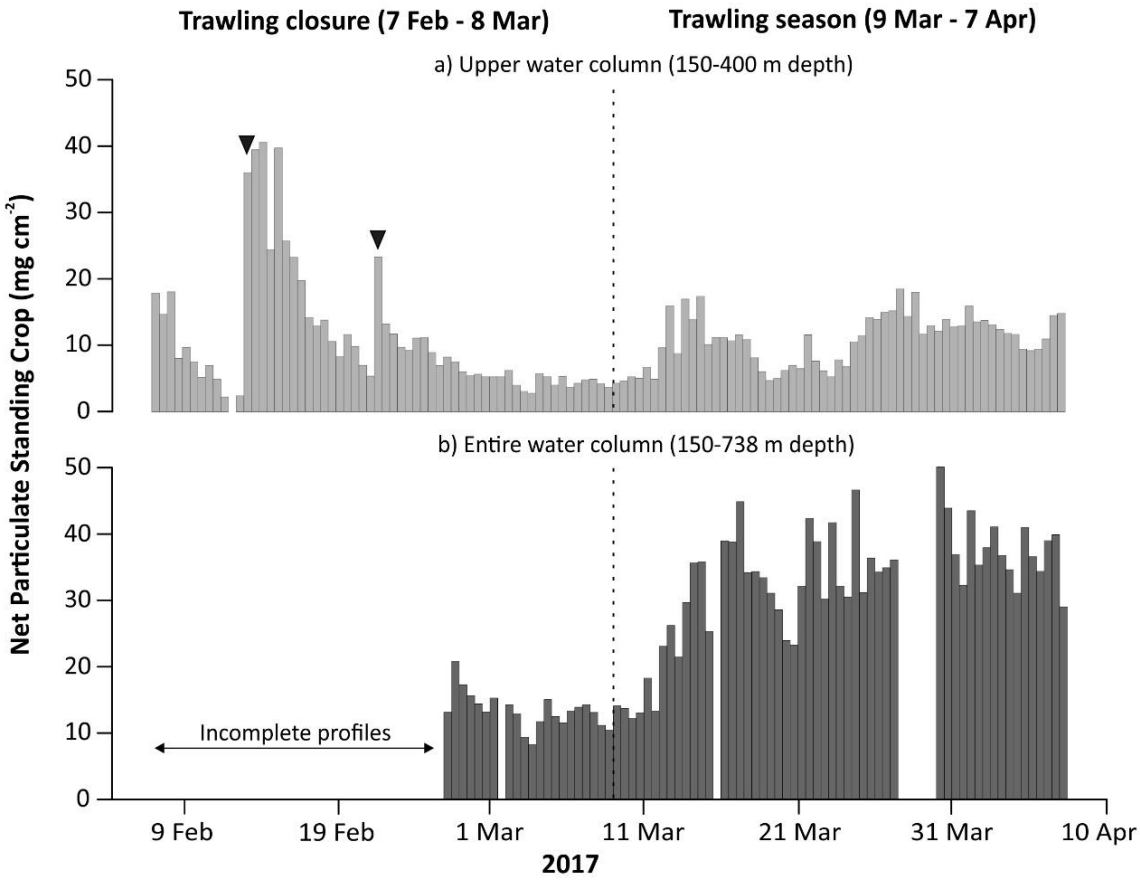

Figure 5.8. Net Particulate Standing Crop (NPSC) for a) the upper water column (150-400 m depth) and for b) water depths between 150 to 738 m depth during the study period. The occurrence of two DSWC events is indicated by a black triangle. The dashed line separates the trawling closure from the trawling season.

5.3.3.3. Near-bottom currents

During most of the study period, near-bottom currents followed the currents axis (Figs. 5.9a, b). Current speeds varied between 0.05 and 0.25 m·s^{-1} during most of the monitoring in both along- and across-canyon directions (Figs. 5.9c, d), although periodic reversals in the current direction mainly oriented up- and down-canyon were observed (Fig. 5.9c).

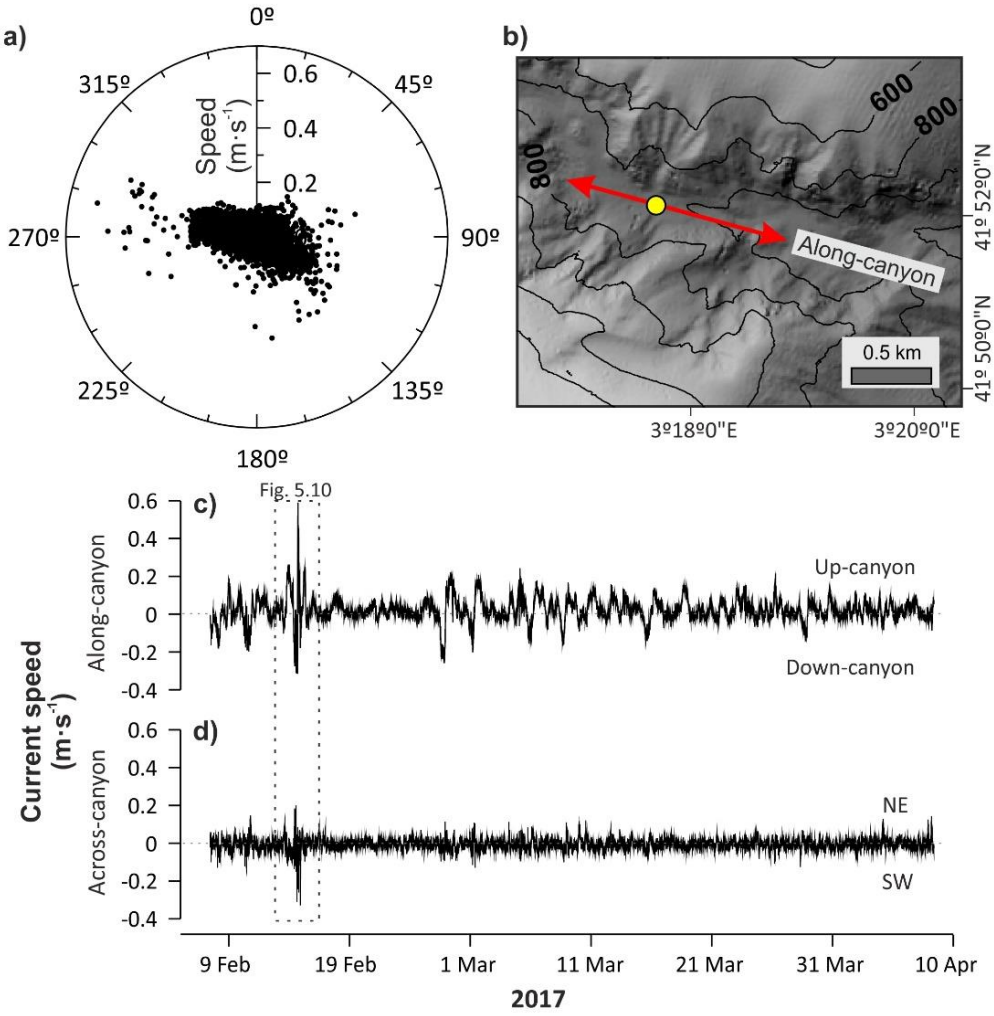

Figure 5.9. Time series of near-bottom currents during the study period. a) Polar plot of current direction and current speed (radius) measured by the near-bottom current meter at 923 m depth. b) Close-up of the mooring location in Palamós Canyon and the main sediment current pathway at this particular location. Panels c) and d) correspond to the time series of along-canyon and across-canyon current speed, respectively.

This general current pattern was altered between February 14 and February 15, during the first DSW pulse, when near-bottom currents and SSC changed drastically (Figs. 5.9 and 5.10). During the first stages of this event, temperature experimented a slight increase of 0.2 ºC (Fig 5.10a), concurrent with an increase of the down-canyon current velocity up to 0.2 $m \cdot s^{-1}$ (Fig. 10b) but slightly oriented towards the NE sector (Fig. 5.10c), while turbidity progressively increased up to 75 $mg \cdot L^{-1}$ (Fig. 5.10d). A sharp decrease in near-bottom temperature (~0.5 ºC) reaching down to 12.6 ºC (Fig. 5.10a) was recorded afterwards and, simultaneously, currents reached speeds of 0.3 $m \cdot s^{-1}$ with dominant down-canyon direction but oriented towards the SW (Figs. 5.10b, c), while near-bottom turbidity increased up to 160.1 $mg \cdot L^{-1}$ (Fig. 5.10d). Three hours later, the temperature increased to 13.3 ºC (Fig. 5.10a), which was concurrent with a maximum peak in current speed up to 0.6 $m \cdot s^{-1}$ directed up-canyon (Fig. 5.10c). When this current reversal occurred, a sharp increase in turbidity was observed, reaching maximum SSC of ~234 $mg \cdot L^{-1}$ (Fig.

5.10d). Near-bottom currents maintained the up-canyon flow direction for almost 5 hours (Fig. 5.10b), and turbidity values gradually decreased to 4 mg·L^{-1} (Fig. 5.10d). Afterwards, the near-bottom current flow reversed following the down-canyon direction (Fig. 5.10b) and slightly towards the SW (Fig. 5.10c). Another current reversal of up to 0.3 m·s^{-1} was detected up-canyon (Fig. 5.10b), while another concurrent important turbidity peak of 96 mg·L^{-1} was recorded (Fig. 5.10d). Towards the end of this event, the current speed and turbidity decreased to baseline values (Figs. 5.10b-d).

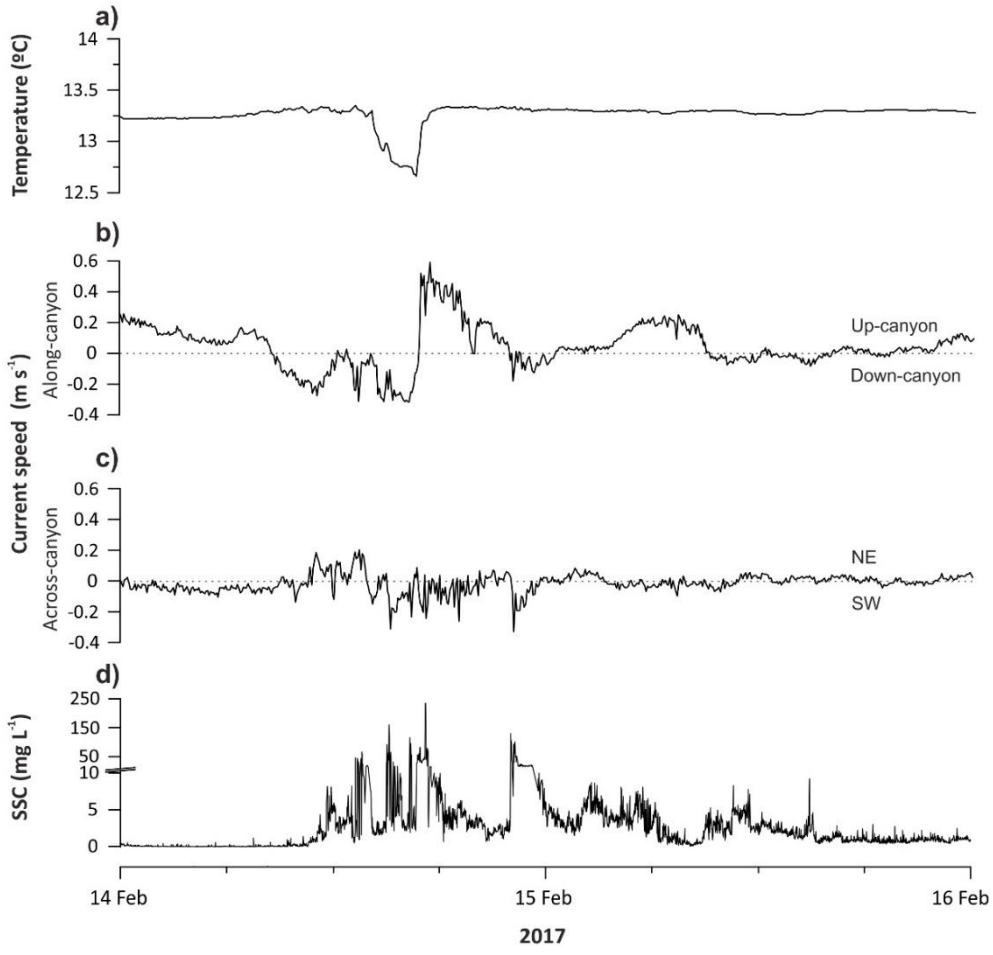

Figure 5.10. Time series of a) temperature (ºC), b) along-canyon current speed (m·s^{-1}), c) across-canyon current speed (m·s^{-1}), and d) SSC (mg·L^{-1}) measured during the first DSWC event.

5.3.3.4. Suspended sediment fluxes and cumulative transport

During most of the trawling closure, instantaneous along-canyon near-bottom suspended sediment fluxes fluctuated between 0.02 and 0.1 g·m^{-2}·s^{-1} (Fig. 5.11a) and between 0.01 and 0.06 g·m^{-2}·s^{-1} in the across-canyon direction (Fig. 5.11b). However, during the first DSWC pulse, there was an increase in both along- and across-canyon suspended sediment fluxes. In the along-

canyon direction, suspended sediment flux increased up to 19 g $m^{-2}·s^{-1}$ down-canyon, but the more important suspended sediment flux was registered up-canyon, reaching values of 44 g $m^{-2}·s^{-1}$ (Fig. 5.11a). In the across-canyon direction, suspended sediment flux increased up to 8.8 g $m^{-2}·s^{-1}$ towards the NE, although the maximum suspended sediment flux was registered towards the SW reaching up to 35 g $m^{-2}·s^{-1}$ (Fig. 5.11b). The cumulative transport after this event was up-canyon (Fig. 11c) and towards the SW (Fig. 5.11d), reaching values of 50 $kg·m^{-2}$ and 80 $kg·m^{-2}$, respectively.

During the trawling season, instantaneous along-canyon suspended sediment flux ranged from 0.1 to 0.7 g $m^{-2}·s^{-1}$ and was predominantly in the up-canyon direction, and across-canyon suspended sediment flux reached maximum values of 1.4 g $m^{-2}·s^{-1}$ mainly towards the SW (i.e., coming from the northern flank) (Figs. 5.11a, b). Therefore, throughout the trawling season, the resultant cumulative suspended sediment transport was in the up-canyon direction and from the northern flank (towards the SW) in the across-canyon component, reaching 40 $kg·m^{-2}$ and 20 $kg·m^{-2}$, respectively (Figs. 5.11c, d).

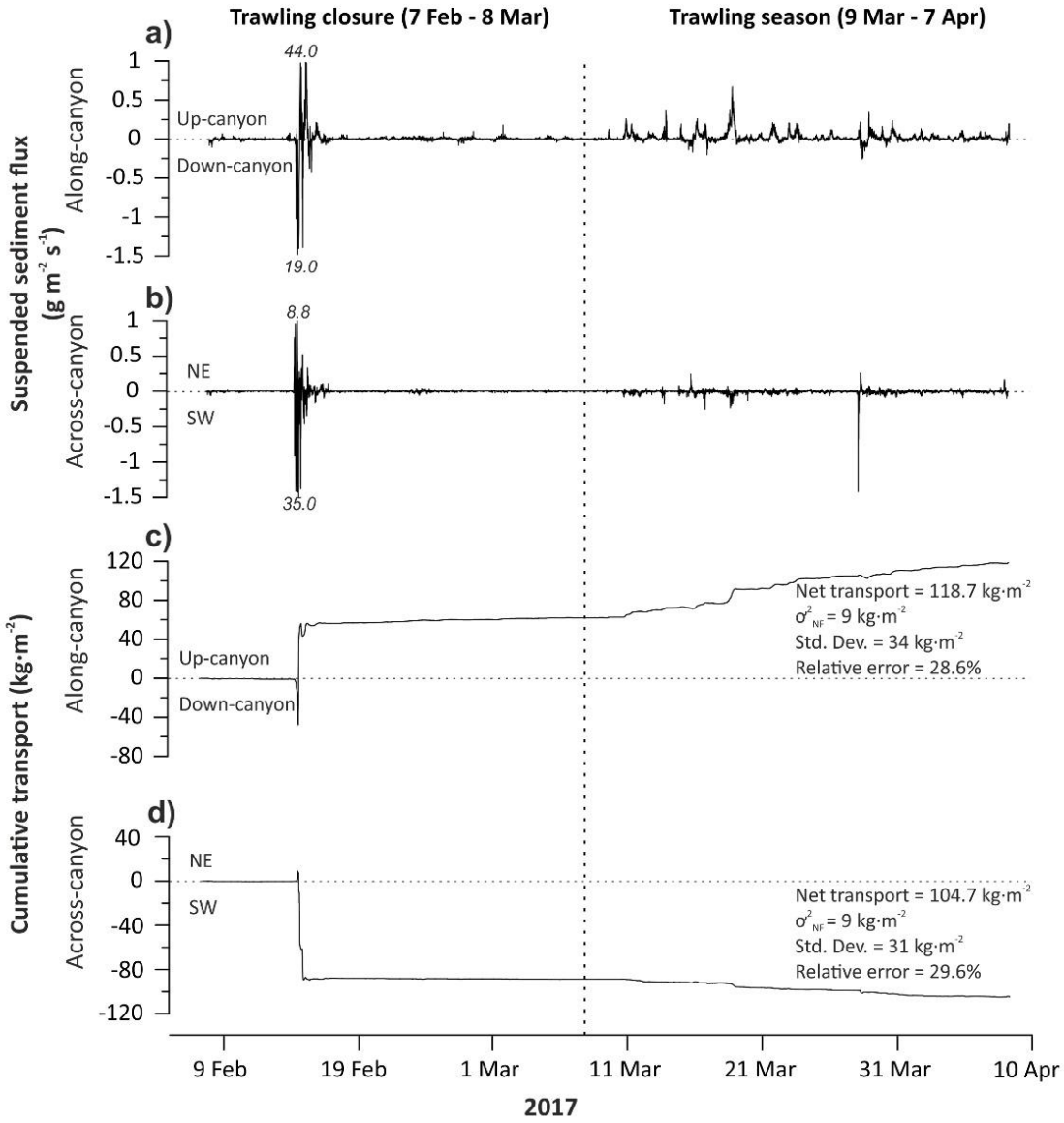

Figure 5.11. a) Instantaneous along-canyon suspended sediment flux ($g \cdot m^{-2} \cdot s^{-1}$), b) instantaneous across-canyon suspended sediment flux ($g \cdot m^{-2} \cdot s^{-1}$), c) along-canyon cumulative transport ($kg \cdot m^{-2}$) and d) across-canyon cumulative transport ($kg \cdot m^{-2}$) at the mooring site during the monitoring period. Maximum sediment fluxes reached during DSWC events are indicated in italics. The dashed line separates the trawling closure from the trawling season. Inset on panels c) and d) provides the time-integrated cumulative transport (net transport) for the along- and across-canyon components and their uncertainty (σ^2_{NF}), the standard deviation and the relative error derived from these calculations for the entire monitoring period.

5.3.4. CTD transect

The hydrographic data obtained during the CTD transect across the Palamós canyon head from the surface down to 925 m depth revealed distinct changes in temperature and salinity throughout the water column (Fig. 5.12). In the first 50 m of the water column, waters with distinctly low salinities (38.0-38.2) and high temperatures (15-19 ºC) were observed (Figs. 5.12a,

b), most probably corresponding to the influence of the seasonal thermocline. The signature of the old Atlantic Water (oAW), characterized by temperatures > 13 ºC (Fig. 5.12a) and salinity values ranging from 38.0 to 38.4 (Fig. 5.12b), was found underneath, reaching water depths down to 200 m in the northern canyon flank and ~300 m in the southern canyon flank. Below (down to ~800 m water depth), the temperature and salinity along the transect showed the more saline LIW core, which displayed a salinity maximum (S > 38.5) centered ~500 m water depth (Figs. 5.12a, b). The deepest part of the water column was occupied by the WMDW that exhibited temperature minima of 13 ºC and salinity values of 38.5 (Figs. 5.12a, b).

The suspended particulate matter (SPM) distribution across the studied canyon section showed a surface clear water layer down to ~100 m water depth and a continuous INL with concentrations ~ 0.5 mg·L^{-1} extending over the entire canyon width in the water parcel occupied by the oAW (Fig. 5.12c). Within the canyon confinement, the central part of the water column mainly corresponded to the upper levels of the LIW core and was characterized by low SSC, whereas near-bottom waters in both canyon flanks and close to the canyon axis displayed higher SSC. Over the southern canyon wall, there was a detachment of a thin BNL mainly centered at ~300 m depth, reaching SSC up to 3 mg·L^{-1} (Fig. 5.12c, station #2). This detachment extended ~450 m horizontally towards the canyon interior as an INL, which was observed in station #3 at the same water depth, but with SSC values of 0.5 mg·L^{-1}. On the northern canyon wall, a well-developed BNL displaying SSCs up to 1.5 mg·L^{-1} was observed at ~450 m water depth (Fig. 5.12c, station #11), which evolved towards the canyon interior and to a less concentrated and thicker BNL, with SSC ~1 mg·L^{-1} extending from 550 to 700 m depth (Fig. 5.12c, station #10). The lower part of the profiled water column over the canyon axis (stations #5 to #9) showed SSC > 0.5 mg·L^{-1} that corresponded to scattered and isolated INLs showing poor lateral continuity among consecutive hydrographic casts (Fig. 5.12c).

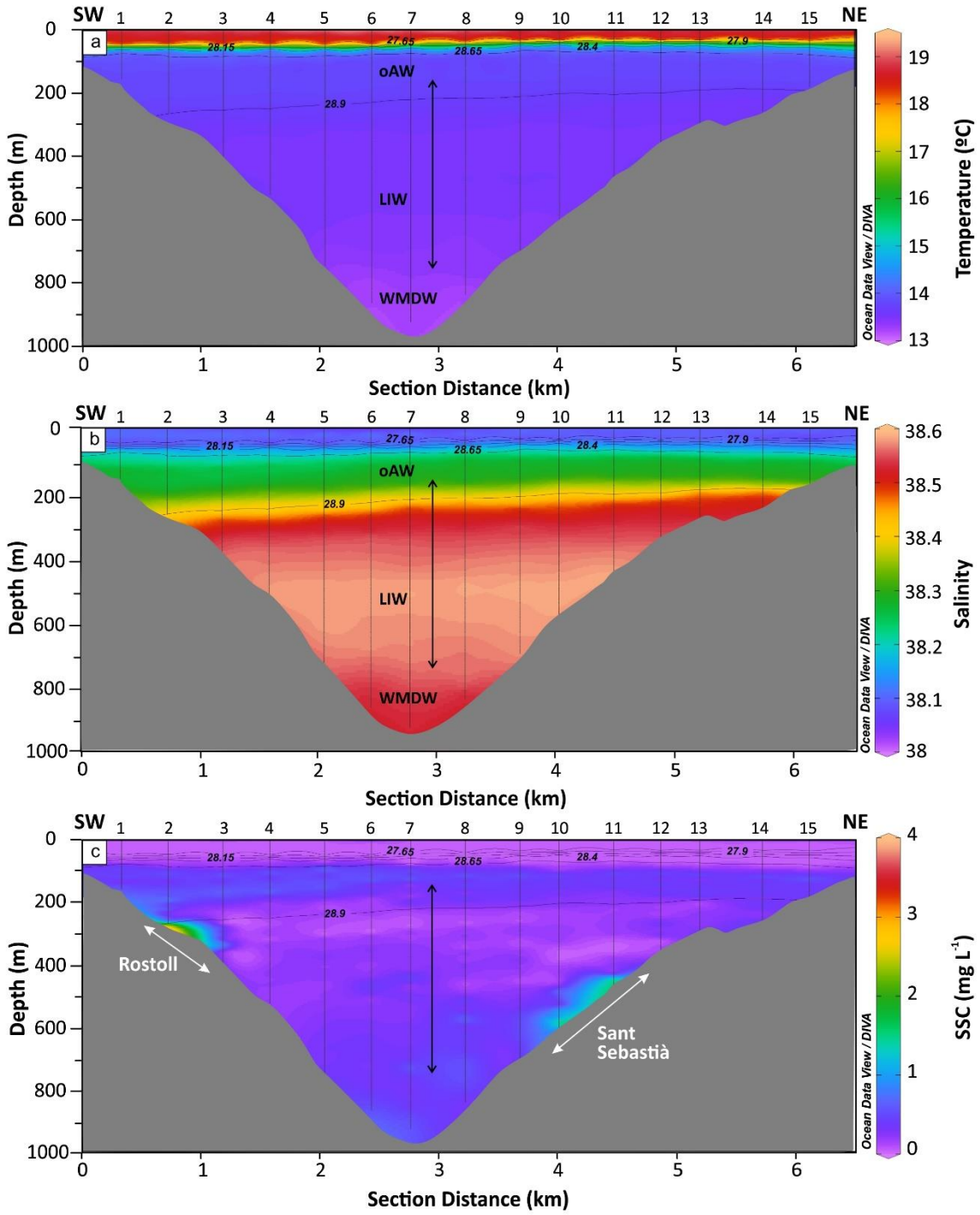

Figure 5.12. CTD transect conducted on June 7, 2017 across the Palamós Canyon showing the distribution of a) potential temperature (ºC), b) salinity, with the different water masses present in the study area (see Figure 5.6 for details), and c) SSC (mg·L^{-1}). The black arrow indicates the working depth range of the autonomous hydrographic profiler (Aqualog) and the white arrows indicate the bathymetric range occupied by the Sant Sebastià and Rostoll fishing grounds extracted from the AIS spatial distribution at the location where the CTD transect was conducted (see location in Figure 5.2).

5.4. Discussion

5.4.1. Natural-induced water turbidity and suspended sediment transport

The earlier studies using moored instrumentation demonstrated that river floods and storms enhanced particle fluxes inside submarine canyons and on the continental slope (Monaco et al., 1990; Puig and Palanques, 1998b), and for a long time, these processes were considered the major contemporary mechanisms able to transport sediments from shallow water environments to deeper environments. Recent studies conducted in the northwestern Mediterranean also recognize the importance of the formation of dense shelf waters (DSW) and their subsequent downslope cascading, exporting sediment particles towards deep-sea regions (Canals et al., 2006; Palanques et al., 2006b).

In the Palamós Canyon, Ribó et al. (2011) reported for the first time the presence of dense shelf water cascading (DSWC) events related to eastern storms. In this investigation, priority was given to the deployment of near-bottom instruments at the canyon head, on the assumption that most of the suspended sediment transport and water turbidity increases were coming from the shelf and relatively confined near the canyon seafloor. The results presented in this Chapter contribute to refine the sedimentary dynamics associated with DSWC events in Palamós Canyon providing additional information throughout the water column, as well as near the bottom at a deeper canyon axis location (Figs. 5.7, 5.8, 5.9, 5.10, 5.11). During the study period, the first DSWC event was enhanced by a major eastern storm that occurred between February 12 and February 16, which also led to a torrential water discharge from the Ter River. The eastern storm was most probably responsible for the expulsion of dense coastal waters present on the shelf upstream of the canyon, which alongside with the ephemerally sediment deposited on the shelf by the Ter River, generated high downslope and down-canyon sediment transport into Palamós Canyon. The DSW signal was detected along the profiled water column from 150 to 377 m depth and also near the bottom at 923 m depth (Fig. 5.7), which suggests an increase of turbidity throughout the entire water column. Although relatively high SSC increases were recorded at intermediate water depths (> 3.5 $mg \cdot L^{-1}$) (Fig. 5.7c), very strong SSC increases (> 200 $mg \cdot L^{-1}$) occurred near the bottom (Fig. 5.7e). This indicates that the cascade of DSW during this event caused a rapid advection of cold and turbid waters down to the deepest part of the surveyed water column, presumably transporting easily erodible sediment particles on their way as they moved down-canyon, generating high near-bottom suspended sediment fluxes (Figs. 5.11a, b; Table 5.2). Previously recorded DSWC events in Palamós Canyon by Ribó et al. (2011) were specific for the canyon head (325 m depth) and accounted for lower down-canyon current velocities (> 0.4 $m \cdot s^{-1}$ versus 0.6 $m \cdot s^{-1}$) and lower SSC peaks (~6 $mg \cdot L^{-1}$ versus > 200 $mg \cdot L^{-1}$) than in the canyon axis. However, DSWC events of similar magnitude to that observed during the present study have been recorded in the Cap de Creus Canyon, where near-bottom SSC > 170 $mg \cdot L^{-1}$ and currents of ~0.6 $m \cdot s^{-1}$ were registered (Ribó et al., 2011).

During the first stages of the major DSWC event recorded during the study, the near-bottom suspended sediment fluxes were mainly directed down-canyon and towards the SW (Figs. 5.11a, b), suggesting the arrival of a non-channeled cascade coming predominantly from the northern canyon flank. As the dominant eastern field veered to south-westerlies (not shown) and the storm ceased (Fig. 5.4b), currents inside the canyon reversed from down-canyon to up-canyon, peaking up to 0.6 $m \cdot s^{-1}$ (Fig. 5.10b), and the DSW turbid plume was retained within the canyon's interior, increasing near-bottom SSC up to ~234 $mg \cdot L^{-1}$ (Figs. 5.10d), generating an abrupt peak in near-bottom suspended sediment flux of 44 $g \cdot m^{-2} \cdot s^{-1}$ directed up-canyon (Fig. 5.11a). This sudden change in current flow, due to the compensation of the isopycnals, has been previously described as the reversal (relaxation) phase of cascading/downwelling events (Ulses et al., 2008b), and described in detail in the Cap de Creus Canyon during a similar storm event in winter 2011 (Martín et al., 2013). The second DSW pulse detected on February 21 was not associated with any storm event nor a flash flood river discharge (Fig. 5.4), and in contrast to the first DSW pulse, it was shorter and only reached about 200 m depth (Fig. 5.7). This event generated lower SSC at the upper part of the hydrographic profiles, and no signal was recorded in the near-bottom instrumentation (Fig. 5.7). This mild and shallow DSW pulse was therefore smaller in magnitude and resembled those recorded at similar depths (~300 m depth) in this submarine canyon by Ribó et al. (2011).

During the trawling closure period, the presence of the WIW was detected at the hydrographic profiles reaching maximum water depths of ~400 m, alongside with relatively high SSC values in the profiled water column (Figs. 5.7a-c). The WIW observed during the study period could have been formed earlier during the winter season by DSWC events affecting the upper slope of the GoL (Lapouyade and Durrieu de Madron, 2001; Dufau-Julliand et al., 2004; Durrieu de Madron et al., 2005a). This seasonal water mass could have then been advected southwards towards the Palamós Canyon, following the general circulation, and carrying an increased SSC signature. These high turbidity values, alongside with the increased SSC associated with the two DSW pulses, were also translated into higher NPSC during this period (Fig. 5.8a). Towards the end of the trawling closure period, the presence of waters generated by cooling and densification during winter (WIW and DSW) was no longer detected along the hydrographic profiles, and water turbidity decreased to almost baseline SSCs and NPSC in the upper water column, reaching the lowest values in the entire record (Figs. 5.7 and 5.8a).

Table 5.2. Near-bottom instantaneous suspended sediment (SS) fluxes ($g \cdot m^{-2} \cdot s^{-1}$) and cumulative transport ($kg \cdot m^{-2}$) calculated for the along- and across-canyon components during the trawling closure, which includes the DSWC period, and the trawling season. For the along-canyon component, up-canyon flux values and cumulative transport are positive, whereas for the down-canyon flux they are negative. For the across-canyon component NE orientation flux values are positive, whereas for the SW orientation they are negative.

	Instantaneous SS flux		**Cumulative transport**	
	Along-canyon	Across-canyon	Along-canyon	Across-canyon
Trawling closure	0.02-0.1	0.01-0.06	+50	-80
DSWC period (max.)	+44	-35		
Trawling season	0.1-0.7	1.4	+40	-20

5.4.2. Trawling-induced water turbidity and suspended sediment transport

Considering the absence of major storms or flooding events during the trawling season (Fig. 5.4) and the position of OTB vessels and number of daily hauls (Figs. 5.2 and 5.5), we can infer that the occurrence of frequent events of increased water turbidity within the Palamós Canyon (Fig. 5.7c) was induced by the passage of OTB vessels along the canyon flanks.

Throughout the monitored trawling season, the more intense fishing activity was particularly detected at depths between 250 and 600 m at the southern canyon wall (Rostoll fishing ground), and between 400 and 800 m depth at the northern canyon wall (Sant Sebastià fishing ground) (Fig. 5.2). Based on the relative depths at which the trawling activities occur on each flank next to the mooring location, the shallower INLs (250-350 m water depth) observed in the hydrographic profiles and the CTD transect most probably correspond to resuspended sediment detached from the Rostoll fishing ground, whereas most of the SSC increases detected below 500 m depth could correspond to resuspension from the Sant Sebastià fishing ground (Figs. 5.7c and 12c). These well-developed INLs and BNLs detected at depths > 500 m are in agreement with previous observations reported by Martín et al. (2014a). In their study, a hydrographic transect conducted across the Sant Sebastià fishing ground revealed the presence of enhanced INLs and BNLs coinciding with the depth range exploited by otter trawlers. The higher number of hauls carried out at this fishing ground in contrast with the lower number of hauls occurring at the Rostoll fishing ground (Fig. 5.5) suggest that most of the increases in water turbidity during the trawling season were generated in the northern canyon wall. Moreover, the Sant Sebastià fishing ground is closer to the canyon axis (~1.5 km) than the Rostoll fishing ground (~2.5 km), which would favor that most of SSC increases reaching the mooring location were detached from the northern canyon wall as nepheloid layers. Over this period, near-bottom suspended sediment fluxes presented a dominant direction towards the SW (Fig. 5.11b; Table 5.2), following the main flow of the geostrophic circulation in this margin, which also suggests that most of the

resuspended sediment came from the northern flank. Nonetheless, the time-integrated cumulative near-bottom transport over the trawling period showed a persistently up-canyon direction (Fig. 5.11c; Table 5.2). This fact seems to confirm previous time series observations within the Palamós Canyon, revealing the presence of a residual up-canyon flux superimposed to the periodical (i.e., inertial) up- and down-canyon flow oscillations along the canyon axis (Martín et al., 2006, 2007). This has important implications for the redistribution and final fate of bottom trawling resuspended sediments in the canyon, as sediment transported down-slope from the canyon flanks' fishing grounds would be retained by the up-canyon residual flow and rapidly deposited along the canyon axis, without being exported further down-canyon towards greater depths. This continuous up-canyon cumulative transport (Fig. 5.11c) may also explain the increase of sediment accumulation rates in Palamós Canyon (Martín et al., 2008; Puig et al., 2015), a phenomenon observed in other trawled submarine canyons of this margin (Paradis et al., 2017, 2018a, 2018b), leading to the formation of canyon axes anthropogenic depocenters next to trawling grounds.

Trawling at the Palamós Canyon also occur with minimal frequency at the northern upper slope (Fig. 5.2). Nevertheless, the few hauls carried out at this particular location could have contributed to feed the particulate matter detachments observed between 90 and 200 m depth during the CTD transect conducted on June 7 (Fig. 12c), which generated an INL too shallow to be recorded by the moored instruments. The pycnocline between the oAW and the LIW (Figs. 5.12a, b) could have favoured the retention of suspended particles at this depth range, which are advected towards the southwest by the geostrophic circulation, above the profiling range of the moored instruments (Fig. 5.7).

Overall, these new data from the Palamós Canyon supports the hypothesis that resuspension induced by bottom trawling activities can play a significant role in increasing SSC in the water column and generating INLs and BNLs at certain depths based on the locations of the fishing grounds. No other submarine canyon has been studied as intensively as the Palamós Canyon regarding the effects of bottom trawling on the sediment dynamics but given that canyons are very often targeted by demersal fisheries, it is likely that similar impacts have occurred and are occurring in other submarine canyons elsewhere. Similar enhanced trawling-induced nepheloid layers such as those reported in this Chapter have been reported in Whittard Canyon (NE Atlantic) (Wilson et al., 2015b; Daly et al., 2018). As discussed by Wilson et al. (2015b), although the trawling activity was not always adjacent to where these enhanced nepheloid layers were observed, the canyon would have likely transported the material down to deeper regions. However, due to limited dataset consisting in discrete CTD casts, these authors were not able to conclude the frequency of these events, nor their temporal evolution during the active trawling period at the Whittard Canyon (Wilson et al., 2015b).

5.4.3. Comparison between water turbidity during the trawling closure and the trawling season

Remarkable aspects during the trawling closure in February 2017 were the high SSC increases related to the two DSWC events in the canyon (Fig. 5.7), and the relatively high SSC values at the upper levels of the water column associated with the presence of WIW (Figs. 5.6 and 5.7). This generated high NPSC values computed for the upper levels of the profiled water column (Fig. 5.8a). By the end of the trawling closure period, water turbidity, as well as computed NPSC, decreased to baseline values (Figs. 5.7c and 5.8a), coinciding with the disappearance of the seasonal WIW and the subsequent reestablishment of the more general hydrographic structure of this region (Figs. 5.6 and 5.7a, b). As it has been previously stated, the formation of WIW over the GoL is directly affected by strong atmospheric events (Duffau-Julliand et al., 2004; Juza et al., 2019), being especially intense between late January to early March. However, changes in these atmospheric forcing and/or inflowing of AW and water properties including changes in LIW, can affect its horizontal advection and mixing with surrounding waters (Juza et al., 2019) and, subsequently, control its presence within the Palamós Canyon. These multiple factors could explain the rapid disappearance of the WIW from the hydrographic profiles by the end of the trawling closure season (Figs. 5.7a, b).

During the trawling season, almost all increases in water turbidity were associated with the trawling activities in the study area. This was translated into higher NPSC during the trawling season, which were almost two times those calculated at the end of the trawling closure (Fig. 5.8a). This was not only observed in the upper water column NPSC water column inventories, which allowed us to compare both periods, but also in the entire profiled water column (Fig. 5.8b). The higher values calculated for the trawling season indicate that trawling can more than double the suspended sediment load in the water column, which is in agreement with suspended sediment inventories previously documented in other trawling grounds, both in shallow and deep-sea environments (Palanques et al., 2001, 2014). Suspended sediment concentrations in the water column did not vary significantly when the trawling fleet was not operating on weekends and holidays at the flanks of the canyon. These results contrast with previous observations from a canyon tributary next to the Sant Sebastià fishing ground, which documented the occurrence of frequent events of high turbidity (i.e., sediment gravity flows) during working days and working hours of the local trawling fleet (Palanques et al., 2006a; Puig et al., 2012; Martín et al., 2014a). Additionally, this data showed that these events occurred once or twice a day when the trawling fleet went offshore and when it headed back to port (Martín et al., 2014a). However, in the results presented in this Chapter the near-bottom time series collected at 923 m depth in the canyon axis did not record such periodic sediment gravity flow events (Figs 5.7 and 5.10), as the instruments of the mooring were not receiving channeled trawled resuspended sediment through any canyon tributary. Instead, they received the less dense sediment particles that were scattered from the trawling grounds and remained in suspension after the passage of the sediment gravity flows. Once particles were detached in the water column, they remained in suspension for long periods of time, contributing to feed quasi-

permanent INLs and BNLs, where SSC was higher. Because of this, these increases of SSC did not show differences between working days and weekends.

5.5. Conclusions

The data presented in this Chapter show different turbidity and suspended sediment transport patterns between the trawling closure and the trawling season at the Palamós Canyon.

During the trawling closure period, natural increases in water turbidity and near-bottom suspended sediment fluxes occurred mainly during DSWC events. These observations provided further insight of the sediment transport associated with this oceanographic process in Palamós Canyon and showed evidence, for the first time, of the presence of DSWC reaching 929 m depth in the canyon axis. During the trawling season, increases in water turbidity linked to trawling activities occurred regularly and were recorded mainly concentrated at depths where the Sant Sebastià and the Rostoll fishing grounds are located. Bottom trawling introduced sediment into the water column that more than doubled the suspended sediment background values recorded during calm sea conditions of the trawling closure, in absence of dense shelf waters within the canyon. Near-bottom instantaneous suspended sediment fluxes caused by the passage of OTB vessels were some orders of magnitude smaller than those generated by DSWC events. However, the chronic trawling activities for at least 30 days over the same fishing ground are capable of producing similar cumulative suspended sediment transport to that generated by a major DSWC event.

The main difference between natural and trawling-induced mechanisms is that natural turbidity and suspended sediment transport occurs sporadically, whereas trawling-induced water turbidity and transport is periodic and constant. Taking into account that bottom trawling is practiced on a daily basis throughout the year at the flanks of Palamós Canyon, with the exception of the 60-day seasonal trawling closure, weekends and holidays, much higher suspended sediment transport would be expected for a complete trawling season. Results presented in this Chapter provide further inside on how bottom trawling activities are able to overcome natural processes as the main mechanism of sediment resuspension, capable of changing the natural patterns of particulate matter dispersion and accumulation in submarine canyon environments.

The capacity of bottom trawling to produce similar accumulated impacts to those resulting from sudden and sporadic natural high-energy events points out the necessity of addressing the effect of anthropogenic activities in studies of sediment dynamics in deep-sea environments where fishing activities are practiced.

Chapter 6. Influence of natural processes and bottom trawling in the nepheloid layer structure off Vancouver Island (British Columbia, Canada, NE Pacific)

6.1. Context and objectives

For the Cascadia margin (Canadian NE Pacific; Fig. 2.3), very little information exists on particulate matter dispersion and sediment dynamics within and around submarine canyons, despite that there are at least 40 canyons incising this margin, between the Juan de Fuca Strait, at 48 ºN, and the northern tip of the Queen Charlotte Islands, at 54 ºN (Harris et al., 2014a, 2014b). Although several studies have been recently conducted in Barkley Canyon using the NEPTUNE cabled seafloor observatory addressing topics such as methane release from gas hydrate outcrops (Thomsen et al., 2012), the role of phytoplankton blooms in the export of organic matter (Thomsen et al., 2017), the population dynamics of benthic organisms (Juniper et al., 2013; Matabos et al., 2014; Doya et al., 2014), and deep ontogenetic migrations of zooplankton (De Leo et al., 2018), up to date, no research has addressed the study of contemporary mechanisms that control the sedimentary dynamics in this canyon environment and its adjacent continental slope.

Previous studies in the NE Pacific margin during the 80s in the neighbour Quinault Canyon (off Olympic Peninsula; Fig. 6.1) suggested that most of the off-shelf sediment transport in this margin occurs during storm events (Carson et al., 1986). Monitoring in this canyon showed that sediment resuspended on the shelf during storm events is advected over the upper slope and canyon forming a shelf-break INL (Carson et al., 1986; Hickey et al., 1986) that increases particle fluxes at intermediate depths in the upper canyon region and near the bottom (Baker and Hickey, 1986). In addition, resuspended fine-grained sediments preferentially accumulate in the canyon head thalweg due to constrained circulation within the canyon (Thorbjarnarson et al., 1986). The same dispersion/accumulation pattern is likely occurring in Barkley Canyon, although no study has yet been conducted to verify it. Moreover, this margin has been exploited by an active bottom trawling fishing fleet since the 1990s (Kulka and Pitcher, 2001; Haigh and Schnute, 2003). Bottom trawling data from Canada's Department of Fisheries and Oceans (DFO) from 1996 to 2005 have shown that this fishery's footprint extends over ~38.000 km^2 along Canada's Pacific coast from 115 to 1100 m depth (Sinclair, 2007). Therefore, the contemporary sedimentary dynamics on the continental slope could also be affected by this human activity, as it has been observed in other margins (Puig et al., 2012; Martín et al., 2014b, c).

This chapter aims to investigate the hydrographic and nepheloid layer distribution through the water column in the upper slope region of Vancouver Island (British Columbia, Canada), as well as to assess and discuss the potential resuspension mechanisms -natural and anthropogenic- that contribute to present-day sedimentary dynamics in this region. To do so, ~4 months of time series of hydrographic vertical profiles (temperature, salinity, pressure, turbidity, fluorescence, and

oxygen) combined with low frequency ADCP data from Barkley Canyon's node of ONC's NEPTUNE cabled seafloor observatory, off Vancouver Island were analysed (Fig. 6.1).

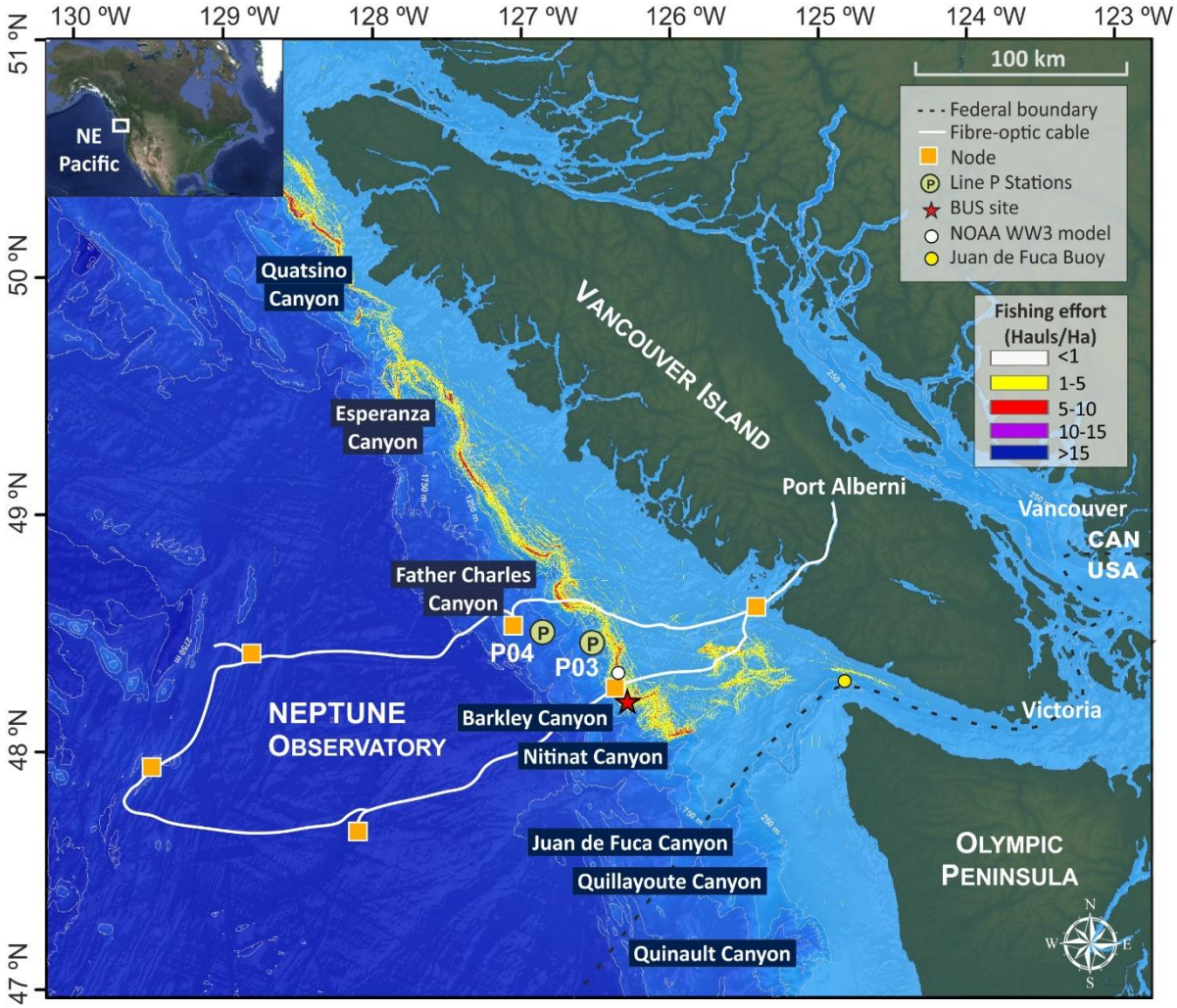

Figure 6.1. Bathymetric map of the study area highlighting Ocean Networks Canada's NEPTUNE cabled seafloor observatory (white line) and nodes (orange squares) and the submarine canyons incising the Cascadia margin. The location of the instrumented platform used in this study (BUS site) is illustrated with a red star and the long-term monitoring stations from Line P (P03 and P04) monitoring program are indicated in green circles. The location of the Juan de Fuca Buoy (yellow dot) and the NOAA WW3 model (white dot) are also shown, from which meteorological (wave and wind conditions) data were retrieved. The overlying density raster represents an estimate of the trawling effort on the Canadian territorial slope waters based on the number of hauls per hectare obtained from AIS data of 2018, which includes the monitoring period from August 14 to November 23 of November (note that the map does not include data from the USA territorial waters).

6.2. Methods

6.2.1. Study site

The study area is located in the continental slope off Vancouver Island (Fig. 6.1). As previously mentioned (see 2.2.1.2), the sediment distribution pattern shows a general trend from gravelly to boulder sediments inshore to sand and gravel on the mid-shelf and to muddy sands on the outer shelf (Bornhold and Yorath, 1984; Bornhold and Barrie, 1991). The shelf edge presents a narrow band of well-sorted sands due to energetic breaking of internal waves or currents along the upper slope and outer shelf. The continental slope mainly presents glaciomarine sediments (Cosma and Hendy, 2008), and can present fine-grained terrigenous material from the Columbia River (Chase et al., 2002).

The hydrographic structure in this area is composed of several water masses: the Subarctic Upper Water (PSUW) in the upper layer (0-500 m depth), the Pacific Subarctic Intermediate Water (PSIW) at intermediate depths (500-1500 m depth), the Eastern North Pacific Transition Water (ENPTW) between the PSUW and the PSIW, and the Circumpolar Deep Water (CDW) occupying the entire basin below 1500 m depth (Table 2.2; see 2.2.1.1 for more details). The physical circulation dynamics at the region are influenced by the California Current System, which forms from the bifurcation of the eastward flowing Subarctic and North Pacific currents into the northward flowing Alaska Current and the southward California Current (CC) (Fig. 2.3). This current system presents important intra-annual seasonal variations (see 2.2.1.1 for more details). In this Chapter, it is analysed the transition between summer and fall months, which captures the physical variations of the California Current System in the region.

Besides, the Vancouver Island continental slope has been subjected to active bottom trawling activity since 1994, covering a wide bathymetric range from shelf depths (~150 m) to the deep slope (~2000 m) (Kulka and Pitcher, 2001; Sinclair, 2007).

6.2.2. Data collection

From August 14 to November 23, 2018, data time-series were acquired from instruments on the Barkley Upper Slope (BUS) Instrument platform from the NEPTUNE seafloor cabled observatory deployed at 390 m depth (Figs. 6.1, 6.2). A total of 765 up and down hydrographic profiles were obtained by a Vertical Profiling System (VPS), which performed several profiles a day from 374 m to almost the surface at ~25 m water depth (Fig. 6.2). In addition, data of water currents were obtained from an ADCP connected to the BUS Instrument platform, which provided current velocity and direction estimates up to ~400 m above the bottom at high sampling frequency (Table 3.1; Fig. 6.2). The sensors installed in the BUS Instrument platform used in this study, as well as their configuration are described in 3.2.2.1 and 3.2.2.2.

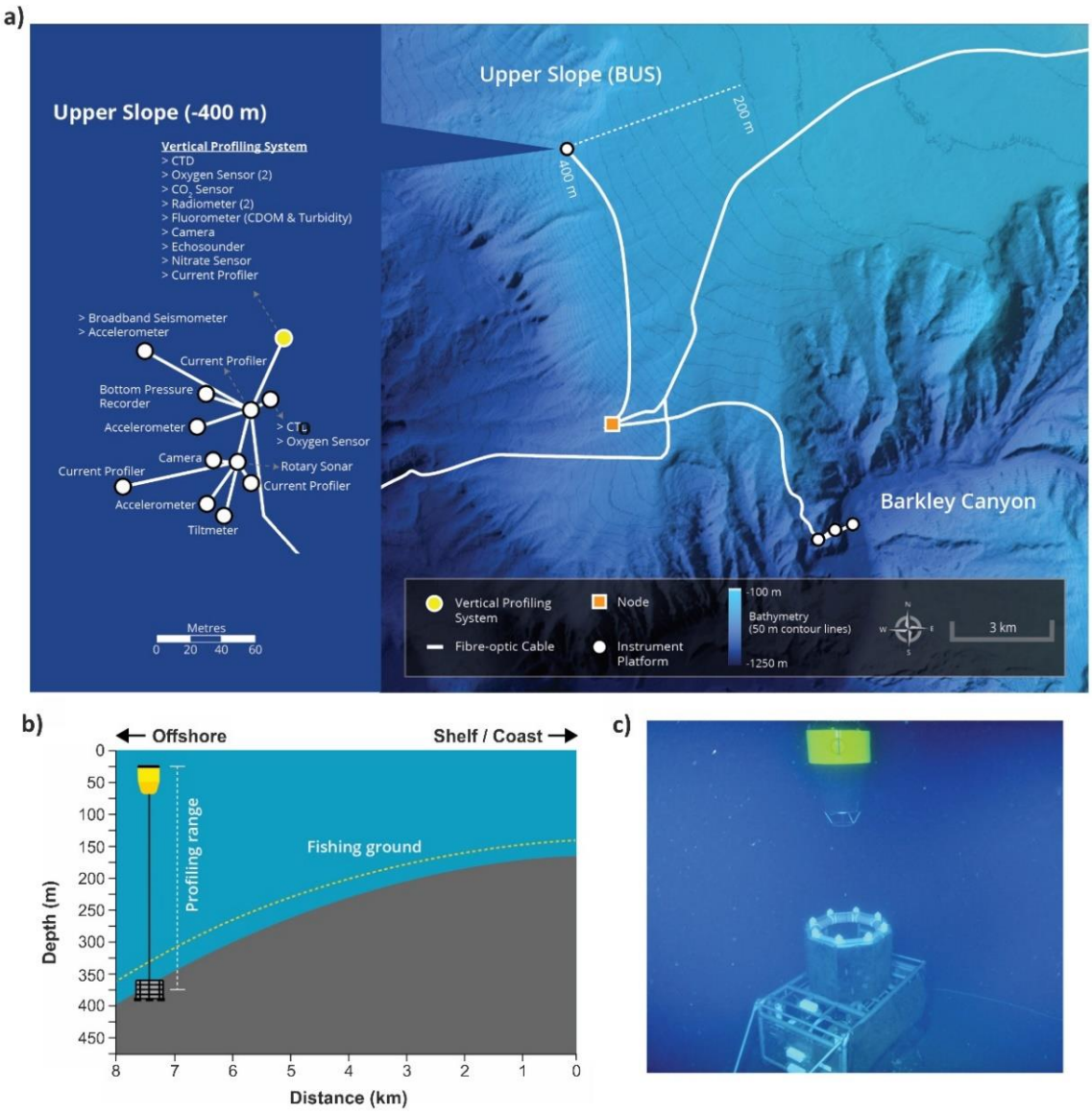

Figure 6.2. a) Detailed bathymetric map of the Barkley Canyon and its upper slope, and the instrument platforms/pods (white dots) that are installed within the Barkley Canyon node (orange square) as part of the Ocean Networks Canada's NEPTUNE cabled seafloor observatory. A detailed description of the different sensors and instruments installed in the VPS is also provided in this figure. b) Scheme of the bathymetric cross-section, obtained from the white dotted line in a), and the location of the VPS at the upper slope region off Vancouver Island. c) Underwater photography of the VPS and its cage.

6.2.3. Data analyses

Data collected with the VPS were first pre-processed to remove outliers and spikes following the procedures explained in 3.4.1. Moreover, the data processing for the low-frequency 75 kHz ADCP was carried out following the procedures described in 3.4.6.

6.2.4. Ancillary data

6.2.4.1. Hydrographic data

Complementary to hydrographic and currents data from the VPS, we also analysed CTD and turbidity profiles from the long-term Line P (http://www.waterproperties.ca/linep/) monitoring program (Boyd et al., 1999). For the purpose of this study, we considered stations P03 and P04, both located over the upper continental slope at 25-40 km to the northwest from the BUS Instrument platform (Fig. 6.1), during summer (June 5-19) and fall (September 11-28) cruises, which took place during the monitoring period. At each station, a SeaBird 9 plus CTD was mounted in a rosette attached with a WET Labs CSTAR transmissometer to measure water turbidity, a SBE 43 dissolved oxygen sensor, a SeaPoint Fluorometer, a Biospherical QSP-400 PAR sensor and an altimeter. During the summer cruise, CTD casts were hauled from the surface down to 740 m and 1307 m depth at station P03 and P04, respectively, whereas during the fall cruise they were hauled down to 798 m and 1300 m depth, respectively.

6.2.4.2. Sea surface meteorological data

Wave and wind data during the study period were obtained from the Strait of Juan de Fuca Traffic Separation Lighted Buoy (hereafter referred to as "Juan de Fuca Buoy") (station 46087; latitude: 48º 29,58' N and longitude: 124º 43.58' W), which is owned and maintained by the U.S. National Data Buoy Centre (http://www.ndbc.noaa.gov/). This buoy is located 123.2 km E from the BUS Instrument platform, over the 260 m isobath, and was the closest operative meteorological buoy to the study site during the monitoring period (Fig. 6.1). Significant wave height (*Hs*, m), primary wave mean period (*Tp,* m) and mean wave direction (Θ, ºC), as well as wind speed and direction were recorded every 30 minutes.

Buoy measurements were compared and crosschecked against model data from the NOAA WAVEWATCH III model (hereafter referred to as "NOAA WW3"). NOAA WW3 has a global coverage and temporal resolution of 0.5 º and 3 h, respectively, and the data are available from https://polar.ncep.noaa.gov/waves. This model is forced with wind data from the Global Forecast System (GFS) that has a resolution of 0.5 degrees at 1-hour intervals. In this study, data from the model was selected for the U.S. West Coast region from 25º to 55º North and from 110º and 140º West, with a spatial resolution of 10 minutes in both x and y directions (Fig. 6.1). Model results included wave (*Hs, Tp,* and Θ) and wind (U and V components of the wind) parameters stored every 3 hours at each grid point, from August to November 2018. For this study, data were only plotted for a particular grid point (latitude: 48º 30' N and longitude: 126º 10' W), which was the closest point within the U.S. West Coast grid to the BUS Instrument platform (Fig. 6.1). This location was carefully chosen to allow for more accurate correlation between wind and wave conditions, and turbidity and currents measured at the study site. Correlation coefficients were calculated between the NOAA WW3 model grid point output and the data from the Juan de Fuca Buoy for the entire period of measurements. The buoy data was extracted at the same time intervals as the NOAA WW3 model data.

6.2.5. Trawling effort from AIS data

For this chapter, fishing effort along Vancouver Island's slope region was obtained using AIS data of bottom trawlers extracted from SiiTech web platform (http://www.siitech.com), which allows for real-time and historical data tracking vessels with AIS positional data. For more details on AIS, see section 3.5. Access to archived AIS data was possible through a data sharing agreement between ONC and the Canadian Coast Guard, which allows distribution and publication for research purposes of only vessel positional data without disclosure of vessel identity (e.g., contained as MMSI strings).

The spatial fishing effort was estimated using AIS data from August to November 2018, and consisted in static data (vessel identifier, dimensions, ship type) and their dynamic data (vessel position, speed over ground, course over ground), as well as voyage information (destination, draught, current activity status). Since the total volume of the AIS dataset exceeded our available computational capacity, a filter was applied to select and keep only "fishing" class vessels with the Canadian flag. The AIS dataset was further reduced by excluding signals received within a 5-km buffer zone surrounding the Vancouver Island coastline to account for vessels slowing while entering the harbour, or those anchored inshore. A final selection of AIS signals was carried out for vessels that held commercial "trawling" licenses, which allows both pelagic and bottom-trawling activity from the same vessel (DFO, 2019).

AIS data were then filtered according to speed to infer whether an AIS message corresponded to fishing activity, following similar criteria used in previous studies (e.g., Natale et al., 2015; Oberle et al., 2016a; Paradis et al., 2021) or in **Chapter 5**. Speed over ground (SOG) histograms were created for all vessels, from which multi-modal distribution was obtained that portrayed travel speeds (high speeds), trawling speeds (mid-speeds) and an unknown third distribution that was hypothesized to be related to fishing gear retrieval or non-power drifting (low speeds) (Fig. 6.3). The EM-algorithm was used to obtain the statistically upper and lower limits of the mid-speed fishing speed distribution, at 2 standard deviations from the mean, obtaining fishing speed of 1.5 to 4.0 knots. However, simply filtering according to this trawling speed range may lead to false-positives and false-negatives. In this case, such interruptions were solved by considering a minimum length of 20 minutes per haul to correct for false-positives, whereas a maximum length of 5 minutes of anomalous trawling speeds between hauls was considered to correct for false-negatives. Hauls per vessel were calculated as consecutive entries that met the trawling criteria for a minimum time of 100 min, and trawling effort was finally approached as the number of fishing hauls that overlapped within a given area. Although metrics used to calculate door's spread were not available during the present study, a grid of one hectare (100 x 100 m) was used to calculate bottom trawling intensity, which accounts for the maximum ~100 m spread of the trawler's nets reported in other continental margins (e.g., NW Mediterranean, Palanques et al., 2006a). Trawling effort was finally represented and plotted using ArcGIS © 10.4 software (Fig. 6.1).

Nevertheless, this classification alone did not suffice to determine which vessels used each specific type of trawling gear during the study period. To address this uncertainty, AIS data were further classified using a vessel speed criterion, assuming that higher velocities (2.7-4 knots) corresponded to vessels that held pelagic trawling licenses (hereafter referred to simply as "pelagic trawling"), while lower velocities (< 2.7 knots) corresponded to vessels holding demersal trawling licenses (hereafter referred to as "demersal trawling"). This classification has been used according to published literature and reports (e.g., Earys and Pol, 2014; Nielsen et al., 2014).

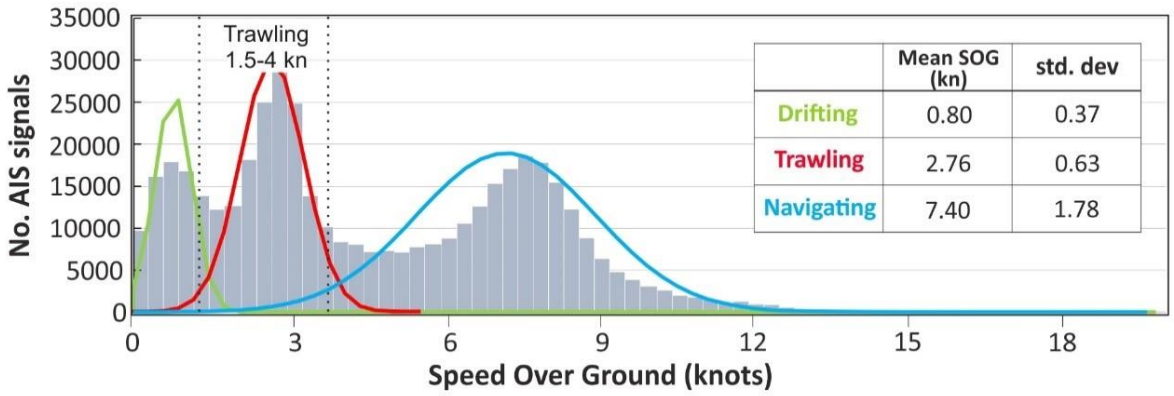

Figure 6.3. Speed over ground (SOG) histogram and fitting of the multi-modal distribution through the EM-algorithm for all trawling vessels, using AIS signals from August to November 2018. The first distribution (green line) is hypothesized to be associated with fishing gear retrieval or non-power drifting. The second distribution (red line) is associated with trawling activity, and the third distribution (blue line) is associated with travelling speeds. The black dashed line indicates the upper and lower limits used to classify vessels as trawling. Inset table includes, for each distribution: mean SOG in knots and the corresponding standard deviation.

6.3. Results

6.3.1. Temporal variability

6.3.1.1. Meteorological data validation

The temporal variability of most meteorological (wind and wave data) variables measured at the Juan de Fuca Buoy was highly correlated with the NOAA WW3 model output (Fig. 6.4).

Overall, the coefficient of determination (R^2) for the regression models of *Hs* and *Tp*, as well as the *p-values* (< 0.0001), indicate a reasonable correlation between the datasets (Figs. 6.4a, b). The R^2 values for the regression model of Θ is noticeably small, and according to the *p-value* (n.s.), the relation between model and buoy data for this wave parameter is not statistically significant. Moreover, the fact that they do not follow the 1:1 ratio shows that the two datasets for this wave parameter are not comparable (Fig. 6.4c). The R^2 values for the regression model for wind

parameters (speed and direction) are distinctly small, but the p-values (< 0.0001) show a statistically significant correlation between the model and buoy data (Figs. 6.4d, e).

The predicted wind and wave parameters show that the NOAA WW3 follows the buoy measurements quite accurately indicating an overall good agreement with the Strait of Juan de Fuca Buoy dataset. Therefore, for the purpose of the study, we used the wind and wave time-series from NOAA WW3 model, which is also closer to the BUS Instrument platform, to describe the temporal variability within the study area.

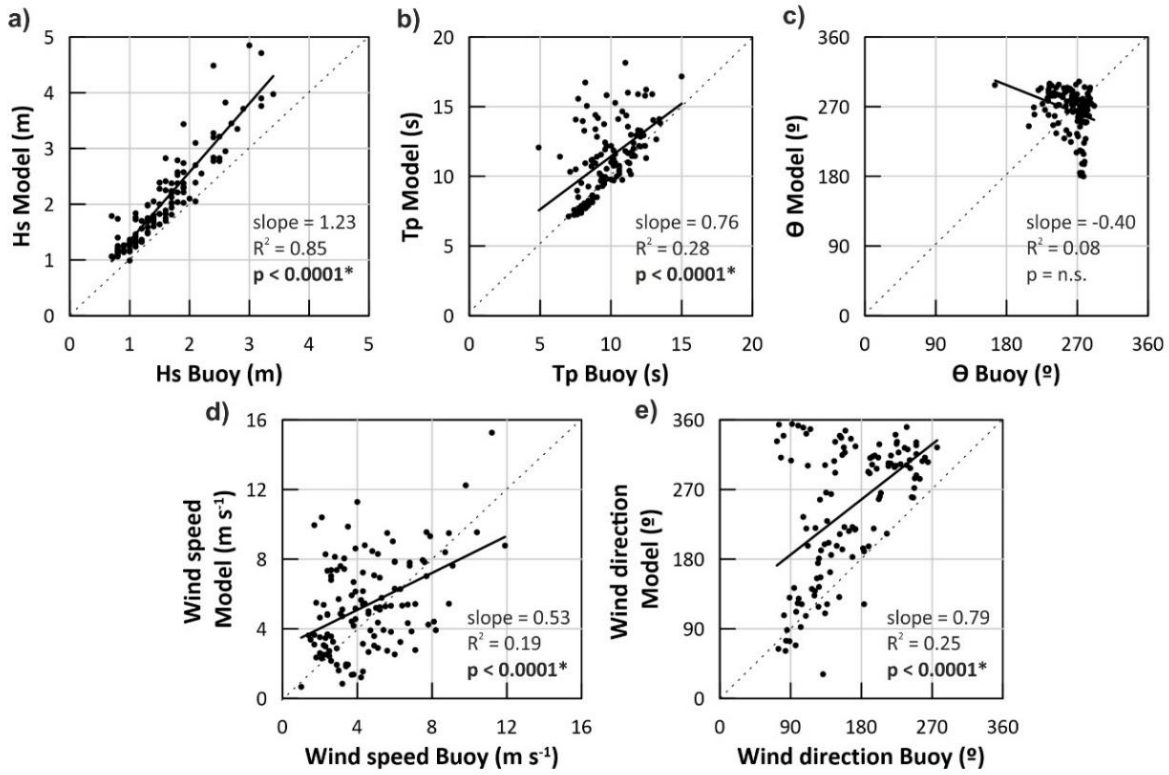

Figure 6.4. Scatter plots of buoy (Juan de Fuca Buoy) vs. model (NOAA WW3) meteorological (wave and wind) data. Correlations for wave parameters are shown in panels a), b) and c), corresponding to significant wave height (Hs), primary wave mean period (Tp), and mean wave direction (Θ), respectively. Correlations for wind parameters are shown in panels d) and e), which correspond to wind speed and wind direction, respectively. Linear regressions statistics (slope, R^2 correlation coefficient, and p-value) are given for wave and wind parameters. Asterisks denote statistically significant correlation between buoy and model data: * p < 0.0001; n.s. denotes not significant.

6.3.1.2. Wind and wave conditions

Sea-surface time-series, as well as wind and wave conditions (Fig. 6.5) provided the climatological context and allowed us to characterize both “late-summer” (August and September) and “fall” (October and November) months. Late-summer months were influenced by high sea surface atmospheric pressures (≥ 1013 hPa) over the region, which was translated into sea surface

temperatures (SST) > 10 ºC, often reaching ~15 ºC (Fig. 6.5a). During fall months, sea surface atmospheric pressure fluctuated between high and low pressures, with lower SST (10-12 ºC) than during late-summer months (Fig. 6.5a).

Significant wave heights (Hs) were between 1 and 2.2 m during the more quiescent late-summer months (Fig. 6.5b), while *Tp* displayed values of 8-12 s, being often > 15 s in mid-September (Fig. 6.5c). Nevertheless, occasional summer storms caused small peaks in *Hs* (3 m) in early September (Fig. 6.5b). Fall months were influenced by the development of larger waves (*Hs* of between 2 and 4 m) with longer *Tp* (10-14 s) (Figs. 6.5b, c). Several storms were recorded that caused *Hs* of 4 m from late October to early November (Fig. 6.5b). Wave direction (Θ) was variable during both late-summer and fall months, although the change in direction was more pronounced in fall months due to the passage of storms (Fig. 6.5b). These events were generally caused by southeastern winds and rapid fluctuations in atmospheric pressure (Fig. 6.5d). Wind speeds were relatively weak and showed almost constant values (< 5 $m \cdot s^{-1}$) in August and beginning of September, and then they started to pick up reaching up to 7.5 $m \cdot s^{-1}$ (Fig. 6.5d). Wind direction varied from NW-SE during this period (Fig. 6.5d). During the fall months, winds changed direction, shifting northward with speeds of 3 to 8.5 $m \cdot s^{-1}$, eventually reaching ~10 $m \cdot s^{-1}$ (Fig. 6.5d).

6.3.2. Trawling activity

Trawling effort estimated from AIS data from August to November 2018 indicates that fishing vessels followed the bathymetric contours, and most of the trawling activity along the west coast of Vancouver Island took place between 250 and 800 m depth (Fig. 6.1). Based on the spatial distribution of fishing hauls determined from the AIS data, it is possible to identify fishing hotspots around Quatsino, Father Charles, Barkley and Nitinat submarine canyons (Fig. 6.1), where the predominating trawling frequency during August-November was between 5 and 15 hauls per hectare, higher than the average trawling effort (1-5 hauls per hectare) observed along the entire coast of Vancouver Island (Fig. 6.1).

The position of fishing vessels operating near the study area was also plotted in detail, in ten consecutive periods (Fig. 6.6). Table 6.1 summarizes the main characteristics of each period in terms of number of hauls and trawlers. Time-series observations on AIS data revealed no trawling activity around the study site during mid-August and early September (Figs. 6.6a-c; Table 6.1). The remaining periods were characterized by the presence of hauls corresponding to demersal and pelagic trawling. During September, fishing hauls were mostly observed between 200 and 600 m depth at Barkley Canyon's head (Figs. 6.6c, d). Highest fishing intensity occurred during fall months (Figs. 6.6e-j), particularly in late September, late October, and November, when the majority of trawling hauls were detected on the open slope between 200 and 600 m depth. Only during early October there was lower fishing activity at the study area, and the majority of trawling hauls were detected on the open slope between 200 and 400 m depth (Figs. 6.6f, g).

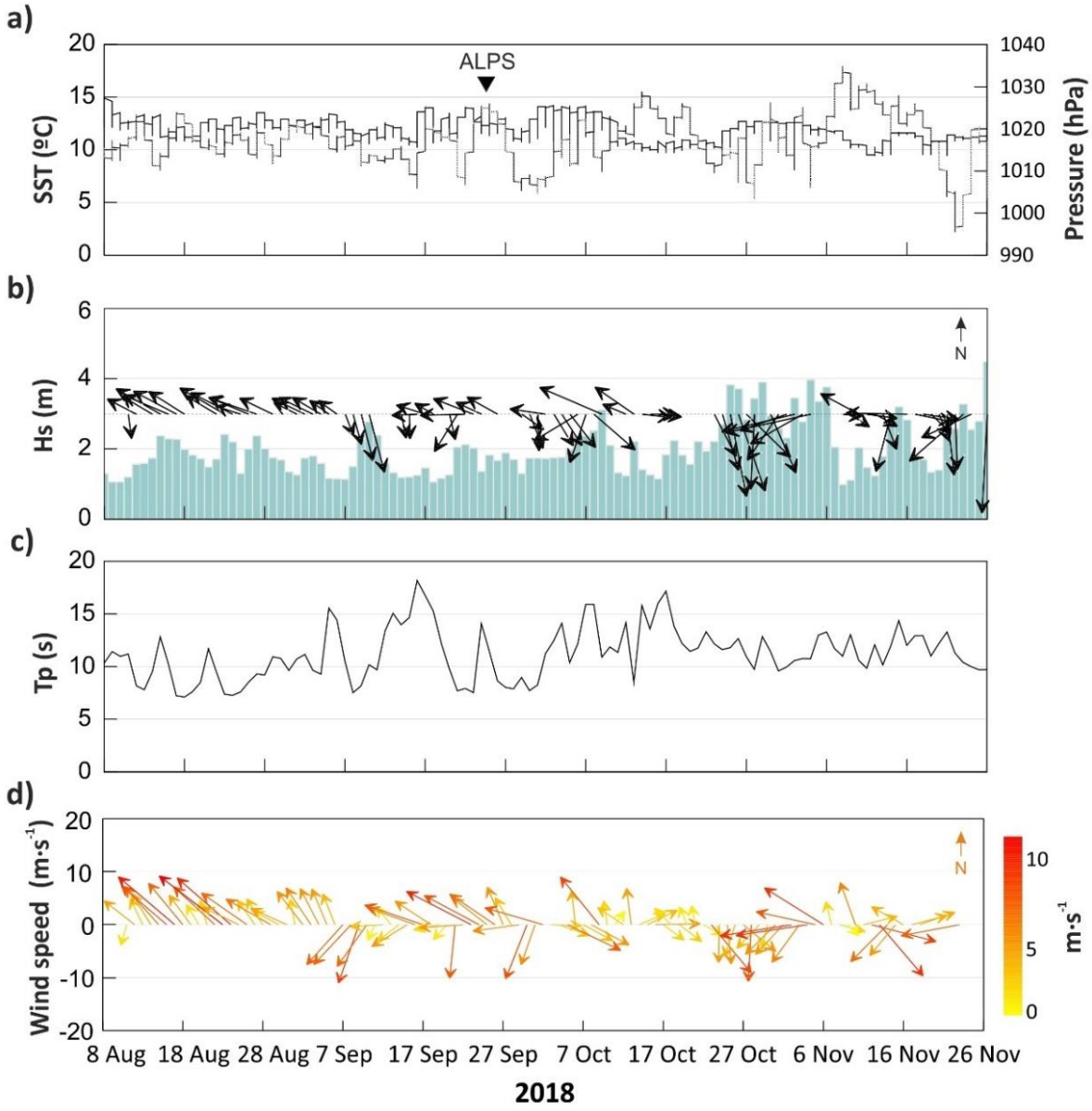

Figure 6.5. Time series of meteorological (wave and wind) conditions measured by the NOAA WW3 model during the study period, spanning from August 14 to November 23, 2018. Atmospheric conditions are based on a) sea surface temperature (SST, ºC) (black line) and sea level atmospheric pressure (hPa) (grey line). The presence of the Aleutian low-pressure system (ALPS), which intensified during fall months over the region, is indicated with a black triangle. Wave conditions are b) significant wave height (Hs, m) (blue bars), mean wave period (Θ, º) (black arrows), and c) primary wave period (Tp, s). Wind parameters are d) speed and direction. The length and color-scale of the arrows represent wind speed, whereas their direction provide wind direction.

Table 6.1. Main characteristics of the defined periods. Number of trawlers and number of hauls are presented for each trawling method. The first column indicates the correspondence with Figure 6.6.

	Season	Date (2018)	Trawling gear			
			Demersal		Pelagic	
			# Hauls	# Trawlers	# Hauls	# Trawlers
Fig. 6.6a	Late-summer	Aug 14-23	0	0	0	0
Fig. 6.6b		Aug 24-31	0	0	0	0
Fig. 6.6c		Sept 1-10	3	2	2	2
Fig. 6.6d		Sept 11-20	20	5	12	6
Fig. 6.6e	Fall	Sept 21-30	35	6	48	6
Fig. 6.6f		Oct 1-10	3	2	7	4
Fig. 6.6g		Oct 11-20	8	2	8	3
Fig. 6.6h		Oct 21-31	14	4	39	3
Fig. 6.6i		Nov 1-10	5	3	17	3
Fig. 6.6j		Nov 11-23	13	3	9	2

Overall, the number of trawling hauls for fall months was higher than for late-summer months. Moreover, the number of fishing hauls corresponding to pelagic trawling was higher than those corresponding to demersal trawling, except for late September and late November (Fig. 6.6; Table 6.1). However, the number of trawlers did not differ much amongst the different periods (Table 6.1), most probably because the same vessel held both demersal and pelagic licenses. In fact, several vessels were identified in both demersal and pelagic AIS signals' trawling speeds throughout the study period.

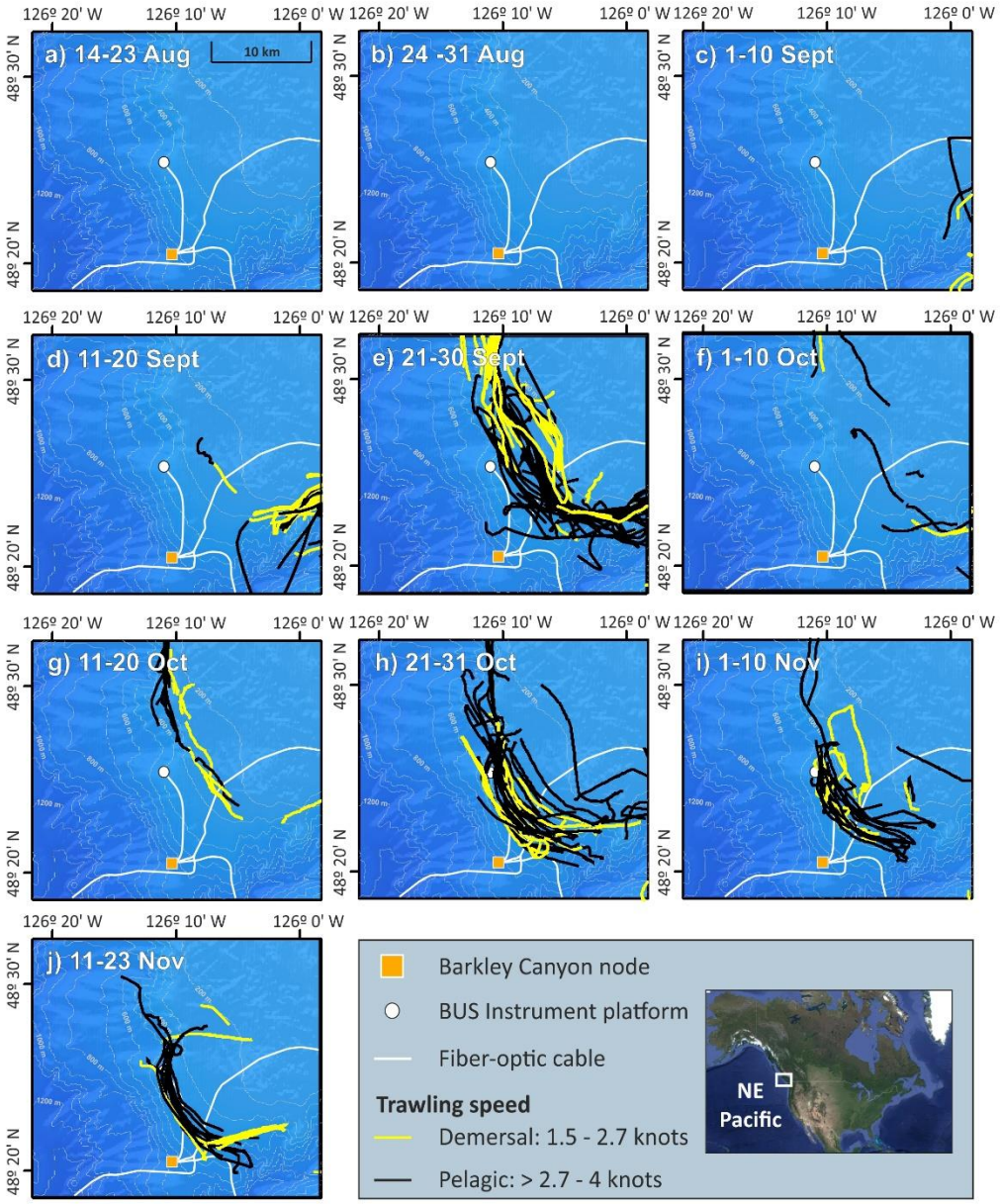

Figure 6.6. Detailed bathymetric map of the study site showing the variability in the number of hauls for late-summer (a-d) and fall months (e-j). Yellow and black lines represent fishing hauls calculated from Automatic Identification System (AIS) data of trawlers during the study period potentially using demersal (1.5-2.7 knots) and pelagic (> 2.7-4 knots) trawling gear.

6.3.3. Time-series data

6.3.3.1. Hydrographic structure, dissolved oxygen, fluorescence, and suspended particulate matter

The hydrographic structure obtained by the CTD measurements from the VPS from 25 to 374 m water depth revealed distinct changes in temperature and salinity throughout the water column. These are ascribed to the different water masses present in the study area (Fig. 6.7). In the upper

~100 m of the water column, temperatures were between 8 and 12.5 ºC and salinities ranged between 32.5 and 33.6 (Fig. 6.7 and Figs. 6.8a, b), which corresponded to Pacific Subarctic Upper Water (PSUW). Below, the Eastern North Pacific Transition Water (ENPTW) was found, characterized by a temperature range from 7.0 to 9.3 ºC and a salinity range from 33.8 to 34.3, and occupied the water column from 100-150 to ~300 m depth (Fig. 6.7 and Figs. 6.8a, b). Underneath these two water masses, the Pacific Subarctic Intermediate Water (PSIW) was generally observed at the deepest part of the hydrographic profiles, exhibiting a temperature minimum of 5.5 ºC and salinity values that ranged from 33.8 to 34.3 (Fig. 6.7 and Figs. 6.8a, b).

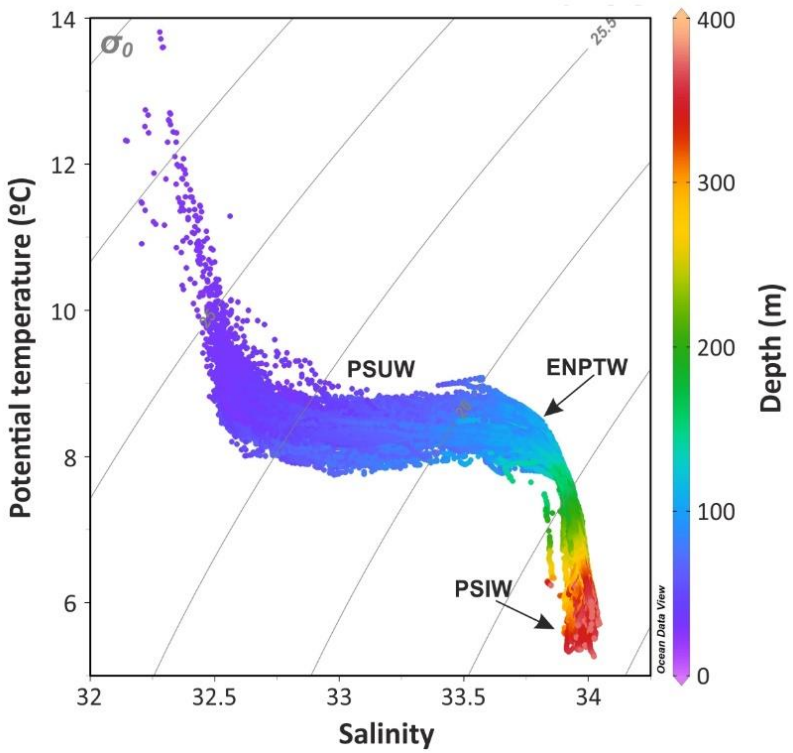

Figure 6.7. *TS* diagram for all the CTD casts sampled with the Vertical Profiling System (VPS) during the study period, spanning from the August 14 to the November 23, 2018, identifying the different water masses present in the study area: Pacific Subarctic Upper Water (PSUW), Eastern North Pacific Transition Water (ENPTW) and Pacific Subarctic Intermediate Water (PSIW) (data plotted using Ocean Data View 4.7.10; http://odv.awi.de; Schlitzer, 2010).

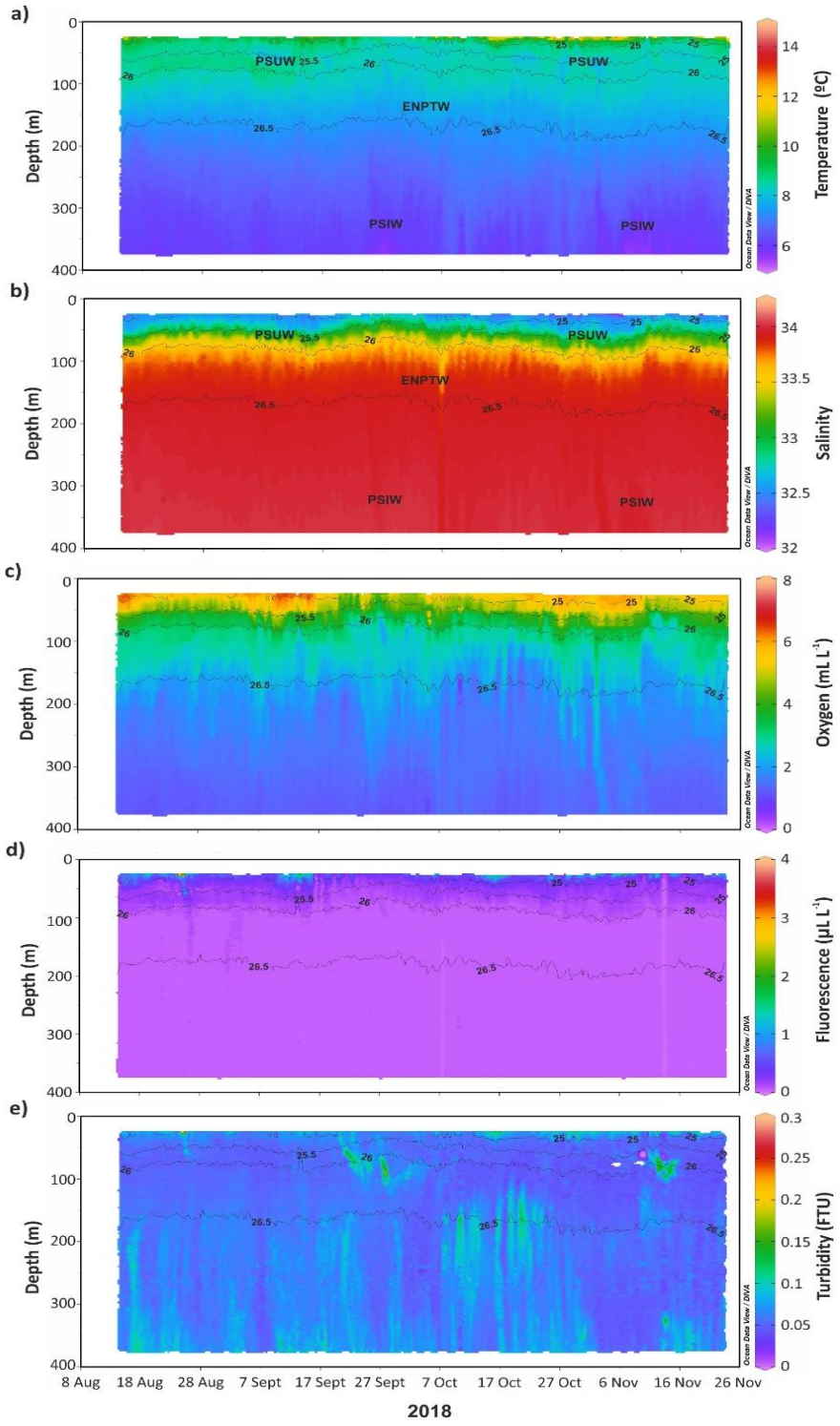

Figure 6.8. Time series of a) potential temperature (ºC), b) salinity, c) dissolved oxygen (mL·L^{-1}), d) fluorescence (µL·L^{-1}) and e) turbidity in FTU measured by the VPS during the study period, spanning from August 14 to November 23, 2018, showing the different water masses being present in the study area: Pacific Subarctic Water (PSUW), Eastern North Pacific Transition Water (ENPTW) and Pacific Subarctic Intermediate Water (PSIW) (data plotted using Ocean Data View 4.7.10; http://odv.awi.de; Schlitzer, 2010).

The VPS time series showed decreasing DO (dissolved oxygen) concentration from the surface (7 $mL \cdot L^{-1}$) towards the deepest part of the sampled water column, where the lowest DO concentrations were found (< 1.2 $mL \cdot L^{-1}$) (Fig. 6.8c). Within the upper water column, between 50 and 150 m depth, there was a relatively sharp change in DO concentrations that corresponded to the limit between the PSUW and the ENPTW. In this region of the water column, oxygen saturation went from 99% at the upper boundary to ~40% at the lower limit. Anomalously low DO values (1.8-2.4 $mL \cdot L^{-1}$) were also found at 87 m water depth compared to surrounding higher DO concentrations between September 26 and October 2 (Fig. 6.8c). Similarly, lower DO concentrations (2.4-2.8 $mL \cdot L^{-1}$) than those of the surrounding waters were observed between November 11 and November 15 at ~70 m water depth (Fig. 6.8c).

Within the surface layer, highest fluorescence (> 1.5 $\mu L \cdot L^{-1}$) was observed, whereas it was not traceable below the surface layer (> 70 m water depth) (Fig. 6.8d).

The distribution of SPM and the nepheloid structure in the water column during the study period is shown in Figure 6.8e. Generally, increases in turbidity were observed near the seafloor and at mid-water depths, generating INLs and BNLs. INLs were mainly recorded between 150 and 300 m depth, centered about 200 m water depth. These increases corresponded to ~150 m thick INLs developed at the shelf-break and showed turbidity values of ~0.1 FTU (Fig. 6.8e). Also, BNLs were recorded at water depths > 300 m depth and displayed thicknesses of almost ~74 m and turbidity values typically ranging between 0.05 and 0.14 FTU (Fig. 6.8e). However, these features (both INLs and BNLs) were not always permanently observed in the turbidity profiles, being interrupted by periods of clear waters of variable duration (from 2 to 10 days) at certain timespans (Fig. 6.8e).

Moreover, increased turbidity was occasionally observed at water depths < 100 m depth distributed in punctual sub-SNLs, in which turbidity values ranged from 0.05 and 0.15 FTU (Fig. 6.8e). Particularly, the hydrographic profiles showed highest turbidity at these SNLs on September 27 and November 12, peaking at 0.19 FTU and 0.14 FTU, respectively, at 88 m water depth (Fig. 6.8e). Overall, these SNLs were observed during the entire study period, with no significant differences between late-summer and fall months (Fig. 6.8e).

6.3.3.2. Line P water mass properties over the slope

The hydrographic data obtained from Line P monitoring stations on the adjacent continental slope (P03 and P04) during summer and fall cruises of 2018 showed a close correspondence to the VPS time-series observations. Moreover, it also provided us with confidence in asserting that the different water masses and turbidity structure are characteristic of the study area. From stations P03 and P04 during summer and fall cruises (Fig. 6.1) we observed the same water structure composed of PSUW at the upper levels of the water column (< 100 m depth), the transition to ENPTW (100-300 m depth) and the PSIW towards the deepest part of the hydrographic profiles (> 300 m depth) (Figs. 6.9a, b).

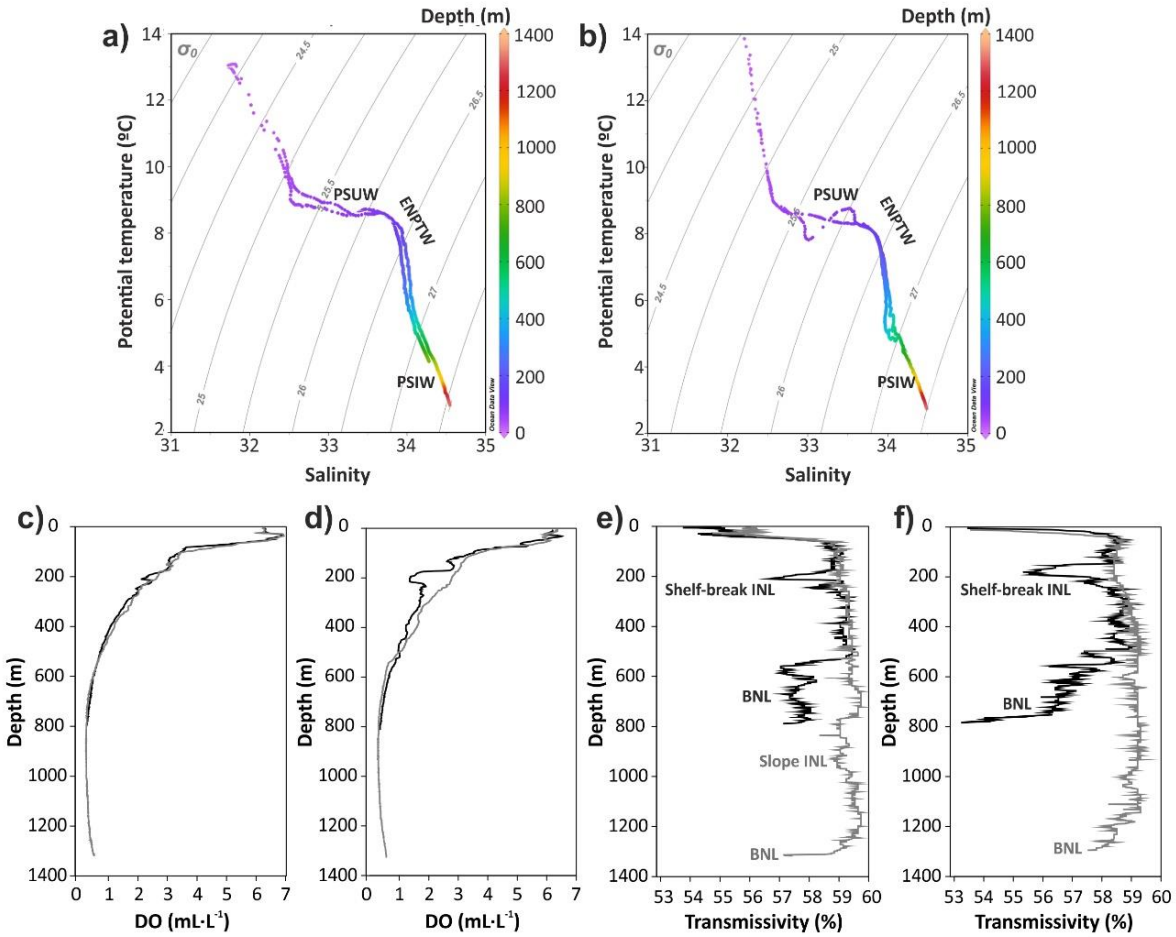

Figure 6.9. Hydrographic data collected during Line P cruises from year 2018. a) and b) *TS* diagrams in P03 and P04 stations in summer and fall cruises, respectively, showing the different water masses observed (PSUW: Pacific Subarctic Upper Water; ENPTW: Eastern North Pacific Transition Water; PSIW: Pacific Subarctic Intermediate Water). c) and d) dissolved oxygen (DO, mL·L^{-1}) profiles collected in P03 (black line) and P04 (grey line) stations during summer and fall cruises, respectively. e) and f) Transmissivity (%) profiles collected in P03 (black line) and P04 (grey line) stations during summer and fall cruises, respectively. (data plotted using Ocean Data View 4.7.10; http://odv.awi.de; Schlitzer, 2010).

Additionally, data collected from both cruises showed decreasing dissolved oxygen (DO) profiles (Figs. 6.9c, d). The highest concentrations were found at the surface, where DO values were ~7 mL·L^{-1}, whereas lowest values were normally found at the deepest part of the hydrographic profiles (1 mL·L^{-1}). During the summer cruise, the DO profile at station P03 showed a relative increase in concentration at 140 m water depth of 3.1 mL·L^{-1}. Between 140 and 265 m depth, the DO concentrations varied between 1.9 and 3.1 mL·L^{-1}, from which DO values decreased until reaching lowest values towards the deepest part of the water column at 800 m water depth (Fig. 6.9c). Only during the fall cruise, the DO profile of station P03 also presented a sharp drop in DO concentrations from 2.7 mL·L^{-1} to 1.3 mL·L^{-1} from 140 to 210 m water depth (Fig. 6.9d). During the fall cruise, the deeper station P04 did not show such variations in DO concentrations. Conversely, it showed monotonically decreasing DO concentrations down to 0.2 mL·L^{-1} from ~100

m to almost 900 m water depth, from which DO concentrations slightly increased to 0.5 $mL \cdot L^{-1}$ towards the bottom at 1,300 m water depth (Fig. 6.9d).

During both summer and fall cruises, the turbidity profile (expressed in % of transmissivity) at station P03 showed an INL at the shelf-break depth (~200 m water depth) and a BNL at 560 m water depth that extended to the bottom (Figs. 6.9e, f). The shelf-break INL was more intense during the fall cruise (Fig. 6.9f) than in summer (Fig. 6.9e) and was not observed farther offshore at P04 (Figs. 6.9e, f). Similarly, the BNL observed at P03 was slightly more intense in fall than in summer, whereas it was not observed at the turbidity profiles recorded farther offshore at station P04. Nevertheless, a diluted slope-INL was identified at 780 m depth during summer at P04, most probably generated from the detachment of the BNL observed at station P03. This appeared to be a transient nepheloid layer, as it was not observed during fall (Fig. 6.9f). Finally, a BNL was recorded at 1,300 m water depth during both summer and fall cruises at station P04 (Figs. 6.9e, f).

6.3.4. Dynamics of water currents

The speed and directions of water currents measured by the low-frequency ADCP at the BUS Instrument platform during the study period were decomposed in across- and along-margin components (Fig. 6.10). Generally, across-margin currents during the study period were weaker than along-margin currents, with maximum across-margin velocities of 0.07 $m \cdot s^{-1}$ during late-summer months and of 0.1 $m \cdot s^{-1}$ during fall months, particularly in early November (Fig .6.10a). They were characterized by a high variability in current direction due to the tidal motion (Fig. 6.10a). In late October, across-margin currents displayed a predominant offshore direction that reversed onshore during early November (Fig. 6.10a). Along-margin currents displayed the strongest velocities recorded during the study period, presenting near-constant values of > 0.1 $m \cdot s^{-1}$ that were mainly directed towards the northwest (Fig. 6.10b). Short periods of south-eastward currents of 0.1 $m \cdot s^{-1}$ were also detected in early and late-September, mid-October, and the first two weeks of November (Fig. 6.10b).

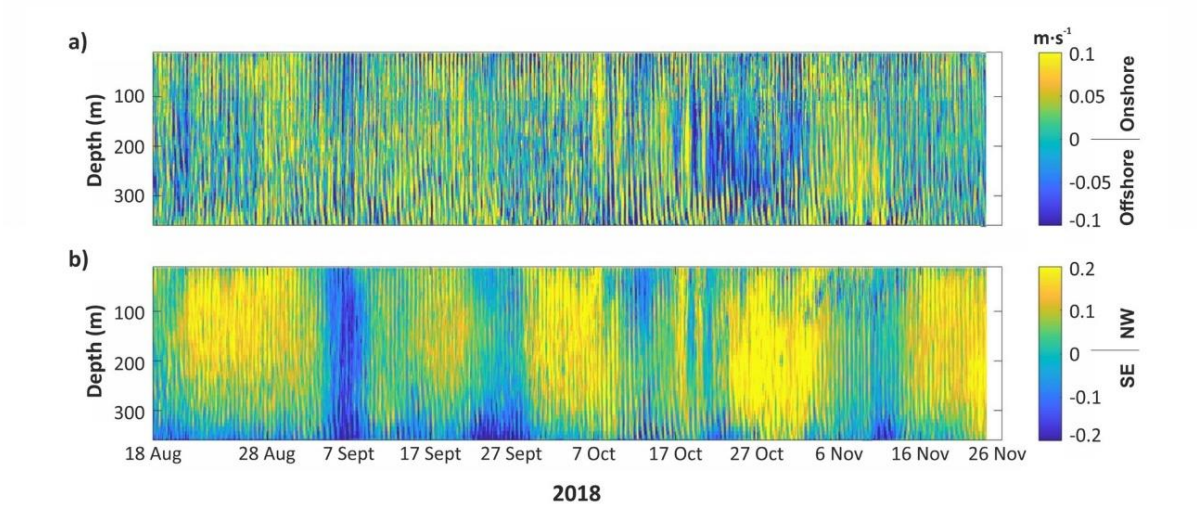

Figure 6.10. a) Across-margin and b) along-margin velocity components, $m \cdot s^{-1}$, measured with the 75 kHz Acoustic Doppler Current Profiler (ADCP) installed at the BUS Instrument platform during the study period, spanning from August 14 to November 23, 2018. Note the change in scale for the along-margin component.

6.4. Discussion

6.4.1. Nepheloid layer distribution

The nepheloid layer distribution over the upper slope region of Vancouver Island exhibited a vertical distribution consisting in: (i) a continuous SNL within the first 70 m of the water column, (ii) intermittent sub-surface turbidity increases between 70 and 90 m water depth, (iii) INLs between 150 and 300 m at the depths of the shelf-break and upper slope, and (iv) a weak discontinuous BNL close to the bottom (Fig. 6.8e).

The SNL maximum (0.16 FTU) at surface levels (Fig. 6.8e) mainly consisted of phytoplankton particles from the euphotic zone, as inferred by the high fluorescence values recorded at this water depth (Fig. 6.8d). This primary productivity is supported by inputs of inorganic nutrients via a number of processes, which include along-shore transport, local wind-driven upwelling, interaction of mesoscale currents with bottom topography, tidal mixing, and estuarine circulation in the Strait of Juan de Fuca (Crawford and Dewey, 1989). In addition to the SNL, elevated turbidity values of 0.14-0.19 FTU were observed sporadically between 70 and 90 m water depth (Fig. 6.8e). The vertical profiles exhibit coherent peaks of decreasing DO at the same water depths (Fig. 6.8c), under upwelling-favourable conditions according to the fluctuation of the isohalines and isotherms (Figs. 6.8a, c), suggesting that these turbidity increases likely corresponded to zooplankton accumulations. From spring to fall, strong upwelling events provide nutrients to the continental shelf to Vancouver Island (Mackas, 1992) that enhance phytoplankton activity, especially during late-summer months, stimulating zooplankton grazing (Simrad and Mackas, 1989). Most of the zooplankton that have been identified in this area are copepods (*Calanus mashallae, Pseudocalanus spp., Neocalanus cristatus* and *N. plumchrus,* and *Metridia pacifica*),

which are known to undergo seasonal ontogenetic vertical migration (Miller et al., 1984; Mackas et al., 1998), including their advection through Barkley Canyon (De Leo et al., 2018); euphausiids (*Euphasia pacifica* and *Thysanoessa spinifera*) (Mackas et al., 1997); chaetognaths (*Sagiita elegans* and *Eukrohnia hamata,* and *Salpa spp.),* hydromedusae (*Aglantha* and *Phialidium), and* ctenophore (*Pleurobrachia*) (Haigh and Schnute, 2003). Despite the high food availability and relatively low predation, surface layer zooplankton populations decline rapidly on the continental shelf area through spring to fall (Mackas, 1992; Venello et al., 2021).

The INLs developed at the shelf-break, mainly centred at ~200 m depth over the upper slope, showed turbidity values of ~0.1 FTU (Fig. 6.8e). Although this INL at the P03 station is only some meters thick (Figs. 6.9e, f), at the VPS station it is often connected with the BNL, displaying continuous turbidity increases from 150 m depth to the bottom (Fig. 6.8e). This probably indicates that sediment particles are detached not only from the shelf but also from deeper regions of the slope, and that particle detachments are then scattered throughout these depths across the slope, rather than being stratified. These connected INL-BNL were frequently interrupted by periods of clear waters and appear to be common in upper slope waters (Fig. 6.8e) but not farther offshore, as they were not recorded in the turbidity profiles of station P04 (Figs. 6.9e, f). In contrast, the BNL extending from ~560 m depth down to 798 m depth (Figs. 6.9e, f) observed at P03 would have detached across-margin, contributing to the development of the slope-INL at similar depths during the summer cruise at station P04 (Fig. 6.9e). This detachment of BNL and its contribution to INLs offshore is further confirmed by the general offshore decrease of turbidity, indicating particle settling and offshore diffusion or dispersal of sediment in weak, detached slope INLs (Hickey et al., 1986).

The across-margin extent of these INLs indicate a complex interaction of the magnitude of the concurrent resuspension events (and the deepest depth of the resuspension), the frequency and the timing of prior resuspension events, as well as the strength, direction and spatial and temporal continuity of flow over the entire open slope (Hickey et al., 1986), which we will attempt to discern in this Chapter.

6.4.2. Potential resuspension mechanisms generating nepheloid layers

6.4.2.1. Fall storms

The INLs developed at the shelf-break depths (~200 m water depth) were more intense (~0.13 NTU) during fall months (Fig. 6.8e), particularly between October 7 and November 6 when several storm events were recorded (Fig. 6.5). During fall months, the passage of the Aleutian low-pressure system (Fig. 6.5a) typically causes rapid fluctuations of wind and wave conditions and high surface waves (Figs. 6.5b-e), which are normally associated to storms, and these are one of the primary mechanisms for resuspension of fine sediments from mid- and outer-continental shelf depths (Sternberg and Larsen, 1975; Walsh and Nittrouer, 1999; McPhee-Shaw et al., 2004).

Storm events usually cause enhanced sediment transport and increase particle fluxes in many submarine canyons by the advection of resuspended sediments from the adjacent shelves (Carson et al., 1986; Puig et al., 2003; Palanques et al., 2008; Puig et al., 2014). For instance, in the neighboring Quinault Canyon off Olympic Peninsula (Fig. 6.1), particulate matter on the shelf is resuspended by storm-induced currents and waves and is subsequently advected by the regional flow (Carson et al., 1986) on a particular isobath, detaching as INL over the shelf-break (Hickey et al., 1986) from which the resuspended particulate material settles rapidly in amorphous aggregates, increasing particle fluxes at intermediate depths in the upper canyon region and near the bottom (Baker and Hickey, 1986).

However, in the present study, the turbidity increases indicated that the passage of storms was not the sole mechanism responsible for resuspending and transporting sediments from the shelf into the slope (Fig. 6.5c and Fig. 6.8e). For instance, the storm recorded on October 25 seemed to generate turbidity increases that reached values of 0.1 FTU at 150-200 m water depth, while a similar storm occurring on October 29 did not produce any apparent resuspension in water turbidity (Fig. 6.5c and Fig. 6.8e). Similarly, the storm recorded on November 4 appeared to generate water turbidity increases to less than 0.1 FTU, whereas the storm occurring on November 6, which had similar characteristics than the former storm, did not appear to generate any water turbidity increases (Fig. 6.5c and Fig. 6.8e). This decoupling between the atmospheric forcing processes and water turbidity indicates that the advection of shelf sediments is not entirely dependent on the storm's magnitude but also on the duration of prevailing currents delivering resuspended sediments towards the shelf edge and deeper areas (Palanques et al., 2008).

Indeed, a close-up analysis of turbidity and current speed between October 20 and October 26 revealed no clear relationship between turbidity increases and current intensity (Fig. 6.11), indicating that although strong storm-induced currents did not reach the BUS Instrument platform, the INL detached from the shelf-break still reached the monitoring station following the main current flow.

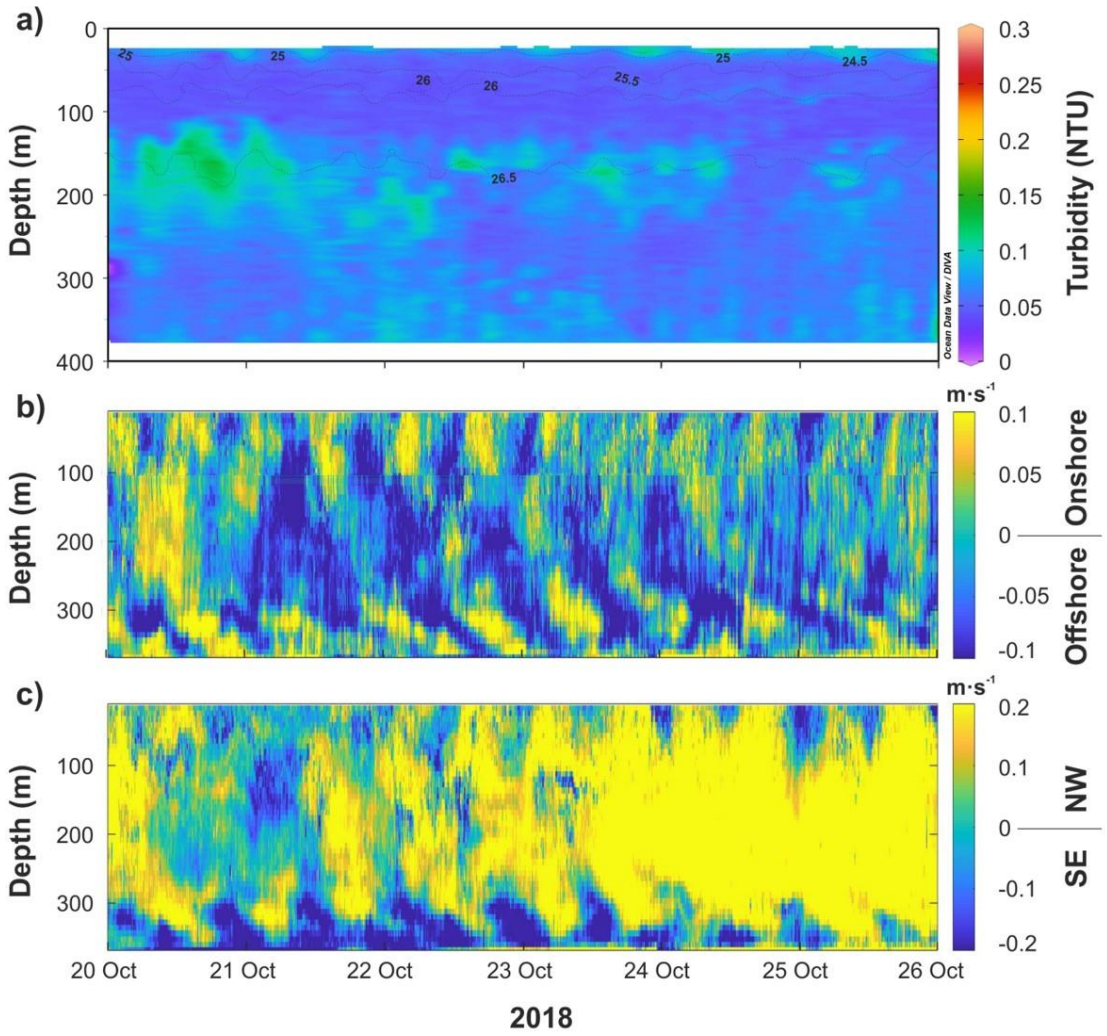

Figure 6.11. Temporal and spatial distribution of a) suspended particulate matter in NTU, and b) across-margin velocity component and c) along-margin velocity component, in $m \cdot s^{-1}$, measured with the 75 kHz Acoustic Doppler Current Profiler (ADCP) installed at the BUS Instrument platform during more intense stormy period in fall 2018. (data plotted using Ocean Data View 4.7.10; http://odv.awi.de; Schlitzer, 2010).

6.4.2.2. Tides and general flow

The interaction of internal waves with the seafloor has been described as the main mechanism responsible for generating and maintaining high near-bottom suspended sediment concentration (Cacchione and Drake, 1986; Palanques and Biscaye, 1992; Puig et al., 2001; 2004; McPhee-Shaw, 2006). At the continental margin of Vancouver Island, internal waves occur at tidal frequencies, being diurnal baroclinic velocities larger than semi-diurnal barotropic velocities (Crawford and Thomson, 1982; Drakopoulos and Marsden, 1993). The internal tide is mainly generated at the shelf-break and has been observed to propagate across-margin (Drakopoulos

and Marsden, 1993). However, during this study, across-margin currents at the study site were generally weak and did not show any clear offshore/onshore pattern (Fig. 6.10a).

Along-margin currents were greater than across-margin currents (> 0.1 m·s-1; Fig. 6.10) and presented dominant north-westward direction at mixed tidal frequencies (Fig. 6.10b). This is in general agreement with a previous study conducted off Vancouver Island (Crawford and Thomson, 1982), as well as with other studies carried out along the west coast of North America which have also suggested that bottom diurnal and semidiurnal barotropic tides propagate northward along the west coast of North America, mainly as Kelvin Waves (Munk et al., 1970; Crawford et al., 1981).

In the neighbouring Quinault Canyon (Fig. 6.1), quasi-geostrophic fluctuations in flow are superimposed on the mean flow every season, exceeding it by an order of magnitude. This means that during any particular season both south-eastward and north-westward flow events can occur (Carson et al., 1986). Battisti and Hickey (1984) demonstrated that fluctuations in the flow field are due to a combination of forcing by the local wind field and freely propagating waves that are generated by the wind field along the coast. The direct effect of these wind-driven fluctuations tends to be confined to the upper water column (250 m depth) and shallower bottom depths (Battisti and Hickey, 1984). Off the Washington State coast, the resulting flow is generally northward during winter when principal sediment transport events occur (Hickey, 1979). Taking this into account, it is very plausible that along-margin currents registered along Vancouver Island are likely affecting the resuspension/advection within slope depths, considering that nearly clear-water periods coincided with south-eastward currents and turbid-water periods with north-westward currents (Fig. 6.8e and Fig. 6.10b). Furthermore, these along-margin currents are likely associated with the California Undercurrent (CUC) which flows north-westward during late-summer and fall months at the depths of the shelf-break (Hickey, 1979; Pierce et al., 2000). Therefore, the CUC may act as a relevant mechanism for both sediment resuspension and advection in our study area.

6.4.2.3. Trawling activities

Although the CUC may exert a controlling role in the sediment transport in our study area, the turbidity increases observed in the water column at the study site could not be conclusively explained by any single hydrodynamic process operating along the margin off Vancouver Island. This suggests that other potential resuspension mechanisms, aside from these natural processes, may also play an important role causing sediment resuspension and contributing to the formation of the INLs and BNLs in the study area.

Several studies have demonstrated that resuspension caused by bottom trawling can create turbid clouds and persistent nepheloid layers with high suspended sediment concentration, which have been observed mainly on continental shelves (Churchill, 1989; Schoellhamer, 1996; Ferré et al., 2008; Palanques et al., 2001; 2014). In contrast, the occurrence of turbidity increases caused by trawling activities in slope environments has been less investigated. Studies conducted

on the NW Mediterranean slope have described that the resuspension created by the trawling gear can be propagated deeper than the trawling grounds (Puig et al., 2012; Martín et al., 2014c). These studies were conducted on a submarine canyon flank, which reported the presence of highly concentrated INLs and BNLs generated after the passage of the trawling fleet. More recent studies recorded quasi-permanent INLs and near-BNLs at the same depths of the canyon fishing grounds of two different submarine canyons incising the Catalan margin (NW Mediterranean) during the trawling season (**Chapters 4** and **5**).

Considering that the Barkley Canyon node is situated very close to currently exploited fishing grounds (Fig. 6.1), and that at least three major trawling hit incidents caused substantial damage to the NEPTUNE cabled seafloor observatory infrastructure, it is highly plausible that bottom trawling activities on the upper slope region is a source of the water turbidity increases recorded by the VPS profiler. To that effect, an artificial AIS signal from the BUS location is now broadcasted to prevent further collisions of trawlers with the NEPTUNE observatory infrastructure. Unfortunately, the available AIS fishing data do not discern between pelagic and demersal trawling, and the AIS data analyses based on vessel speed limits revealed that the most intense fishing activity at the upper slope region was likely attributed to pelagic trawlers and not demersal trawlers (Fig. 6.6; Table 6.2). Nonetheless, the presence of demersal trawlers, particularly in late September and late November, at the depths where INLs and BNLs were observed highlights that bottom trawling might contribute to enhance water turbidity at the study area.

To understand the turbidity increases in the study area we must consider a wider context. The presence of continuous fishing activity along the Vancouver Island's continental slope (Fig. 6.1), combined with the California Current System results in the continuous advection of trawling resuspended particles, playing an important role in their transport along the margin via nepheloid layers. Some turbidity increases recorded at the study site can be the result of trawling resuspension in farther fishing grounds, where the resulting detachments are advected by the mean flow and can reach the VPS site without direct concordance with the local AIS data around our study site (Fig. 6.6), therefore making it difficult to the relationship between trawling and sediment resuspension in such a highly dynamic region.

Trawling activities at the Cascadia margin mainly occur at ~400 m depth targeting groundfish species such as cod, pollock, rockfish (*Sebastes spp.*), sablefish (*Anopoloma fimbria*), and thornyheads (*Sebastopolus spp.*) (FAO, 2019). However, the continuous expansion of trawling activities to deeper regions (Norse et al., 2012; Watson and Morato, 2013) is evident in this margin due to the presence of trawl marks below 900 m depth, further expanding the impacts of bottom trawling to greater depths (Friedlander et al., 1999; De Leo et al., 2017). In an effort to mitigate and abate the impacts of bottom trawling, closure areas have been established (Iriondo et al., 2019). However, the sediment resuspension by bottom trawling in areas adjacent to protected areas can still affect them (Linders et al., 2018). Our results are a clear evidence that

long-lasting detachments of INLs in this highly dynamic margin may need to be taken into account when delimiting protected areas.

6.5. Conclusions

This Chapter provides a first glimpse into the nepheloid layer distribution on the upper slope region of Vancouver Island, discussing the potential mechanisms contributing to the sediment resuspension and advection in continental margin. The high-resolution time-series of turbidity profiles provided in this Chapter illustrate a well-defined turbidity structure consisting in SNLs at < 100 m depth related to primary and secondary productivity, INLs between 150 and 300 m depth at the shelf-break and upper slope domain, and deeper INLs and BNLs found at water depths < 400 m depth. Our data suggests that energetic shelf dynamics induced by fall storms could be generating the more intense INLs found at shelf-break depths. However, INLs are not always concurrent with fall storms, indicating that some INLs are not directly driven by the storm events at the BUS Instrument platform but they rather reach this site through the advection of shelf-break detachments along the slope.

The high number of AIS signals observed over the study area during the ~4-month observational period, and the lack of a clear correspondence of turbidity increases with natural processes and events, suggests that trawling resuspension contributes to increasing suspended particle concentrations in the water column. AIS data reveals that the depths of the observed nepheloid layers coincide with the operating depths of trawlers. Although the most intense fishing activity is likely attributed to pelagic trawling, the presence of demersal trawlers at certain time spans where intermediate and bottom particulate matter detachments were observed highlights the role of bottom trawling in enhancing water turbidity at the study site. The presence of pervasive fishing grounds along the Vancouver Island's continental slope, combined with the currents of the California Current System, results in the continuous advection of trawling resuspended particles, playing a major role in their transport along the margin as nepheloid layers.

General discussion

Part IV

Chapter 7. General discussion

In this Chapter, the usefulness of autonomous hydrographic profiling to study the temporal evolution of nepheloid layers in the water column is discussed, presenting the main advantages of these platforms when compared with classical methods of measurement and detection of nepheloid layers. Furthermore, a joint discussion of the results obtained in this Thesis dissertation is presented, offering an integrated vision of the temporal distribution of nepheloid layers and the main mechanisms that dominate in their generation and formation in continental slope environments. Natural-induced and trawling-induced sediment resuspension processes are compared and discussed, offering a temporal vision of the effects of these processes on the distribution of the suspended particulate matter in the water column of deep-sea environments.

7.1. Usefulness of autonomous hydrographic profiling

In situ ocean observations are limited by the ability of humans to make comprehensive measurements in specific locations because of the remoteness, harshness, or vast geographical extensions of the ocean environment. Ship-based ocean observations are increasingly limited by the cost of the operating platforms that support humans and instruments for detailed measurements, and the monitoring is limited, although oceanographic vessels provide great flexibility and are essential for servicing moorings, buoys, and cabled observatories (Whitt et al., 2020). In this sense, instrumented moorings, cabled observatories, or the use of robotic infrastructures, such as AUVs, ROVs, or gliders, are good monitoring options since they can make measurements over a wide array of spatial and temporal scales. Observations can range from meso-scale processes to small-scale variabilities in oceanographic parameters, such as temperature, salinity, pressure, oxygen, biomass, and many other variables depending on the needs of the research. True autonomy, however, is still unavailable, because autonomous platforms still require human interaction and support from oceanographic vessels (Ramp et al., 2009).

For a long time, the use of instrumented moorings has been a good option for the scientific community to overcome some of the limitations explained above, since they can accommodate numerous pieces of measuring equipment and can obtain long time-series of oceanographic parameters at some levels of the water column at a specific location (Rayner and Kanzow, 2011). Despite the evident spatial limitation, this approach also allows to compare data from the same site, and to observe data patterns that affect natural systems. The majority of moorings, either used for short-term or long-term monitoring studies, are equipped with fixed-depth instruments, which means that a series of sensors (e.g., turbidimeters or current meters) are placed at fixed depth intervals along the mooring line. However, this implies that many oceanographic devices and sensors need to be deployed on the mooring to obtain adequate vertical resolution, which substantially raises the cost of the mooring deployment (Carlson et al., 2013).

Autonomous moored profilers have been developed to provide high-resolution temporal data of the various characteristics of the water column by periodically traveling through the water column at a fixed position. These profilers acquire data in the water column from near the surface to the bottom, thereby allowing one to obtain homogeneous data with uniform accuracy (Ostrovskii et al., 2013). It is worth to mention here that moored profilers were first introduced in the 1970s (Van Leer et al., 1974), although more recently there have been developed more sophisticated tethered profilers including those transported by the bottom mounted winch, such as the VPS (see **Chapter 6**) or by the propulsion system mounted on the profiler suite itself. Among the latter type of profilers, one of the most prominent examples is the Russian Aqualog (Ostrovskii et al., 2013), which has been presented in this Thesis (see **Chapters 3, 4** and **5***).* Although the great possibilities that moorings offer, they generally present telemetry and power limitations, and data cannot be accessed until the instruments are recovered.

Seafloor observatories, such as the ONC's NEPTUNE observatory (**Chapter 6**), have been recently developed to overcome the limitations of stand-alone moorings. They have the main advantage of continuous operation and large power and bandwidth capabilities, and they provide near real-time communication and integration. Although they are an expensive alternative for sustained observations, they offer the scientific community new opportunities to study multiple, interrelated processes over long-time scales.

7.2. Sediment transport through nepheloid layers

The aim of this Thesis was to study the temporal and spatial variability of the nepheloid layer structure in continental slope environments in the Catalan and Cascadia margins (NW Mediterranean and Canadian NE Pacific, respectively) using autonomous profiling vehicles installed in seafloor cabled observatories and stand-alone moorings. The specific goals of this Thesis were established with special emphasis on addressing the generation mechanisms (natural and anthropogenic) and the implications of these mechanisms in a spatial and, more importantly, temporal context.

The presence of nepheloid layers has been reported in many sites along the NW Mediterranean margin, where the highest suspended sediment concentrations (SSC) have been observed on the terrigenous margins of Catalonia (Puig and Palanques, 1998a) and the Gulf of Lions (Casamor, 2007), being particularly important in presence of submarine canyons (Fig. 7.1).

The first systematic description of the suspended particulate matter (SPM) in the Catalan margin was carried out by Puig and Palanques (1998a), who identified a well-defined pattern consisting in surface, intermediate and bottom nepheloid layers (SNL, INL, and BNLs, respectively). Particles constituting these nepheloid layers were attributed to be mainly supplied by rivers discharging into this margin or resuspended on the shelf during storms (Puig and Palanques, 1998a). Once in suspension, their transport is controlled by the topography, hydrography, distance from the source that originates them, and different physical gradients (Puig and Palanques, 1998a). In this margin, maximum particulate matter concentrations are found near the coast, where the surface

salinity gradient favours the formation of SNL and where the thermocline, intersecting with the seafloor, can generate a BNL, from which sediment particles detach forming an INL at the shelf. In the Foix Canyon and over the continental slope, an increase of SPM concentrations was recorded between 300 and 500 m water depth related to a suggested permanent slope INL (Puig and Palanques, 1998a) (Fig. 7.1).

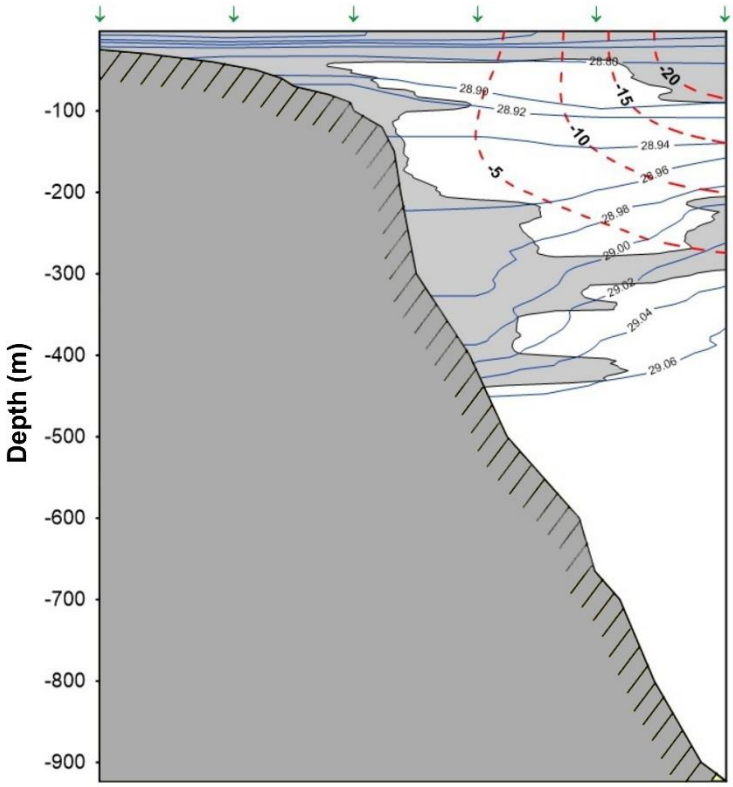

Figure 7.1. Cross-margin section along a hydrographic transect (No. 6) conducted during an oceanographic cruise (April 1993) in the Barcelona continental margin, showing the *sigma t* (blue continuous line) and the beam attenuation coefficient contour higher than 0.4 m^{-1} (stippled area). Dashed lines show the geostrophic current flow (from 5 to 20 $cm \cdot s^{-1}$) and the structure of the current jet inferred from the observed density field (reference level 600 dbar). Note that particulate matter distribution over the slope is controlled by the current jet boundary and by the slope density front. **Source:** Modified from Puig and Palanques, 1998a.

Several mechanisms had been discussed to assess the permanent presence of this nepheloid layer (Puig andPalanques, 1998a). First, the presence of the shelf-slope density front and the geostrophic circulation (Northern Current) associated to this front was discussed, as it is an interface able to retain sediment particles at its foot (~400 m depth) (Fig. 7.1). The location of the density front has been associated with the presence of the Western Intermediate Water (WIW). When the WIW is present, the foot of the front and the slope INL are located at 300-500 m depth, whereas when it is not present, the front migrates upslope, generating particulate matter detachments closer to the shelf. However, the slope-INL was still observed at ~400 m depth as a permanent structure, despite the absence of this water mass at the slope. The

breaking and possibly shoaling of internal waves was then discussed, based on previous observations carried out in other continental slope areas (Cacchione and Drake, 1986) and in submarine canyons (Gardner, 1989) that explained and demonstrated the generation of INLs and near-BNLs related to the action of these waves. Thus, the propagation of internal waves along the foot of the density front intersecting with the seabed was postulated for the Foix Canyon as a mechanism able to resuspend bottom sediments, thereby generating and feeding the slope INL (Puig and Palanques, 1998a).

Repeated mapping of these layers carried out in this Thesis (**Chapter 4**) using an autonomous hydrographic profiler (Aqualog) has yielded to a better definition of the structure and time evolution of the nepheloid layers in the Foix Canyon, recording their persistence in the water column, which was not possible to obtain in previous studies. The study presented in **Chapter 4** is the first work in which the temporal variation of the nepheloid layer structure has been determined in the Catalan margin. The matching of the water depths of the observed slope INLs developed between 300 and 500 m and bottom trawling activities water depths within the Foix Canyon and the adjacent slope (Fig. 4.7) strongly suggest that this human activity is the major mechanism that leads to increasing SSCs in the water column at the Foix Canyon (**Chapter 4**).

On the other hand, a preferentially retention close to the seabed of the resuspended sediment sediments by bottom trawling activities within the canyon was shown. Although the current regime within the Foix Canyon interior could not be determined, the periodical vertical oscillations of 4-10 days of the water masses were observed during the deployment (Fig. 4.5), which were in agreement with the periodicity of the near-bottom along-canyon flow reversals observed by Puig et al. (2000). This suggests that the Foix Canyon contributes to the cross-margin transport of trawling-induced resuspended particulate matter.

In fact, the nepheloid layer structure observed at the Foix Canyon (**Chapter 4**) highly resembles that describe for the entire Catalan margin (Casamor, 2007; Fig. 7.2). The SNL is observed in the entire margin and its presence is linked to the seasonal thermocline. The BNL is especially developed at continental shelf depths (< 120 m), and it has been hypothesized to be fed by sediment particles from riverine origin and *in-situ* resuspended sediments on the shelf. The main INL is located below the shelf break (~120 m depth), extending towards the basin of the Catalan margin, and other INLs appear between 300 and 500 m depth, particularly in the section of the margin comprised between the Lacaze-Duthiers and the Foix submarine canyons (Fig. 7.2), which can laterally spread towards the canyon flanks and to adjacent areas between canyons.

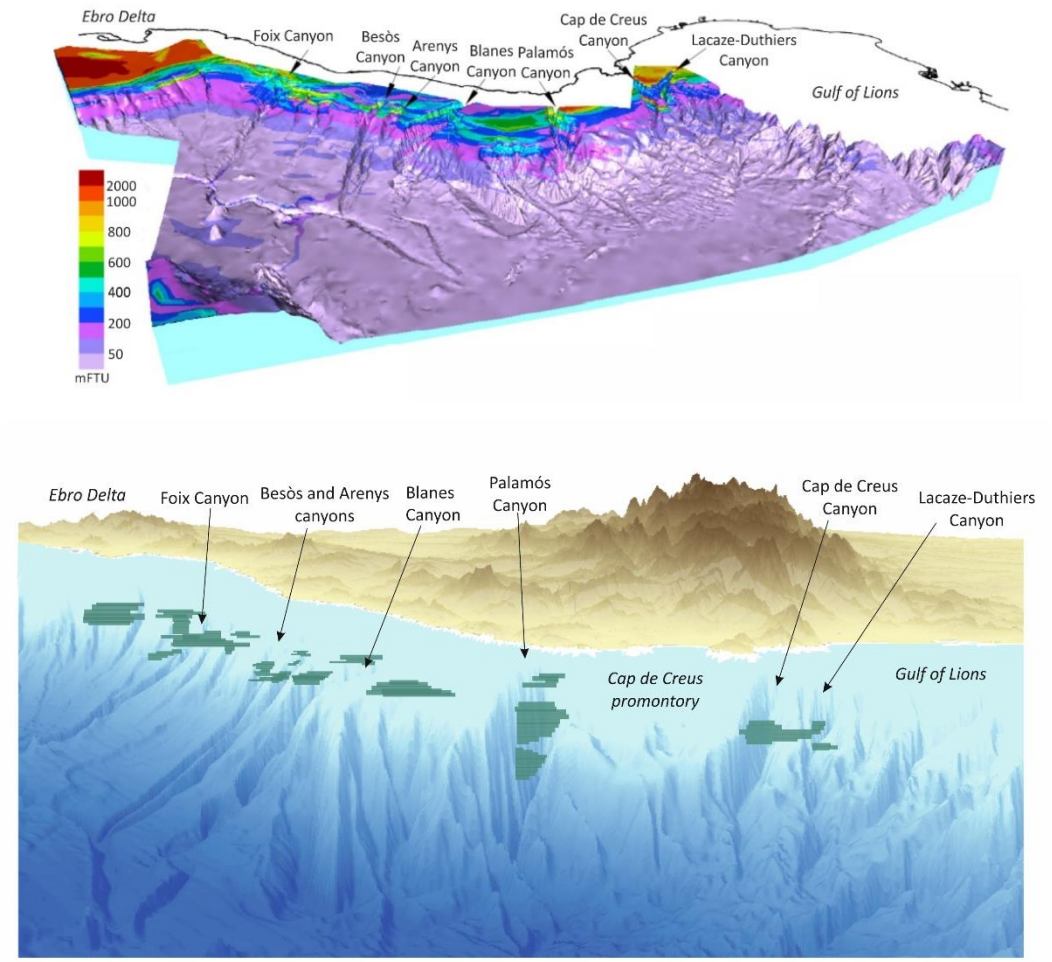

Figure 7.2. 3-D view from the E of the intermediate nepheloid layers (INLs) of the Catalan margin (NW Mediterranean), displaying concentrations between 500 and 600 mFTU. The majority of these INLs are located over the axes of the main submarine canyons incising this margin. Towards the southern section, these INLs are observed to spread along the slope between canyons. Also, towards the south, it can be observed that the depths of these INLs progressively decrease. **Source:** Modified and adapted from Casamor, 2007.

The nepheloid layer structure and variability in the SPM patterns were also studied in the Palamós Canyon (**Chapter 5**) on the assumption that a similar nepheloid layer structure and comparable resuspension processes affecting the Foix Canyon (and other canyons of the margin) could be also affecting the Palamós Canyon. This new study (**Chapter 5**) builds on data from a CTD transect conducted at a fished tributary of the Palamós Canyon (Martín et al., 2014a). This study identified a well-defined nepheloid layer structure consisting of INLs and BNLs between 500 and 700 m depth related to trawling activities along the northern flank of the canyon, and an INL between 150 and 220 m depth, constrained by the density gradient between the Atlantic Water (AW) and the Levantine Intermediate Water (LIW) (Martín et al., 2014a). The data presented in **Chapter 5** derived from the deployment of the Aqualog profiler with additional near-bottom instrumentation allowed a high frequency record of turbidity vertical profiles during 4 months of monitoring, including part of a trawling closure period and the beginning of the trawling season (**Chapter 5**).

The quasi-permanent presence of INLs and near-BNLs near the fishing grounds of Palamós Canyon (Sant Sebastià at the northern canyon flank, and Rostoll at the southern canyon flank, respectively) during the monitored trawling season (Fig. 5.7c) resembles the nepheloid structure linked to the trawling activities at fishing grounds of the Foix Canyon (Fig. 4.5c). Both submarine canyons are deeply incised in the Catalan margin, at a relatively close distance from the coast, but are affected differently by the corresponding bottom trawling fleets that operate on them. Trawling activities at the Foix Canyon take place along the canyon axis at 600-800 m depth, and mainly over the upper slope next to the canyon (200-500 m depth), from where resuspended particles are advected along-margin by ambient currents and cross over the canyon as nepheloid layers (**Chapter 4**). In contrast, trawling activities at the Palamós Canyon are not carried out along its axis, and occur mainly at the flanks of the canyon, with minimal activity on the northern upper slope (Figs. 5.2 and 5.5). Nevertheless, the low trawling activity at the upper slope of the Palamós Canyon is able to contribute to the advection of resuspended sediments between 80 and 200 m depth (Fig. 5.12c), and to the detachment of an INL at these depths. In agreement with the observations made in the study by Martín et al. (2014a), the isopycnal surface created between the oAW and the LIW could favour the retention of suspended particles along this depth range, which are advected afterwards towards the southwest by the geostrophic circulation. Nonetheless, despite the different locations where trawling activities take place at the Foix and Palamós submarine canyons, the nepheloid structure developed in both canyons is remarkably similar. Sediment concentrations in the nepheloid layers developed at both submarine canyons are also very similar, usually showing concentrations up to 1 $mg \cdot L^{-1}$ and displaying maximum concentrations of ~3.8 $mg \cdot L^{-1}$ (Figs. 4.5c and 5.7c).

In contrast to the preceding study conducted in the Foix Canyon (**Chapter 4**), in which the Aqualog was only tested during the trawling season at the canyon, the study conducted in Palamós Canyon (**Chapter 5**) represents an advance in terms of data acquisition and in the knowledge of sediment dynamics in submarine canyons affected by trawling activities. Firstly, the frequency at which the Aqualog was programmed during the study at the Palamós Canyon doubled that at which the same profiler was programmed at the Foix Canyon (2 up-and down-casts per day vs. 1 up-and down-casts per day, respectively). However, the increased frequency, which was initially used to discern any daily variations on the water column turbidity due to trawling activities, was not sufficient for capturing the supposedly higher concentration of particles during the day profile at 2 p.m. (during the working schedule of the local trawling fleet) and the lower concentration of particles during the night profile at 2 a.m. (when water column turbidity is supposedly decreasing due to the cessation of trawling activities) (Fig. 7.3). Additionally, no clear decrease on suspended sediment concentrations was observed during weekends, when the trawling fleet rest at the harbour. This points out that the water column turbidity structure of a fished submarine canyon can remain relatively unchanged during hours and even days when it is constantly being fed by the less dense fraction of sediment particles put in suspension after the repeated passage of the trawling vessels feeding quasi-permanent INLs and BNLs during the trawling season (Fig. 5.7c).

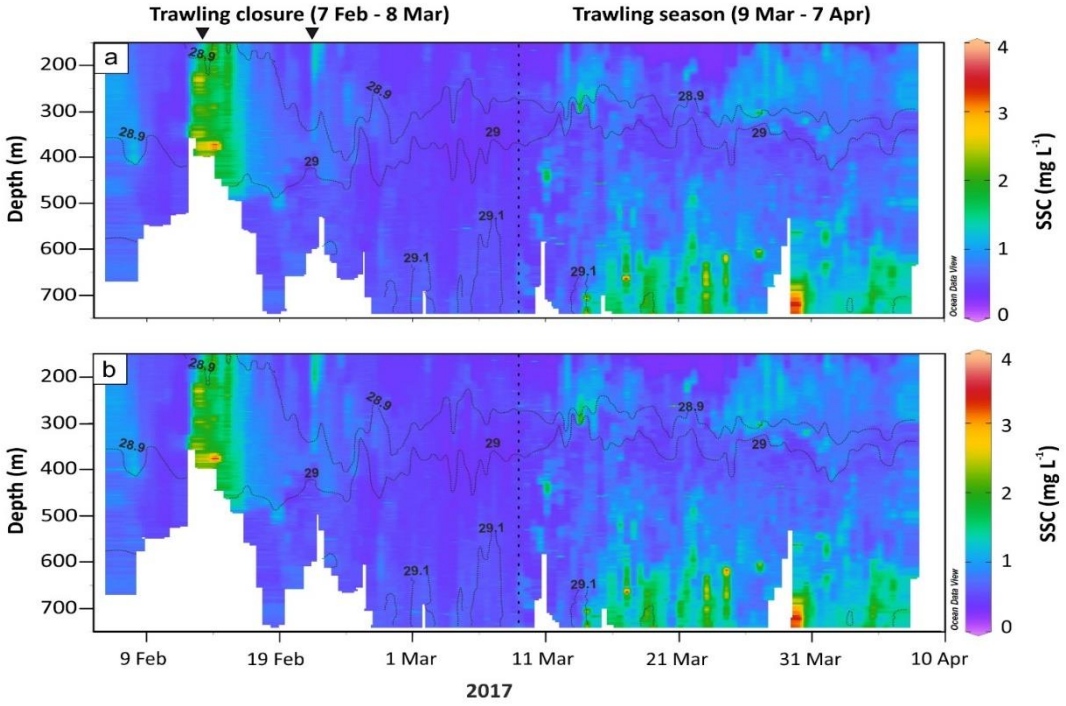

Figure 7.3. Time series of the SSC (mg·L^{-1}) measured at a) 2 a.m. and at b) 2 p.m. by the Aqualog during the study conducted at the Palamós Canyon (Catalan margin, NW Mediterranean), basically showing the same nepheloid structure. The dashed line separates the trawling closure from the trawling season.

In addition, in this new study it has been possible to examine the evolution of the water column turbidity structure of the Palamós Canyon when it is unaffected by fishing activities (i.e., during the trawling closure period), thereby being able to discern between the natural and anthropogenic resuspension processes affecting the canyon nepheloid layer structure (Fig. 5.7c). Findings from this study (**Chapter 5**) have shown that, in absence of trawling activities, the water column turbidity structure in the Palamós Canyon can be mainly dominated by sediment particles resuspended by high-energetic oceanographic processes such as storms, flash-floods from nearby rivers, and dense shelf water cascading (DSWC) events. Particularly, DSWC has been intensively studied in the neighbouring Cap de Creus Canyon at the northern sector of the Catalan margin (Fig. 2.1), as well as in other canyon head regions at the Gulf of Lions, associated with high-near bottom speeds and significant suspended sediment transport (Palanques et al., 2006b; Puig et al., 2008; Ogston et al., 2008; Palanques et al., 2012). DSWC had not been yet observed in the Catalan margin south of the Cap de Creus Canyon until Ribó et al. (2011) reported the first evidence of the presence of these events in the Palamós Canyon head (300 m depth) related to eastern storms. The results presented in **Chapter 5** contribute to a better understanding of the sedimentary dynamics of this canyon related to DSWC events, evidencing for the first time the effects on the water column turbidity structure, as well as additional near-bottom data at a deeper location at the canyon, almost reaching 1000 m water depth. The SSCs reached at the water column during this event ranged between 1.1 and 3.8 mg·L^{-1} (Fig. 5.7c), whereas near-

bottom SSC increased up to 234 mg·L^{-1} and current speeds up to ~0.6 m·s^{-1} (Figs. 5.7d, e). This data shows a higher magnitude of DSWC events in Palamós Canyon in terms of down-canyon current velocities and SSC peaks than the previous records from Ribó et al (2011).

The results obtained in **Chapter 5** allowed to discern between the effects of both natural and anthropogenic processes (bottom trawling) in the water column turbidity and associated nepheloid layer structure, which was not assessed in the study conducted in the Foix Canyon (**Chapter 4**). In the Palamós Canyon, trawling activities supplied resuspended sediment that doubled the sediment load measured in the water column during the trawling closure period. This actually seems to be in coincidence with the double-fold increase of natural sedimentation rates registered at this canyon in a sediment core collected at the canyon axis (Martín et al., 2008), indicating that trawling activities increase the sediment load in the water column and the sediment accumulation rates where trawling resuspended sediment is deposited.

Findings from **Chapter 5** have also highlighted the important role of currents inside the Palamós Canyon in the redistribution and final fate of resuspended particles in the canyon. Near-bottom currents registered during the Palamós Canyon deployment confirmed the presence of a predominantly up-canyon flux superimposed to the regular up- and down-canyon current oscillations along the axis (Fig. 5.11). In fact, previous studies (Martín et al., 2006; 2007) had already proposed a division of the Palamós Canyon in two domains: an outer domain (down to 1200 m depth), where slope dynamics and seasonal trends are the main factors controlling the magnitude of suspended sediment fluxes, and an inner domain (up to 1200 m depth) constricted by the canyon topography and mainly influenced by lateral transport of SPM from the adjoining shelf and adjacent slope (Palanques et al., 2005).

In the NE Pacific margin, the body of literature addressing the nepheloid layer structure and main sediment transport processes is very slim, with only one work conducted back in the 1980s off in Quinault Canyon, off Olympic Peninsula (NE American Pacific; Fig. 6.1), assessing the sedimentary dynamics at this particular location of the margin (Carson et al., 1986). No other studies have addressed the processes responsible for the transference of sediments at the NE Pacific margin, nor the nepheloid structure, leaving a big gap of knowledge in this sense. The results presented in this Thesis for the Cascadia margin at Vancouver Island's continental slope constitute the first observations on the nepheloid layer structure on this margin and the NE Pacific region, and propose a first tentative on the processes dominating the sediment transport in this margin alongside with the main controlling factors of nepheloid layer formation (**Chapter 6**). These results present a similar approximation to the study of the nepheloid layer structure as that used in the Catalan margin in this Thesis, also using an autonomous vertical profiling device (the Vertical Profiling System, VPS), but installed in a seafloor cabled observatory rather than in a mooring, as in the Foix and Palamós canyons (**Chapters 4** and **5**). An Acoustic Doppler Current Profiler (ADCP) installed close to the VPS provided additional information of the water column current dynamics. The water column studied in Vancouver Island's continental slope (**Chapter 6**) presented a nepheloid layer structure consisting in SNLs, INLs and BNLs, which resembles that

observed on the Catalan margin (Figs. 4.5c, 5.7c, and 6.8e). Differently from the Catalan margin, in which the resuspension processes generating nepheloid layers in each of the studied areas could be constrained, the Cascadia margin off Vancouver Island presents great complexity of the sedimentary and oceanographic dynamics, thereby making it difficult to determine the precise source of suspended sediments and the specific action of the different processes able to generate nepheloid layers.

In **Chapter 6**, several processes have been discussed that could potentially explain the SPM detachments observed in this margin. In the first place, fall storms were considered as a very plausible mechanism generating nepheloid layers in the area, particularly during the most intense stormy period. The only studies to build these results on were conducted at the Quinault Canyon, where storm-induced currents and waves resuspended sediment on the shelf were detached as an INL over the shelf-break (Hickey et al., 1986; Baker and Hickey, 1986). However, after a detailed analysis in the study site off Vancouver Island, a direct coupling between the atmospheric conditions and the increases in water turbidity was discarded (Fig. 6.11). Although internal waves at tidal frequencies were postulated as a dominant sediment transport mechanism in this region (Crawford and Thomson, 1982; Drakopoulos and Marsden, 1993), very weak current activity across the margin was observed at the VPS study site, without a clear offshore-onshore pattern and without a relationship with the nepheloid layer structure. In contrast, along-margin currents associated with the California Current System showed a clear relation with the presence/absence of water turbidity increases (Fig. 6.7e and Fig. 6.9b), thereby highlighting the important role of the geostrophic circulation in controlling sediment transport. Nonetheless, there was not a solely natural mechanism that could explain, by itself, the high variability on the nepheloid layer structure in this area.

The presence of trawling activities in the continental slope area, when crossed with the presence and water depths of the observed INLs and BNLs, also suggests that this anthropogenic process could be injecting resuspended sediments into the water column, and therefore, it has been hypothesized as a contributor to the nepheloid layer structure in this area. In comparison with the NW Mediterranean, trawling activities at the continental margin of Vancouver Island are less intense and patchy (Fig. 6.1), with a proportion of trawlers using pelagic trawling gear. Nevertheless, the available AIS data used in this study area do not discern between pelagic and demersal trawling. This fact poses a difficulty in discriminating the contribution of fishing activities to the sedimentary dynamics on this continental slope region. Despite that the analysis conducted in this study area based on vessel speed limits revealed a high frequency of pelagic trawling signals (Fig. 6.6; Table 5.2), it has been hypothesised that the presence of bottom trawling activity along the Vancouver Island's continental slope, in combination with the California Current System, could be contributing to resuspend sediments and advect them as nepheloid layers, even if these activities take place in farther fishing grounds and not directly close to the study area.

7.3. Bottom trawling as a contributor in the formation of nepheloid layers in fished continental slope areas and submarine canyons

There are many causes for the formation of nepheloid layers in the different oceans of the world (McCave, 1986). Amongst them, in continental slope regions, internal waves have been proposed as one of the major mechanisms that initiates sediment resuspension and therefore, in generating nepheloid layers (see 1.4.2.1). Submarine canyons can play a major role in determining the characteristics of internal waves' interaction with the seafloor and control the transport of suspended sediment particles transport at intermediate and deeper sections of continental margins (Gardner, 1989; Kunze et al., 2002; Puig et al., 2003). However, in open continental slope environments, it is difficult to observe this mechanism directly and to evaluate its contribution to the sediment dynamics. In the Gulf of Valencia (W Mediterranean), where internal wave activity was properly characterized (van Haren et al., 2013), the presence of high SSC peaks was unrelated to hydrographic processes, proposing trawling activities as the main source of sediment resuspension in this area (Ribó et al., 2015). Previous hydrographic transects conducted on this area identified INLs and BNLs that by their water depth and location were also attributed to trawling (Ribó et al., 2013).

Data presented in this Thesis corroborates that resuspension induced by trawling activities in slope and canyon environments can play a significant role as initiator of sediment resuspension at slope depths, generating INLs and BNLs at certain water depths based on the locations of the fishing grounds. This mechanism is particularly relevant in the Mediterranean Sea, where, in absence of tides, the internal wave activity is rather weak and occurs mostly at near-inertial frequencies, having a minimal effect on sediment resuspension and water column turbidity.

Nonetheless, only a few studies have addressed the effects of bottom trawling activities in deep-sea environments. The first comprehensive studies were centered in the Palamós Canyon (NW Mediterranean). Briefly, these studies observed that bottom trawling smoothened the complex morphology of the canyon and modified natural sediment dynamics along with resuspension and erosion of large volumes of sediment, triggering sediment gravity flows into the canyon interior and enhancing the formation of nepheloid layers (Palanques et al., 2006a; Martín et al., 2008; Puig et al., 2012; Martín et al., 2014a, b). In the southern margin of the Aegean Sea (NE Mediterranean), Chronis et al. (2000) found near-BNLs and detached INLs in the vicinity of the shelf-break and over the slope region, suggesting that, besides near-bottom current activity and breaking of internal waves, demersal fishing activities developed over the area might be likely causing the sharpest SSC recorded near the seabed. However, other studies in the Aegean Sea (Karageorgis and Anagnostou, 2003) proposed opposite results, reporting deep slope INLs in regions where fishing occurs at shallower depths, attributing the formation of these INLS to natural processes, such as strong currents or internal waves. Therefore, both natural and anthropogenic processes seem to coexist and generate sediment resuspension that, ultimately, can lead to the formation of nepheloid layers at continental slope depths. Outside the Mediterranean, in the Whittard Canyon region (NE Atlantic), unusual high peaks of suspended

particulate matter in nepheloid layers were also observed to be linked to trawling activities near the canyon (Wilson et al., 2015b; Daly et al., 2018). Through the use and presence of vessel identification data (i.e., VMS data), as it has been used in this Thesis, the locations and presence of bottom trawlers in the area provided evidence for the relationship between trawling activity and the occurrence of enhanced nepheloid layers which displayed anomalous high SSC values, exceeding those in the INLs typically observed in the region (Wilson et al., 2015a).

Although the formation of trawling-induced nepheloid layers on deep-sea environments has only been documented in these few studies, and the temporal evolution of the nepheloid layer structure had not been assessed before, it is important to point out that bottom trawling might be affecting in a similar way other submarine canyons and continental slope regions targeted by fisheries worldwide.

Bottom trawling has lately gained attention on the scientific community and policy makers (European Parliament, 2008), not only for the impacts on marine biodiversity and living resources, but also for its destructive effects on the seabed and its strong potential in altering sediment transport processes and turbidity conditions in the deep-sea environment at large spatial and temporal scales (Puig et al., 2012). The identification and assessment of these impacts, together with the quantification of the ecological status of the deep-sea environment, has become increasingly important, especially after the implementation of the European Marine Strategy Framework Directive (MSFD; 2008/56/EC, descriptors #6 and #7), but it is still an ongoing challenge (Gislason et al., 2017).

Conclusions and future perspectives

Part V

Chapter 8. Conclusions

Throughout this Thesis, the main resuspension mechanisms on continental slope environments and the associated distribution of surface, intermediate and bottom nepheloid layers in two different geographic and oceanographic settings has been assessed. Special emphasis has been placed on addressing these mechanisms in a temporal context by using multiparametric instrument platforms such as autonomous profiling vehicles installed in moorings and in a seafloor cabled observatory.

The hydrographic and nepheloid layer structure identified in the water column of submarine canyons incising the Catalan margin were studied through the analysis of over 170 hydrographic profiles collected by an autonomous hydrographic profiler deployed at the axes of two submarine canyons incising this margin. Through a dedicated hydrographic and nephelometric study in the Foix (**Chapter 4**) and Palamós (**Chapter 5**) submarine canyons, a well-defined water turbidity structure consisting in INLs and near-BNLs was identified. The nepheloid layers detected in both canyons have comparable concentrations of suspended particulate matter, although they present almost doubled concentrations and particulate standing crops when trawling activities are present. The locations and presence of bottom trawlers in both canyons provide evidence for the relationship between trawling activities practised in and around the Foix and Palamós canyons, and the occurrence of trawling-induced nepheloid layers. The use of VMS and AIS vessel tracking data have been proven as a useful tool to establish such a link and they also show that sustained bottom trawling over the same fishing ground is able to generate quasi-permanent nepheloid layers and maintain high concentrations of SPM in the water column of these two submarine canyons.

In absence of trawling activities nearby the study sites, the water column shows lower SPM concentrations and sporadic increases during high energetic natural events, such as storms, flash-floods, or dense shelf water cascading (DSWC). The results obtained in **Chapter 5** reveal that turbidity and sediment transport induced by natural processes in the Palamós Canyon occur sporadically, whereas turbidity and sediment transport related to trawling activities occur periodically, but overtime, they can overcome natural processes as the main resuspension mechanism by reaching similar cumulative sediment fluxes. Trawling activities are able to change the natural patterns of suspended particulate matter dispersion and accumulation in some submarine canyons. This is especially important in regions such as the Catalan margin, where trawling activities are practised on a daily basis throughout the year and high-energy processes are more sporadic.

The hydrodynamics in submarine canyons can also contribute to the maintenance of high concentrations of suspended particulate matter in their interior. The net suspended sediment transport in the Foix and Palamós canyons is mainly up-canyon, which implies that sediment transported down-canyon during gravity or density (i.e., DSWC and trawling) is retained in the

canyon axis and not exported down-canyon for long distances towards greater depths. This ultimately has a key role in the redistribution and final fate of resuspended sediments in the canyon interior.

The sediment resuspension and nepheloid layers generated in the submarine canyons by both natural and anthropogenic processes can also be advected along-slope by currents, eventually affecting the water column turbidity structure in further areas outside submarine canyon domains, as suggested in the Vancouver Island's continental slope (**Chapter 6**). Even the physical processes in this area are very complex, both in terms of oceanography and hydrodynamics, and that it is difficult to identify how natural mechanisms contribute to the nepheloid layer structure in the area, the entire margin presents high trawling activity (Fig. 6.1). Although the trawling effort is less intense and more spread than in the Catalan margin, with a proportion of pelagic trawlers, trawling-induced resuspended sediments can be ultimately transported by along-slope currents, affecting the water column turbidity in further regions.

This along-slope transport of trawling-induced suspended sediment particles seems evident in the Catalan margin, where the development of INLs over the axes and flanks of submarine canyons incising the margin coincide with the depths affected by bottom trawling activities (Casamor, 2007; Fig. 8.1). The sediment particles put in suspension by this human activity, in combination with the Northern Current (Fig. 2.1), and the associated shelf-slope density front, are advected along the margin contributing to feed quasi-permanent INLs and BNLs.

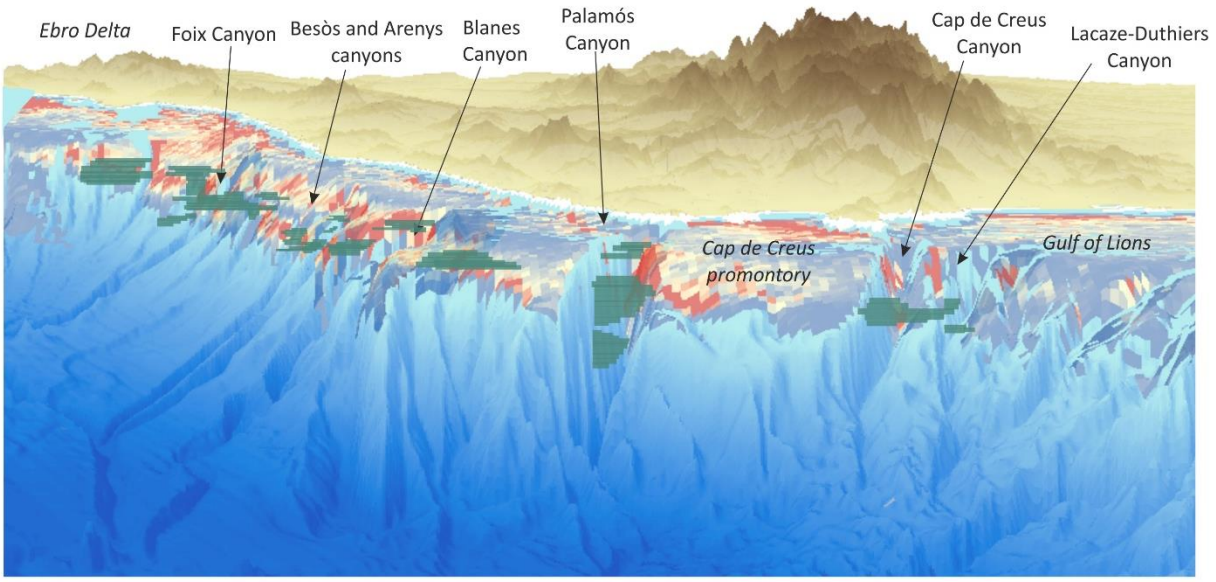

Figure 8.1. 3-D view, from the E, of the Catalan margin and the Gulf of Lions showing the presence of nepheloid layers along the margin (green-coloured) displaying values between 500 and 600 FTU. The overlying raster represents the fishing effort, which has been extracted from the Global Fishing Watch database (Global Fishing Watch, 2020). The majority of these INLs are located over the axes of the main submarine canyons incising this margin and the Gulf of Lions, which are affected by bottom trawling activities. **Source:** Modified from Casamor, 2007.

The results presented in this Thesis highlight the importance of taking into account the vulnerability of deep-sea environments, and stress that trawling activities affect the good status of the water column, altering sediment transport processes and turbidity conditions at long spatial and temporal scales. Trawling activities can produce impacts in the water column, even overcoming those of natural processes, altering natural conditions in deep ecosystems. This highlights the necessity to address the effects of anthropogenic activities and incorporate them in studies of sediment dynamics in deep-sea environments where fishing activities are practised.

Chapter 9. Future perspectives

Overall, this Thesis has contributed to the understanding of the impacts that natural and anthropogenic mechanisms, particularly trawling activities, exert on the nepheloid layer structure, both on submarine canyon and open continental slope environments. Some of the current and future research areas that this Thesis arose are summarised in this section.

9.1. Open issues and recommendations for future work

- *Long-term monitoring*

Although this Thesis has made significant progress in determining the main controlling factors of the presence of nepheloid layers, the duration of the different experiments was rather short (covering from 2 to 4 months) and, in some cases, only the trawling season could be monitored. Longer water-column monitoring, both in the Catalan and Cascadia margins (or elsewhere), would allow for a better characterization of the nepheloid layer structures over time. A year-round experiment would allow to improve our knowledge of the sediment dynamics and it would help us identifying the potential seasonal variations on the nepheloid layer structures developed in the study sites. Also, it would allow us to constrict the relationship of the seasonal patterns of trawling activities and the generation of nepheloid structures.

However, a longer monitoring would require a high maintenance of the instruments, especially those installed in stand-alone moorings which are fed by batteries, and the optical sensors should be equipped with anti-fouling systems. In that sense, seafloor cabled observatories are more prepared for longer experiments, allowing for continuous monitoring and large power supply, although in turns they are very expensive to maintain, and the location of the instrumented platforms can be in conflict with the presence of trawling activities that could damage them.

- *Towards more sustainable trawling activities*

With the increasing awareness of the adverse effects of trawling gears on the seafloor, certain measures and management strategies have been taken to lessen its impacts (McConnaughey et al., 2020). Some of these measures include spatial and temporal trawling closures. Results from **Chapter 5** highlight that temporal trawling closures are sufficient to reduce the amount of suspended particulate matter being injected to the water column, although they are insufficient to restore the seafloor in terms of sediment coverage and biogeochemical composition (Paradis et al., 2021).

Other measures have been towards limit seabed contact by adopting new fishing gears or altering existing ones that minimise the pressure on the bottom, and therefore, minimise the impacted area while trawling (He et al., 2004; He and Winger, 2010; Rijnsdorp et al., 2017). In this regard, the fishermen guild of Palamós harbour, in collaboration with the Catalan Regional Government

and the Spanish Central Government, initiated in 2013 a long-term self-management plan with the main goal to increase the sustainability of the blue and the red deep-sea shrimp (*Aristeus antennatus*) in the trawling grounds of the Palamós Canyon, and to reduce the intensive erosion created by demersal trawling gears along the canyon flanks (BOE, 2013). During the PORTES Project in 2015, which involved scientists and the local fishermen guild of Palamós harbour, several experimental trials with different pelagic and semi-pelagic trawl doors were carried out in order to investigate their impact on the sediment resuspension (Palanques et al., 2018). The pelagic trawl models, which have no contact with the seabed, were selected to be in use in all trawling vessels of the Palamós fleet, and the complete shift of the trawling gear was accomplished in September 2017. Since then, a reduction of almost half of the sediment load and suspended sediment transport in the water column has been observed.

Therefore, management strategies reinforcing both trawling closures and low-impact fishing gears would help achieving the good status of the water column in this (and other areas) in terms of water turbidity and sediment transport by reducing the amount of particulate matter introduced into the water column.

- *Improvement of fishing vessel tracking data*

With further extension of trawling grounds, we might see an increase in trawling-induced resuspension events and/or increased activity at vulnerable deep-sea sites. Thus, there is an urgent need to examine this issue. In this Thesis, the trawling fleets mobility patterns by using either VMS data (**Chapter 4**) or AIS data (**Chapters 5** and **6**) have been examined. The latter offer far greater resolution in comparison to the former (data points every 6 seconds in the AIS method vs. to every 2 hours in the VMS method, respectively), although AIS signal can be manually disconnected by fishermen, while VMS is transmitting permanently.

In this Thesis, it has been observed that both VMS and AIS technologies generate data with several limitations, making them often ineffective when used in isolation. This can lead to significant underestimation of fishing effort. For future research, integrating data from both methodologies in an ensemble approach could provide more accurate fishing information for marine spatial planning, as well as for assessing the impacts of this anthropogenic activity.

- *Composition of nepheloid layers*

Although considerable improvement on previous knowledge on the nepheloid layer structure has been made in both study areas, particularly in the Catalan margin, the composition of these nepheloid layers and the duration that the particulate matter remains in suspension remain unknown.

Further studies could include the sampling of the water column at the depths where these nepheloid layers are detected by using a CTD lowered from a ship equipped with a rosette of Niskin bottles or in-situ pumps. Analysis of particles in these nepheloid layers could include the

use of stable isotopes (e.g., ^{13}C and ^{15}N) to assess temporal and seasonal variations on particulate matter, as well to trace energy flow between different trophic levels. Analysing the suspended particulate matter from nepheloid layers by radioactive isotopes would also aid our understanding on the source of material and the constant changes it undergoes. In combination with isotopic analyses of sediments from the shelf, questions related to the source of material could be addressed. Analyses of ^{234}Th and ^{210}Pb have also been carried out in the exploration of particle exchanges, as in Inthorn (2006), Owens et al. (2015), or in Marchal and Lam (2012).

Therefore, by studying the composition of nepheloid layers, one could assess the mechanisms that have originated them, and even distinguish their natural or anthropogenic origin.

- *Application of acoustic methods to assess the nepheloid layer structure*

The application of acoustic methods for the quantification of suspended sediment concentrations and flow velocities has been recently demonstrated (Simmons et al., 2009; Best et al., 2010; O'Neill et al., 2013), enabling the imaging of sediment dynamics in a 2-dimensional flow field. Acoustic devices (such as ADCPs or multibeam echosounders) can be used to quantify the sediment concentrations by using backscatter information, and therefore, identify the sediment loads that are mobilised into the water column by different mechanisms.

In this Thesis, the nepheloid layer structure of the covered study sites using optical instrumentation (i.e., turbidimeters equipped with optical backscatter sensors) installed in autonomous vertical profiling devices (Aqualog profiler and VPS, respectively) could be identified. Acoustic instrumentation was only used in **Chapter 5** to study the near-bottom current dynamics of Palamós by means of a near-bottom current meter, and in **Chapter 6** to study the current dynamics in the upper continental slope off Vancouver Island by means of an Acoustic Doppler Current Profiler (ADCP). Further studies should consider combining both methods to fully quantify the sediment concentrations in the water column.

- *Towards a more comprehensive study of the nepheloid layer structure in the Catalan margin*

In this Thesis, it has been possible to assess the role of bottom trawling activities in increasing the concentration of suspended particulate matter in the water column and in generating INLs and BNLs at certain depths based on the location of fishing grounds. However, deep bottom trawling grounds are ubiquitous in the whole Catalan margin, being present in almost all submarine canyons incising it (Fig. 2.1 and Fig. 8.1), and therefore, similar impacts could be occurring in these deep-sea environments. Further studies such as those presented in this Thesis could provide additional information on the nepheloid layer structure in other submarine canyons incising the Catalan margin, on which other works could be based in order to study the potential impacts of trawling-induced resuspension on vulnerable benthic communities, such as cold-water corals.

9.2. Future perspectives

Since the 1950s, bottom trawling grounds have been expanding from the shallow sea to deeper and unexplored areas to feed the world's population (Norse et al., 2012; Watson and Morato, 2013). Nowadays, it is estimated that bottom trawling occupies 4.4 million km^2 of the continental slope worldwide (Puig et al.,2012), covering the great majority of continental slopes (Fig. 9.1). Some studies have assessed the damage of deep-sea fisheries on benthic communities (Clark et al., 2016; Sciberras et al., 2018), but there is still a gap of knowledge on the studies assessing the physical impacts of bottom trawling in deep-sea environments, both in the seafloor and in the water column turbidity.

The effects of bottom trawling activities in the nepheloid layer structure in two very different oceanographic settings, the Catalan margin in the NW Mediterranean and the Cascadia margin in the NE Canadian Pacific, have been reported in this Thesis. Due to the ubiquitous presence of bottom trawling in the world's continental slopes, it is likely that these effects can be extrapolated to other regions of the Mediterranean, but also to other ocean margins around the world affected by trawling activities. However, these impacts might be modified by different oceanographic conditions and hydrodynamics forces (i.e., tides and strong bottom currents), along with variable trawling efforts.

As previously stated in this Thesis, many studies in SPM pattern dispersal have noted the presence of nepheloid layers in the continental margins worldwide (Gardner et al., 2018), including a great variety of different oceanographic settings (Fig. 9.1). However, only a few of them have attempted to relate the presence of such features with trawling activities. Therefore, more interdisciplinary studies should be conducted to assess the potential role and contribution of this anthropogenic activity, besides natural processes, to the contemporary sediment dynamics on trawled continental slope areas.

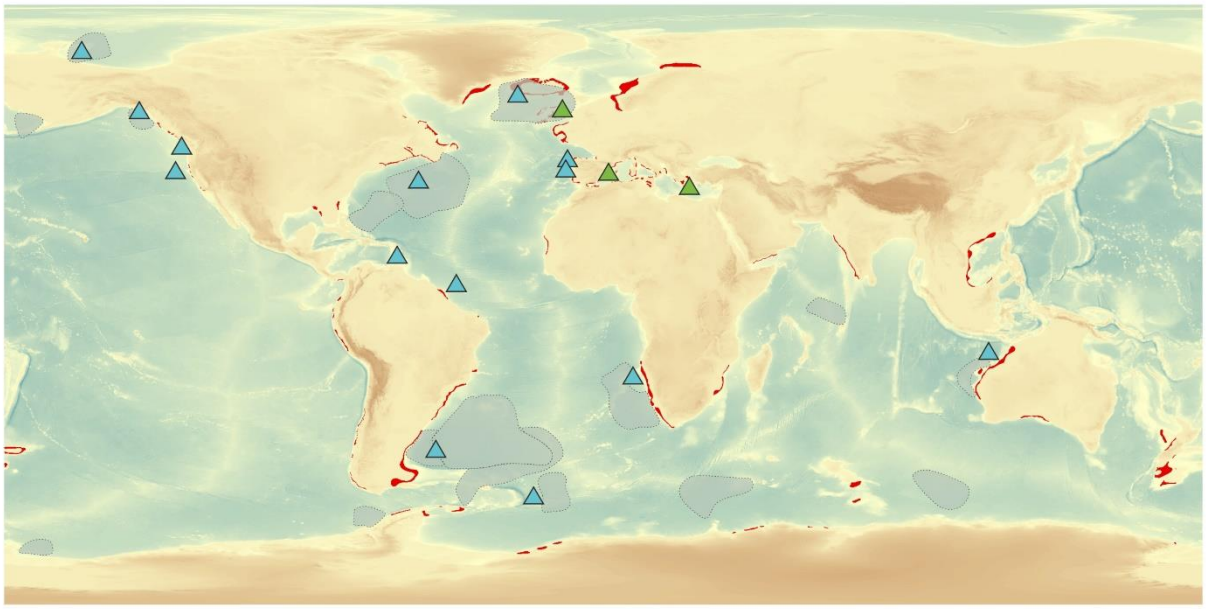

Figure 9.1. Location of the main places where the presence of nepheloid layers has been reported. Green triangles correspond to sites where the presence of nepheloid layers has been related to trawling activities, whereas blue triangles correspond to places where the presence of nepheloid layers has been linked to natural processes. Grey-coloured shaded areas represent sites where particulate matter concentration (in $\mu g \cdot L^{-1}$), averaged in the bottom 10 m of each hydrographic profile, exceeds 200 $\mu g \cdot L^{-1}$ (data obtained from Gardner et al., 2018). The overlying density raster (red) represents the global distribution of trawling grounds in continental slopes. Bottom trawling grounds were obtained from Global Fishing Watch database (Global Fishing Watch, 2020) and extracted in continental slopes according to Global Seafloor Geomorphic Features Map (Harris et al., 2014).

References

References

Agrawal, Y., 2004. Bottom nepheloid layer. Oceanography 17, 79.

Aguzzi, J., Sardà, F., 2008. A history of recent advancements on *Nephrops norvegicus* behavioral and physiological rhythms. Rev. Fish Biol. Fisher. 18(2), 235-248.

Alegret, J.L., Garrido, A., 2008. Historia del puerto pesquero de Palamós: migraciones, asociacionismo y desarrollo. Revista Internacional de Ciencias Sociales, 27, 27-40.

Alldredge, A. L., Silver, M. W., 1988. Characteristics, dynamics, and significance of marine snow. Progr. Oceanogr. 20, 41-82.

Allen, S. E., Durrieu de Madron, X., 2009. A review of the role of submarine canyons in deep-ocean exchange with the shelf. Ocean Sci. 5, 607-620.

Alonso, B., Díaz, J., Farran, M., Giró, S., Maldonado, A., Vázquez, A., 1984. Cañones submarinos del margen Catalán meridional: morfología y evolución. In Congreso Español de Geología vol. 1. Ilustre Colegio Oficial de Geólogos. Segovia, pp. 301-311.

Amblas, D., Canals, M., Urgeles, R., Lastras, G., Liquete, C., Hughes-Clarke, J. E., Casamor, J. L., Calafat, A. M., 2006. Morphogenetic mesoscale analysis of the northeastern Iberian margin, NW Mediterranean Basin. Mar. Geol. 234(1-4), 3-20.

Amin, M., Huthnance, J. M., 1999. The pattern of cross-slope depositional fluxes. Deep Sea Res. I Oceanogr. Res. Pap. 46, 1565-1591.

Antoine, D., André, J. M., Morel, A., 1996. Oceanic primary production: 2. Estimation at global scale from satellite (coastal zone color scanner) chlorophyll. Global Biogem. Cy. 10, 57-69.

Ardron, J. A., Jamieson, G. S., Hangaard, D., 2007.Spatial identification of closures to reduce the by-catch of corals and sponges in the groundfish trawl fishery, British Columbia. B. Mar. Sci. 81, 157-167.

Asper, V. L., Dueser, W. G., Knauer, G. A., Lohrenz, S. E., 1992. Rapid coupling of sinking particle fluxes between surface and deep ocean waters. Nature 357, 670-672.

Baker, E. T., Hickey, B. M., 1986. Contemporary sedimentation processes in and around an active west coast submarine canyon. Mar. Geol. 71, 15-34.

Barber, F. G., 1957. Observations of currents north of Triangle Island, British Columbia. Research Board of Canada, Progress Reports of the Pacific Coast Stations 108, 15-18.

Barnes, C. R., Best, M. M., Pautet, L., Pirenne, B., 2011. Understanding Earth-Ocean Processes using Real-time Data from NEPTUNE, Canada's Widely Distributed Sensor Networks, Northeast Pacific. Geosci. Can. 38(1).

Barrie, J. W., Conway, K. W., Picard, K., Greene, H. G., 2009. Large-scale sedimentary bedforms and sediment dynamics on a glaciated tectonic continental shelf: examples from the Pacific margin of Canada. Cont. Shelf Res. 29, 796-806.

Baschek, B., Schroeder, F., Brix, H., Riethmüller, R., Badewien, T. H., Breitbach, G., Brügge, B., Colijn, F., Doerffer, R., Eschenbach, C., Friedrich, J., Fischer, P., Garthe, S., Horstmann, J., Krasemann, H., Metfies, K., Merckelbach, L., Ohle, L., Petersen, W., Pröfrock, D., Röttgers, R., Schlüter, M., Schulz, J., Schulz-Stellenfleth, J., Stanev, E., Staneva, J., Winter, C., Wirtz, K., Wollschläger, J., Zielinski, O., Ziemer, F., 2017. The coastal observing system for northern and Arctic seas (COSYNA). Ocean Sci. 13, 379–410.

Battisti, D., Hickey, B. M., 1984. Application of remote wind-forced coastal trapped wave theory to the Oregon and Washington coasts. J. Phys. Oceanogr. 14, 887-903.

Bell, M. C., Redant, F., Tuck, I., 2006. Nephrops species. In: Phillips BF (ed) Lobsters: biology, management, aquaculture and fisheries. Blackwell Publishing, Oxford, pp. 412-461.

Benn, A. R., Weaver, P. P., Billet, D. S., Van Den Hove, S., Murdock, A. P., Doneghan, G. B., Le Bas, T., 2010. Human activities on the deep seafloor in the North East Atlantic: an assessment of spatial extent. PloS one 5, e12730.

Beranzoli, L. P., Favali, I., Smriglio, G., 2002. Science-technology synergy for research in marine environment: challenges for the XXI century. Developments in Marine Technology Series (Elsevier, Amsterdam), 12, pp. 268.

Bergman, M. J. N., van Santbrink, J. W., 2000. Mortality in megafaunal benthic populations caused by trawl fisheries on the Dutch continental shelf in the North Sea in 1994. ICES J. Mar. Sci, 57, 1321-1331.

Bertoni, C., Cartwright, J., 2005. 3D seismic analysis of slope-confined canyons from the Plio–Pleistocene of the Ebro Continental Margin (Western Mediterranean). Basin Res. 17, 43-62.

Best, J., Simmons, S., Parsons, D., Oberg, K., Czuba, J., Malzone, C., 2010. A new methodology for the quantitative visualization of coherent flow structures in alluvial channels using multibeam echo-sounding (MBES). Geophys. Res. Lett. 37, L06405.

Best, M., Bornhold, B. D., Juniper, S. K., Barnes, C. R., 2007. NEPTUNE Canada regional cabled observatory: science plan. Sea Technol. 49, 10–14.

Best, M. M. R., Favali, P., Beranzoli, L., Blandin, J., Çağatay, N. M., Cannat, M., Dañobeitia, J. J., Delory, R., de Miranda, J. M. A., Del-Rio Fernandez, J., de Stitger, H., Gillooly, M., Grant, F., Hall, P. O. J., Hartman, S., Hernandez-Brito, J., Lanteri, N., Mienert, J., Oaie, G., Piera, J., Radulescu, V., Rolin, J. F., Ruhl, H. A., Wadmann, C., 2016. The EMSO-ERIC pan-european consortium: data benefits and lessons learned as the legal entity forms. Mar. Technol. Soc. J. 50, 8-15.

Béthoux, J. P., Durrieu de Madron, X., Nyffeler, F., Tailliez, D., 2002. Deep water in the western Mediterranean: peculiar 1999 and 2000 characteristics, shelf formation hypothesis, variability since 1970 and geochemical inferences. J. Mar. Sys. 33, 117-131.

Billett, D. S. M., Lampitt, R. S., Rice, A. L., Mantoura, R. F. C., 1983. Seasonal sedimentation of phytoplankton to the deep sea benthos. Nature 302, 520-522.

Bin Omar, A. F., Bin MatJafri, M. Z., 2009. Turbidimeter design and analysis: a review on optical fiber sensors for the measurement of water turbidity. Sensors, 9, 8311-8335.

Biscaye, P. E., Eittreim, S. L., 1974. Variations in benthic boundary layer phenomena: nepheloid layer in the North American Basin. In Suspended solids in water (pp. 227-260). Springer, Boston, MA.

Biscaye, P. E., Eittreim, S. L., 1977. Suspended particulate loads and transports in the nepheloid layer of the abyssal Atlantic Ocean. Mar. Geol. 23, 155-172.

Biscaye, P. E., Flagg, C. N., Falkowsky, P. G., 1994. The Shelf Edge Exchange Processes experiment: SEEP-II: an introduction to hypotheses, results and conclusions. Deep Sea Res. II Top. Stud. Oceanogr. 41, 231-252.

Bjørkan, M., Company, J.B., Gorelli, G., Sardà, F., Massaguer, C., 2020. When Fishemen Take Charge: The Development of a Management Plan for the Red Shrimp Fishery in Mediterranean Sea (NE Spain). Springer, Cham, pp. 159–178.

Blair, N. E., Aller, R. C., 2012. The fate of terrestrial organic carbon in the marine environment. Annu. Rev. Mar. Sci. 4, 401-423.

Bloesch, J., 1994. A review of methods used to measure sediment resuspension. Hydrobiologia, 284, 13-18.

Blondel, P., 2009. Continental margins. In The Handbook of Sidescan Sonar (pp. 147-183). Springer, Berlin, Heidelberg.

BOE, 2013. Orden AAA/923/2013, de 16 de mayo, por la que se regula la pesca de la gamba rosada (Aristeus antennatus) con arte de arrastre de fondo en determinadas zonas marítimas próximas a Palamós.

BOE, 2017. Resolución de 26 de enero de 2017, de la Secretaría General de Pesca, por la que se fija, para 2017, el periodo de veda establecido en la Orden AAA/923/2013, de 16 de mayo, por la que se regula la pesca de gamba rosada (Aristeus antennatus) con arte de arrastre de fondo en determinadas zonas marítimas próximas a Palamós.

Bograd, S. J., Lynn, R. J., 2003. Long-term variability in the southern California Current System. Deep Sea Res. II Top. Stud. Oceanogr. 50, 2355-2370.

Bornhold, B. D., Yorath, C. J., 1984. Surficial geology on the continental shelf, northwestern Vancouver Island. Mar. Geol. 57, 89-112.

Bornhold, B. D., Barrie, J. V., 1991. Surficial sediments on the western Canadian continental shelf. Cont. Shelf Res. 11, 685-699.

Boyd, P. W., Harrison, P. J., Johnson, B. D., 1999. The Joint Global Ocean Flux Study (Canada) in the NW subarctic Pacific. Deep Sea Res. II Top. Stud. Oceanogr. 46, 2345-2350.

Bradshaw, C., Tjensvoll, I., Sköld, M., Allan, I. J., Molvaer, J., Magnusson, J., Naes, K., Nilsson, H. C., 2012. Bottom trawling resuspends sediment and releases bioavailable contaminants in a polluted fjord. Environ. Pollut. 170, 232-241.

Britannica Concise, 2008. Encylopaedia Britannica. Encylopaedia Britannica 2008 Ultimate Reference Suite. Chicago: Encyclopaedia Britannica.

Broecker, W. S., Takashi, T., 1985. Sources and flow patterns of deep-ocean waters as deduced from potential temperature, salinity and initial phosphate concentration. J. Geophys. Res. 90, 6925-6939.

Buhl-Mortensen, P., Buhl-Mortensen, L., 2018. Impacts of Bottom Trawling and Litter on the Seabed in Norwegian Waters. Front. Mar. Sci. 5, 42.

Cacchione, D. A., Drake, D. E., 1986. Nepheloid layers and internal waves over continental shelves and slopes. Geo-Mar. Lett. 6 (3), 147–152

Cacchione, D. A., Wiberg, P. L., Lynch, J., Irish, J., Traykovski, P., 1999. Estimates of suspended-sediment flux and bedform activity on the inner portion of the Eel continental shelf. Mar. Geol. 154, 83-97.

Cacchione, D. A., Pratson, L. F., Ogston, A. S., 2002. The shaping of continental slopes by internal tides. Science 296, 724-727.

Canals, M., Puig, P., Durrieu de Madron, X., Heussner, S., Palanques, A., Fabres, J., 2006. Flushing submarine canyons. Nature, 444, 354-357.

Canals, M., Danovaro, R., Heussner, S., Vasilis, L., Puig, P., Trincardi, F., Calafat, A. M., Durrieu de Madron, X., Palanques, A., Sánchez-Vidal, A., 2009. Cascades in Mediterranean submarine grand canyons. Oceanography 22, 26-43.

Canals, M., Company, J. B., Martín, D., Sanchez-Vidal, A., Ramirez-Llodra, E., 2013. Integrated study of Mediterranean deep canyons: novel results and future challenges. Prog. Oceanogr. 118, 1-27.

Cannolly, T. P., Hickey, B. M., 2014. Regional impact of submarine canyons during seasonal upwelling. J. Geophys. Res. Oceans 119, 953-975.

Carlson, D. F., Ostrovskii, A. G., Kebkal, K., Gildor, H., Gal, O., 2013. Moored automatic mobile profilers and their applications. Adv. Mar. Rob. LAP LAMBERT Academic Publishing, 169-206.

Carson, B., Baker, E. T., Hickey, B. M., Nittrouer, C. A., DeMaster, D. J., Thorbjarnarson, K. W., Snyder, G. W., 1986. Modern sediment dispersal and accumulation in Quinault submarine canyon – a summary. Mar. Geol. 71(1-2), 1-13.

Casamor, J. L., 2007. Distribución 3-D de la materia particulada en suspensión en el Mar Catalano-Balear (Mediterráneo Noroccidental).

Castellón, A., Font, J., García-Ladona, E., 1990. The Liguro-Provençal-Catalan current (NW Mediterranean) observed by Doppler profiling in the Balearic Sea. Sci. Mar. 54, 269-276.

Chase, Z., van Geen, A., Kosro, P. M., Marra, J., Wheeler, P. A., 2002. Iron nutrient and phytoplankton distributions in Oregon coastal waters. J. Geophys. Res. 107(C10), 3174.

Checa, A., Díaz, J. I., FARRAN, M., Maldonado, A., 1988. Sistemas deltaicos holocenos de los ríos Llobregat, Besós y Foix: modelos evolutivos transgresivos. Acta geológica hispánica, 23, 241-255.

Checkley, D. M., Barth, J. A., 2009. Patterns and processes in the California Current System. Prog. Oceanogr. 83, 49-64.

Chelton, D. B., Bernal, P. A., McGowan, J. A., 1982. Large-scale interannual physical and biological interaction in the California Current. J. Mar. Res. 40, 1095-1125.

Chronis, G., Lykousis, V., Georgopoulos, D., Zervakis, V., Stavrakakis, S., Poulos, S., 2000. Suspended particulate matter and nepheloid layers over the southern margin of the Cretan Sea (NE Mediterranean): seasonal distribution and dynamics. Prog. Oceanogr. 46 (2–4), 163–185.

Churchill, J. H., 1989. The effect of commercial trawling on sediment resuspension and transport over the Middle Atlantic Bight shelf. Cont. Shelf Res. 9, 841-865.

Churchill, J. H., Wirick, C. D., Flagg, C. N., Pietrafesa, L. J., 1994. Sediment resuspension over the continental shelf east of the Delmarcva Peninsula. Deep Sea Res. II Top. Stud. Oceanogr. 41, 341-363.

Clark, M.R., Althaus, F., Schlacher, T.A., Williams, A., Bowden, D.A., Rowden, A.A., 2016. The impacts of deep-sea fisheries on benthic communities: a review. ICES J. Mar. Sci. J. du Cons. 73, i51--i69.

Cochran, J. K., Bokuniewicz, H. I., Yager, P. L., 2019. Encyclopedia of Ocean Sciences. Academic Press.

Coll, M., Carreras, M., Ciércoles, C., Cornax, M. J., Gorelli, G., Morote, E., Saez, R., 2014. Assessing fishing and marine biodiversity changes using fishers' perceptions: the Spanish Mediterranean and Gulf of Cadiz case study. PloS One 9, e85670.

Colloca, F., Scarcella, G., Libralato, S., 2017. Recent trends and Impacts of Fisheries Exploitation on Mediterranean Stocks and Ecosystems. Front. Mar. Sci. 4, 244.

Company, J.B., Puig, P., Sardà, F., Palanques, A., Latasa, M., Scharek, R., 2008. Climate influence on deep sea populations. PLoS One 3, e1431.

Company, J.B., Ramirez-Llodra, E., Sardà, F., Aguzzi, J., Puig, P., Canals, M., Calafat, A., Palanques, A., Solé, M., Sanchez-Vidal, A., Martín, J., Lastras, G., Tecchio, S., Koenig, S., Fernandez-Arcaya, U., Mechó, A., Fernandez, P., 2012. Submarine canyons in the Catalan Sea (NW Mediterranean): megafaunal biodiversity patterns and anthropogenic threats, in: Würtz, M. (Ed.), Mediterranean Submarine Canyons: Ecology and Governance. International Union for Conservation of Nature, Gland, Switzerland, pp. 133–144.

Conan, P., Millot, C., 1995. Variability of the northern current off Marseilles, western Mediterranean Sea, from February to June 1992. Oceanol. Acta 18, 193-205.

Coppola, L., Ntoumas, M., Bozzano, R., Bensi, M., Hartman, S. E., Charcos-Llorens, M. I., Craig, J., Rolin, J. F., Giovanetti, G., Cano, D., Karstensen, J., Cianca, A., Toma, D., Stasch, C., Pensieri, S., Cardin, V., Tengberg, A., Petihakis, G., Cristini, L., 2016. Handbook of Best Practices for Opean Ocean Fixed Observatories. European Commission, FixO3 Project, 127. (European Commission FixO3 project, FP7 Programme 2007-2013 under grant agreement No. 312463). Available online at: http://hdl.handle.net/11329/302.

Cosma, T., Hendy, I. L., 2008. Pleistocene glacimarine sedimentation on the continental slope off Vancouver Island, British Columbia. Mar. Geol. 255, 45-54.

Crawford, W. R., Dewey, R. K., 1989. Turbulence and mixing: Sources of nutrients on the Vancouver Island continental shelf. Atmos.-Ocean 27, 428-442.

Crawford, W. R., Thomson, R. E., 1982. Continental shelf waves of diurnal period along Vancouver Island. J. Geophys. Res. Oceans 87, 9516-9522.

Crawford, W. R., Thomson, R. E., 1991. Physical oceanography of the western Canadian continental shelf. Cont. Shelf Res. 11, 669-683.

Crawford, W. R., Rapatz, W. J., Huggett, W. S., 1981. Pressure and temperature measurements on seamounts in the North Pacific. Mar. Geol. 5, 43-54.

Cullen, E., Chumbinho, R., Breslin, J., 2015. SmartBay Ireland's marine real time data acquisition system. In Proceedings of the 2014 Oceans, St. John's (pp. 1-4). IEEE.

Curtis, J. A., 2007. Summary of Optical-backscatter and Suspended-Sediment Data, Tomales Bay Watershed, California, Water Years 2004, 2005, and 2006. US Department of the Interior, US Geological Survey.

Daly, E., Johnson, M.P., Wilson, A.M., Gerritsen, H.D., Kiriakoulakis, K., Allcock, A.L., White, M., 2018. Bottom trawling at Whittard Canyon: Evidence for seabed modification, trawl plumes and food source heterogeneity. Prog. Oceanogr. 169, 227-240.

Dayton, P. K., Thrush, S. F., Agardy, M. T., Hofman, R. J., 1995. Environmental effects of marine fishing. Aquat. Conserv. Mar. Freshw. Ecosyst. 5, 205-232.

De Leo, F.C., Vetter, E.W., Smith, C.R., Rowden, A.A., McGranaghan, M., 2014. Spatial scale-dependent habitat heterogeneity influences submarine canyon macrofaunal abundance and diversity off the Main and Northwest Hawaiian Islands. Deep Sea Res. Part II Top. Stud. Oceanogr. 104, 267–290.

De Leo, F. C., Gauthier, M., Nephin, J., Mihaly, S., Juniper, S. K., 2017. Bottom trawling and oxygen minimum zone influences on continental slope benthic community structure off Vancouver Island (NE Pacific). Deep Sea Res. II. Top. Stud. Oceanogr. 137, 404-419.

De Leo, F. C., Ogata, B., Sastri, A. R., Heesemann, M., Mihaly, S., Galbraith, M., Morley, M. G., 2018. High-frequency observations from a Deep-sea cabled observatory reveal seasonal overwintering of Neocalanus spp. in Barkley Canyon, NE Pacific: insights into particulate organic carbon flux. Progr. Oceanogr. 169, 120-137.

Dellapenna, T.M., Allison, M.A., Gill, G.A., Lehman, R.D., Warnken, K.W., 2006. The impact of shrimp trawling and associated sediment resuspension in mud dominated, shallow estuaries. Estuar. Coast. Shelf Sci. 69, 519–530.

De Sigter, H. C., Boer, W., de Jesus Mendes, P. A., Jesus, C. C., Thomsen, L., van den Bergh, G. D., van Weering, T. C., 2007. Recent sediment transport and deposition in the Nazaré Canyon, Portuguese continental margin. Mar. Geol. 246, 144-164.

De Stigter, H. C., Jesus, C. C., Boer, W., Richter, T. O., Costa, A., van Weering, T. C., 2011. Recent sediment transport and deposition in the Lisbon–Setúbal and Cascais submarine canyons, Portuguese continental margin. Deep Sea Res. II. Top Stud. Oceanogr. 58(23-24), 2321-2344.

Del-Río, J., Nogueras, M., Toma, D. M., Martinez, E., Artero-Delgado, C., Bghiel, I., Martinez, M., Cadena, J., Garcia-Benadi, A., Sarria, D., Aguzzi, J., Masmitja, I., Carandell, M., Olive, J.,

Gomariz, S., Santamaria, P., Làzaro, A. M., 2020. Obsea: a decadal balance for a cabled observatory deployment. IEEE Access 8, 33163-33177.

Dempster, A. P., Laird, N. M., Rubin, D. B., 1977. Maximum likelihood from Incomplete Data via the EM Algorithm. J. R. Stat. Soc. Ser. B 39, 1-38.

Deuser, W. G., Ross, E. H., 1980. Seasonal change in the flux of organic carbon to the deep Sargasso Sea. Nature 283, 364-365.

Dewey, R., Round, A., Macound, P., Vervynck, J., Tunnicliffe, V., 2007. The VENUS cabled observatory: engineering meets science on the seafloor. In Proceedings of the Oceans 2007, Vancouver, BC, 1-7.

DFO (Department of Fisheries and Oceans Canada), 2019. Commercial Fisheries Licensing Rules and Policies Reference Document Pacific Region. (http://www.pac.dfo-mpo.gc.ca/).

Díaz, J. I., Ercilla, G., 1993. Holocene depositional history of the Fluviá—Muga prodelta, northwestern Mediterranean Sea. Mar. Geol. 111, 83-92.

Dickson, R. R., McCave, I.N., 1986. Nepheloid layers on the continental slope west of Porcupine Bank. Deep-Sea Res. I Oceanogr. Res. Pap. 33 (6), 791–818.

Diercks, A., Ziervogel, K., Sibert, R., Joye, S. B., Asper, V., Montoya, J. P., Thomsen, L., 2019. Vertical marine snow distribution in the stratified, hypersaline, and anoxin Orca Basin (Gulf of Mexico). Elementa: Science of the Anthropocene, 7.

D'Ortenzio, F., Ribera d'Alcalà, M., 2009. On the trophic regimes of the Mediterranean Sea: a satellite analysis. Biogeosciences, 6, 139-148.

Drakopoulos, P. G., Marsden, R. F., 1993. The internal tide off the west coast of Vancouver Island. J. Phys. Oceanogr. 23, 758-775.

Dounas, C., Davies, I., Triantafyllou, G., Koulouri, P., Petihakis, G., Arvanitidis, C., Sourlatzis, G., Elefheriou, A., 2007. Large-scale impacts of bottom trawling on shelf primary productivity. Cont. Shelf Res. 27, 2198-2210.

Doya, C., Aguzzi, J., Pardo, M., Matabos, M., Company, J. B., Costa, C., Mihaly, S., Canals, M., 2014. Diel behavioral rythms in sablefish (Anoplopma fimbria) and other benthic species, as recorded by the Deep-sea cabled observatories in Barkley Canyon (NEPTUNE-Canada). J. Mar. Sys. 130, 69-78.

Downing, J. P., 2006. Twenty-five years with OBS sensors: The good, the bad, and the ugly. Cont. Shelf Res. 26, 2299-2318.

Downing, J. P., Sternberg, R. W., Lister, C. R. B., 1981. New instrumentation for the investigation of sediment suspension processes in the shallow marine environment. Mar. Geol. 42, 19-34.

Druffel, E. R. M., Robinson, B. H., 1999. Is the Deep Sea on a Diet? Science 284, 1139-1140.

Dufau-Julliand, C., Marsaleix, P., Petrenko, A., Dekeyser, I., 2004. Three-dimensional modeling of the Gulf of Lion's hydrodynamics (northwest Mediterranean) during January 1999 (MOOGLI3 Experiment) and late winter 1999: Western Mediterranean Intermediate Water's (WIW's) formation and its cascading over the shelf break. J. Geophys. Res. Oceans, 109(C11).

Durán, R., Canals, M., Sanz, J. L., Lastras, G., Amblas, D., Micallef, A., 2014. Morphology and sediment dynamics of the northern Catalan continental shelf, northwestern Mediterranean Sea. Geomorphology, 204, 1-20.

Durrieu de Madron, X., 2019. Error propagation. Time Series Analysis Conference. Tromsoe (Norway), January 2019.

Durrieu de Madron, X., Castaing, P., Nyffeler, F., Courp, T., 1999. Slope transport of suspended particulate matter on the Aquitanian margin of the Bay of Biscay. Deep Sea Res. II Top. Stud. Oceanogr. 46, 2003-2027.

Durrieu de Madron, X., Zervakis, V., Theocharis, A., Georgopoulos, D., 2005a. Comments on "Cascades of dense water around the world ocean". Prog. Oceanogr. 64, 83-90.

Durrieu de Madron, X, Ferré, B., Le Corre, G., Grenz, C., Conan, P., Pujo-Pay, M., Buscail, R., Bodiot, O., 2005b. Trawling-induced resuspension and dispersal of muddy sediments and dissolved elements in the Gulf of Lion (NW Mediterranean). Cont. Shelf Res. 25, 2387–2409.

Durrieu de Madron, X., Wiberg, P. L., Puig, P., 2008. Sediment dynamics in the Gulf of Lions: The impact of extreme events. Cont. Shelf Res. 28, 1867-1876.

Durrieu de Madron, X., Houpert, L., Puig, P., Sanchez-Vidal, A., Testor, P., Bosse, A., Estournel, C., Somot, S., Bourrin, F., Bouin, M. N., Beauverger, M., Beguery, L., Calafat, A., Canals, M., Cassou, C., Coppola, L., Dausse, D., D'Ortenzio, F., Font, J., Heussner, S., Kunesch, Lefevre, D., Le Goff, H., Martín, J., Mortier, L., Palanques, A., Raimbault, P., 2013. Interaction of dense shelf water cascading and open-sea convection in the northwestern Mediterranean during winter 2012. Geophys. Res. Lett. 40, 1379-1385.

Durrieu De Madron, X., Ramondenc, S., Berline, L., Houpert, L., Bosse, A., Martini, S., Guidi, L., Conan, P., Curtil, C., Delsaut, N., Kunesch, S., Ghiglione, J. F., Marsaleix, P., Pujo-Pay, M., Séverin, T., Testor, P., Tamburini, C., the ANTARES collaboration, 2017. Deep sediment

resuspension and thick nepheloid layer generation by open-ocean convection. J. Geophys. Res. Oceans 122, 2291-2318.

Earys, S., Pol, M., 2014. GEARNET: Northeast groundfish gear conservation engineering and demonstration network. Final Report, National Marine Fisheries Service, Northeast Cooperative Research Program (NRCP).

Eigaard, O.R., Bastardie, F., Breen, M., Dinesen, G.E., Hintzen, N.T., Laffargue, P., Mortensen, L.O., Nielsen, J.R., Nilsson, H.C., O'Neill, F.G., Polet, H., Reid, D.G., Sala, A., Sköld, M., Smith, C., Sørensen, T.K., Tully, O., Zengin, M., Rijnsdorp, A.D., 2016. Estimating seabed pressure from demersal trawls, seines, and dredges based on gear design and dimensions. ICES J. Mar. Sci. 73, i27-i43.

Eittreim, S., Thorndike, E. M., Sullivan, L., 1976. Turbidity distribution in the Atlantic Ocean. Deep Sea Res. Oceanogr. Abstracts 12, 1115-1127.

Emeis, K. C., Mara, P., Schlarbaum, T., Möbius, J., Dähnke, K., Struck, U., Mihalopoulos, N., Krom, M., 2010. External N inputs and internal N cycling traced by isotope ratios of nitrate, dissolved reduced nitrogen, and particulate nitrogen in the eastern Mediterranean Sea. J. Geophys. Res: Biogeosciences, 115.

Emery, W. J., Meincke, J., 1986. Global water masses-summary and review. Oceanol. Acta 9, 383-391.

Esentia, I., Stow, D., Smillie, Z., 2018. Contourite drifts and associated bedforms. In Submarine geomorphology (pp. 301-331). Springer, Cham.

Estournel, C., Durrieu de Madron, X., Marsaleix, P., Auclair, F., Julliand, C., Vehil, R., 2003. Observation and modelling of the winter coastal oceanic circulation in the Gulf of Lion under wind conditions influenced by the continental orography (FETCH experiment). J. Geophys. Res. Oceans 108(C3).

Estrada, M., 1996. Primary production in the northwestern Mediterranean. Sci. Mar. 60, 55-64.

Etcheber, H., Heussner, S., Weber, O., Dinet, A., Durrieu de Madron, X., Monaco, A., Buscail, R., Miquel, J. C., 1996. Organic carbon fluxes and sediment biogeochemistry on the French Mediterranean and Atlantic margins. In: Ittekkot, V., Schäfer, P., Honjo, S., Depetris, P. J. (Eds.), Particle Flux in the Ocean, SCOPE Report 57. John Wiley & Sons, pp. 223-241.

European Commission, 2003. Commission Regulation (EC) No. 2244/2003 of 18 December 2003 laying down detailed provisions regarding satellite-based Vessel Monitoring Systems. Off. J. Eur. Union L333, 17–27.

European Commission, 2009. Council regulation (EC) No. 1244/2009 of 20 November 2009 establishing a Community control system for ensuring compliance with the rules of the

common fishery policy, amending regulations (EC) No. 847/96, (EC) No. 2371/2002, (EC), No. 811/2004, (EC) No, Off. J. Eur. Union L343, 1-50.

European Commission Fisheries & Maritime Affairs, 2014. Fleet Register on the Net. Available at http://ec.europa.eu/fisheries/fleet/index.cfm (1st April 2016).

European Parliament, 2008. Directive 2008/56/EC of the European Parliament and the Council of 17 June 2008 establishing a framework for community action in the field of marine environmental policy (Marine Strategy Framework Directive). Off. J. Eur. Union 1–22.

Ewing, M., Thorndike, E. M., 1965. Suspended matter in deep ocean water. Science 14, 1291-1294.

FAO, 2015. Food and Agriculture Organization of the United Nations. List of major fishing areas. Coordinating Working Party on Fishery Statistics (CWP). http://www.fao.org/3/bt979e/bt979e.pdf.

FAO, 2016. Food and Agriculture Organization of the United Nations. The State of World Fisheries and Aquaculture 2016 (SOFIA). Contributing to food security and nutrition for all. Rome. http://www.fao.org/3/a-i5555e.pdf.

FAO, 2019. Food and Agriculture Organization of the United Nations. FAO Major Fishing Areas. Northeast Pacific (Major Fishing Area 67). http://www.fao.org/fishery/area/Area67/en.

Farrugio, H., 2012. A refugium for the spawners of exploited Mediterranean marine species: the canyons of the continental slope of the Gulf of Lion, in: Würtz, M. (Ed.), Mediterranean Submarine Canyons: Ecology and Governance. International Union for Conservation of Nature, Gland, Switzerland, pp. 45–50.

Favali, P., Beranzoli, 2006. Seafloor observatory science: A review. Ann. Geophys. 49, 515-567.

Favali, P., Person, R., Barnes, C. R., Kaneda, Y., Delaney, J. R., Hsu, S. K., 2010. Seafloor observatory science. P. OceanObs 9, 21-25.

Favali, P., Beranzoli, L., De Santis, A., 2015. SEAFLOOR OBSERVATORIES: A New Vision of the Earth from the Abyss. Springer Science & Business Media.

Fernandez-Arcaya, U., Ramirez-Llodra, E., Aguzzi, J., Allcock, A.L., Davies, J.S., Dissanayake, A., Harris, P., Howell, K., Huvenne, V.A.I., Macmillan-Lawler, M., Martín, J., Menot, L., Nizinski, M., Puig, P., Rowden, A.A., Sanchez, F., Van den Beld, I.M.J., 2017. Ecological Role of Submarine Canyons and Need for Canyon Conservation: A Review. Front. Mar. Sci. 4, 5.

Ferré, B., Guizien, K., Durrieu de Madron, X., Palanques, A., Guillén, J., Grémare, A., 2005. Fine-grained sediment dynamics during a strong storm event in the inner-shelf of the Gulf of Lion (NW Mediterranean). Cont. Shelf Res. 25, 2410-2427.

Ferré, B., Durrieu de Madron, X., Estournel, C., Ulses, C., Le Corre, G., 2008. Impact of natural (waves and currents) and anthropogenic (trawl) resuspension on the export of particulate matter to the open ocean: application to the Gulf of Lion (NW Mediterranean). Cont. Shelf. Res. 28(15), 2071-2091.

Fettweis, M., Riethmüller, R., Verney, R., Becker, M., Backers, J., Baeye, M., Chapalain, M., Claeys, S., Tom Cox, J. C., Deloffre, J., Depreiter, D., Druine, F., Flöser, G., Grünler, S., Jourdin, F., Lafite, R., Nauw, J., Nechad, B., Röttgers, R., Sottolichio, A., van Engeland, T., Vanhaverbeke, W., Vereecken, H., 2019. Uncertainties associated with in situ high-frequency long-term observations of suspended particulate matter concentration using optical and acoustic sensors. Prog. Oceanogr. 178, 102162.

Finney, J. L., 2009. Overlap of predicted cold-water coral habitat and bottom-contact fisheries in British Columbia (Doctoral dissertation, School of Resource and Environmental Management-Simon Fraser University).

Fischer, P., Brix, H., Baschek, B., Kraberg, A., Brand, M., Cisewski, B., Rietmüller, R., Breitbach, G., Möller, K. O., Gattuso, J. P., Alliouane, S., van de Poll, W. H., Witbaard, R., 2020. Operating cabled underwater observatories in rough shelf-sea environments: A technological challenge. Front. Mar. Sci. 7, 551.

Flexas, M. D., Boyer, D. L., Espino, M., Puigdefàbregas, J., Rubio, A., Company, J. B., 2008. Circulation over a submarine canyon in the NW Mediterranean. J. Geophys. Res. Oceans, 113(C12).

Foerster, J. W., 1993. Northeast North Pacific Ocean: Surface Current Pattern Shifts During the Spring. Remote Sens. Environ. 43, 149-159.

Fohrmann, H., Backhaus, J. O., Blaume, F., Rumohr, J., 1998. Sediments in bottom-arrested gravity plumes: Numerical case studies. J. Phys. Oceanogr. 28, 2250-2274.

Font, J., 1987. The path of the Levantine intermediate water to the Alboran Sea. Deep Sea Res. Pt. I. 34, 1745-1755.

Font, J., Miralles, L., 1978. Circulación geostrófica en el Mar Catalán.

Font, J., Salat, J., Tintoré, J., 1988. Permanent features of the circulation in the Catalan Sea. Ocenol. Acta 9, 51-57.

Font, J., Millot, C., Salas, J., Julià-Brugues, A., Chic, Ò., 1998. The drift of Modified Atlantic Water from the Alboran Sea to the eastern Mediterranean.

Font, J., Puig, P., Salat, J., Palanques, A., Emelianov, M., 2007. Sequence of hydrographic changes in the NW Mediterranean deep water due to the exceptional winter of 2005. Sci. Mar. 71, 339-346.

Forrester, N. C., Stokey, R. P., von Alt, C., Allen, B. G., Goldsborough, R. G., Purcell, M. J., Austin, T. C. 1997. The LEO-15 long-term ecosystem observatory: Design and installation. In Oceans' 97. MTS/IEEE Conference Proceedings (Vol. 2, pp. 1082-1088). IEEE.

Freeland, H. J., Crawford, W. R., Thomson, R. E., 1984. Currents along the Pacific coast of Canada. Atmos. Ocean 22, 151-172.

Friedlander, A. M., Boehlert, G. W., Field, M. E., Mason, J. E., Gardner, J. V., Dartnell, P., 1999. Sidescan-sonar mapping of benthic trawl marks on the shelf and slope off Eureka, California. Fish. Bull. 97, 786-801.

Gage, J. D., Roberts, J. M., Hartley, J. P., Humphrey, J. D., 2005. Potential impacts of deep-sea trawling on the benthic ecosystem along the Northern European Continental Margin: a review.

García, M. L., Millot, C., Font, J., García-Ladona, E., 1994. Surface-circulation variability in the Balearic Basin. J. Geophys. Res. Oceans, 99, 3285-3296.

Gardner, W. D., 1989. Baltimore Canyon as a modern conduit of sediment to the deep ocean. Deep Sea Res. I Oceanogr. Res. Pap. 36, 323-358.

Gardner, W. D., Walsh, I. D., 1990. Distribution of macroaggregates and fine-grained particles across a continental margin and their potential role in fluxes. Deep Sea Res. I Oceanogr. Res. Pap. 37, 401-411.

Gardner, W. D., Richardson, M. J., Walsh, I. D., Berglund, B. L., 1990. In-situ optical sensing of particles for determination of oceanic processes: what satellites can’t see, but transmissometers can. Oceanography 3, 11-17.

Gardner, W. D., Walsh, I. D., Richardson, M. J., 1993. Biophysical forcing of particle production and distribution during a spring bloom in the North Atlantic. Deep Sea Res. II Top. Stud. Ocenogr. 40, 171-195.

Gardner, W. D., Richardson, M. J., Carlson, C. A., Hansell, D., Mishonov, A. V., 2003. Determining true particulate organic carbon: bottles, pumps and methodologies. Deep Sea Res. II Top Stud. Oceanogr. 50, 655-674.

Gardner, W. D., Richardson, M. J., Mishonov, A. V., Biscaye, P. E., 2018. Global comparison of benthic nepheloid layers based on 52 years of nephelometer and transmissometer measurements. *Prog. Oceanogr. 168*, 100-111.

Gargett, A. E., Stucchi, D., Whitney, F., 2003. Physical processes associated with high primary production in Saanich Inlet, British Columbia. Est. Coast. Shelf Sci. 56, 1141-1156.

Gerritsen, H D., Minto, C., Lordan, C., 2013. How much of the seabed is impacted by mobile fishing gear? Absolute estimates from Vessel Monitoring System (VMS) point data. ICES J. Mar. Sci. 70, 523–531.

Gianni, M., 2004. High Seas Bottom Trawl Fisheries and their Impacts on the Biodiversity of Vulnerable Deep-Sea Ecosystems: Options for International Action. IUCN, Gland, Switzerland.

Gibbs, R. J., 1974. Principles of studying suspended materials in water. In Suspended Solids in Water (Eds). Gibss, R. J., Springer, New York, USA (1974). Pp. 3-15.

Gibbs, R. J., Wolanski, E., 1992. The effect of flocs on optical backscattering measurements of suspended material concentration. Mar. Geol. 107, 289-291.

Giering, S. L. C., Sanders, R., Lampitt, R. S., Anderson, T. R., Tamburini, C., Boutrif, M., Zubkov, M. V., Marsay, C. M., Henson, S. A., Saw, K., Cook, K., Mayor, D. J., 2014. Reconciliation of the carbon budget in the ocean's twilight zone. Nature 507, 480-483.

Giering, S. L. C., Humphreys, M. P., 2018. Biological pump. Encyclopedia of Geochemistry, Encyclopedia of Earth Sciences Series, 1-6.

Gislason, H., Bastardie, F., Dinesen, G.E., Egekvist, J., Ritzau-Eigaard, O., 2017. Lost in translation? Multi-metric macrobenthos indicators and bottom trawling. Ecol. Indic. 82, 260‑270.

Glover, A. G., Smith, C. R., 2003. The deep-sea floor ecosystem: current status and prospects of anthropogenic change by the year 2025. Environ. Conserv. 30, 219-241.

Godø, O. R., Johnsen, S., and Torkelsen, T. 2014. The LoVe ocean observatory is in operation. Mar. Technol. Soc. J. 48, 24–30.

Gorelli, G., Company, J.B., Sardà, F., 2014. Management strategies for the fishery of the red shrimp Aristeus antennatus in Catalonia (NE Spain). Mar. Steward. Counc. Sci. Ser. 2, 116–127.

Gorelli, G., Sardà, F., Company, J.B., 2016. Fishing Effort Increase and Resource Status of the Deep-Sea Red Shrimp Aristeus antennatus (Risso 1816) in the Northwest Mediterranean Sea Since the 1950s.

Granata, T. C., Vidondo, B., Duarte, C. M., Satta, M. P., García, M., 1999. Hydrodynamics and particle transport associated with a submarine canyon off Blanes (Spain), NW Mediterranean Sea. Cont. Shelf Res. 19, 1249-1263.

Gruber, P., Felix, D., Storti, G., Lattuada, M., Fleckenstein, P., Deschwanden, F., 2016. Acoustic measuring techniques for suspended sediment. In IOP Conference Series: Earth and Environmental Science (Vol. 49, No. 12, p. 122003). IOP Publishing.

Guidi, L., Legendre, L., Reygondeau, G., Uitz, J., Stemmann, L., Henson, S. A., 2015. A new look at ocean carbon remineralization for estimating deepwater sequestration. Global Biogeochem. Cycles 29, 1044-1059.

Guillén, J., Palanques, A., Puig, P., De Madron, X. D., Nyffeler, F., 2000. Field calibration of optical sensors for measuring suspended sediment concentration in the western Mediterranean. Sci. Mar. 64, 427-435.

Guillén, J., Bourrin, F., Palanques, A., Durrieu de Madron, X., Puig, P., Buscail, R., 2006. Sediment dynamics during the wet and dry storm events on the Têt inner shelf (SW Gulf of Lions). Mar. Geol. 234, 129-142.

Haalboom, S., de Sigter, H., Duineveld, G., van Haren, H., Reichart, G. J., Mienis, F., 2021. Suspended particulate matter in a submarine canyon (Whittard Canyon, Bay of Biscay, NE Atlantic Ocean): Assessment of commonly used instruments to record turbidity. Mar. Geol. 434, 106439.

Haigh, R., Schnute, J. T., 2003. The longspine thornyhead fishery along the west coast of Vancouver Island, British Columbia, Canada: portrait of a developing fishery. N. Am. J. Fish. Manage. 23(1), 120-140.

Hall, R. A., Aslam, T., Huvenne, V. A., 2017. Partly standing internal tides in a dendritic submarine canyon observed by an ocean glider. Deep Sea Res. I Oceanogr. Res. Pap. 126, 73-84.

Harris, P. T., Whiteway, T., 2011. Global distribution of large submarine canyons: Geomorphic differences between active and passive continental margins. Mar. Geol. 285, 69-86.

Harris, P. T., Macmillan-Lawler, M., Rupp, J., Baker, E. K., 2014a. Geomorphology of the oceans. Mar. Geol. 352, 4-24.

Harris, P. T., Barrie, J. V., Conway, K. W., Greene, H. G., 2014b. Hanging canyons of Haida Gwaii, British Columbia, Canada: Fault-control on submarine canyon geomorphology along active continental margins. Deep-Sea Res. II Top. Stud. Oceanogr. 104, 83-92.

Hartley, H. O., 1958. Maximum likelihood estimation from incomplete data. Biometrics 14, 174-194.

He, P., Winger, P., Fonteyne, R., Pol, M., MacMullen, P., Løkkeberg, S., van Marlen, B., Moth-Poulsen, T., Zachariassen, K., Sala, A., Thiele, W., Hansen, U., Grimaldo, E., Revill, A., Polet, A., 2004. Mitigation measures against seabed impact of mobile fishing gears. Report of the ICES Fisheries Technology Committee Working Group on Fishing Technology and Fish Behaviour, Gdynia, Poland. ICES CM, 160-172.

He, P. G., Winger, P. D., 2010. Effect of trawling on the seabed and mitigation measures to reduce impact. Behavior of marine fishes: Captures processes and conservation challenges, 295-314.

Henson, S. A., Sanders, R., Madsen, E., Morris, P. J., LeMoigne, F., Quartly, G. D., 2011. A reduced estimate of the strength of the ocean's biological carbon pump. Geophys. Res. Lett. 38, L04606.

Hickey, B. M., 1979. The California current system – hypotheses and facts. Prog. Oceanogr. 8(4), 191-279.

Hickey, B., Baker, E., Kachel, N., 1986. Suspended particle movement in and around Quinault submarine canyon. Mar. Geol. 71, 35-83.

Hickey, B. M., 1989. Patterns and processes of circulation over the Washington continental shelf and slope. In Elsevier Oceanography Series 47, 41-115. Elsevier.

Hickey, B. M., 1997. The response of a steep-sided, narrow canyon to time-variable wind forcing. J. Phys. Oceanogr. 27, 697-726.

Hickey, B., Baker, E., Kachel, N., 1986. Suspended particle movement in and around Quinault submarine canyon. Mar. Geol. 71, 35-83.

Hiddink, J. G., Jennings, S., Kaiser, M. J., 2006. Indicators of the ecological impact of bottom-trawl disturbance on seabed communities. Ecosystems, 9(7), 1190-1199.

Hill, P. S., Boss, E., Newgard, J. P., Law, B. A., Milligan, T. G., 2011. Observations of the sensitivity of beam attenuation to particle size in a coastal bottom boundary layer. J. Geophys. Res. Oceans, 116(C2).

Hinz, H., Prieto, V., Kaiser, M. J. 2009. Trawl disturbance on benthic communities: chronic effects and experimental predictions. Ecol. App., 19, 761-773.

Hollister, C. D., McCave, I. N., 1984. Sedimentation under deep-sea storms. Nature 309, 220-225.

Hollister, C. D., Nowell, A. R. M., 1991. HEBBLE epilogue. Mar. Geol. 99, 445-460.

Hollowed, A. B., 1992. Spatial and temporal distributions of Pacific hake, Merluccius productus, larvae and estimates of survival during early life stages. Calif. Coop. Oceanic Fish. Invest. Rep. 33, 100-123.

Honjo, S., Manganini, S. J., Krishfield, R. A., Francois, R., 2008. Particulate organic carbon fluxes to the ocean interior and factors controlling the biological pump. A synthesis of global sediment trap programs since 1983. Prog. Oceanogr. 76, 217-285.

Hopkins, T. S., 1978. Physical processes in the Mediterranean basins. Est. Transp. Proc. 269-310.

Huang, Z., Nichol, S. L., Harris, P. T., Caley, M. J. 2014. Classification of submarine canyons of the Australian continental margin. Mar. Geol. 357, 362-383.

Huthnance, J. M., 1995. Circulation, exchange and water masses at the ocean margin: the role of physical processes at the shelf edge. Prog. Oceanogr. 35, 353-431.

Ianson, D., Allen, S. E., Harris, S. L., Orians, K. J., Varela, D. E., Wong, C. S., 2003. The inorganic carbon system in the coastal upwelling region west of Vancouver Island, Canada. Deep Sea Res. Part. I. Oceanogr. Res. 50, 1023-1042.

Inthorn, M., 2005. Lateral particle transport in nepheloid layers-a key factor for organic matter distribution and quality in the Benguela high-productivity area (Doctoral dissertation, Universität Bremen).

Inthorn, M., Wagner, T., Scheeder, G., Zabel, M., 2006. Lateral transport controls distribution, quality, and burial of organic matter along continental slopes in high-productivity areas. Geology 34, 205-208.

Iriondo, A., Santiago, J., Murua, H., Granado, I., Taconet, M., Kroodsma, D., Miller, N. A., Fernandes, J. A., 2019. FAO Area 67 – AIS-based fishing activity in the Northeast Pacific. In Taconet, M., Kroodsma, D., Fernandes, J. A. (eds) Global Atlas of AIS-based fishing activity – Changes and opportunities. Rome, FAO.

ISO, 1999. ISO 7027: Water quality—Determination of turbidity. International Organization for Standardization.

Ivanov, V. V., Shapiro, G. I., Huthnance, J. M., Aleynik, D. L., Golovin, P. N., 2004. Cascades of dense water around the world ocean. Prog. Oceanogr. 60, 47-98.

Iversen, M. H., Ploug, H., 2010. Ballast minerals and the sinking carbon flux in the ocean: carbon-specific respiration rates and sinking velocity of marine snow aggregates. Biogeosciences 7, 2613-2624.

Iversen, M. H., Pakhomov, E. A., Hunt, B. P. V., van der Jagt, H., Wolf-Gladrow, D., Klaas, C., 2017. Sinkers or floaters? Contribution from salp pellets to the export flux during a large bloom event in the Southern Ocean. Deep Sea Res. II Top. Stud. Oceanogr. 138, 116-125.

Jackson, J.B., Kirby, M.X., Berger, W.H., Bjorndal, K.A., Botsford, L.W., Bourque, B.J., Bradbury, R.H., Cooke, R., Erlandson, J., Estes, J.A., Hughes, T.P., Kidwell, S., Lange, C.B., Lenihan, H.S., Pandolfi, J.M., Peterson, C.H., Steneck, R.S., Tegner, M.J., Warner, R.R., 2001. Historical overfishing and the recent collapse of coastal ecosystems. Science 293, 629–37.

Jennings, S., Dinmore, T. A., Duplisea, D. E., Warr, K. J., Lancaster, J. E., 2001. Trawling disturbance can modify benthic production processes. J. Anim. Ecol. 70, 459-475.

Jerlov, N. G., 1953. Particle distribution in the ocean. Reports of the Swedish Deep Sea Expedition 3, 73-97.

Jones, J. B., 1992. Environmental impact of trawling on the seabed: a review. New Zeal. J. Mar. Fresh., 26, 59-67.

Jordi, A., Orfila, A., Basterretxea, G., Tintoré, J., 2005. Shelf-slope exchanges by frontal variability in a steep submarine canyon. Prog. Oceanogr. 6(2-4), 120,141.

Juniper, S. K., Matabos, M., Mihaly, S., Ajayamohan, R. S., Gervais, F., Bui, A. O., 2013. A year in Barkley Canyon: A time-series observatory study of mid-slope benthos and habitat dynamics using the NEPTUNE Canada network. Deep-Sea Res. II. Top.Stud. Oceanogr. 92, 114-123.

Juza, M., Escudier, R., Vargas-Yáñez, M., Mourre, B., Heslop, E., Allen, J., Tintoré, J., 2019. Characterization of changes in Western Intermediate Water properties enabled by an innovative geometry-based detection approach. J. Mar. Sys. 191, 1-12.

Kaiser, M. J., Collie, J. S., Hall, S. J., Jennings, S., Poiner, I. R., 2002. Modification of marine habitats by trawling activities: prognosis and solutions. Fish Fish. 3, 114-136.

Karageorgis, A. P., Anagnostou, C. L., 2003. Seasonal variation in the distribution of suspended particulate matter in the northwest Aegean Sea. J. Geophys. Res. Oceans 108 (C8(.

Karageorgis, A. P., Georgopoulos, D., Kanellopoulos, T. D., Mikkelsen, O. A., Pagou, K., Kontoyiannis, H. K., Pavlidou, A., Anagnostou, C., 2012. Spatial and seasonal variability of particulate matter optical and size properties in the Eastern Mediterranean Sea. J. Mar. Sys. 105, 123-134.

Kasahara, J., Chave, A. D., 2003. Proceedings 3rd International Workshop on Scientific Use of Submarine Cables and Related Technologies, Tokyo, Japan, edited by J. KASAHARA and A.D. CHAVE, IEEE Catalogue No. 03EX660, pp. 315.

Kelleher, K., 2005. Discards in the world's marine fisheries: An update. FAO Fish. Tech. Pap. 470, 131 pp.

Kennett, J. P. 1982. Marine Geology. Prentice-Hall, Englewood Cliffs, NJ. 813 pp.

Kiko, R., Biastoch, A., Brandt, P., Cravatte, S., Hauss, H., Hummels, R., Kriest, I., Marin, F., McDonnell, A. M. P., Oschlies, A., Picheral, M., Schwarzkopf, F. U., Thurnherr, A. M., Stemmann, L., 2017. Biological and physical influences on marine snowfall at the equator. Nat. Geosci. 10, 852-858.

Kitazato, H., Shirayama, Y., Nakatsuka, T., Fujiwara, S., Shimanaga, M., Kato, Y., Okada, Y., Kanda, J., Yamaoka, A., Masuzawa, G., Suzuki, K., 2000. Seasonal phytodetritus deposition and responses of bathyal benthic foraminiferal populations in Sagami Bay, Japan: preliminary results from "Project Sagami 1996-1999". Mar. Micropalentol. 40, 135-149.

Kulka, D. W., Pitcher, D. A., 2001. Spatial and temporal patterns in trawling activity in the Canadian Atlantic and Pacific. Fisheries and Oceans Canada.

Kunze, E., Rosenfeld, L. K., Carter, G. S., Gregg, M. C., 2002 Internal waves in Monterey submarine canyon. J. Phys. Oceanogr. 32, 1890–1913.

Kwon, E. Y., DeVries, T., Galbraith, E. D., Hwang, J., Kim, G., Timmermann, A., 2021. Stable Carbon Isotopes Suggest Large Terrestrial Carbon Inputs to the Global Ocean. Global Biogeochem. Cy. 35, e2020GB006684.

Lambert, G.I., Jennings, S., Hiddink, J.G., Hintzen, N.T., Hinz, H., Kaiser, M.J., Murray, L.G., 2012. Implications of using alternative methods of vessel monitoring system (VMS) data analysis to describe fishing activities and impacts. ICES J. Mar. Sci. 69, 682–693.

Lampitt, R. S., Raine, R. C. T., Billet, D. S. M., Rice, A. L., 1995. Material supply to the European continental slope: A budget based on benthic oxygen demand and organic supply. Deep Sea Res. I Oceanogr. Res. Pap. 42, 1865-1880.

Lapouyade, A., Durrieu de Madron, X., 2001. Seasonal variability of the advective transport of particulate matter and organic carbon in the Gulf of Lion (NW Mediterranean). Oceanol. Acta 24, 295-312.

Lastras, G., Canals, M., Urgeles, R., Amblas, D., Ivanov, M., Droz, I., Dennielou, B., Fabrés, J., Schoolmeester, T., Akhmetzhanov, A., Orange, D., García-García, A., 2007. A walk down the Cap de Creus canyon, Northwestern Mediterranean Sea: Recent processes inferred from morphology and sediment bedforms. Mar. Geol. 246, 176-192.

Lastras, G., Canals, M., Amblas, D., Lavoie, C., Church, I., De Mol, B., Duran, R., Calafat, A. M., Hughes-Clarke, J. E., Smith, C. J., Heussner, S., “Euroléon” cruise shipboard party, 2011. Understanding sediment dynamics in two large submarine valleys from seafloor data: Blanes and La Fonera canyons, northwestern Mediterranean Sea. Mar. Geol. 280(1-4), 20-39.

Leduc, D., Rowden, A. A., Nodder, S. D., Berkenbusch, K., Probert, P. K., Hadfield, M. G., 2014. Unusually high food availability in Kaikoura Canyon linked to distinct deep-sea nematode community. Deep Sea Res. II Top. Stud. Oceanogr. 104, 310-318.

Levin, L. A., Sibuet, M., 2012. Understanding continental margin biodiversity: a new imperative. Annu. Rev. Mar. Sci. 4, 79-112.

Lévy, M., Memery, L., Madec, G., 1998. The onset of a bloom after deep winter convection in the northwestern Mediterranean Sea: mesoscale process study with a primitive equation model. J. Mar. Sys. 16, 7-21.

Linders, T., Nilsson, P., Wikström, A., Sköld, M., 2018. Distribution and fate of trawling-induced suspension of sediments in a marine protected area. ICES J. Mar. Sci. 75, 785-795.

Linnane, A., Ball, B., Munday, B., Marlen, B. V, Fonteyne, R., 2000. A review of potential techniques to reduce the impact of demersal trawls. Irish Fish. Investig. 7, 1–32.

Liquete, C., Canals, M., Ludwig, W., Arnau, P., 2009. Sediment discharge of the rivers of Catalonia, NE Spain, and the influence of human impacts. J. Hydrol. 366, 76-88.

Liu, J. T., Wang, Y. H., Lee, I. H., Hsu, R. T., 2010. Quantifying tidal signatures of the benthic nepheloid layer in Gaoping Submarine Canyon in Southern Taiwan. Mar. Geol. 271, 119-130.

Liu, Z., Zhao, Y., Colin, C., Stattegger, K., Wiesner, M. G., Huh, C-A., Liu, J. T., Siringan, F. P., Phon Le, K., Sathiamurthy, E., Hantoro, W. S., Liu, J., Tuo, J., Zhao, S., Zhou, S., He, Z., Wang, Y., Bunsomboonsakul, S., Li, Y., 2016. Source-to-sink transport processes of fluvial sediments in the South China Sea. Earth-Sci. Rev. 153, 238-273.

Lleonart, J., 1990. La pesqueria de Cataluna y Valencia: descripcion global y planteamiento de bases para su seguimiento. (Informe final. EEC DG XP/-CSIC, 2).

Lluch-Belda, D., Laurs, R. M., Lluch-Cota, D. B., Lluch-Cota, S. E., 2001. Long-term trends of interannual variability in the California Current System. Cal. Coop. Ocean. Fish. 14, 458-467.

Longhurst, A. R., 2009. Chapter 9: The Atlantic Ocean. Ecol. Geogr. of the Sea, 131-273.

Longhurst, A. R., Sathyendranath, S., Platt, T., Caverhill, C., 1995. An estimate of global primary production in the ocean from satellite radiometer data. J. Plankton Res. 17, 1245-1271.

Lorenzoni, L., Thunell, R. C., Benitez-Nelson, C. R., Hollander, D., Martinez, N., Tappa, E., Varela, R., Astor, Y., Muller-Karger, F. E., 2009. The importance of subsurface nepheloid layers in transport and delivery of sediments to the eastern Cariaco Basin. Deep Sea Res. I Oceanogr. Res. Pap. 56, 2249-2262.

Lorenzoni, L., Thunell, R. C., Benitez-Nelson, Montes, E., Varela, R., Astor, Y., Muller-Karger, F. E., 2019. From Land to the Ocean: The Interplay Between Allochthonous and Autochthonous Contribution to Particles in Nepheloid Layers of the Cariaco Basin, Venezuela. J. Geophys. Res. Biogeosciences 124, 3191-3207.

Lowes, F. J., 2002. Why global geomagnetism needs ocean bottom observatories, in Science-Technology Synergy for Research in the Marine Environment: Challenges for the XXI Century, edited by L. Beranzoli, P. Favali and G. Smriglio, Developments in Marine Technology Series (Elsevier, Amsterdam), 12, 27-35.

Lynn, R. J., Simpson, J. J., 1987. The California Current System: The seasonal variability of its physical characteristics. J. Geophys. Res. Oceans 92, 12947-12966.

Mackas, D. L. 1992. Seasonal cycle of zooplankton off southwestern British Columbia. Can. J. Fish. Aquat. Sci. 49, 903-921.

Mackas, D. L., Louittit, G. C., Austin, M. J., 1980. Spatial distribution of zooplankton and phytoplankton in British Columbian coastal waters. Can. J. Fish. Aquat. Sci. 37, 1476-1487.

Mackas, D.L., Kieser, R., Saunders, M., Yelland, D.R., Brown, R.M., Moore, D.F., 1997. Aggregation of euphausiids and Pacific hake (*Merluccius productus*) along the outer continental shelf off Vancouver Island. Can. J. Fish. Aquat. Sci. 54, 2080–2096.

Mackas, D. L., Goldblatt, R., Lewis, A. L., 1998. Interdecadal variation in developmental timing of *Neocalanus plumchrus* populations at Ocean Station P in the subarctic North Pacific. Can. J. Fish. Aquat. Sci., 55, 1878-1893.

Malej, A., Mozetič, P., Malačč, V., Turk, V., 1997. Response of summer phytoplankton to episodic meteorological events (Gulf of Trieste, Adriatic Sea). Mar. Ecol. 18, 273-288.

Marchal, O., Lam, P. J., 2012. What can paired measurements of Th isotope activity and particle concentration tell us about particle cycling in the ocean? Geochim. Cosmochim. Ac. 90, 126 – 148.

Martín, J., Palanques, A., Puig, P., 2006. Composition and variability of downward particulate matter fluxes in Palamós submarine canyon (NW Mediterranean). J. Mar. Sys. 60, 75-97.

Martín, J., Palanques, A., Puig, P., 2007. Near-bottom horizontal transfer of particulate matter in the Palamós Submarine Canyon (NW Mediterranean). J. Mar. Res. 65(2), 193-218.

Martín, J., Puig, P., Palanques, A., Masqué, P., García-Orellana, J., 2008. Effect of commercial trawling on the deep sedimentation in a Mediterranean submarine canyon. Mar. Geol. 252, 150–155.

Martín, J., Palanques, A., Vitorino, J., Oliveira, A., De Stigter, H. C., 2011. Near-bottom particulate matter dynamics in the Nazaré submarine canyon under calm and stormy conditions. Deep Sea Res. II Top. Stud. Oceanogr. 58, 2388-2400.

Martín, J., Durrieu de Madron, X., Puig, P., Bourrin, F., Palanques, A., Houpert, L., Higueras, M., Sanchez-Vidal, A., Calafat, A. M., Canals, M., Heussner, S., Delsaut, N., Sotin, C., 2013. Sediment transport along the Cap de Creus Canyon flank during a mild, wet winter. Biogeosciences, 10(5), 3221-3239.

Martín, J., Puig, P., Palanques, A., Ribó, M., 2014a. Trawling-induced daily sediment resuspension in the flank of a Mediterranean submarine canyon. Deep Sea Res. Part II Top. Stud. Oceanogr. 104, 174–183.

Martín, J., Puig, P., Masqué, P., Palanques, A., Sánchez-Cabeza, A., 2014b. Impact of bottom trawling on deep-sea sediment properties along the flanks of a submarine canyon. PLoS One, 9(8), e104536.

Martín, J., Puig, P., Palanques, A., Giamportone, A., 2014c. Commercial bottom trawling as a driver of sediment dynamics and deep seascape evolution in the Anthropocene. Anthropocene 7, 1–15.

Masó, M., Tintoré, J., 1991. Variability of the shelf water off the northeast Spanish coast. J. Mar Sys. 1, 441-450.

Masson, D. G., Huvenne, V. A. I., De Stigter, H. C., Wolff, G. A., Kiriakoulakis, K., Arzola, R. G., Blackbird, S. 2010. Efficient burial of carbon in a submarine canyon. Geology, 38, 831-834.

Masson, D. G., Huvenne, V. A. I., de Stigter, H. C., Arzola, R. G., LeBas, T. P., 2011. Sedimentary processes in the middle Nazaré Canyon. Deep Sea Res. II Top Stud. Oceanogr. 58, 2369-2387.

Matabos, M., Bui, A. O., Mihaly, S., Aguzzi, J., Juniper, S. K., Ajayamohan, R. S., 2014. High-frequency study of epibenthic megafaunal community dynamics in Barkley Canyon: A multi-disciplinary approach using the NEPTUNE Canada network. J. Mar. Sys. 130, 56-68.

Matabos, M., Best, M. M. R., Blandin, J., Hoeberechts, M., Juniper, S. K., Pirenne, B., Robert, K., Ruhl, H. A., Sarrazin, J., Vardaro, M., 2016. Seafloor observatories. Biol. Sampl. Deep Sea, 306-337.

Maynou, F., Conan, G. Y., Cartes, J. E., Company, J. B., Sardà, F., 1996. Spatial structure and seasonality of decapod crustacean populations on the northwestern Mediterranean slope. Limnol. Oceanogr. 41, 113-125.

Maynou, F., Sardà. F., 2001. Influence of environmental factors in commercial trawl catches of *Nephrops norvegicus* (L.). ICES J. Mar. Sci. 58, 1318-1325.

Maynou, F., Sardà, F., Tudela, S., Demestre, M., 2006. Management strategies for red shrimp (Aristeus antennatus) fisheries in the Catalan sea (NW Mediterranean) based on bioeconomic simulation analysis. Aquat. Living Resour. 19, 161–171.

McCave, I. N., 1983. Particulate size spectra, behavior and origin of nepheloid layers over the Nova Scotian continental rise. J. Geophys. Res. Oceans 88, 7647-7666.

McCave, I. N., 1986. Local and global aspects of the bottom nepheloid layers in the world ocean. Neth. J. Sea Res. 20, 167-181.

McCave, I. N., Carter, L., 1997. Recent sedimentation beneath the deep Western Boundary Current off northern New Zealand. Deep Sea Res. I Oceanogr. Res. Pap. 44, 1203-1237.

McCave, I. N., Hall, I. R., Antia, A. N., Dehairs, Lampitt, R. S., Thomsen, L., van Weering, T. C. E., Wollast, R., 2001. Distribution, composition and flux of particulate material over the European margin at 47º-50º N. Deep Sea Res. II Top. Stud. Oceanogr. 48, 3107-3139.

McCave, I. N., Hall, I. R., 2002. Turbidity of waters over the Northwest Iberian continental margin. Prog. Oceanogr. 52, 299-313.

McConnaughey, R. A., Hiddink, J. G., Jennings, S., Pitcher, C. R., Kaiser, M. J., Suuronen, P., Sciberras, M., Rijnsdorp, A., Collie, J., Mazor, T., Amoroso, R. O., Parma, A. M., Hilborn, R., 2020. Choosing best practices for managing impacts of trawl fishing on seabed habitats and biota. Fish Fish. 21, 319-337.

McDonell, A. M. P., Buesseler, K. O., 2010. Variability in the average sinking velocity of marine particles. Limnol. Oceanogr. 55, 2085-2096.

McPhee-Shaw, E. E., 2006. Boundary-interior exchange: reviewing the idea that internal-wave mixing enhances lateral dispersal near continental margins. Deep Sea Res. II. Top. Stud. Oceanogr. 53, 42-59.

McPhee-Shaw, E. E., Sternberg, R. W., Mullenbach, B., Ogston, A. S., 2004. Observations of intermediate nepheloid layers on the northern California continental margin. Cont. Shelf Res. 24, 693-720.

Mendoza, E. T., Jimenez, J. A., 2009. Vulnerability assessment to coastal storms at a regional scale. In Coastal Engineering 2008 (vol. 5 pp. 4154-4166).

Mengual, B., Cayocca, F., Le Hir, P., Draye, R., Laffargue, P., Vincent, B., Garlan, T., 2016. Influence of bottom trawling on sediment resuspension in the 'Grande-Vasière'area (Bay of Biscay, France). Ocean Dynam. 66, 1181-1207.

Mengual, B., Le Hir, P., Cayocca, F., Garlan, T., 2019. Bottom trawling contribution to the spatio-temporal variability of sediment fluxes on the continental shelf of the Bay of Biscay (France). Mar. Geol. 414, 77–91.

Menot, L., Sibuet, M., Carney, R. S., Levin, L. A., Rowe, G. T., Billett, D. S. M., Poore, G., Kitazato, H., Vanreusel, A., Galéron, J., Lavrado, H. P., Sellanes, J., Ingole, B., Krylova, E., 2010. New perceptions of continental margin biodiversity. In: Life in the World's Oceans Diversity, Distribution and Abundance (Edited by Alistair D McIntyre) Wiley-Blackwell.

Mienis, F., De Sigter, H. C., De Haas, H., van Weering, T. C. E., 2009. Near-bed particle deposition and resuspension in a cold-water coral mound area at the Southwest Rockall Trough margin, NE Atlantic. Deep Sea Res. I Oceanogr. Res. Pap. 56, 1026-1038.

Miller, C. B., Frost, B. W., Batchelder, H. P., Clemons, M. J., Conway, R. E., 1984. Life histories of large, grazing copepods in a subarctic ocean gyre: Neocalanus plumchrus, Neocalanus cristatus, and Euclanus bungii in the Northeast Pacific. Prog. Oceanogr. 13, 201-243.

Milliman, J. D., Farnsworth, K. L., 2013. River discharge to the coastal ocean: a global synthesis. Cambridge University Press.

Millot, C., 1990. The Gulf of Lions' hydrodynamics. Cont. Shelf Res. 10, 885-894.

Millot, C., 1999. Circulation in the western Mediterranean Sea. J. Mar. Sys. 20, 423-442.

Millot, C., Taupier-Letage, I., 2005. Circulation in the Mediterranean Sea. In The Mediterranean Sea (pp. 29-66). Springer, Berlin, Heidelberg.

Monaco, A., Courp, T., Heussner, S., Carbonne, J., Fowler, S. W., Deniaux, B., 1990. Seasonality and composition of particulate fluxes ECOMARGE-I, western Gulf of Lions. Cont. Shelf Res. 10, 959-987.

Monaco, A., Biscaye, P. E., Laborde, P., 1999. The ECOFER (ECOsystéme du canyon du cap FERret) experiment in the Bay of Biscay: introduction, objectives and major results. Deep Sea Res. II Top. Stud. Oceanogr. 46, 1967-1978.

Montagner, J. P., Lancelot, Y., 1995. Proceedings International Workshop Multidisciplinary Observatories on the Deep Seafloor (INSU/CNRS, IFREMER, OSN/USSAC, ODP-France and ODP-Japan, Marseille, France), pp. 229.

Morato, T., Watson, R., Pitcher, T.J., Pauly, D., 2006. Fishing down the deep. Fish Fish. 7, 24–34.

Mordecai, G., Tyler, P. A., Masson, D. G., Huvenne, V. A., 2011. Litter in submarine canyons off the west coast of Portugal. Deep Sea Res. II Top. Stud. Oceanogr. 58, 2489-2496.

Mortensen, P. B., Buhl-Mortensen, L., 2004. Distribution of deep-water gorgonian corals in relation to benthic habitat features in the Northeast Channel (Atlantic Canada). Mar. Biol. 144, 1223-1238.

Munk, W., Snodgrass, F., Wirebush, M., 1970. Tides offshore: transition from California coastal to deep-sea water. Geophys. Fluid Dyn. 1, 161-235.

Nash, J. D., Kunze, E., Toole, J. M., Schmitt, R. W., 2004. Internal tide reflection and turbulent mixing on the continental slope. J. Phys. Oceanogr. 34, 1117-1134.

Natale, F., Gibin, M., Alessandrini, A., Vespe, M., Paulrud, A., 2015. Mapping fishing effort through AIS Data. PloS One 10(6), e0130746.

Naudin, J. J., Cauwet, G., 1997. Transfer mechanisms and biogeochemical implications in the bottom nepheloid layer. A case study of the coastal zone off the Rhone River (France). Deep Sea Res. II Top. Stud. Oceanogr. 44, 551-575.

Nielsen, O. E., Lunde, A., Shephard, N., Veraart, A. E., 2014. Integer-valued trawl processes: A class of stationary infinitely divisible processes. Scand. J. Stat. 41, 693-724.

Nittrouer, C. A., 1999. STRATAFORM: overview of its design and synthesis of its results. Mar. Geol. 154, 3-12.

Norse, E. A., Brooke, S., Cheung, W. W. L., Clark, M. R., Ekeland, I., Froese, R., Gjerde, K. M., Haedrich, R. L., Heppell, S. S., Morato, T., Morgan, L. E., Pauly, D., Sumaila, R., Watson, R., 2012. Sustainability of deep-sea fisheries. Mar. Policy 36, 307-320.

NRC (National Research Council), 2000. Illuminating the Hidden Planet. The Future of Seafloor Observatory Science (National Academy Press,Washington DC), pp. 135.

NRC (National Research Council), 2003. Enabling ocean research in the 21st century: implementation of a network of ocean observatories. Washington DC: National Academy Press, 240 pp.

Oberle, F. K. J., Storlazzi, C. D., Hanebuth, T. J. J., 2016a. What a drag: Quantifying the global impact of chronic bottom trawling on continental shelf sediment. J. Mar. Syst. 159, 109–119.

Oberle, F. K. J., Swarzenski, P. W., Reddy, C. M., Nelson, R. K., Baasch, B., Hanebuth, T. J. J., 2016b. Deciphering the lithological consequences of bottom trawling to sedimentary habitats on the shelf. J. Mar. Syst. 159, 120–131.

Oberle, F. K. J., Puig, P.; Martín J., 2018. Fishing Activities. In: Micallef, A., Krastel, S., Savini, A. (Eds.). Submarine Geomorphology. Springer. ISBN 978-3-319-57851-4, pp 503-534.

Ogston, A. S., Drexler, T. M., Puig, P. 2008. Sediment delivery, resuspension, and transport in two contrasting canyon environments in the southwest Gulf of Lions. Cont. Shelf Res. 28, 2000-2016.

Oliveira, A., Vitorino, J., Rodrigues, A., Jouanneau, J. M., Días, J. A., Weber. O., 2002. Nepheloid layer dynamics in the northern Portuguese shelf. Prog. Oceanogr. 52, 195-213.

Oliveira, A., Santos, A. I., Rodrigues, A., Vitorino, J., 2007. Sedimentary particle distribution and dynamics on the Nazaré canyon system and adjacent shelf (Portugal). Mar. Geol. 246, 105-122.

O'Neill, F.G., Summerbell, K., 2011. The mobilisation of sediment by demersal otter trawls. Mar. Pollut. Bull. 62, 1088–1097.

O'Neill, F. G., Robertson, M., Summerbell, K., Breen, M. Robinson, L. A., 2013. The mobilisation of sediment and benthic infauna by scallop dredges. Mar. Environ. Res. 90, 104-112.

O'Neill, F.G., Ivanović, A., 2016. The physical impact of towed demersal fishing gears on soft sediments. ICES J. Mar. Sci. J. du Cons. 73, i5-i14.

Orr, M. H., Hess, F. R., 1978. Remote acoustic monitoring of natural suspensate distributions, active suspensate resuspension, and slope/shelf water intrusions. J. Geophys. Res. Oceans, 83, 4062-4068.

Ostrovskii, A. G., Zatsepin, A. G., Soloviev, V. A., Tsybulsky, A. L., Shvoev, D. A., 2013. Autonomous system for vertical profiling of the marine environment at a moored station. Oceanology 53, 233–242.

Owens, S. A., Pike, S., Buesseler, K. O., 2015. Thorium-234 as a tracer of particle dynamics and upper ocean export in the Atlantic Ocean. Deep Sea Res. Top. Stud Oceanogr. 116, 42-59.

Palanques, A., Biscaye, P. E., 1992. Patterns and controls of the suspended matter distribution over the shelf and upper slope south of New England. Cont. Shelf Res. 12, 577-600.

Palanques, A., Guillén, J., Puig, P., 2001. Impact of bottom trawling on water turbidity and muddy sediment of an unfished continental shelf. Limnol. Oceanogr. 46, 1100–1110.

Palanques, A., Puig, P., Guillén, J., Jiménez, J., Gràcia, V., Sánchez-Arcilla, A., Madsen, O., 2002. Near-bottom suspended sediment fluxes on the microtidal low-energy Ebro continental shelf (NW Mediterranean). Cont. Shelf Res. 22, 5-303.

Palanques, A., García-Ladona, E., Gomis, D., Martín, J., Marcos, M., Pascual, A., Puig, P., Gili, J. M., Emelianov, M., Montserrat, S., Guillén, J., Tintoré, J., Segura, M., Jordi, A., Ruiz, S., Basterretxea, G., Font, J., Blasco, D., Pagès, F., 2005. General patterns of circulation, sediment fluxes and ecology of the Palamós (La Fonera) submarine canyon, northwestern Mediterranean. Prog. Oceanogr. 66, 89-119.

Palanques, A., Martín, J., Puig, P., Guillén, J., Company, J. B., Sardà, F., 2006a. Evidence of sediment gravity flows induced by trawling in the Palamós (Fonera) submarine canyon (northwestern Mediterranean). Deep Sea Res. Part I Oceanogr. Res. Pap. 53, 201–214.

Palanques, A., Durrieu de Madron, X., Puig, P., Fabres, J., Guillén, J., Calafat, A., Canals, M., Bonnin, J., 2006b. Suspended sediment fluxes and transport processes in the Gulf of Lions submarine canyons: the role of storms and dense shelf water cascading. Mar. Geol. 234(1-4), 43-61.

Palanques, A., Guillén, J., Puig, P., Durrieu de Madron, X., 2008. Storm-driven shelf-to canyon suspended sediment transport at the southwestern Gulf of Lions. Cont. Shelf Res. 28(15), 1947-1956.

Palanques, A., Puig, P., Durrieu de Madron, X., Sanchez-Vidal, A., Pasqual, C., Martín, J., Calafat, A., Heussner, S., Canals, M., 2012. Sediment transport to the deep canyons and open-slope of the western Gulf of Lions during the 2006 intense cascading and open-sea convection period. Prog. Oceanogr. 106, 1-15.

Palanques, A., Puig, P., Guillén, J., Demestre, M., Martín, J., 2014. Effects of bottom trawling on the Ebro continental shelf sedimentary system (NW Mediterranean). Cont. Shelf Res. 72, 83–98.

Palanques, A., Puig, P., 2018. Particle fluxes induced by benthic storms during the 2012 dense shelf water cascading and open sea convection period in the northwestern Mediterranean basin. Mar. Geol. 406, 119-131.

Palanques, A., Puig, P., Arjona-Camas, M., 2018. Self-regulated deep-sea trawling fishery management in La Fonera Canyon (NW Mediterranean) towards reduction of sediment resuspension and seabed impact. In: AGU Ocean Sciences Meeting, Portland, Oregon, USA.

Paradis, S., Puig, P., Masqué, P., Juan-Díaz, X., Martín, J., Palanques, A., 2017. Bottom trawling along submarine canyons impacts deep sedimentary regimes. Sci. Rep. 7, 43332.

Paradis, S., Puig, P., Sánchez-Vidal, A., Masqué, P., García-Orellana, J., Calafat, A., Canals, M., 2018a. Spatial distribution of sedimentation-rate increases in Blanes Canyon caused by technification of bottom trawling fleet. Prog. Oceanogr. 169, 241-252.

Paradis, S., Masqué, P., Puig, P., Juan-Diaz, X., Gorelli, G., Palanques, A., 2018b. Enhancement of sedimentation rates in the Foix Canyon after the renewal of trawling fleets in the early XXI st century. Deep Sea Res. I Oceanogr. Res. Pap. 132, 51-59.

Paradis, S., Goñi, M., Masqué, P., Durán, R., Arjona-Camas, M., Palanques, A., Puig, P., 2021. Persistence of biogeochemical alterations of deep-sea sediments by bottom trawling. Geophys. Res. Lett., e2020GL091279.

Parsons, J. D., Whipple, K. X., & Simoni, A. (2001). Experimental Study of the Grain-Flow, Fluid-Mud Transition in Debris. The Journal of Geology, 109, 427-447.

Pasqual, C., Goñi, M., Tesi, T., Sanchez-Vidal, A., Calafat, A., Canals, M., 2013. Composition and provenance of terrigenous organic matter transported along submarine canyons in the Gulf of Lion (NW Mediterranean Sea). Prog. Oceanogr. 118, 81–94.

Pedrosa-Pàmies, R., Sanchez-Vidal, A., Calafat, A., Canals, M., Durán, R., 2013. Impact of storm-induced remobilization on grain size distribution and organic carbon content in sediments from the Blanes Canyon area, NW Mediterranean Sea. Prog. Oceanogr. 118, 122–136.

Petrenko, A. A. 2003. Variability of circulation features in the Gulf of Lion NW Mediterranean Sea. Importance of inertial currents. Oceanol. Acta, 26, 323-338.

Pham, C. K., Ramirez-Llodra, E., Alt, C. H. S., Amaro, T., Bergmann, M., Canals, M., Company, J. B., Davies, J., Duinevals, G., Galgani, F., Howell, K. L., Huvenne, V. A. I., Isidro, E., Jones, D. O. B., Lastras, G., Morato, T., Gomes-Pereira, J. N., Purser, A., Stewart, H., Tojeira, I., Tubau, X., van Rooij, D., Tyler, P. A., 2014. Marine litter distribution and density in European seas, from the shelves to deep basins. PloS One 9, e95839.

Pierce, S. D., Smith, R. L., Kosro, P. M., Barth, J. A., Wilson, C. D., 2000. Continuity of the poleward undercurrent along the eastern boundary of the mid-latitude north Pacific. Deep Sea Res. II Top. Stud. Oceanogr. 47, 811-829.

Pilskaln, C. H., Churchill, J. H., Mayer, L. M., 1998. Resuspension of Sediment by Bottom Trawling in the Gulf of Maine and Potential Geochemical Consequences. Conserv. Biol. 12, 1223–1229.

Pinardi, N., Masetti, E., 2000. Variability of the large-scale general circulation of the Mediterranean Sea from observations and modelling: a review. Paleogeography, Palaeoclimatology, Palaeoecology, 158, 153-173.

Pitcher, C. R., Poiner, I. R., Hill, B. J., Burridge, C. Y., 2000. Implications of the effects of trawling on sessile megazoobenthos on a tropical shelf in northeastern Australia. ICES Journal of Mar. Sci. 57, 1359-1368.

Pitcher, C. R., Ellis, N., Venables, W. N., Wassenberg, T. J., Burridge, C. Y., Smith, G. P., Browne, M., Pantus, F., Poiner, I. R., Doherty, J., Hooper, J. N. A., Gribble, N., 2016. Effects of trawling on sessile megabenthos in the Great Barrier Reef and evaluation of the efficacy of management strategies. ICES Journal of Marine Science,73, i115-i126.

Porter, M., Inall, M. E., Hopkins, J., Palmer, M. R., Dale, A. C., 958 Barth, J. A., Mahaffey, C., Smeed, D. A., 2016. Glider observations of enhanced deep water upwelling at a shelf break canyon: A mechanism for cross-slope carbon and nutrient. J. Geophys. Res. Oceans, 121, 7575-7588.

Pratson, L.F., Nittrouer, C.A., Wiberg, P.L., Steckler, M.S., Swenson, J.B., Cacchione, D.A., Karson, J.A., Murray, A.B., Wolinsky, M.A., Gerber, T.P., Mullenbach, B.L., Spinelli, G.A., Fulthorpe, C.S., O'Grady, D.M., Parker, G., Driscoll, N.W., Burger, R.L., Paola, C., Orange, D.L., Field, M.E., Friedrichs, C.T., Fedele, J.J., 2007. Seascape evolution on clastic continental shelves and slopes, in: Continental Margin Sedimentation: from sediment transport to sequence stratigraphy. Int. As. Sed. 37, pp. 339-380.

Puertos del Estado, ShipLocus, 2017. Available at ⟨https://shiplocus.puertos.es/⟩ (Accessed 1 January 2018).

Puig, P., Palanques, A., 1998a. Nepheloid structure and hydrographic control on the Barcelona continental margin, northwestern Mediterranean. Mar. Geol. 149, 39-54.

Puig, P., Palanques, A., 1998b. Temporal variability and composition of settling particle fluxes on the Barcelona continental margin (Northwestern Mediterranean). J. Mar. Res. 56, 639-654.

Puig, P., Palanques, A., Guillén, J., García-Ladona, E., 2000. Deep slope currents and suspended particle fluxes in and around the Foix submarine canyon (NW Mediterranean). Deep Sea Res. I Oceanogr. Res. Pap. 47, 343-366.

Puig, P., Palanques, A., Guillén, J., 2001. Near-bottom suspended sediment variability caused by storms and near-inertial internal waves on the Ebro mid continental shelf (NW Mediterranean). Mar. Geol. 178, 81-93.

Puig, P., Ogston, A. S., Mullenbach, B. L., Nittrouer, C. A., Sternberg, R. W., 2003. Shelf-to-canyon sediment-transport processes on the Eel continental margin (northern California). Mar. Geol. 193, 129-149.

Puig, P., Ogston, A. S., Mullenbach, B. L., Nittrouer, C. A., Parsons, J. D., Sternberg, R. W., 2004. Storm-induced sediment gravity flows at the head of the Eel submarine canyon, northern California margin. J. Geophys. Res. Oceans, 109(C3).

Puig, P., Palanques, A., Guillén, J., El Khatab, M., 2004b. Role of internal waves in the generation of nepheloid layers on the northwestern Alboran slope: Implications for the continental margin shaping. J. Geophys. Res. Oceans 109(C9).

Puig, P., Palanques, A., Orange, D. L., Lastras, G., & Canals, M., 2008. Dense shelf water cascades and sedimentary furrow formation in the Cap de Creus Canyon, northwestern Mediterranean Sea. Cont. Shelf Res. 28, 2017-2030.

Puig, P., Canals, M., Company, J.B., Martín, J., Amblas, D., Lastras, G., Palanques, A., 2012. Ploughing the deep sea floor. Nature 489, 286-289.

Puig, P., Durrieu de Madron, X., Salat, J., Schroeder, K., Martín, J., Karageorgis, A. P., Palanques, A., Roullier, F., Lopez-Jurado, J. L., Emelianov, M., Moutin, T., Houpert, L., 2013. Thick bottom nepheloid layers in the western Mediterranean generated by deep dense shelf water cascading. Prog. Oceanogr. 111, 1-23.

Puig, P., Palanques, A., Martín, J., 2014. Contemporary Sediment-Transport Processes in Submarine Canyons. Annu. Rev. Mar. Sci., 6: 53-77.

Puig, P., Martín, J., Masqué, P., Palanques, A., 2015. Increasing sediment accumulation rates in La Fonera (Palamós) submarine canyon axis and their relationship with bottom trawling activities. Geophys. Res. Lett. 42, 8106-8113.

Pusceddu, A., Mea, M., Canals, M., Heussner, S., Durrieu de Madron, X., Sanchez-Vidal, A., Bianchelli, S., Corinaldesi, C., Dell'Anno, A., Thomsen, L., Danovaro, R., 2013. Major consequences of an intense dense shelf water cascading event on deep-sea benthic trophic conditions and meiofaunal biodiversity. Biogeosciences 10, 2659–2670. https://doi.org/10.5194/bg-10-2659-2013.

Pusceddu, A., Bianchelli, S., Martín, J., Puig, P., Palanques, A., Masqué, P., Danovaro, R., 2014. Chronic and intensive bottom trawling impairs deep-sea biodiversity and ecosystem functioning. Proc. Natl. Acad. Sci. U. S. A. 111, 8861–8866.

Quaresma, L. S., Vitorino, J., Oliveira, A., da Silva, J., 2007. Evidence of sediment resuspension by nonlinear internal waves on the western Portuguese mid-shelf. Mar. Geol. 246, 123-143.

Quattrini, A. M., Nizinski, M. S., Chaytor, J. D., Demopoulos, A. W. J., Roark, E. B., France, S. C., Moore, J. A., Heyl, T., Auster, P. J., Kinlan, B., Ruppel, C., Elliott, K. P., Kennedy, B. R. C., Lobecker, E., Skarke, A., Shank, T. M., 2015. Exploration of the canyon-incised continental margin of the northeastern United States reveals dynamic habitats and diverse communities. PLoS One 10, e0139904.

Ragnarsson, S., Steingrímsson, S. A., 2003. Spatial distribution of otter trawl effort on Icelandic waters: comparison of measures of effort and implications for benthic community effects of trawling activities. ICES J. Mar. Sci. 60, 1200- 1215.

Ramirez-Llodra, E., Tyler, P. A., Baker, M. C., Bergstad, O. A., Clark, M. R., Escobar, E., Levin, L. A., Menot, L., Rowden, A. A., Smith, C. R., van Dover, C. L., 2011. Man and the last great wilderness: human impact on the deep sea. PLoS One 6, e22588.

Ramp, S. R., Davis, R. E., Leonard, N. E., Shulman, I., Chao, Y., Robinson, A. R., Marsden, J., Lermusiaux, P. F. J., Fratantoni, D. M., Paduan, J. D., Chavez, F. P., Bahr, F. L., Liang, S., Leslie, W., Li, Z., 2009. Preparing to predict: The Second Autonomous Ocean Sampling Network (AOSN-II) experiment in the Monterey Bay. Deep Sea Res. Part II Top. Stud. Oceanogr. 56, 68–86.

Ransom, B. B. R. H., Bennett, R. H., Baerwald, R., Shea, K., 1997. TEM study of in situ organic matter on continental margins: occurrence and the "monolayer" hypothesis. Mar. Geol. 138, 1-9.

Rayner, D., Kanzow, T., 2011. The design strategy and methodology of the RAPID-MOC project moorings. Underwater Technol., 29, 159-171.

Rebesco, M., Hernández-Molina, F. J., van Rooij, D., Wåhlin, A., 2014. Contourites and associated sediments controlled by deep-water circulation processes: State-of-the-art and future considerations. Mar. Geol. 352, 111-154.

Reid, J. L., 1997. On the total geostrophic circulation of the Pacific Ocean: Flow patterns, tracers and transports. Prog. Oceanogr. 39, 263-352.

Ribera d'Alcalà, M., Civitarese, G., Conversano, F., and Lavezza, R., 2003. Nutrient fluxes and ratios hint at overlooked processes in the Mediterranean sea, J. Geophys. Res., 108, 8106.

Ribó, M., Puig, P., Palanques, A., Lo Iacono, C., 2011. Dense shelf water cascades in the Cap de Creus and Palamós submarine canyons during winters 2007 and 2009. Mar. Geol. 284, 175-188.

Ribó, M., Puig, P., Salat, J., Palanques, A., 2013. Nepheloid layer distribution in the Gulf of Valencia, northwestern Mediterranean. J. Mar. Syst. 111, 130-138.

Ribó, M., Puig, P., van Haren, H., 2015. Hydrodynamics over the Gulf of Valencia continental slope and their role in sediment transport. Deep Sea Res. I Oceanogr. Res. Pap. 95, 54-66.

Rijnsdorp, A. D., Eigaard, O. R., Kenny, A., Hiddink, J. G., Hamon, K., Piet, G. J., Sala, A., Nielsen, J. R., Polet, H., Laffargue, P., Zengin, M., Gregersen, O., 2017. Assessing and mitigating of bottom trawling. Final BENTHIS project Report (Benthic Ecosystem Fisheries Impact Study).

Robert, K., Jones, D. O., Tyler, P. A., van Rooij, D., Huvenne, V. A., 2015. Finding the hotspots within a biodiversity hotspot: fine-scale biological predictions within a submarine canyon using high-resolution acoustic mapping techniques. Mar. Ecol. 36, 1256-1276.

Robinson, A. R., Leslie, W. G., Theocharis, A., Lascaratos, A., 2001. Mediterranean sea circulation. Ocean currents, 1, 19.

Romanowicz, B., Suyehiro, K., & Kawakatsu, H., 2001. OHP/ION joint symposium long-term observations in the oceans. Current status and perspectives for the future. In Workshop Rep (p. 188).

Royer, T. C., 1982. Coastal fresh water discharge in the Northeast Pacific. J. Geophys. Res. 87, 2017-2021.

Russo, T., D'Andrea, L., Parisi, A., Martinelli, M., Belardinelli, A., Boccoli, F., Cignini, I., Tordoni, M., Cataudella, S., 2016. Assessing the fishing footprint using data integrated from different tracking devices: issues and opportunities. Ecol. Indic. 69, 818-827.

Ryan, J. P., Chavez, F. P., Bellingham, J. G., 2005. Physical-biological coupling in Monterey Bay, California: topographic influences on phytoplankton ecology. Mar. Ecol. Prog. Ser. 287, 23-32.

Salat, J., Cruzado, A., 1981. Water masses in the Western Mediterranean Sea: Catalan Sea and adjacent waters. Rap. Proc. CIESM v.27(6).

Salat, J., Font, J., 1987. Water mass structure near and offshore the Catalan coast during the winters of 1982 and 1983. In Annales geophisicae, Series B. Terrestrial and planetary physics (vol. 5, num. 1., pp. 48-54).

Salat, J., García, M. A., Cruzado, A., Palanques, A., Arín, L., Gomis, D., Guillén, J., de León, A., Puigdefàbregas, J., Sospedra, J., Velásquez, Z. R., 2002. Seasonal changes of water mass structure and shelf slope exchanges at the Ebro Shelf (NW Mediterranean). Cont. Shelf Res. 22, 327-348.

Sanchez-Cabeza, J. A., Masqué, P., Ani-Ragolta, I., Merino, J., Frignani, M., Alvisi, F., Palanques, A., Puig, P., 1999. Sediment accumulation rates in southern Barcelona continental margin (NW Mediterranean Sea) derived from 210Pb and 137Cs chronology. Prog. Oceanogr. 44, 313-332.

Sanchez-Vidal, A., Pasqual, C., Kerhervé, P., Calafat, A., Heussner, S., Palanques, A., Durrieu de Madron, X., Canals, M., Puig, P., 2008. Impact of dense shelf water cascading on the transfer of organic matter to the deep western Mediterranean basin. Geophys. Res. Lett. 35(5).

Sanchez-Vidal, A., Canals, M., Calafat, A.M., Lastras, G., Pedrosa-Pàmies, R., Menéndez, M., Medina, R., Company, J.B., Hereu, B., Romero, J., Alcoverro, T., 2012. Impacts on the Deep-Sea Ecosystem by a Severe Coastal Storm. PLoS One 7, e30395.

Sanchez-Vidal, A., Higueras, M., Martí, E., Liquete, C., Calafat, A., Kerhervé, P., Canals, M., 2013. Riverine transport of terrestrial organic matter to the North Catalan margin, NW Mediterranean Sea. Prog. Oceanogr. 118, 71-80.

Sardà, F., Demestre, M., 1987. Estudio biológico de la gamba *Aristeus antennatus* (Risso, 1816) en el Mar Catalán (NW de España).

Sardà, F., Cartes, J. E., 1994. Spatio-temporal variations in megabenthos abundance in three different habitats of the Catalan deep-sea (Western Mediterranean). Mar. Biol. 120, 211-219.

Sardà, F., Peired, C., 1998. Long-term morphometric variations in a population of the deep-sea shrimp *Aristeus antennatus* (Risso, 1816) (*Decapoda, Aristeidae*). Crustaceana (Leiden, Print).

Sardà, F., Company, J.B., Castellón, A., 2003. Intraspecific aggregation structure of a shoal of a Western Mediterranean (Catalan coast) deep-sea shrimp, Aristeus antennatus (Risso, 1816), during the reproductive period. J. Shellfish Res. 22, 569–579.

Sardà, F., D'Onghia, G., Politou, C.Y., Company, J.B., Maiorano, P., Kapiris, K., 2004. Deep-sea distribution, biological and ecological aspects of Aristeus antennatus (Risso, 1816) in the western and central Mediterranean Sea. Sci. Mar., 68, 117-127.

Sartor, P., Sbrana, M., Chato Osio, G., Ligas, A., Reale, B., Colloca, F., Ferretti, F., De Ranieri, S., Marvelias, C., Kavadas, S., Damalas, D., Klaoudatos, D., Papaconstantinou, C., Maynou, F., Cartes, J., Miriani, A., Lariccia, M., Bartoli, A., Vazzoloretto, S., Rossetti, I., Sartini, M., Vannucci, A., Balducci, G. M., 2011. The 20th Century evolution of Mediterranean exploited demersal resources under increasing fishing disturbance and environmental change.

Schlitzer, R., 2002. Interactive analysis and visualization of geoscience data with Ocean Data View. Comput. Geosci. 28, 1211-1218.

Schlitzer, R., 2010. Ocean Data View. http://odv.awi.de.

Schoellhamer, D. H., 1996. Anthropogenic sediment resuspension mechanisms in a shallow microtidal estuary. Estuar. Coast. Mar. Sci. 43, 533-548.

Sciberras, M., Hinz, H., Bennell, J. D., Jenkins, S. R., Hawkins, S. J., Kaiser, M. J., 2013. Benthic community response to a scallop dredging closure within a dynamic seabed habitat. Mar. Ecol. Prog. Ser. 480, 83-98.

Sciberras, M., Hiddink, J.G., Jennings, S., Szostek, C.L., Hughes, K.M., Kneafsey, B., Clarke, L.J., Ellis, N., Rijnsdorp, A.D., McConnaughey, R.A., Hilborn, R., Collie, J.S., Pitcher, C.R., Amoroso, R.O., Parma, A.M., Suuronen, P., Kaiser, M.J., 2018. Response of benthic fauna to experimental bottom fishing: A global meta-analysis. Fish Fish. 19, 698–715.

Serra, J., 1981. Els canyons submarins del marge Català. Treb. Inst. Cat. Hist. Nat. 9, 53-57.

Shanmugam, G., 2008. Deep-water bottom currents and their deposits. Developments in sedimentology, 60, 59-81.

Shanmugan, G., 2014. Modern internal waves and internal tides along oceanic pycnoclines: Challenges and implications for ancient deep-marine baroclinic sands: Reply. AAPG bulletin, 98, 858-879.

Shapiro, G. I., Huthnance, J. M., Ivanov, V. V., 2003. Dense water cascading off the continental shelf. J. Geophys. Res. Oceans, 108(C12).

Shatova, O., Branch, B. S., 2008. Understanding Intermediate Nepheloid Layers: A Multi-platform Approach.

Shepard, F. P., Dill, R. F., 1966. Submarine Canyos and Other Sea Valleys. USA: Rand McNally.

Simmons, S. M., Parsons, D. R., Best, J. L., Orfeo, O., Lane, S. N., Kostaschuk, R., Hardy, R. J., West, G., Malzone, C., Marcus, J., Pocwiardowski, P., 2009. Monitoring suspended sediment dynamics using MBES. J. Hydraul. Eng. 136, 45-49.

Simrad, Y., Mackas, D. K., 1989. Mesoscale aggregations of euphausiid sound scattering layers on the continental shelf Seabirds off Vancouver Island. BC, 83.

Sinclair, A., 2007. Trends in groundfish bottom trawl fishing activity in BC. Research Document 006. Fisheries and Oceans Canada Pacific Biological Station Nanaimo, 22.

Siokou-Frangou, I., Christaki, U., Mazzochi, M. G., Montresor, M., Ribera d'Alcalà, M., Vaqué, D., Zingone, A., 2010. Plankton in the open Mediterranean Sea: a review. Biogeosciences, 7, 1543-1586. https://doi.org/10.5194/bg-7-1543-2010, 2010.

Smith, C. R., 1994. Tempo and mode in deep-sea benthic ecology: punctuated equilibrium revisited. Palaios 9, 3-13.

Smith, C. R., 2006. Bigger is better: the role of whales as detritus in marine ecosystems. In Estes, J., DeMaster, D. P., Doak, D. F., Williams, T. M., Brownell, R. L. J. (eds), 2006. Whales, whaling and ocean ecosystems. University of California Press, pp. 286-301.

Smith, C. R., Kukert, H., Wheatcroft, R. A., Jumars, P. A., Deming, J. W., 1989. Vent fauna on whale remains. Nature 341, 27-28.

Smith, C., Rumohr, H., Karakassis, I., Papadopoulou, K.N., 2003. Analysing the impact of bottom trawls on sedimentary seabeds with sediment profile imagery. J. Exp. Mar. Biol. Ecol. 285, 479-496.

Sobarzo, M., Figueroa, M., Djurfeldt, L., 2001. Upwelling of subsurface water into the rim of the Biobio submarine canyon as a response to surface winds. Cont. Shelf Res. 21, 279-299.

Solé, J., Emelianov, M., Ostrovskii, A., Puig, P., García-Ladona, E., 2016. Fine-scale water mass variability inside a narrow submarine canyon (the Besòs Canyon) in the NW Mediterranean Sea. Sci. Mar. 80S1, 195-204.

Solomon, O. M., Larson, D. R., Paulter, N. G., 2001. Comparison of some algorithms to estimate the low and high state level of pulses. In IMTC 2001. Proceedings of the 18th IEEE Instrumentation and Measurement Technology Conference. Rediscovering Measurement in the Age of Informatics (Cat. No. 01CH 37188) (Vol. 1, pp. 96-101). IEEE.

Stefanescu, C., Nin-Morales, B., Massuti, E., 1994. Fish assemblages on the slope in the Catalan Sea (Western Mediterranean): influence of a submarine canyon. J. Mar. Biol. Assoc. UK, 74, 499-512.

Sternberg, R. W., Larsen, L. H., 1975. Threshold of sediment movement by open ocean waves: observations. In Deep Sea Res. And Ocean. Abstracts (vol. 22, 5, pp. 299-309). Elsevier.

Svensen, C., Morata, N., Reigstad, M., 2014. Increased degradation of copepod faecal pellets by co-acting dinoflagellates and *Centropages hamatus*. Mar. Ecol. Prog. Ser. 516, 61-70.

Sverdrup, H. V., Johnson, M. W., Fleming, R. H., 1942. The Oceans. Their Physics, Chemistry and General Biology. Prentice-Hall, Englewood Cliffs NJ, 1087 pp.

Syvitski, J. P. M., Peckham, S. D., Hilberman, R. D., Mulder, T. 2003. Predicting the terrestrial flux of sediment to the global ocean: a planetary perspective. Sedimentary Geology 162, 5-24

Talley, L. D., 1993. Distribution and formation of North Pacific intermediate water. J. Phys. Oceanogr. 23, 517-537.

Talley, L. D., 1997. North Pacific Intermediate Water transports in the mixed region. J. Phys. Oceanogr. 27, 1795-1803.

Thiel, H., Pfannkuche, O., Schriever, G., Lochte, K., Gooday, A. J., Hemleben, C, Mantoura, R. F. G., Turley, C. M., Pathing, J. W., Riemann, F., 1989. Phytodetritus on the Deep-Sea Floor in a Central Oceanic Region of the Northeast Atlantic. Biol. Oceanogr. 6, 203-239.

Thistle, D., 2003. The deep-sea floor: an overview. Ecosystems of the deep oceans, 5.

Thomsen, C., Blaume, F., Fohrmann, H., Peeken, I., Zeller, U., 2001. Particle transport processes at slope environments – event driven flux across the Barents Sea continental margin. Mar. Geol. 175, 237-308.

Thomsen, L., 1999. Processes in the benthic boundary layer at continental margins and their implication for benthic carbon cycle. J. Sea Res. 41, 73-86.

Thomsen, L., van Weering, T. C., 1998. Spatial and temporal variability of particulate matter in the benthic boundary layer at the NW European Continental Margin (Goban Spur). Prog. Oceanogr. 42, 61-76.

Thomsen, L., Barnes, C., Best, M., Chapman, R., Pirenne, B., Thomson, R., Vogt, J., 2012. Ocean circulation promotes methane release from gas hydrate outcrops at the NEPTUNE Canada Barkley Canyon node. Geophys. Res. Lett. 39(16).

Thomsen, L., Aguzzi, J., Costa, F.C., De Leo, F.C., Ogston, A., Purser, A., 2017. The oceanic biological pump: rapid carbon transfer to depth at continental margins during winter. Sci. Reports 7, 10763.

Thomson, R. E., Emery, W. J., 2014. Data analysis methods in physical oceanography. Newnes.

Thorpe, S. A., 2005. The turbulent ocean. C. U. P. ISBN-100-521-83543-7.

Thorbjarnarson, K. W., Nittrouer, C. A., & DeMaster, D. J., 1986. Accumulation of modern sediment in Quinault submarine canyon. Mar. Geol. 71(1-2), 107-124.

Thrush, S. F., Dayton, P. K., 2002. Disturbance to marine benthic habitats by trawling and dredging: implications for marine biodiversity. Ann. Rev. Ecol. Syst. 33, 449-473.

Thunell, R. C., Varela, R., Llano, M., Collister, J., Karger, F. M., Bohrer, R., 2000. Organic carbon fluxes, degradation, and accumulation in an anoxic basin: sediment trap results from the Cariaco Basin. Limnol. Oceanogr. 45 300-308.

Tillin, H. M., Hiddink, J. G., Jennings, S., Kaiser, M. J., 2006. Chronic bottom trawling alters the functional composition of benthic invertebrate communities on a sea-basin scale. Mar. Ecol. Prog. Ser. 318, 31-45.

Tintoré, J., Wang, D. P., La Violette, P. E., 1990. Eddies and thermohaline intrusions of the shelf/slope front off the northeast Spanish coast. J. Geophys. Res. Oceans, 1627-1633.

Troupin, C., Barth, A., Sirjacobs, D., Ouberdous, M., Brankart, J. M., Brasseur, P., Rixen, M., Alvera-Azcárate, A., Belounis, M., Capet, A., Lenartz, F., Toussaint, M. E., Beckers, J. M., 2012. Generation of analysis and consistent error fields using the Data Interpolating Variational Analysis (DIVA). Ocean Model. 52, 90-101.

Tubau, X., Lastras, G., Canals, M., Micallef, A., Amblas, D., 2013. Significance of the fine drainage pattern for submarine canyon evolution: the Foix Canyon system, northwestern Mediterranean Sea. Geomorphology 184, 20-37.

Tubau, X., Canals, M., Lastras, G., Rayo, X., Rivera, J., Amblas, D., 2015. Marine litter on the floor of deep submarine canyons of the Northwestern Mediterranean Sea: the role of hydrodynamic processes. Prog. Oceanogr. 134, 379-403.

Tudela, S., Sardà. F., Maynou, F., Demestre, M., 2003. Influence of submarine canyons on the distribution of the deep-water shrimp, Aristeus antennatus (Risso, 1816) in the NW Mediterranean. Crustaceana 76, 217-226.

Turner, J. T., 2002. Zooplankton fecal pellets, marine snow and sinking phytoplankton blooms. Aquat. Microb. Ecol. 27, 57-102.

Turner, J. T., 2015. Zooplankton fecal pellets, marine snow, phytodetritus and the ocean's biological pump. Prog. Oceanogr. 130, 205-248.

Tsuchiya, M., Talley, L. D., 1996. Water-property distributions along an eastern Pacific hydrographic section at 135 W. J. Mar. Res. 54, 541-564.

Tyler, P. A., Gage, J. D., 1982. The reproductive Biology of Ophiacantha bidentata (Echinodermata: Ophiuroidea) from the Rockall Trough. J. Mar. Biol. Assoc. UK 62, 45-55.

Ulses, C., Estournel, C., Puig, P., Durrieu de Madron, X., Marsaleix, P., 2008a. Dense shelf water cascading in the northwestern Mediterranean during the cold winter 2005: Quantification of the export through the Gulf of Lion and the Catalan margin. Geophys. Res. Lett. 35, L07610.

Ulses, C., Estournel, C., Bonnin, J., Durrieu de Madron, X., Marsaleix, P., 2008b. Impact of storms and dense water cascading on shelf-slope exchanges in the Gulf of Lion (NW Mediterranean). Journal of Geophysical Research 113, C02010.

USEPA, 1993. Method 180.1 Determination of turbidity by nephelometry (revision 2.0). In: J.W. O'Dell (Ed.), Methods for the Determination of Inorganic Substances in Environmental Samples (EPA/600/R-93/100) (p. 10). Cincinnati, Ohio: U. S. Environmental Proctection Agency.

van den Beld, I. M., Guillaumont, B., Menot, L., Bayle, C., Arnaud-Haond, S., Bourillet, J. F., 2017. Marine litter in submarine canyons of the Bay of Biscay. Deep Sea Res. II Top. Stud. Oceanogr. 145, 142-152.

van Haren, H., Ribó, M., Puig, P., 2013. (Sub-) inertial wave boundary turbulence in the Gulf of Valencia. J. Geophys. Res. 118, 2067-2073.

van Leer, J., Düing, W., Erath, R., Kennelly, E., Speidel, A., 1974. The Cyclesonde: An unattended vertical profiler for scalar and vector quantities in the upper ocean. In Deep Sea Research Oceanographic Abstracts (Vol. 21, No. 5, pp. 385-400).

van Weering, T. C. E., McCave, I. N., 2002. Benthic processes and dynamics at the NW Iberian margin: an introduction. Prog. Oceanogr. 52, 123-128.

van Weering, T. C. E., de Stitger, H. C., Boer, W., de Haas, H., 2002. Recent sediment transport and accumulation on the NW Iberian margin. Prog. Oceanogr. 52, 349-371.

Venello, T. A., Sastri, A. R., Galbraith, M. D., Dower, J. F. 2021. Zooplankton functional group responses to environmental drivers off the west coast of Vancouver Island, Canada. Prog. Oceanogr. 190, 102482.

Venkatesan, R., Ramesh, K., Kishor, A., Vedachalam, N., Atmanand, M. A., 2018. Best practices for the ocean moored observatories. Front. Mar. Sci. 5, 469.

Volk, T., Hoffert, M. I., 1985. Ocean carbon pumps: Analysis of relative strengths and efficiencies in ocean-driven atmospheric CO2 changes. The carbon cycle and atmospheric CO2: natural variations Archean to present, 32, 99-110.

Walsh, J. J., 1991. Importance of continental margins in the marine biogeochemical cycling of carbon and nitrogen. Nature 350, 53-55.

Walsh, J. P., Nittrouer, C. A., 1999. Observations of sediment flux to the Eel continental slope, northern California. Mar. Geol. 154, 55-68.

Walsh, J. P., Nittrouer, C. A., 2009. Understanding fine-grained river-sediment dispersal on continental margins. Mar. Geol. 263, 34-45.

Walsh, J. J., Rowe, G. T., Iverson, R. L., McRoy, C. P., 1981. Biological export of shelf carbon is a sink of the global CO2 cycle. Nature 291, 196-201.

Walsh, J. J., Biscaye, P. E., Csanady, G. T., 1988. The 1983-1984 Shelf Edge Exchange Processes (SEEP)-1 experiment: hypotheses and highlights. Cont. Shelf Res. 8, 435-457.

Watling, L., Norse, E. A., 1998. Disturbance of the Seabed by Mobile Fishing Gear: A Comparison to Forest Clearcutting. Conserv. Biol. 12, 1180–1197.

Watson, R. A., Morato, T., 2013. Fishing down the deep: Accounting for within-species changes in depth of fishing. Fish. Res. 140, 63–65.

Watson, R. A., Tidd, A., 2018. Mapping nearly a century and a half of global marine fishing: 1869-2015. Mar. Policy 171-177.

WET Labs, 2011. Sea-Bird Electronics Inc., Transmissometer C-Star User's Guide Revision V Dec. 2011.

White, M., Ullgren, J., Goodjin, L., Mohn, C., 2008. Appendic I RV Celtic Voyager CTD User's Guide. Department of Earth and Ocean Sciences, NUI Galway.

Whitney, F., Robert, M., 2002. Structure of Haida eddies and their transport of nutrient from coastal margins into the NE Pacific Ocean. J. Oceanogr. 58, 715-723. https://doi.org/10.1023/A:1022850508403.

Whitney, F. A., Crawford, W. R., Harrison, P. J., 2005. Physical processes that enhance nutrient transport and primary productivity in the coastal and open ocean of the subarctic NE Pacific. Deep Sea Res. Part II Top. Stud. Oceanogr. 52, 681-706.

Whitney, F. A., Freeland, H. J., Robert, M., 2007. Persistently declining oxygen levels in the interior waters of the eastern subarctic Pacific. Prog. Oceanogr. 75, 179-199.

Whitt, C., Parlman, J., Polagye, B., Caimi, F., Muller-Karger, F., Copping, A., Spence, H., Madhusudhana, S., Kirkwood, W., Grosjean, L., Fiaz, B. M., Singh, S., Singh, S., Manalang, D., Sen Gupta, A., Maguer, A., Buck, J. J. H., Marouchos, A., Atmanand, M. A., Venkatesan, R., Narayanaswamy, V., Testor, P., Douglas, E., de Halleux, S., Khalsa, S. J., 2020. Future vision for autonomous ocean observations. Front. Mar. Sci. 7, 697.

Wilson, A. M., Raine, R., Mohn, C., White, M., 2015a. Nepheloid layer distribution in the Whittard Canyon, NE Atlantic margin. Mar. Geol. 367, 130-142.

Wilson, A. M., Kiriakoulakis, K., Raine, R., Gerritsen, H. D., Blackbird, S., Allcock, A. L., White, M., 2015b. Anthropogenic influence on sediment transport in the Whittard Canyon, NE Atlantic. Mar. Pollut. Bull. 101, 320–329.

Wilson, A. M., 2016. Lateral transport of suspended particulate matter in nepheloid layers along the Irish continental margin–A case study of the Whittard Canyon, North-East Atlantic Ocean. (Doctoral dissertation, National University of Ireland).

Wollast, R., 1998. Evaluation and comparison of the global carbon cycle in the coastal zone and in the open ocean. In The Sea (Eds.) K. H., Brink and A. R., Robinson. Wiley & Sons (1998), pp. 213-252.

Wollast, R., Chou, L., 2001a. Ocean Margin Exchange in the Northern Gulf of Biscay: OMEX I. An introduction. Deep Sea Res. II Top. Stud. Oceanogr. 48, 2971-2978.

Wollast, R., Chou, L., 2001b. The carbon cycle at the ocean margin in the northern Gulf of Biscay. Deep Sea Res. II Top. Stud. Oceanogr. 48, 3265-3293.

Wooster, W. S., Hollowed, A. B., 1995. Decadal-scale variations in the eastern subarctic Pacific: 1. Winter ocean conditions. Can. Spe. Fish. Aquat. Sci. 81-85.

Xu, J. P., 2011. Measuring currents in submarine canyons: Technological and scientific progress in the past 30 years. Geosphere 7, 868-876.

Xu, J. P., Noble, M., Eittreim, S. L., Rosenfeld, L. K., Schwing, F. B., Pilskaln, C. H., 2002. Distribution and transport of suspended particulate matter in Monterey Canyon, California. Mar. Geol. 181, 215-234.

Yada, T., Namba, N., Ura, T., 2004. Proceedings OCEANS'04 MTS/IEEE TECHNO-OCEAN'04, Kobe, Japan, IEEE Catalogue No. 04CH37600C, pp. 2365.

Zenk, W., 2008. Abyssal and contour currents. Developments in Sedimentology, 60, 35-57.

Zheng, G., DiGiacomo, P. M., 2017. Uncertainties and applications of satellite-derived coastal water quality products. Prog. Oceanogr. 159, 45-72.

Zúñiga, D., Flexas, M. M., Sanchez-Vidal, A., Coenjaerts, J., Calafat, A., Jordà, G., García-Orellana, J., Puigdefàbregas, J., Espino, M., Sardà, F., Company, J. B., 2009. Particle fluxes dynamics in Blanes submarine canyon (Northwestern Mediterranean). Prog. Oceanogr. 82, 239-251.

Appendix

List of Figures

List of Tables

List of Abbreviations

ABIDES: Assessment of Bottom-trawling Impacts in DEep-sea Sediments

ADCP: Acoustic Doppler Current Profiler

AIS: Automatic Identification System

ALPS: Aleutian Low-Pressure System

AW: Atlantic Water

BNL: Bottom Nepheloid Layer

BUS: Barkley Upper Slope

CARIACO: CARbon Retention in A Colored Ocean

CC: California Current

CDW: Circumpolar Deep Water

CIW: Cretan Interemediate Water

COSYNA: Coastal Observing System for Northern and Arctic Seas

CPUE: Catch Per Unit Effort

CTD: Conductivity, Temperture, Depth

CUC: California Undercurrent

CWM: Clear Water Minimum

DMAS: Data Management and Archive Station

DO: Dissolved Oxygen

DSW: Dense Shelf Water

DSWC: Dense Shelf Water Cascading

ECOFER: ECOsystem du canyon du cap FERret

ECOMARGE: ECOsystèmes des MARGEs continentales

EM: Expectation-Maximization

ENPTW: Eastern North Pacific Transition Water

EPA: Environmental Protection Agency

FORMED: FORmas de fondo y su dinámica actual en el margen continental MEDiterráneo español

FTU: Formazin Turbidity Units

GFS: Global Forecast System

GPS: Global Positioning System

GPSC: Gross Particulate Standing Crop

HEBBLE: High Energy Benthic Boundary Layer Experiment

HERMIONE: Hotspot Ecosystem Research and Man's Impact ON European seas

Hs: Significant Wave Height

IMO: International Maritime Organization

INL: Intermediate Nepheloid Layer

ISO: International Organization for Standardization

LIW: Levantine Intermediate Water

MARS: Monterey Accelerated Research System

MAW: Modified Atlantic Water

MedFlux: Mineral Ballast and Organic Matter Compositions as Determinants of Particle Setting Velocities and Fluxes in the Sea (Mediterranean Sea)

MU: Microcontroller Unit

NEPTUNE: North-East Pacific Time-Series Undersea Networked Experiments

NOAA WW3: NOAA Wavewatch III

NPSC: Net Particulate Standing Crop

NTU: Nephelometric Turbidity Units

OBS: Optical Backscatter Sensor

OMEX: Ocean Margin Exchange

ONC: Ocean Networks Canada

OTB: Otter Trawl Boards

PSIW: Pacific Subarctic Intermediate Water

PSUW: Pacific Suarctic Upper Water

ROV: Remoted Operated Vehicle

SEEP: Shelf Edge Exchange Processes

SEGEMAR: Segretaria General del Mar

SNL: Surface Nepheloid Layer

SPM: Suspended Particulate Matter

SOG: Speed Over ground

SOSUS: Sound Surveillance System

SSC: Suspended Sediment Concentration

SST: Sea Surface Temperature

STRATAFORM: STRATA FORmation on Margins

Tp: Primary wave mean period

VENUS: Victoria Experimental Network Under the Sea

VERTEX: VERtical Transport and Exchange

VMS: Vessel Monitoring System

VPS: Vertical Profiling System

WIW: Western Intermediate Water

WMDW: Western Mediterranean Deep Water

Θ: Mean wave direction

Supplementary information to Chapter 3

Table A.1. Weights (initial, dry, and averaged) of the Nucleopore membranes used in the laboratory calibration. The volume of water filtered for each turbidity reading, as well as the rendered SSC (in $mg \cdot L^{-1}$) obtained from dividing the weight of the dry residue by the volume of water filtered, are provided.

Filter code	Initial weight (g)	Averaged initial weight (g)	Dry weight (g)	Averaged dry weight (g)	Final weight (g)	Filtered volume (L)	SSC (mg L^{-1})
CALIB-01	0.01550	0.01550	0.01604	0.01604	0.00054	1	0.54
CALIB-01	0.01550		0.01603				
CALIB-02	0.01585	0.01586	0.01790	0.01790	0.00205	1	2.05
CALIB-02	0.01586		0.01790				
CALIB-03	0.0519		0.02018				
CALIB-03	0.01512	0.01515	0.02019	0.02018	0.00503	1	5.03
CALIB-03	0.01515		0.02018				
CALIB-04	0.01500		0.02046				
CALIB-04	0.01503	0.01501	0.02044	0.02045	0.00544	0.5	10.87
CALIB-04	0.01501		0.02045				
CALIB-05	0.01542		0.02590				
CALIB-05	0.01541	0.01541	0.02586	0.02589	0.01047	0.5	20.95
CALIB-05	0.01541		0.02590				
CALIB-06	0.01542		0.02851				
CALIB-06	0.01543	0.01543	0.02854	0.02851	0.01308	0.25	53.352
CALIB-06	0.01545		0.02849				
CALIB-07	0.01558		0.04582				
CALIB-07	0.01557	0.01557	0.04575	0.04576	0.03019	0.25	120.77
CALIB-07	0.01556		0.04572				
CALIB-08	0.01533		0.07319				
CALIB-08	0.01534	0.01533	0.07318	0.07317	0.05784	0.25	231.35
CALIB-08	0.01532		0.07313				
CALIB-09	0.01550		0.15612				
CALIB-09	0.01550	0.01550	0.15614	0.15611	0.14061	0.25	562.44
CALIB-09	0.01551		0.15608				

Scientific output related to this Thesis

Journal of Marine Systems 196 (2019) 86–96

Contents lists available at ScienceDirect

Journal of Marine Systems

journal homepage: www.elsevier.com/locate/jmarsys

Evidence of trawling-induced resuspension events in the generation of nepheloid layers in the Foix submarine canyon (NW Mediterranean)

Marta Arjona-Camas[a,b,*], Pere Puig[a], Albert Palanques[a], Mikhail Emelianov[a], Ruth Durán[a]

[a] Institute of Marine Sciences, CSIC, Passeig Maritim de la Barceloneta, 37-49, 08003 Barcelona, Spain
[b] Department of Earth and Ocean Dynamics, University of Barcelona, c/Martí Franquès s/n, 08028 Barcelona, Spain

ARTICLE INFO

Keywords:
Submarine canyon
Sediment transport
Nepheloid structure
Bottom trawling
Resuspension
Northwestern Mediterranean

ABSTRACT

The temporal evolution of water column turbidity was studied on a submarine canyon on the Barcelona continental margin. From April to June 2014, an instrumented mooring array equipped with an autonomous hydrographic profiler with a CTD and a turbidimeter was deployed in the Foix canyon axis at 870 m depth. The instruments were programmed to collect hydrographic profiles once per day to provide a view of the temporal evolution of water column characteristics from 200 to 800 m water depth. The results illustrate a well-defined water turbidity structure of particulate matter distributed in intermediate nepheloid layers (INLs) developed between 300 and 500 m water depth and above the canyon rims, and INLs and near-bottom nepheloid layers (BNLs) confined inside the canyon between 650 and 800 m water depth. Data from fishing vessels activity at the time of the deployment was obtained from Vessel Monitoring System (VMS). The presence and location of the fishing vessels in the study area suggested a relationship between trawling activity and the generation of such layers. Nepheloid layers were absent during the first part of the deployment, when there was no fishing activity within the Foix Canyon axis or at the adjacent continental slope. Later, with the beginning of trawling activity on the fishing grounds close to the canyon, both INLs and BNLs were observed in the profiling casts, suggesting a causative relationship with fishing activities. Additionally, the hydrodynamic conditions within the canyon also seem to favour particle retention and to increase water turbidity in thick BNLs when water circulation is directed up-canyon. Bottom trawling appears to act as a main sediment resuspension mechanism in the Barcelona continental slope regions, increasing suspended sediment concentration at specific water depths where fishing grounds are located. Suspended particles are then advected and propagate along and across-margin by ambient currents via nepheloid layers.

1. Introduction

The transport of matter and energy from the upper ocean to the seafloor is especially important in continental margins due to the large material inputs from both terrestrial sources and high productivity coastal waters (Walsh, 1991). Particulate matter is often introduced into the ocean by biological production, riverine and aeolian supplies or glaciers (Gardner et al., 1990; Gardner and Walsh, 1990). Once in the water column, the distribution of suspended particulate matter strongly depends on the regional and physical conditions, as well as the hydrographic structure and the hydrodynamic processes. Particularly, physical gradients, such as thermoclines or density fronts, and geostrophic currents are some of the most common factors controlling particulate matter distribution and exchanges in the water column (Palanques and Biscaye, 1992; Spurgin and Allen, 2014). Additionally, topographic structures, such as submarine canyons incising continental margins, can promote complex hydrographic and sedimentary conditions that also favour the transport of material from the continental shelves to deeper environments (Gardner, 1989; Puig et al., 2001; Canals et al., 2013; Puig et al., 2014; Wilson et al., 2015a).

Nepheloid layers (i.e., cloudy layers within the water column with high concentrations of suspended particulate material compared with the surrounding clear waters) are considered as the diluted product of sediment transport processes and are significant contributors to the shelf-slope exchanges of material (McCave, 1986; Amin and Huthnance, 1999; Wilson et al., 2015a, 2015b). They are formed by a balance of settling and resuspension processes and are considered as important lateral transporters of sediments and organic matter (Amin and Huthnance, 1999; Wilson, 2016). These turbid layers can regularly be observed at the upper ocean, where they form surface nepheloid layers

* Corresponding author.
E-mail address: marjona@icm.csic.es (M. Arjona-Camas).

https://doi.org/10.1016/j.jmarsys.2019.05.003
Received 2 August 2018; Received in revised form 8 February 2019; Accepted 14 May 2019
Available online 17 May 2019

(SNLs), and very often near the seabed, forming bottom or benthic nepheloid layers (BNLs). Additionally, they can be detected along isopycnals at different water depths as intermediate nepheloid layers (INLs) (Dickson and McCave, 1986; McCave, 1986; Puig et al., 2004; Karageorgis et al., 2017).

In deep-sea environments (> 200 m water depth), the energy associated with internal waves has been hypothesized as the main mechanism that initiates periodic sediment resuspension on continental margins and slopes as well as within submarine canyons (Cacchione and Drake, 1986). Bottom shear stress caused by internal waves can be large enough to resuspend sediment over these areas, and lead to the formation of localised intermediate and bottom nepheloid layers at certain depths (McCave, 1986; Cacchione and Drake, 1986; Gardner, 1989; Puig et al., 2004). However, bottom fishing activities can resuspend as well surface sediments and contribute to the transport of suspended particles (e.g. Durrieu de Madron et al., 2005; Martín et al., 2014a; Palanques et al., 2014; Linders et al., 2017), since the trawling gear produces relative high bed shear stress and high turbulence when it interacts with the seabed (O'Neill and Summerbell, 2011). As such, in certain continental margins, deep-sea trawling has been recognized as an important source of suspended material over slope regions (e.g. Chronis et al., 2000; Puig et al., 2012; Wilson et al., 2015b; Daly et al., 2017), being able to overcome natural processes as the main mechanism of sediment resuspension.

On the Barcelona continental margin (NW Mediterranean), Puig and Palanques (1998a) described the general pattern of water column suspended particles distribution. This study revealed that particulate matter was consistently distributed in surface, intermediate and near-bottom nepheloid layers that were related to topographic and hydrographic structures. These authors suggested natural processes (i.e., internal waves' activity focussed along the permanent shelf-slope density front) as the main mechanisms that could contribute to form and maintain these nepheloid layers. Nonetheless, in the NW Mediterranean margin, deep-sea trawling activities have been identified as an important mechanism causing resuspension and erosion of sediments from fishing grounds (Puig et al., 2012; Martín et al., 2014b; Pusceddu et al., 2014). This mechanism has caused increased sediment accumulation rates within several submarine canyon axes of this margin since the 1960–70s, as a result of the expansion and industrialization of the trawling fleets at that time (Martín et al., 2008; Puig et al., 2015; Paradis et al., 2017). In the Foix submarine canyon (Fig. 1), Paradis et al. (2018) reported recent sediment accumulation rates from a core collected in 2013 at the canyon axis at 860 m depth, and compared them with a sediment core retrieved in 1993 at the same location (Sanchez-Cabeza et al., 1999). At this site, it was recorded an almost two-fold increase in the sedimentation rates in the 1960–70s, from 0.5 cm/y to 0.9 cm/y, and a further increase (up to 1.8 cm/y) in the early 2000s, after a new renewal of the trawling fleet (Paradis et al., 2018).

In the present paper, we aim to assess the role of trawling fisheries in resuspending bottom sediments within the Foix Canyon and discuss the implications of trawl-induced resuspension events in the generation of nepheloid layers in the NW Mediterranean margin. With this purpose in mind, from April to June 2014, a mooring array equipped with an autonomous hydrographic profiler was deployed at the Foix canyon axis at a water depth of 870 m, a slightly deeper location that the maximum working depth of the local trawling fleet. Vessel Monitoring System (VMS) was used in order to assess the position of fishing vessels at the time of the instrumented mooring deployment.

2. Materials and methods

2.1. Study area

The Foix Canyon system is located in the Catalan margin a few kilometres south of Barcelona (Fig. 1). This canyon incises the shelf-break at 90 m depth and moulds the seafloor down to its confluence with the Valencia channel at a water depth of 2180 m (Canals et al., 2013; Tubau et al., 2013). It consists of two sinuous branches, the eastern Foix and the western Foix branches, that conjoin at 1340 m water depth (Tubau et al., 2013). The canyon cross section at its eastern branch is V-shaped along the first 3.7 km and is defined by an axial incision, while the western branch is U-shaped, characterized by the presence of small tributaries and sedimentary instabilities (Alonso et al., 1984; Tubau et al., 2013). On the upper slope, its steep walls can reach heights of 400 m and maximum gradients of 23° at the mid canyon (Alonso et al., 1984). It also becomes narrow with depth, decreasing from 4 km at the shelf-break to 2 km at a depth of 1200 m (Fig. 1).

This canyon intercepts particulate matter from the continent and acts as a preferential conduit for such sediments to the slope during sporadic events such as storms or river discharges (Puig and Palanques, 1998b). It is influenced by the geostrophic circulation of the Liguro-Provençal-Catalan current (NW Mediterranean), that flows towards the southwest and along the continental slope (Millot, 1999; Font et al., 1988).

Current speed fluctuations along this canyon are mainly controlled by the local inertial motion and by low-frequency oscillations (from 6 to 10 days) linked to meteorological forcing conditions (Puig et al., 2000). Near-bottom currents recorded inside the canyon are highly constrained by the canyon topography, and are mainly oriented along the canyon axis both in the up- and down-canyon directions, although at the canyon head currents do not display such a clear trend of up- and down-canyon alternations. In intermediate waters at the slope depths, currents are mainly oriented along the margin towards the southwest, according to the main flow direction of the geostrophic circulation (Puig et al., 2000).

The fisheries that at present are economically more important on the Catalan continental margin take place on slope fishing grounds and are targeting the Norway lobster *Nephrops norvegicus* at depths ~300–500 m, and the blue and red deep-sea shrimp *Aristeus antennatus*, at depths ~600–900 m (Sardà et al., 1994; Lleonart, 1990; Maynou et al., 1998). The spatial distribution of these two main fishing grounds in some areas can be easily recognized in the bottom trawling footprint of Fig. 1. The Foix Canyon and its surrounding waters are mainly frequented by trawling vessels from Vilanova i la Geltrú and Barcelona harbours (Fig. 1). The local fleets on the study area operate on a daily basis during weekdays, from 7 a.m. to 4 p.m., remaining at the harbours on weekends, holidays and local festivities.

2.2. Time-series observations

From April to June 2014, a total of 58 hydrographic profiles were obtained by an instrumented mooring array equipped with an autonomous hydrographic profiler (Aqualog) deployed in the Foix canyon axis (41° 05.55820′ N; 001° 55.58104′ E) at 870 m depth (Figs. 1, 2). The Aqualog moves up and down along a fixed vertical line at a fixed position at programmed frequencies, collecting regular profiles over a large depth range at high temporal and vertical resolutions (Ostrovskii et al., 2013; Kershaw and Liu, 2015; Solé et al., 2016). In this deployment, the Aqualog profiler was programmed to perform one up- and down-cast per day at 12 a.m., profiling from 800 m to 200 m, and back to 800 m (parking depth), at a relative speed of 25 cm/s. Every up- and down-cast took approximately 1 h to be completed. The profiler was equipped with a SeaBird 19 plus v2 CTD probe configured to measure temperature, salinity and pressure at 1 second intervals. Temperature and salinity were used to characterize the hydrographic structure of the study site. The profiler was also equipped with a SeaPoint turbidity sensor, programmed to measure turbidity, expressed in mV, at 1 second intervals. The sensor gain was set at 0–5 V, and a range of 0–25 FTU. The readings were transformed into Formazin Turbidity Units (FTU), and since water samples were not taken for calibration, reported values

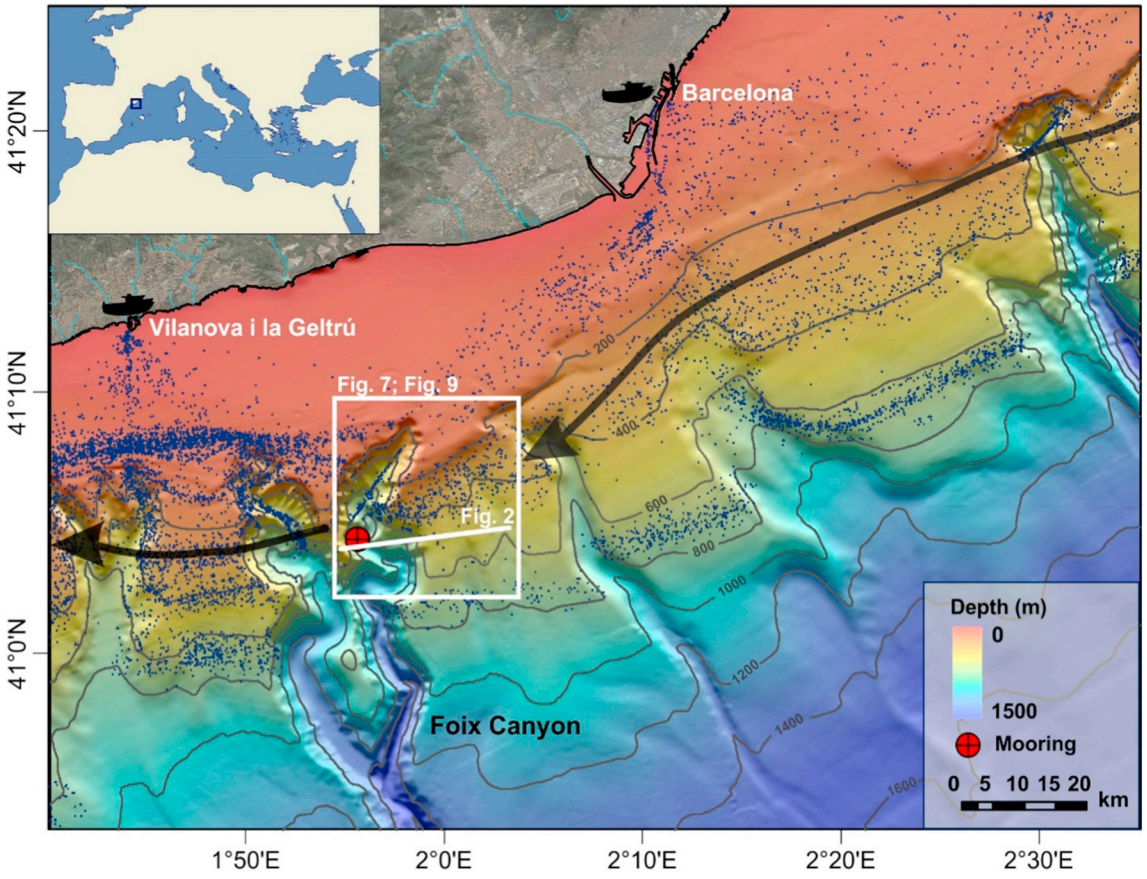

Fig. 1. Bathymetric map of the Catalan margin (NW Mediterranean) showing the location of the Foix Canyon, and the main fishing grounds and harbours. The red dot indicates the position of the mooring array used in this study. Blue dots represent Vessel Monitoring System (VMS) positions of trawlers during the monitoring period and the black arrow represents the geostrophic current. The white line depicts the transect showed in Fig. 2. (For interpretation of the references to colour in this figure legend, the reader is referred to the web version of this article.)

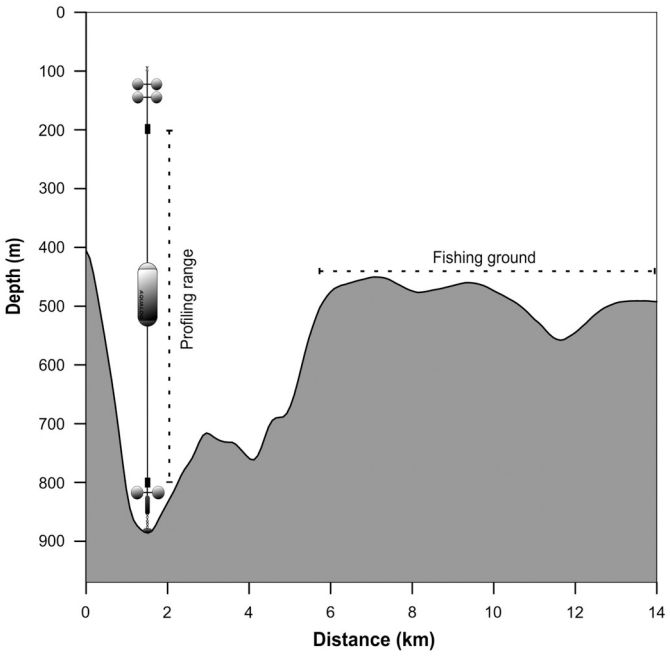

Fig. 2. Bathymetric cross section and scheme of the mooring array deployed at the Foix canyon axis. See location in Fig. 1.

were converted to estimates of suspended sediment concentration (SSC) in mg/L using the general calibration of Guillén et al. (2000) for the Western Mediterranean. Estimates of SSC values were reported above a background concentration corresponding to the clear water minimum of each profile.

To proceed with a homogenous methodology for all parameters, all the data was interpolated to 1 m vertical resolution, obtaining a matrix for the whole sampling period composed of 58 down-casts. The measured and calculated parameters were represented using Ocean Data View (ODV) software (Schlitzer, 2010).

According to the bathymetric section in Fig. 2 and the Aqualog profiling range, and based on the position of the canyon rims and the position of trawlers throughout the monitoring period, data was described and analysed considering two depth ranges: 1) canyon-unconfined waters (depths between 200 and 500 m) and 2) canyon-confined waters (depths > 500 m).

2.3. Computation of the net particulate standing crop

A depth-average vertical integration of SSC was computed to calculate the net particulate standing crop on each down-cast (Fig. 3). This parameter was calculated for the concentration excess over the value of the clear water minimum on each cast and integrated over the height of the profiling range following:

$$Net\ particulate\ standing\ crop = \frac{1}{h}\int_0^h SSC\ (z)\ dz$$

where h is the depth of the considered water column and $SSC\ (z)$ represents the estimated SSC values, in mg/L (Karageorgis and

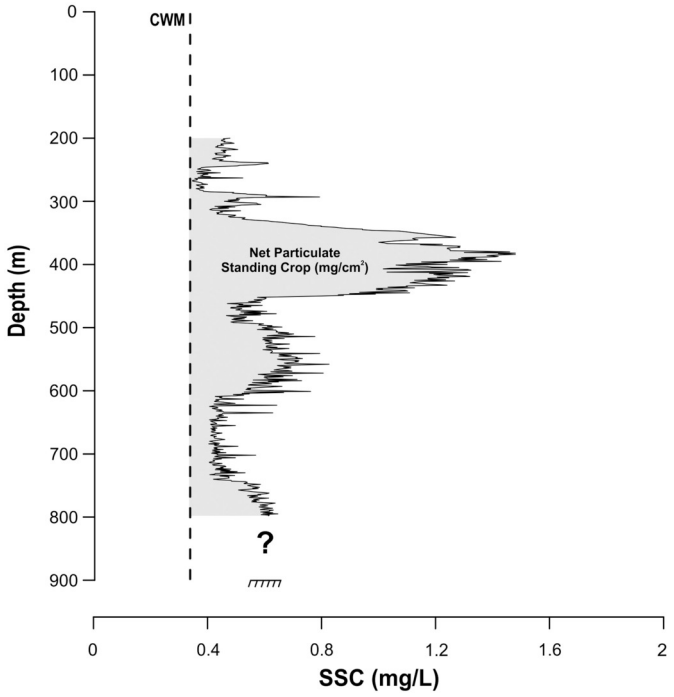

Fig. 3. Example of a suspended sediment concentration (SSC) profile with a strong nepheloid layer. The suspended matter which is in excess of the clear water minimum (CWM) concentrations represents the net particulate standing crop (mg/cm^2) (grey-coloured area). SSCs below 800 m are not shown due to the limited working range of the Aqualog (see Fig. 2).

Anagnostou, 2003).

The net particulate standing crop provides an estimation of the input of particles introduced in the water column from bottom resuspension. This estimation differs from the original methodology used by Biscaye and Eittreim (1977), as these authors defined this parameter in oceanic waters for BNLs, as the suspended matter which is found below the clear water minimum. Here, we also took into account the contribution of INLs at various levels in the water column (Fig. 3).

2.4. Fishing fleet data

The activity of the fishing vessels operating in the Foix Canyon fishing grounds near the mooring location was obtained from the Fishing Monitoring Centre of the Spanish General Secretariat of Maritime Fishing (SEGEMAR) through Vessel Monitoring System (VMS). Vessels with VMS provide their position using Global Positioning System (GPS) and transmit this information in approximately 10 min at intervals of 2 h or less. This system also gives vessels' direction and speed, which is also useful to determine whether they are sailing, fishing or drifting.

However, VMS data for research and impact assessment has some limitations, including incomplete coverage of vessel activities, long durations between position records, and a lack of information on whether a vessel is actually fishing when the position is recorded. Hence, it is necessary to make assumptions and interpretations when using VMS data as the principal source of information on fishing activities (Lambert et al., 2012).

The recorded VMS for the period from April 6 to June 2 included vessels' position, heading and speed measurements, port of origin and ID code. The total records for this period were reduced to those fitting the criteria for trawling activity. VMS data were filtered by speed (< 5

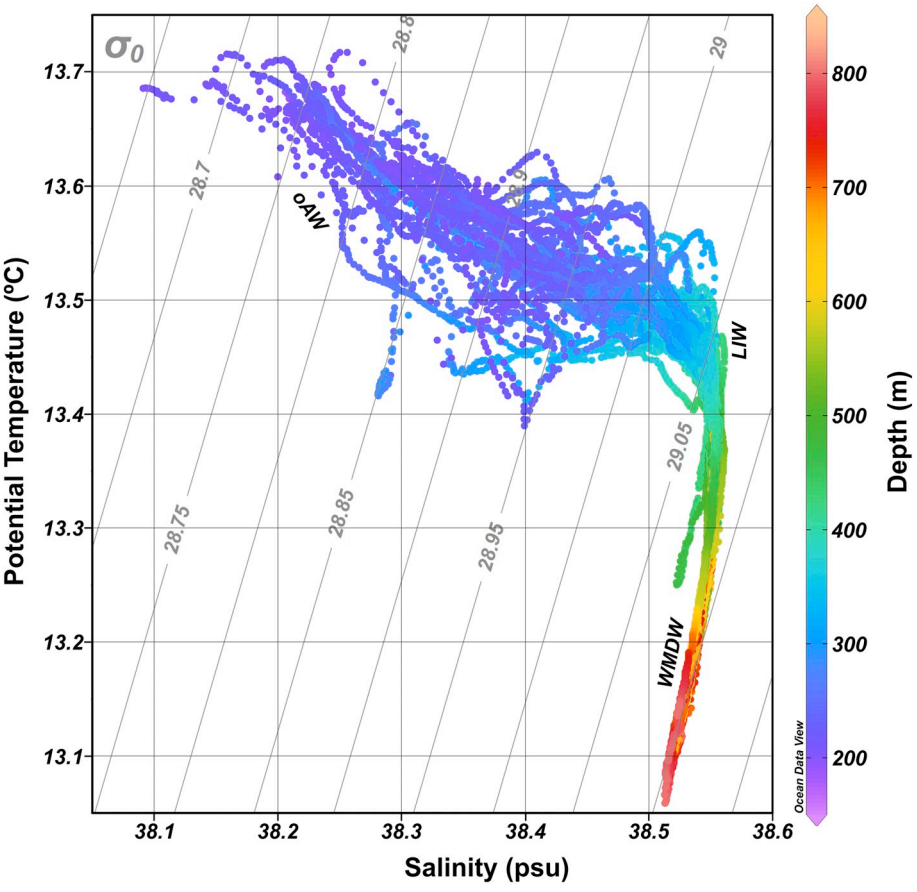

Fig. 4. General θ-S diagram for all the CTD casts sampled in April–June 2014 (oAW: Old Atlantic Waters; LIW: Levantine Intermediate Waters; WMDW: Western Mediterranean Deep Waters). Colour scale indicates the depth (m). (For interpretation of the references to colour in this figure legend, the reader is referred to the web version of this article.)

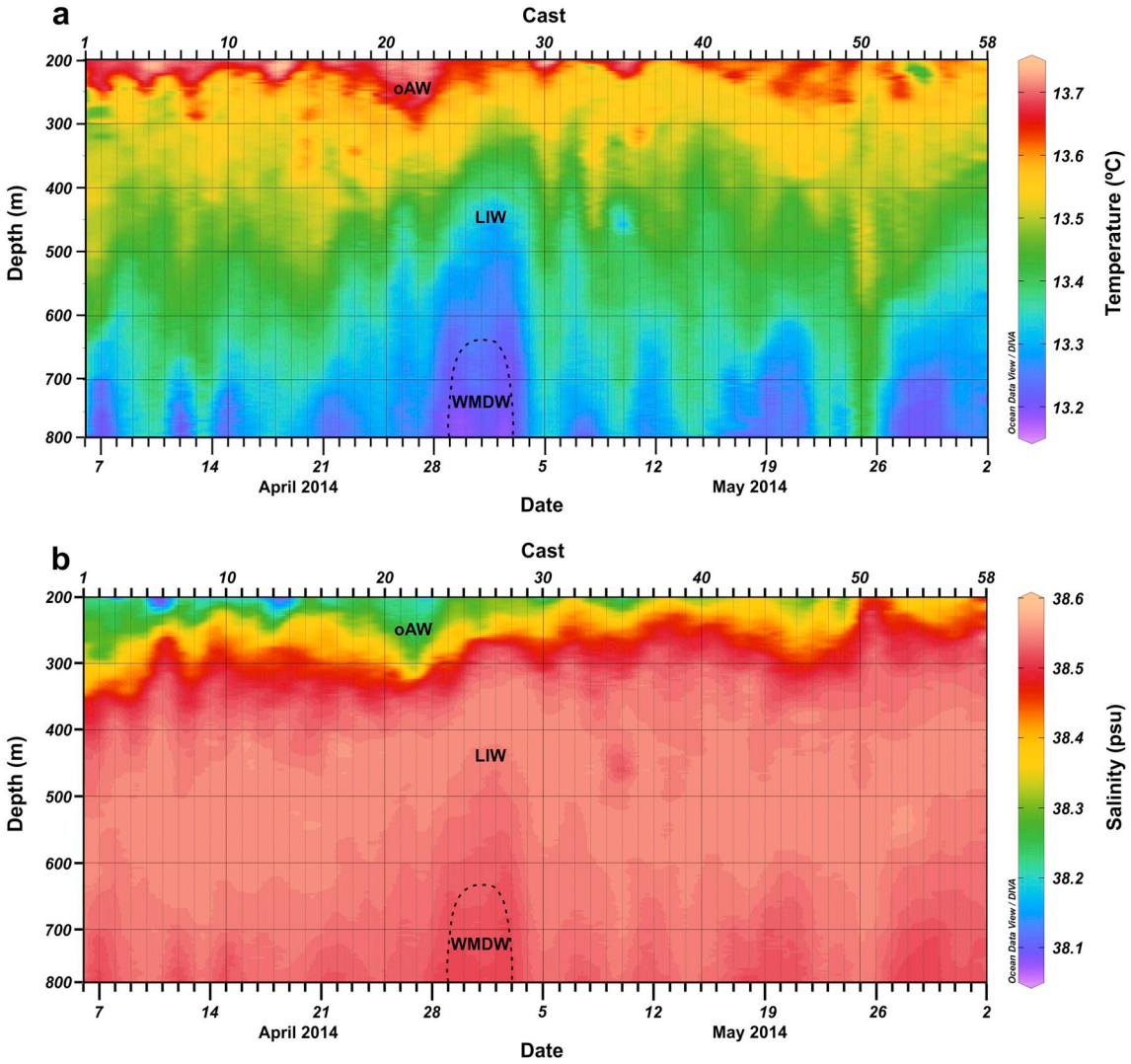

Fig. 5. Temporal variability of the vertical distribution of a) potential temperature, ˚C, and b) salinity, psu. (For interpretation of the references to colour in this figure legend, the reader is referred to the web version of this article.)

knots), allowing the identification of the vessels while fishing and not while navigating towards the harbour or other fishing grounds. Additionally, VMS data points were also filtered by working depth (> 200 m) to match the Aqualog profiling range. The total number of hauls were also considered, as they are an indicator of the times that a trawler tows an area and, hence, of trawlers' capacity to resuspend bottom sediments (Ragnarsson and Steingrímsson, 2003; Martín et al., 2014a). Finally, fishing vessels position at the study site was represented and plotted using ArcGis© v. 10.3.

3. Results

3.1. Hydrographic structure

Compiled data of all CTD casts revealed the presence of the three water masses permanently found in the NW Mediterranean basin, clearly distinguished by their characteristic potential temperature and salinity profiles (Fig. 4).

The shallowest waters (200–350 m water depth) were occupied by relatively warm (13.6–13.7 ˚C) and low salinity (38.0–38.2 psu) old Atlantic Waters (oAW) (Figs. 4, 5a, b). Below (350–600 m water depth), the θ-S diagram showed the more saline Levantine Intermediate Waters (LIW), characterized by both temperature and salinity relative maxima of 13.75 ˚C, and 38.55 psu, respectively (Figs. 4, 5a, b). The deepest waters (600–800 m water depth) were occupied by Western Mediterranean Deep Waters (WMDW) that exhibited temperature relative minima of 13.0 ˚C and salinity values between 38.4 and 38.55 psu (Figs. 4, 5a, b). The seasonal Western Intermediate Water (WIW), occasionally found between the oAW and the LIW, was absent in the profiles (see https://www.ciesm.org/catalog/WaterMassAcronyms.pdf for more details).

Overall, temperature and salinity showed fluctuations of a hundred meters in depth throughout the 58 days of sampling, displaying a periodicity of 4–10 days (Fig. 5a, b). Several up-canyon water intrusions were also observed. The most relevant was detected from April 29 to May 3, when a cold (13 ˚C) and relatively less salty (38.5 psu) pool of WMDW occupied the lowest part of the profiled water column (Fig. 5a, b).

3.2. Suspended particulate matter distribution

Fig. 6 shows the temporal variability in the distribution of the suspended sediment concentration (SSC) during the deployment. From April 6 to April 17, the vertical particulate matter distribution was quite homogenous and no SSC increases were observed in the profiled water column. From April 17, several increases of SSC (up to 1 mg/L) were

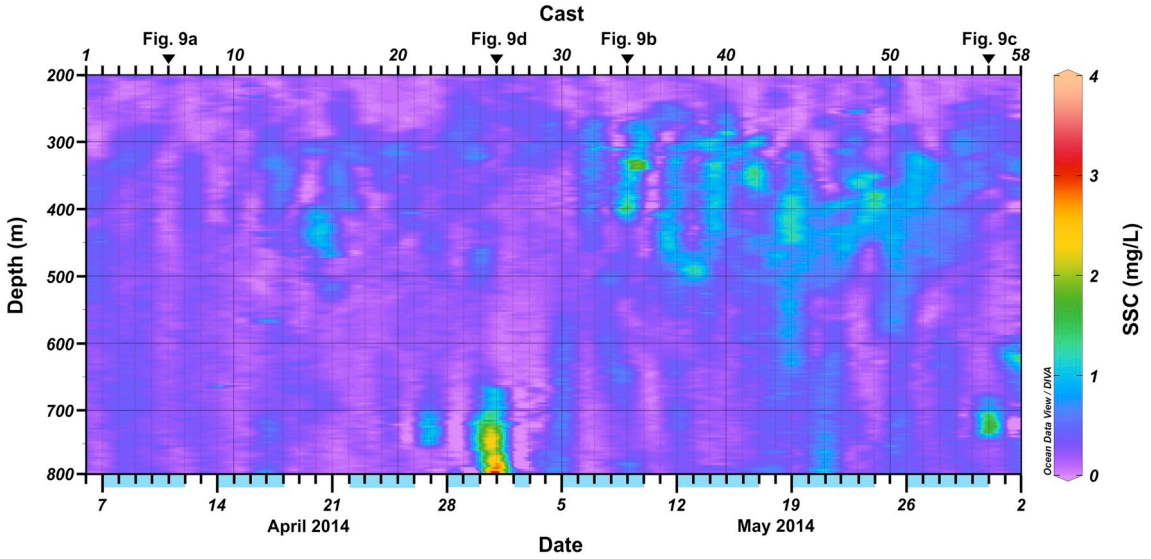

Fig. 6. Temporal variability of the distribution of the suspended sediment concentration (SSC) during the monitoring period. Fishing days are indicated as blue bars on the bottom x-axis. SSC vertical profiles which were examined (Fig. 9a, b, c, d) are also shown in this figure. (For interpretation of the references to colour in this figure legend, the reader is referred to the web version of this article.)

recorded at intermediate water depths (300–500 m), mainly centred at ~400 m. These increases corresponded to ~150 m-thick INLs developed at depths of canyon-unconfined waters (Fig. 2). Deeper INLs were recorded sporadically within the canyon confined waters at ~700 m water depth, being thinner (60–90 m) than the shallower ones and reaching estimated SSC up to 1.2 mg/L, as in the case of the profiles on April 27 (cast #22) or April 30 (cast #25).

On May 1, the occurrence of a relative high turbidity event was observed particularly at the lowest part of cast #26, which most probably continued below the profiling range, down to the seafloor, generating a ~150 m thick BNL. This layer displayed the highest concentrations for the whole sampling period, reaching estimated SSC of 3.8 mg/L at 77 m above the bottom (Fig. 6).

Afterwards, several INLs were detected through the second half of the recording period, mainly in the profiling range corresponding to canyon-unconfined waters (Fig. 6). These INLs were found at the same depth ranges (300–500 m) as observed in the first half of the sampling period, showing similar thickness, although during this part of the deployment they displayed higher estimates of SSC (1.1–1.6 mg/L). The distribution of the suspended particulate matter depicted the presence of a turbid water mass at intermediate depths that remained in the water column at least until the end of the experiment.

Within the canyon confined waters, no more significant near-BNLs were detected by the end of the experiment, but an INL was clearly noticeable at ~700 m water depth on May 31 (Fig. 6, cast #56). This deep INL was similar to one detected previously at the same depth range on April 27 (Fig. 6, cast #22). However, it was narrower (50 m thick) and had a maximum estimated SSC of 1.9 m/L (Fig. 6).

3.3. Trawling activity

During the experiment, VMS data showed that the fishing grounds around the Foix Canyon were exploited by 22 trawlers, mostly from Barcelona and Vilanova i la Geltrú harbours (Fig. 1). After speed and depth were filtered, vessels positions recorded by VMS appeared to follow the bathymetric contours and most of the trawling activity took place at 200–500 m water depth outside the canyon, along the fishing ground named *Can Pere Negre*, and at 600–800 m water depth inside the canyon, following the axis, along the fishing ground known as *Sant Salvador* (Figs. 1, 7, Lleonart, 1990).

The position of fishing vessels operating near the mooring site was plotted in detail, in six consecutive periods, each of them spanning 10 days of VMS data points except for the last one that lasted 8 days (Fig. 7). Table 1 summarizes the main characteristics of each period in terms of number of hauls and number of trawlers for the identified fishing grounds. Few isolated trawlers were observed to be fishing on the slope at depths > 600 m (Fig. 7), but since they were far from the mooring location, they have not been taken into account in this analysis.

Time-series observations on VMS data revealed nearly no trawling activity around the mooring site during the first period (Fig. 7a). Only 10 hauls were counted, corresponding to five active vessels that were working at the slope fishing ground (Table 1). No fishing activity was detected at the axis fishing ground (Table 1; Fig. 7a).

The remaining periods (Fig. 7b–f) were characterized by the presence of trawlers both at the axis and at the slope fishing grounds. During the second period, VMS data points were mostly clustered between the 200 m and the 500 m isobaths, suggesting that the majority of trawlers were working at the slope fishing ground (Table 1; Fig. 7b). Trawling activity throughout the third period remained similar to the previous period, although trawlers were concentrated at both the axis and the slope fishing grounds, but none of them were detected at depths > 400 m outside the canyon confinement (Fig. 7c). The number of trawlers and hauls was the same for both fishing grounds during this period (Table 1).

As far it concerns the last three periods, these were characterized by a relatively higher number of trawlers and hauls at both fishing grounds (Fig. 7d–f; Table 1). The majority of trawling activity was detected along the axis and the slope fishing grounds between the 200–500 m isobaths. Particularly, recordings for this second half of the survey showed that the highest number of hauls for both fishing grounds occurred during the fourth period (Fig. 7d; Table 1).

3.4. Relationship between net particulate standing crop and number of hauls

The number of hauls identified from the activity of trawlers operating nearby the Foix Canyon (Table 1) was used to infer trawlers' capacity to resuspend bottom sediments. Fig. 8 illustrates the relation between the net particulate standing crop for each hydrographic cast and the number of hauls identified from the activity of trawlers operating at around the Foix Canyon fishing grounds on the previous day. Two approaches were considered, first the net particulate standing crop

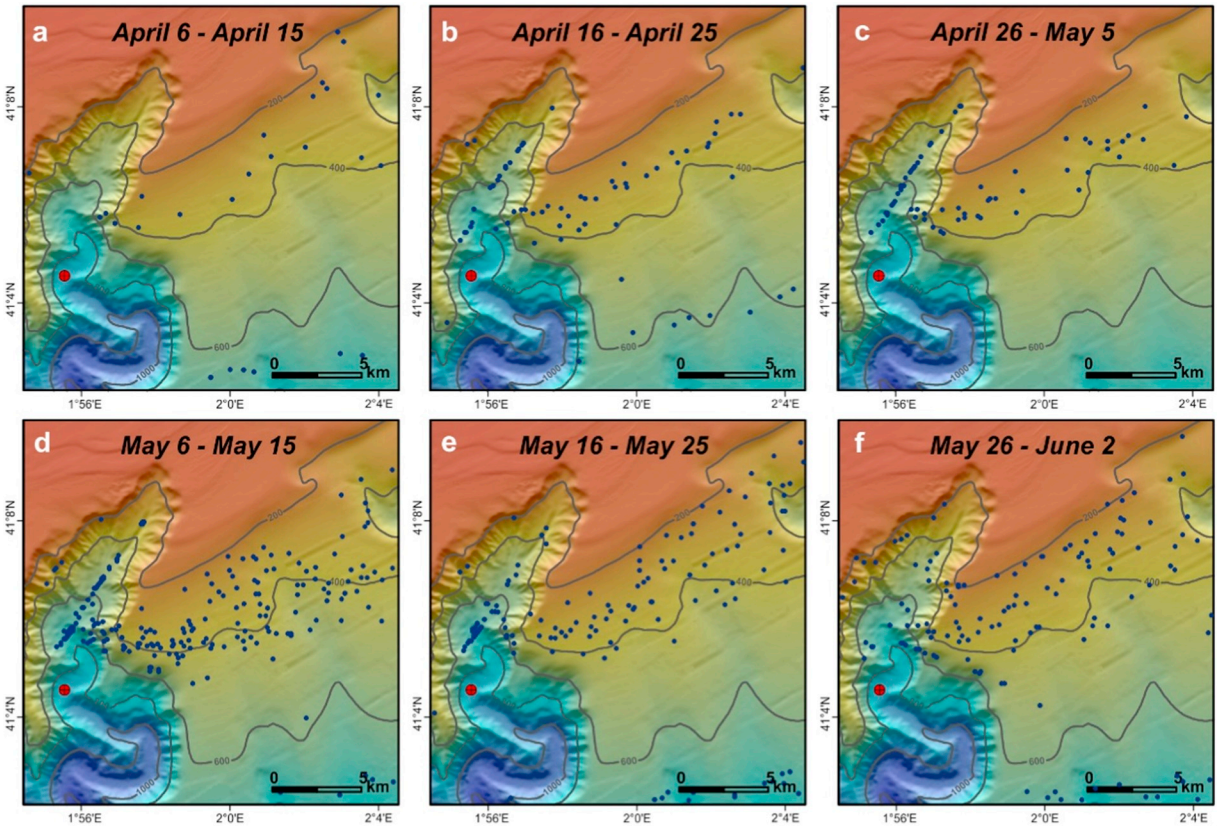

Fig. 7. Bathymetry of the eastern branch of the Foix Canyon and the main fishing grounds. The red dot indicates the position of the mooring array used in this study. Blue dots represent Vessel Monitoring System (VMS) positions of trawlers during the monitoring period (a: first period, April 6 to April 15; b: second period, April 16 to April 25; c: third period, April 26 to May 5; d: fourth period, May 6 to May 15; e: fifth period, May 16 to May 25; f: sixth period, May 26 to June 2). (For interpretation of the references to colour in this figure legend, the reader is referred to the web version of this article.)

Table 1
Main characteristics of the defined periods. Number of hauls (#) and number of trawlers (#) are presented for the identified fishing grounds. The first column indicates the correspondence with Fig. 7.

	Period	Date (2014)	Fishing ground			
			Slope		Axis	
			# trawlers	# hauls	# trawlers	# hauls
Fig. 7a	1	April 6–April 15	5	10	0	0
Fig. 7b	2	April 16–April 25	6	12	4	7
Fig. 7c	3	April 26–May 5	5	13	5	13
Fig. 7d	4	May 6–May 15	12	52	9	32
Fig. 7e	5	May 16–May 25	13	38	6	15
Fig. 7f	6	May 26–June 2	12	45	6	14

values of the entire hydrographic profiles (200–800 m depth) were plotted against the total number of hauls on the slope and within the canyon (Fig. 8a), and second, the net particulate standing crop of the profiled section outside the canyon confinement (200–500 m depth) was plotted against the hauls of the slope fishing ground (Fig. 8b).

Despite the small number of hydrographic profiles obtained during fishing days, due to the exclusion of data during weekends and holidays, the overall fit of the two variables is fairly good. The correlation coefficients for the regression models are noticeably small, but according to the *p-values* ($p < 0.05$), both relations are statistically significant. The *r value* for the relation between the net particulate standing crop at intermediate waters and the number of hauls at the slope (Fig. 8b), where the major fishing activity took place (Fig. 7; Table 1), is slightly bigger than for the relation between the computed standing crop for the entire profiled depth range and the total number of hauls (Fig. 8a).

4. Discussion

4.1. Evidence of trawling-induced nepheloid layers using VMS data

The nepheloid structure of the Barcelona continental margin was determined by Puig and Palanques (1998a) using data from three hydrographic surveys conducted in 1992–93. These results showed that suspended particulate matter was mainly distributed at surface, intermediate and near-bottom nepheloid layers, and that nepheloid layer detachments were related to hydrographic structures. The maximum suspended sediment concentrations observed in the area occurred at the Foix submarine canyon, more specifically, at intermediate depths (between 300 and 500 m) associated with a suggested permanent INL. This layer was also observed at the adjacent continental slope (Puig and Palanques, 1998a). According to these authors, this slope INL was controlled by the shelf-slope density front and by the Liguro-Provençal-Catalan current, and was probably re-fed by sediment particles from other submarine canyons incising the margin. Some authors (Cacchione and Drake, 1986; Gardner, 1989) explained that shoaling and breaking of internal waves could lead to the formation and maintenance of INLs and near-BNLs over certain slopes and continental shelves. Therefore, in the Foix submarine canyon it was also suggested that breaking of near-inertial internal waves at the upper slope could resuspend bottom sediments where the foot of the density front intersects with the seabed and, thus, feeding this slope INL (Puig and Palanques, 1998a).

During the present study, several particulate matter detachments were found at intermediate depths within the unconfined canyon waters, mainly centred at 400 m over the slope region (Fig. 6). Even

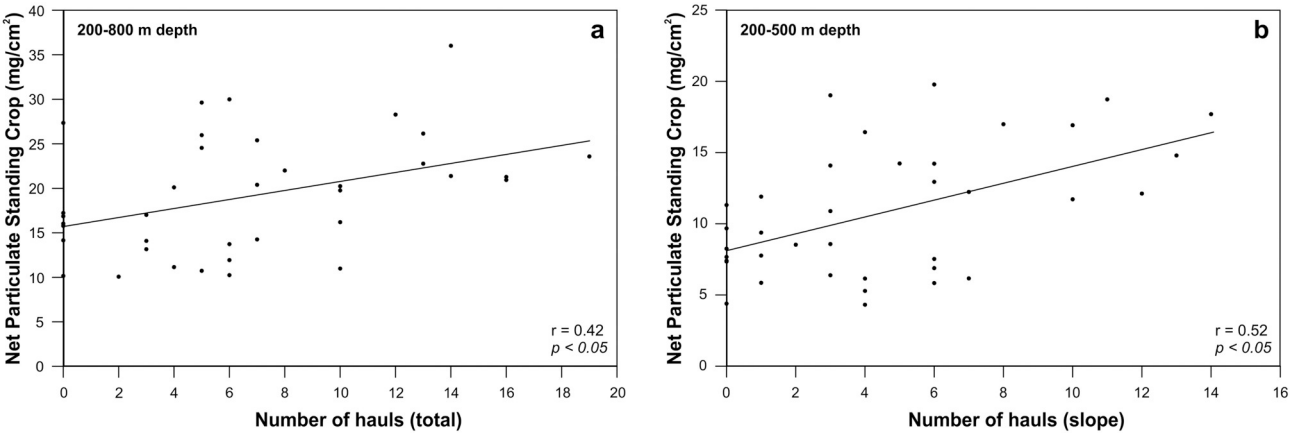

Fig. 8. Relation between net particulate standing crop (mg/cm^2) and number of hauls from trawlers operating nearby the mooring location at the fishing grounds around the Foix Canyon (see Table 1). Linear relationships are shown for the (a) total computed net particulate standing crop and the total number of hauls, considering those at the axis and at the slope fishing grounds, and for the (b) computed net particulate standing crop at the slope (between the 200 and 500 m isobath) and the number of hauls counted at the slope fishing ground. Only fishing days were used to calculate the standing crop in both cases (see blue bars on the bottom x-axis of Fig. 6 for the exact dates).

though the mechanism proposed by the latter authors involving internal waves' activity could be plausible, these slope INLs were not permanent and were just observed at specific time-spans throughout the sampling period (Fig. 6). The results presented in this study, when combined with data from fishing vessels positioning, suggest that trawling activity is likely responsible for most of the sediment resuspension that ultimately generates these INLs.

Analyses on VMS data revealed that all the observed nepheloid layers were detected during or after a period of trawling activity along the neighbouring fishing grounds of the Foix Canyon. When no particulate matter detachments were observed at the mooring location, particularly at the beginning of the monitoring period (Fig. 6), there was a low trawling activity at the neighbouring fishing grounds of the Foix Canyon (Fig. 7a). As an example, on April 9 there were no trawlers fishing near the mooring, neither at the slope nor at the axis fishing ground. At that time, the lowest suspended sediment concentration of the entire record was observed and VMS data identified a single trawler fishing at the 200 m depth isobath, far from the mooring location at shallower depths than the Aqualog profiling range (Fig. 9a). During the first 10-day period of monitoring (Fig. 7a), fishing activity was only detected on the slope fishing ground by 5 trawlers working at around the 400 m isobath (Table 1). This low trawling activity seems to be insufficient to induce any particulate matter detachments that could be subsequently detected by the Aqualog at the mooring site (Figs. 1, 7, 9a).

Throughout the monitoring period, the presence of a higher number of trawlers on the slope fishing ground coincided with the INLs centred at 400 m water depth observed in the hydrographic profiles (Fig. 6). For instance, the position of trawlers on May 8 coincided temporally and spatially with the observed INL on May 9 (Figs. 6, 9b). Other hydrographic profiles, corresponding to the same monitoring period (Figs. 6, 7d), showed similar SSC levels related to the presence of trawlers operating on the slope fishing ground (Fig. 6). In fact, higher net particulate standing crops at this depth range (200–500 m) responded to a major number of hauls at the same bathymetric range, hence, to a higher trawling activity at the slope fishing ground (Fig. 8b). Therefore, it seems plausible that all observed particulate matter detachments at these depths were generated by the same mechanism. Once resuspension is generated by trawling, the presence of the geostrophic current flowing towards the southwest (Fig. 1) could have favoured particle transport from the slope, where fishing vessels were located (Fig. 7d), towards the canyon-unconfined waters over the mooring array (Fig. 2). Therefore, the Aqualog could have detected these increases in SSC as particulate matter was being detached from the slope over the canyon rims. The positive relationship between the quantification of the net particulate standing crop of the profiled section outside the canyon confinement and the number of hauls on the slope fishing ground supports this hypothesis (Fig. 8b). Nevertheless, previous hydrographic transects conducted along the axis of this canyon suggest that these INLs could have also been detached from the canyon head region (see Fig. 11 in Puig and Palanques, 1998a), from resuspension of trawlers operating along the canyon axis. Therefore, due to the presence of trawlers working simultaneously at both fishing grounds (Fig. 7d; Table 1), it is difficult to determine where these INLs were exactly generated, and probably both sources of resuspended particles contributed to the observed INL detachments around 400 m water depth.

Within the canyon confinement, several deep INLs were also observed at ~700 m throughout the sampling period (Fig. 6). These confined INLs were recorded sporadically and displayed higher concentrations (~2 mg/L) than the slope unconfined INLs (Fig. 6). As an example, Fig. 9c illustrates the confined INL observed on May 31 at the time that two trawlers were operating at the axis fishing ground. The development of these deep INLs is likely related to the presence of trawlers working along the main axis fishing ground, which can reach greater depths than the hauls on the adjacent slope. In this case, the natural conduit of the canyon and the alternation up- and down-canyon current regime (Puig et al., 2000) could have helped retaining sediment particles in the canyon interior, as they remain outside the influence of the geostrophic flow that just affects canyon-unconfined waters (Fig. 2).

Within the canyon, a thick near-BNL was also detected on May 1 (Fig. 9d), displaying the highest SSCs of the sampling period. The high concentration and thickness of this layer seem to be related to an up-canyon intrusion of WMDW (Fig. 5a), that could have favoured the retention at this depth range of sediment particles resuspended at the canyon axis fishing ground. The vertical oscillations of the water masses observed during the deployment had a frequency of 4–10 days, which are in agreement with the periodicity of the near-bottom along-canyon flow reversals observed by Puig et al. (2000) in this canyon. Even so, our data do not allow us to determine the concentration of this BNL at depths > 800 m due to the limited working range of the Aqualog (Fig. 2). Nonetheless, the SSC profile (Fig. 9d) suggests that the concentration tends to increase with depth. This limitation also prevented us to detect other potential BNLs developed by trawling activities along the canyon axis and that could have been extending closer to the bottom, without reaching the lower operational depths of the Aqualog.

Overall, our findings support the idea that resuspension induced by trawling activities can play a significant role in increasing SSC levels in the water column within the Foix Canyon, causing higher net

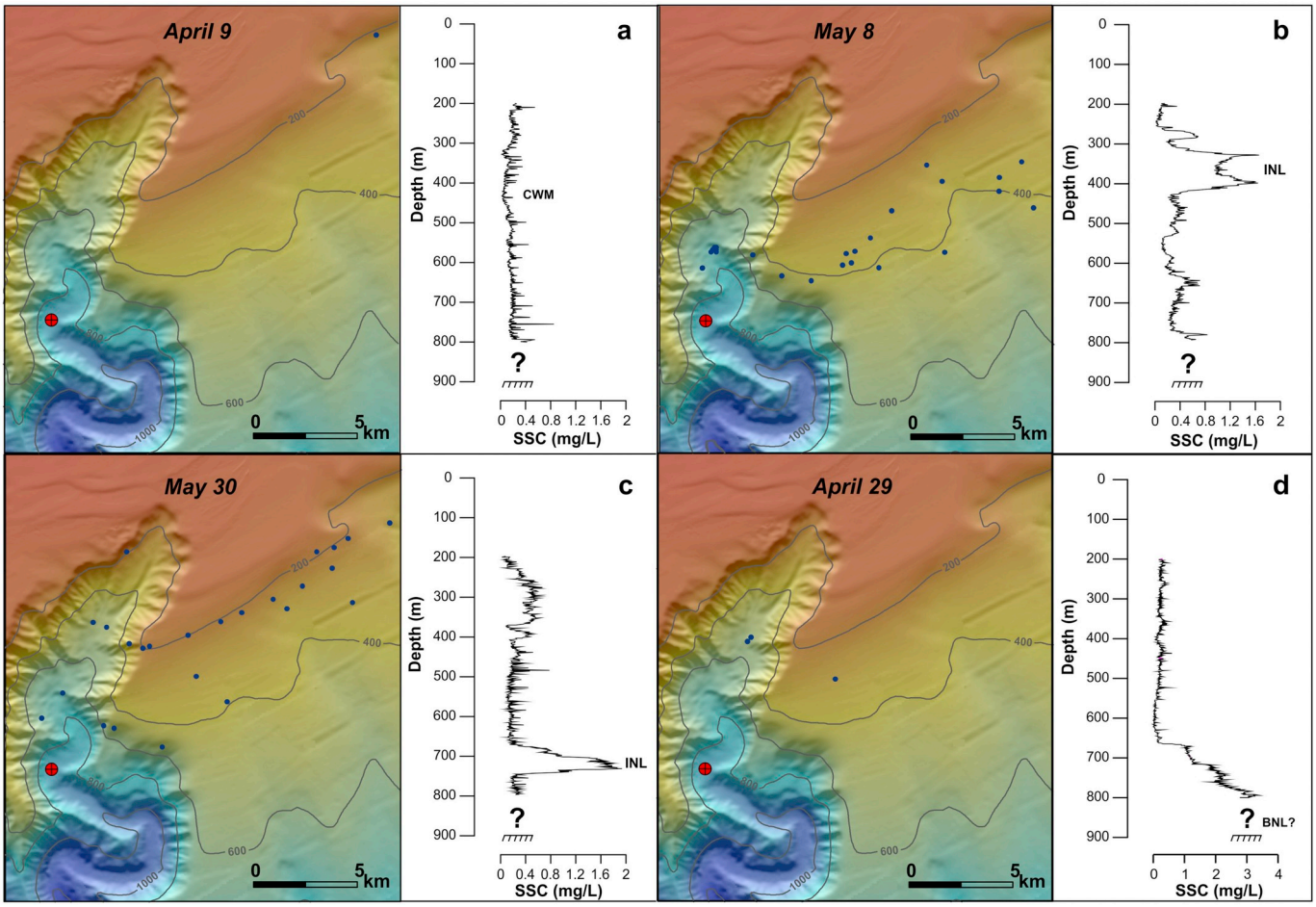

Fig. 9. Daily VMS recordings in the study area (blue dots) when nepheloid layers were absent (a) or present at different water depths: ~400 m (b), ~700 m (c) and near the bottom (d). See Fig. 6 for profile timing throughout the entire record. Note the change of scale for the SSC axis of the (d) vertical profile. (For interpretation of the references to colour in this figure legend, the reader is referred to the web version of this article.)

particulate standing crop values as the number of hauls increases, whether they occur at canyon-confined or unconfined waters (Fig. 8).

4.2. Bottom trawling as a major contributor in the formation of nepheloid layers in fished submarine canyons

There are many causes for the formation of nepheloid layers in the different oceans of the world (McCave, 1986). As it has been mentioned previously, in continental slope regions and submarine canyons, internal waves have been proposed as one of the major mechanisms that initiates sediment resuspension and, therefore, in generating nepheloid layers (Gardner, 1989; Puig and Palanques, 1998a; Puig et al., 2004; Martín et al., 2014a). The potential of internal waves in maintaining particles in suspension has been demonstrated in several studies (e.g. Gardner, 1989; Palanques and Biscaye, 1992; Puig et al., 2001). Submarine canyon morphologies can play a major role in determining the characteristics of internal waves' interaction with the seafloor and control suspended sediment particles transport at intermediate and deeper sectors of continental margins. Several studies have observed that some submarine canyons are shaped so they efficiently trap wave energy that, ultimately, can help to the generation of INLs at certain water depths (Gardner, 1989; Kunze et al., 2002; Puig et al., 2003). However, in open continental slope environments, it is difficult to observe this mechanism directly and to evaluate its contribution to the sediment dynamics. Indeed, in the Gulf of Valencia (western Mediterranean), where internal wave activity was properly characterized (van Haren et al., 2013), it was found that the presence of high SSC peaks recorded was unrelated to hydrodynamic processes, proposing trawling activities as the main sources of sediment resuspension on this area (Ribó et al., 2015). Previous hydrographic transects conducted on this area identified INLs and BNLs that by their water depth location were also attributed to trawling (Ribó et al., 2013).

Our data in the Foix Canyon corroborates that resuspension induced by trawling activities on slope and canyon environments can play a significant role as initiator of sediment resuspension at slope depths, generating INLs and BNLs at certain depths based on the locations of the fishing grounds. This mechanism might be particularly relevant in the Mediterranean Sea, where, in absence of tides, the internal wave activity is rather weak and occurs mostly at near-inertial frequencies.

Indeed, some previous observational field studies in the Mediterranean Sea, besides the previous described example of the Gulf of Valencia, have proposed trawling as a main driving force of sediment resuspension in continental slope regions. In the Catalan margin, Martín et al. (2014a) recorded the presence of nepheloid layers in a CTD + turbidimeter transect, conducted across a fishing ground in La Fonera Canyon. In the southern margin of the Aegean Sea (NE Mediterranean), Chronis et al. (2000) found near-BNLs and detached INLs in the vicinity of the shelf-break and over the upper slope region, suggesting that, besides near-bed current activity and breaking of internal waves, demersal fishing activities developed over the area might be likely causing the sharpest SSC recorded near the seabed. However, other studies in the Aegean Sea (e.g., Karageorgis and Anagnostou, 2003) have reported deep slope INLs in regions where fishing occurs at shallower depths. These authors attributed the formation of those INLs

to natural processes, such as strong current velocities or internal waves. Therefore, both natural and anthropogenic mechanisms can coexist and generate sediment resuspension that, ultimately, can lead to the formation of nepheloid layers at continental slope depths.

Outside the Mediterranean, in the Whittard Canyon region (NE Atlantic), unusual high peaks of suspended particulate matter in nepheloid layers were also observed to be linked to trawling activities near the canyon (Wilson et al., 2015b; Daly et al., 2017). Through the use of VMS data, as in the present study, the locations and presence of bottom trawlers in the area provided evidence for the relationship between trawling activity and the occurrence of enhanced nepheloid layers, that displayed anomalous high SSC values, exceeding those in the INLs typically observed in the region (Wilson et al., 2015a).

Given that submarine canyons incising continental margins are often targeted by fisheries, it is likely that similar or other impacts have occurred and are occurring in other submarine canyons elsewhere in the world (Martín et al., 2014c; Oberle et al., 2018).

Bottom trawling has lately gained attention on the scientific community and policy makers (European Parliament, 2008), not only for the impacts on marine diversity and living resources, but also for its destructive effects on the seabed and its strong potential in altering sediment transport processes and turbidity conditions in the deep-sea environment at large spatial and time scales (Puig et al., 2012). The identification and assessment of these impacts, together with the quantification of the ecological status of the deep sea environment, has become increasingly important in Europe, especially after the implementation of the European Marine Strategy Framework Directive (MSFD; 2008/56/EC, descriptors #6 and #7) but it is still an ongoing challenge (Gislason et al., 2017). Accordingly, more measurements are necessary elsewhere to understand the effects of bottom trawling in deep ecosystems, including fished submarine canyons. Identifying and assessing the impacts of fishing activities could help us to reduce their negative effects.

5. Conclusions

Daily hydrographic profiles collected throughout this field study illustrate a well-defined water turbidity structure consisting in INLs, found between 300 and 500 m water depth and above the canyon rims at canyon-unconfined waters, and INLs and near-BNLs, confined within the canyon at depths > 650 m.

Using vessels' positioning through Vessel Monitoring System (VMS), the temporal and spatial distribution of the local trawling fleet over the study area at the time of the deployment strongly suggests that trawling resuspension is likely the major mechanism that leads to increasing SSCs in the water column. VMS logs revealed that the presence and water column levels of the observed nepheloid layers strongly depend on the operating depths of trawlers and on the specific fishing grounds being exploited.

Nonetheless, even bottom trawling appears to act as the main sediment resuspension mechanism, natural processes and ambient currents contribute to the advection and/or retention in suspension of resuspended particles, playing a major role in their transport along and across the margin via nepheloid layers.

The present study describes, for the first time, the temporal evolution of water column turbidity using an autonomous hydrographic profiler deployed at the canyon axis of a trawled submarine canyon on the NW Mediterranean region. Our study provides only a set of vertical profiles of the water column in the Foix Canyon, and more extensive studies are required to fully understand the turbidity structure at this or other comparable sites. For further studies, higher sampling frequency and working depth range of the hydrographic profiler would greatly increase our understanding of trawling-induced resuspension events.

Acknowledgements

The authors are very grateful to the captain, crew and scientists involved in *R/V* García del Cid cruises, and also the UTM technicians and the Instrumental Service for their guidance and assistance during the sampling. We also thank the Spanish General Secretariat of Maritime Fishing for providing VMS data. Special gratitude is dedicated to Alexander Ostrovskii from the P.P. Shirshov Institute of Oceanology of Moscow (Russia) for his assistance with the autonomous hydrographic profiler (Aqualog) data processing. This work has been supported by FORMED (CGL2012-33989) and ABIDES (CTM2015-65142-R) Spanish Projects. M. Arjona-Camas is supported by a predoctoral F.P.I. grant from the Spanish Ministry of Economy, Industry and Competitiveness. M. A-C, P. P., A. P. and R. D. belong to CRG on Littoral and Oceanic Processes, supported by Grant 2017 SGR 863 of the Generalitat de Catalunya, and M. E. belongs to CRG on Physical and Technological Oceanography (SGR 1241, 2017 of the Generalitat de Catalunya).

References

Alonso, B., Díaz, J., Farran, M., Giró, S., Maldonado, A., Vázquez, A., 1984. Cañones submarinos del margen Catalán meridional: morfología y evolución. In: I Congreso Español de Geología. vol. 1. Ilustre Colegio Oficial de Geólogos, Segovia, pp. 301–311.

Amin, M., Huthnance, J.M., 1999. The pattern of cross-slope depositional fluxes. Deep-Sea Res. I Oceanogr. Res. Pap. 46 (9), 1565–1591.

Biscaye, P.E., Eittreim, S.L., 1977. Suspended particulate loads and transports in the nepheloid layer of the abyssal Atlantic Ocean. Mar. Geol. 23, 155–172.

Cacchione, D.A., Drake, D.E., 1986. Nepheloid layers and internal waves over continental shelves and slopes. Geo-Mar. Lett. 6 (3), 147–152.

Canals, M., Companys, J.B., Martín, D., Sanchez-Vidal, A., Ramirez-Llodra, E., 2013. Integrated study of Mediterranean deep canyons: novel results and future challenges. Prog. Oceanogr. 118 (1–27).

Chronis, G., Lykousis, V., Georgopoulos, D., Zervakis, V., Stavrakakis, S., Poulos, S., 2000. Suspended particulate matter and nepheloid layers over the southern margin of the Cretan Sea (NE Mediterranean): seasonal distribution and dynamics. Prog. Oceanogr. 46 (2–4), 163–185.

Daly, E., Johnson, M.P., Wilson, A.M., Gerritsen, H.D., Kiriakoulakis, K., Allcock, A.L., White, M., 2017. Bottom trawling at Whittard Canyon: evidence for seabed modification, trawl plumes and food source heterogeneity. Prog. Oceanogr 169, 227–240.

Dickson, R.R., McCave, I.N., 1986. Nepheloid layers on the continental slope west of Porcupine Bank. Deep-Sea Res. I Oceanogr. Res. Pap. 33 (6), 791–818.

Durrieu de Madron, X., Ferré, B., Le Corre, G., Grenz, C., Conan, P., Pujo-Pay, M., Buscail, R., Bodiot, O., 2005. Trawling-induced resuspension and dispersal of muddy sediments and dissolved elements in the Gulf of Lion (NW Mediterranean). Cont. Shelf Res. 25 (19–20), 2387–2409.

European Parliament, 2008. Directive 2008/56/EC of the European Parliament and the Council of 17 June 2008 establishing a framework for community action in the field of marine environmental policy (Marine Strategy Framework Directive). Off. J. Eur. Union 1–22.

Font, J., Salat, J., Tintoré, J., 1988. Permanent features of the circulation in the Catalan Sea. Oceanol. Acta 9, 51–57.

Gardner, W.D., 1989. Periodic resuspension in Baltimore Canyon by focusing of internal waves. J. Geophys. Res. Oceans 94 (C12), 18185–18194.

Gardner, W.D., Walsh, I.D., 1990. Distribution of macroaggregates and fine-grained particles across a continental margin and their potential role in fluxes. Deep-Sea Res. I Oceanogr. Res. Pap. 37 (3), 401–411.

Gardner, W.D., Richardson, M.J., Walsh, I.D., Berglund, B.L., 1990. In-situ optical sensing of particles for determination of oceanic processes: what satellites can't see, but transmissometers can. Oceanography 3 (2), 11–17.

Gislason, H., Bastardie, F., Dinesen, G.E., Egekvist, J., Ritzau-Eigaard, O., 2017. Lost in translation? Multi-metric macrobenthos indicators and bottom trawling. Ecol. Indic. 82, 260–270.

Guillén, J., Palanques, A., Puig, P., Durrieu de Madron, X., Nyffeler, F., 2000. Field calibration of optical sediment concentration in the western Mediterranean. Sci. Mar. 64 (4), 427–435.

Karageorgis, A.P., Anagnostou, C.L., 2003. Seasonal variation in the distribution of suspended particulate matter in the northwest Aegean Sea. J. Geophys. Res. Oceans 108 (C8), 3274.

Karageorgis, A.P., Drakopoulos, P.G., Psarra, S., Krasakopoulou, E., Banks, A.C., Velaoras, D., Spyridakis, N., Papathanassiou, E., 2017. Particle characterization and composition in the Aegean Sea: combining optical methods and biogeochemical parameters. Cont. Shelf Res. 149, 96–111.

Kershaw, S., Liu, M., 2015. Modern Black Sea oceanography applied to the end-Permian extinction event. J. Palaeogeogr. 4 (1), 52–62.

Kunze, E., Rosenfeld, L.K., Carter, G.S., Gregg, M.C., 2002. Internal waves in Monterey submarine canyon. J. Phys. Oceanogr. 32 (6), 1890–1913.

Lambert, G.I., Jennings, S., Hiddink, J.G., Hintzen, N.T., Hinz, H., Kaiser, M.J., Murray,

L.G., 2012. Implications of using alternative methods of vessel monitoring system (VMS) data analysis to describe fishing activities and impacts. ICES J. Mar. Sci. 69 (4), 682–693.
Linders, T., Nilsson, P., Wikström, A., Sköld, M., 2017. Distribution and fate of trawling-induced resuspension of sediments in a marine protected area. ICES J. Mar. Sci. 75 (2), 785–795.
Lleonart, J., 1990. La pesquería de Cataluña y Valencia: descripción global y planteamiento de bases para su seguimiento. (Informe final. EEC DG XP/-CSIC, 2).
Martín, J., Puig, P., Palanques, A., Masqué, P., García-Orellana, J., 2008. Effect of commercial trawling on the deep sedimentation in a Mediterranean submarine canyon. Mar. Geol. 252 (3–4), 150–155.
Martín, J., Puig, P., Palanques, A., Ribó, M., 2014a. Trawling-induced daily sediment resuspension in the flank of a Mediterranean submarine canyon. Deep-Sea Res. II Top. Stud. Oceanogr. 104, 174–183.
Martín, J., Puig, P., Masqué, P., Palanques, A., Sánchez-Gómez, A., 2014b. Impact of bottom trawling on deep-sea sediment properties along the flanks of a submarine canyon. PLoS One 9 (8), e104536.
Martín, J., Puig, P., Palanques, P., Giamportone, A., 2014c. Commercial bottom trawling, a driver of sediment dynamics and deep seascape evolution in the Anthropocene. Anthropocene 7, 1–15.
Maynou, F.X., Sardà, F., Conan, G., 1998. Assessment of the spatial structure and biomass evaluation of Nephrops norvegicus (L.) populations in the northwestern Mediterranean by geostatistics. ICES J. Mar. Sci. 55 (1), 102–120.
McCave, I.N., 1986. Local and global aspects of the bottom nepheloid layers in the world ocean. J. Sea Res. 20 (2–3), 167–181.
Millot, C., 1999. Circulation in the western Mediterranean Sea. J. Mar. Syst. 20 (1–4), 423–442.
Oberle, F.K., Puig, P., Martín, J., 2018. Fishing activities. In: Submarine Geomorphology. Springer, Cham, pp. 503–534.
O'Neill, F.G., Summerbell, K., 2011. The mobilisation of sediment by demersal otter trawls. Mar. Pollut. Bull. 62 (5), 1088–1097.
Ostrovskii, A.G., Zatsepin, A.G., Soloviev, V.A., Tsybulsky, A.L., Shvoev, D.A., 2013. Autonomous system for vertical profiling of the marine environment at a moored station. Oceanology 53 (2), 233–242.
Palanques, A., Biscaye, P.E., 1992. Patterns and controls of the suspended matter distribution over the shelf and upper slope south of New England. Cont. Shelf Res. 12 (5–6), 577–600.
Palanques, A., Puig, P., Guillén, J., Demestre, M., Martín, J., 2014. Effects of bottom trawling on the Ebro continental shelf sedimentary system (NW Mediterranean). Cont. Shelf Res. 72, 83–98.
Paradis, S., Puig, P., Masqué, P., Juan-Díaz, X., Martín, J., Palanques, A., 2017. Bottom-trawling along submarine canyons impacts deep sedimentary regimes. Sci. Rep. 7, 43332.
Paradis, S., Masqué, P., Puig, P., Juan-Díaz, X., Gorelli, G., Palanques, A., 2018. Enhancement of sedimentation rates in the Foix Canyon after the renewal of trawling fleets in the early XXI st century. Deep-Sea Res. I Oceanogr. Res. Pap. 132, 51–59.
Puig, P., Palanques, A., 1998a. Nepheloid structure and hydrographic control on the Barcelona continental margin, northwestern Mediterranean. Mar. Geol. 149 (1–4), 39–54.
Puig, P., Palanques, A., 1998b. Temporal variability and composition of settling particles fluxes on the Barcelona continental margin (Northwestern Mediterranean). J. Mar. Res. 56 (3), 639–654.
Puig, P., Palanques, A., Guillén, J., García-Ladona, E., 2000. Deep slope currents and suspended particle fluxes in and around the Foix submarine canyon (NW Mediterranean). Deep-Sea Res. I Oceanogr. Res. Pap. 47 (3), 343–366.
Puig, P., Sardà, F., Palanques, A., 2001. Responses of deep-water shrimp populations to intermediate nepheloid layer detachments on the Northwestern Mediterranean continental margin. Deep-Sea Res. I Oceanogr. Res. Pap. 48 (10), 2195–2207.
Puig, P., Ogston, A.S., Mullenbach, B.L., Nittrouer, C.A., Sternberg, R.W., 2003. Shelf-to-canyon sediment-transport processes on the Eel continental margin (northern California). Mar. Geol. 193 (1–2), 129–149.
Puig, P., Palanques, A., Guillén, J., El Khatab, M., 2004. Role of internal waves in the generation of nepheloid layers on the northwestern Alboran slope: implications for continental margin shaping. J. Geophys. Res. Oceans 109 (C9).
Puig, P., Canals, M., Martín, J., Amblas, D., Lastras, G., Palanques, A., Calafat, A.M., 2012. Ploughing the deep-sea floor. Nature 489 (7415), 286.
Puig, P., Palanques, A., Martín, J., 2014. Contemporary Sediment-Transport Processes in Submarine Canyons. Ann. Rev. Mar. Sci. 6, 53–77.
Puig, P., Martín, J., Masqué, P., Palanques, A., 2015. Increasing sediment accumulation rates in La Fonera (Palamós) submarine canyon axis and their relationship with bottom trawling activities. Geophys. Res. Lett. 42 (19), 8106–8113.
Pusceddu, A., Bianchelli, S., Martín, J., Puig, P., Palanques, A., Masqué, P., Danovaro, R., 2014. Chronic and intensive bottom trawling impairs deep-sea biodiversity and ecosystem functioning. Proc. Natl. Acad. Sci. U. S. A. 111 (24), 8861–8866.
Ragnarsson, S.A., Steingrímsson, S.A., 2003. Spatial distribution of otter trawl effort in Icelandic waters: comparison of measures of effort and implications of benthic community effects of trawling activities. ICES J. Mar. Sci. 60 (6), 1200–1215.
Ribó, M., Puig, P., Salat, J., Palanques, A., 2013. Nepheloid layer distribution in the Gulf of Valencia, northwestern Mediterranean. J. Mar. Syst. 111, 130–138.
Ribó, M., Puig, P., van Haren, H., 2015. Hydrodynamics over the Gulf of Valencia continental slope and their role in sediment transport. Deep-Sea Res. I Oceanogr. Res. Pap. 95, 54–66.
Sanchez-Cabeza, J.A., Masqué, P., Ani-Ragolta, I., Merino, J., Frignani, M., Alvisi, F., Palanques, A., Puig, P., 1999. Sediment accumulation rates in the southern Barcelona continental margin (NW Mediterranean Sea) derived from ^{210}Pb and ^{137}Cs chronology. Prog. Oceanogr. 44 (1–3), 313–332.
Sardà, F., Cartes, J.E., Norbis, W., 1994. Spatio-temporal structure of the deep-water shrimp Aristeus antennatus (Decapoda: Aristeidae) population in the western Mediterranean. Fish. Bull. 92 (3), 599–607.
Schlitzer, R., 2010. Ocean Data View. http://odv.awi.de.
Solé, J., Emelianov, M., Ostrovskii, A., Puig, P., García-Ladona, E., 2016. Fine-scale water mass variability inside a narrow submarine canyon (Besòs Canyon) in the NW Mediterranean Sea. Sci. Mar. 80 (S1), 195–204.
Spurgin, J.M., Allen, S.E., 2014. Flow dynamics around downwelling submarine canyons. Ocean Sci. 10, 799–819.
Tubau, X., Lastras, G., Canals, M., Micallef, A., Amblas, D., 2013. Significance of the fine drainage pattern for submarine canyon evolution: the Foix Canyon system, northwestern Mediterranean Sea. Geomorphology 184, 20–37.
van Haren, H., Ribó, M., Puig, P., 2013. (Sub-) inertial wave boundary turbulence in the Gulf of Valencia. J. Geophys. Res. 118 (4), 2067–2073.
Walsh, J.J., 1991. Importance of continental margins in the marine biogeochemical cycling of carbon and nitrogen. Nature 350 (6313), 53.
Wilson, A.M., Raine, R., Mohn, C., White, M., 2015a. Nepheloid layer distribution in the Whittard Canyon, NE Atlantic margin. Mar. Geol. 367, 130–142.
Wilson, A.M., Kiriakoulakis, K., Raine, R., Gerritsen, H.D., Blackbird, S., Allcock, A.L., White, M., 2015b. Anthropogenic influence on sediment transport in the Whittard Canyon, NE Atlantic. Mar. Pollut. Bull. 101 (1), 320–329.
Wilson, A.M., 2016. Lateral transport of suspended particulate matter in nepheloid layers along the Irish continental margin - a case study of the Whittard Canyon, North-East Atlantic Ocean (Doctoral dissertation, National University of Ireland Galway, Galway, Ireland). Retrieved from. http://hdl.handle.net/10379/6047.

Marine Geophysical Research _####################_
https://doi.org/10.1007/s11001-021-09457-7

ORIGINAL RESEARCH PAPER

Natural vs. trawling-induced water turbidity and suspended sediment transport variability within the Palamós Canyon (NW Mediterranean)

Marta Arjona-Camas[1,2] · Pere Puig[1] · Albert Palanques[1] · Ruth Durán[3] · Martin White[4,5] · Sarah Paradis[6] · Mikhail Emelianov[1]

Received: 3 June 2021 / Accepted: 12 September 2021

Abstract

Increases of water turbidity and suspended sediment transport in submarine canyons have been associated with high-energy events such as storms, river floods and dense shelf water cascading (DSWC), and occasionally with bottom trawling along canyon flanks and rims. To assess the variations on the water column turbidity and sediment transport in the Palamós Canyon linked to both natural and trawling-induced processes, an autonomous hydrographic profiler, as well as a near-bottom current meter and a turbidimeter were deployed in the canyon axis (929 m depth) from February to June 2017, covering a trawling closure (February) and trawling activities (March-June). Periods of enhanced water turbidity during the trawling closure were mostly associated with storms and DSWC events, transporting turbid dense waters into the canyon. In absence of such events, the water column displayed low suspended sediment concentrations (~0.3 mg L^{-1}) until the trawling season began, when particulate matter detachments, ranging between > 1 mg L^{-1} and 3.8 mg L^{-1}, were observed at the water depths where the trawling grounds are found. During the trawling closure, high near-bottom suspended sediment fluxes (35–44 g m^{-2} s^{-1}) were sporadically registered at ~ 920 m depth associated with a major storm and DSWC event. Smaller but more frequent increases of near-bottom suspended sediment fluxes (0.1–1.4 g m^{-2} s^{-1}) were recorded during trawling activities. Despite these smaller trawling-induced suspended sediment fluxes, 30 days of continuous bottom trawling activity transported a total amount of 40 kg m^{-2}, of similar magnitude to that generated by a major DSWC event (50 kg m^{-2}). Since bottom trawling in Palamós Canyon is practiced on a daily basis throughout the year, a much larger contribution of anthropogenically derived water turbidity and suspended sediment transport can be expected.

Keywords Palamós Canyon · Dense shelf water cascading (DSWC) · Bottom trawling · Sediment transport · Nepheloid structure · NW Mediterranean

Introduction

Submarine canyons are widespread morphological features incising continental margins (Shepard and Dill 1966; Shepard 1972; Harris and Whiteway 2011) considered to be preferential pathways for the transference of water and sediments between nearshore areas and deep-sea environments (e.g., García et al. 2008; Allen and Durrieu de Madron 2009; Puig et al. 2014; Porter et al. 2016). For this reason, several studies have focused on studying the shelf-slope exchanges of downward particle fluxes and water turbidity by means of moored oceanographic instruments (see review by Puig et al. 2014). In these investigations, increases in sediment fluxes have been generally associated with lateral inputs of particulate matter by the action of different mechanisms such as breaking and/or shoaling of internal waves and tidal

✉ Marta Arjona-Camas
marjona@icm.csic.es

[1] Institute of Marine Sciences (CSIC), Passeig Marítim de la Barceloneta, 37-49, 08003 Barcelona, Spain

[2] Department of Earth and Ocean Dynamics, University of Barcelona, c/Martí i Franquès s/n, 08028 Barcelona, Spain

[3] Marine Geology & Seafloor Surveying, Department of Geosciences, University of Malta, Msida, Malta

[4] Earth and Ocean Sciences, Ryan Institute, National University of Ireland, Galway, Ireland

[5] Irish Centre for Research in Applied Geosciences (iCRAG), Galway, Ireland

[6] Geological Institute, ETH Zurich, Zurich, Switzerland

motions (e.g., Gardner 1989; Kunze et al. 2002; Cacchione and Ogston 2002; Puig et al. 2004b; Pomar et al. 2012) or high-energy storms affecting the upper portion of submarine canyons and hyperpycnal plumes formed during river floods (Monaco et al. 1990; Puig et al. 2004a; Palanques et al. 2006b, 2008; Bonnin et al. 2008; Ulses et al. 2008a). Occasionally, increases in turbidity have been associated with sediment gravity flow related events, such as slope failure on canyon walls (e.g., Paull et al. 2003; Puig et al., 2003, 2004a; Xu et al. 2004; Piper and Normark et al. 2009; Völker et al. 2011). Additionally, it has been demonstrated that dense shelf water cascading (DSWC) can also transport particles and erode and reshape the seafloor of submarine canyons, thereby increasing suspended sediment concentrations and transport towards the slope (Canals et al. 2006; Palanques et al. 2006b, 2008; Puig et al. 2008; Allen and Durrieu de Madron 2009). This later phenomenon is particularly relevant in the NW Mediterranean. Dense-shelf water formation tends to occur in winter over the Gulf of Lions (GoL) induced by dry and cold north and northwesterly winds (Tramontane and Mistral, respectively), which cause the cooling and heat loos of surface coastal waters. Eventually, these shelf waters become denser than the surrounding waters and sink over the shelf-edge and cascade downslope, mainly through submarine canyons until they reach their equilibrium depth, and continue flowing along the margin towards the southwest (Millot 1990; Durrieu de Madron 2005a). During mild or average winters, which are the most common in the study site, they are detached at intermediate depths, contributing to the formation of the seasonal Western Intermediate Water (WIW) found at the upper slope depths (Lapouyade and Durrieu de Madron 2001; Dufau-Julliand et al. 2004). In very dry, cold and windy winters, DSWC can be exceptionally intense, and dense shelf waters can affect the entire continental slope and even reach the basin floor (Canals et al. 2006; Palanques et al. 2012; Durrieu de Madron et al. 2013; Palanques and Puig 2018).

In addition to these various natural transport mechanisms, human activities, such as bottom trawling practiced at the flanks and rims of submarine canyons, have also been shown to contribute substantially to present-day sediment resuspension and water column turbidity (Palanques et al. 2006a; Puig et al. 2012; Martín et al. 2014a; Wilson et al. 2015b; Daly et al. 2018). Generally, the impacts of bottom trawling activities have been studied in shallow water environments, and mostly include the scraping and ploughing of the seabed by the use of heavy trawl doors that leave big furrows behind (Krost et al. 1990; Smith et al. 2003). The design of these heavy trawls also causes increases in near-bottom turbidity due to the sediment resuspension (O'Neill and Summerbell 2011), which contributes to the formation of turbid plumes and persistent nepheloid layers that are afterwards advected by local currents, waves and tides (Churchill 1989; Durrieu de Madron et al. 2005b; Palanques et al. 2001, 2014). However, shallow water environments on the continental shelf (< 120 m depth) are periodically impacted by natural sediment resuspension processes, masking the consequences of this anthropogenic activity. Therefore, assessing the relative contribution of oceanographic processes and anthropogenic activities to the sedimentary dynamics is rather complex because each area has its own wave climate, current regime, seabed sediment characteristics and bottom trawling frequency, and only a few studies have attempted to do this (e.g., Pilskaln et al. 1998; Churchill 1989; Ferré et al. 2008; Palanques et al. 2014; Oberle et al. 2016a; Mengual et al. 2016). A common conclusion of all these studies is that bottom trawling has a measurable impact on sediment resuspension in shallow-water environments, comparable to that created by natural forces. In deeper environments on the continental slope, however, bottom trawling disturbances can be more severe and have longer-lasting effects mainly because natural processes capable of overcoming human impacts are generally weaker than in shallower areas (Puig et al. 2012; Martín et al. 2014a; Oberle et al. 2016a).

The Mediterranean Sea hosts important deep-sea bottom trawl fisheries mainly located on the upper slope on the northwestern continental margin, where trawled bottoms exist up to 800 m depth, with greater depths being reached occasionally (Puig et al. 2012). Several studies aimed at understanding the effects of bottom trawling on the sediment dynamics in this area focused on the Palamós Canyon (also known as La Fonera or Llafranc Canyon) (Lastras et al. 2011), one of the most prominent morphological features incising this margin (Serra 1981). Some of these studies have shown that bottom trawling along the flanks of this canyon can trigger sediment gravity flows and transport sediments downslope from the fishing grounds to deeper regions of the canyon (Palanques et al. 2005; Martín et al. 2007, 2014a; Payo-Payo et al. 2017), affecting sediment accumulation rates in the canyon axis (Martín et al. 2006, 2008; Puig et al. 2015), and altering the natural morphology of the canyon flanks due to periodic reworking and removal of sediments (Puig et al. 2012). Additionally, Martín et al. (2014a) reported the presence of bottom and intermediate nepheloid layers (BNLs and INLs, respectively) in several hydrographic profiles conducted after the passage of the trawling fleet over the northern flank of the Palamós Canyon, but the continued effect of bottom trawling in this canyon causing changes in the water column turbidity beyond fishing grounds is an issue that remains largely unexplored.

Trawling-derived increases in suspended sediment concentrations (SSC) on the continental slope were also recorded in hydrographic studies conducted in the Celtic Sea (NE Atlantic). These studies showed unusual turbidity peaks in the water column within the Whittard Canyon that were linked to bottom trawling activities at the adjacent

Journal : Large 11001 | Article No : 9457 | Pages : 22 | MS Code : 9457 | Dispatch : 8-11-2021

canyon spurs (Wilson et al. 2015b; Daly et al. 2018). However, the temporal evolution of such trawling-induced turbidity increases throughout the water column has not been assessed in this submarine canyon. To our knowledge, the only study addressing this aspect in a trawled submarine canyon was conducted by Arjona-Camas et al. (2019) in the Foix Canyon (Catalan margin, NW Mediterranean). Two months of hydrographic profiles were acquired at the axis of this canyon during the trawling season, revealing the occurrence BNLs at the bottom of the canyon and quasi-permanent INLs over the canyon rim, originating from trawling activities on the adjacent continental slope. However, accurate estimates of the quantity of material being introduced by bottom trawling to the water column are still needed to better appreciate its contribution to the sediment dynamics and the potential environmental and ecological impacts associated with it. In this new study, we aim to assess the spatial and temporal variations on the water turbidity structure and near-bottom suspended sediment fluxes linked to both anthropogenic (bottom trawling) and natural (storms and DSWC) processes in the Palamós Canyon, as well as assess the contribution of each mechanism to the sediment fluxes.

Regional setting

The NW Mediterranean margin has a high density of submarine canyons, the Palamós Canyon (Fig. 1) being one of the most prominent examples (Canals et al. 2013). The canyon head is situated closest to the coastline at ~ 1 km and incises the continental shelf at 90 m depth. The first ~ 5 km of the canyon presents a N-S direction parallel to the coastline, after which the canyon's direction turns to WNW-ESE for ~ 35 km, separating the Roses margin to the north, and La Planassa margin to the south (Amblas et al. 2006). This submarine canyon has a total length of 110 km, and a maximum width of 18.4 km, and runs almost from the coastline down to 2550 m water depth. The canyon's steep walls (> 25º) present several well-developed gullies generated by sedimentary instabilities (Lastras et al. 2011), although these complex morphologies have been smoothened on fishing grounds due to recurrent disturbance of the seafloor by the trawling gear (Puig et al. 2012).

The hydrographic structure in this area is composed by a three-layer system (Salat and Cruzado 1981; Salat et al. 2002). Within the first layer, from the surface down to 150–300 m depth, the Atlantic Water (AW) is generally found. AW can be distinguished between "recent" and "old" according to the residence time in the Mediterranean basin that increases its salinity (Salat, 1996). In the NW Mediterranean, the oAW is found and is characterized by temperatures > 13 ºC and salinity values of 38.0–38.2. Mainly during wintertime, cold (~ 13 ºC) and fresh (~ 38.5) lenses of Western Intermediate Water (WIW) can be found at ~ 150 m depth. The second layer is formed by the Levantine Intermediate Water (LIW) between 300 and 600 m depth and is characterized by temperatures ~ 13.5 ºC and salinities of ~ 38.5. The third layer is formed by the near-homogeneous Western Mediterranean Deep Water (WMDW), which is formed in the open ocean resulting from intense sea-atmosphere heat exchanges and the subsequent buoyancy loss of offshore waters induced by cold, dry and persistent N-NW winds (Salat et al. 2002; Font et al. 2007). It covers the entire basin below 1000 m depth and has cold (~ 13 ºC) and salty (~ 38.5) characteristics (Font et al. 2007).

Since the Palamós Canyon is deeply incised in the continental shelf, it is capable of intercepting particulate matter transported by the Northern Current. This baroclinic current follows the continental slope from NE to SW in quasi-geostrophic equilibrium with a shelf-slope density front established between low-salinity coastal waters and the more saline and denser open waters (Font et al. 1988; Millot 1999). Although it approaches the Palamós Canyon mainly in a southwestward direction (Font et al. 1988), the abrupt topography of the canyon forces some adjustments of the Northern Current (Masó et al. 1991), which lead to significant vertical motions (Palanques et al. 2005; Jordi et al. 2005).

This submarine canyon also acts as a preferential conduit for particulate matter transported during sporadic events such as storms or river discharges (Palanques et al. 2005). The most important river in the nearby coast is the Ter River, whose mouth reaches the sea at 25 km north from the canyon. It has a mean annual water discharge of 12.1 $m^3 s^{-1}$ (Liquete et al. 2009). On this margin, northern storms are very frequent and persistent, but due to their reduced fetch they can only generate relatively small waves (~ 2 m) on the inner shelf that have limited capacity to resuspend sediment. Eastern storms are rarer and brief, although they generate larger waves (> 4 m), particularly during fall and winter months (Palanques et al. 2008). They are usually accompanied by heavy rains and torrential river discharges carrying large amounts of sediment to the coast (Ribó et al. 2011).

The Palamós Canyon's flanks are intensively exploited by a local trawling fleet targeting the blue and red shrimp *Aristeus antennatus*. Trawlers are active in this area on a daily basis except for weekends, holidays, and local festivities, mainly along the Sant Sebastià and the Rostoll fishing grounds (Fig. 1). The same vessel usually carries out two hauls per day, starting typically at 7 a.m. in an offshore direction, until 6 p.m. when it heads back to port. The average length of a haul usually ranges from 10 to 20 km, with

Journal : Large 11001 | Article No : 9457 | Pages : 22 | MS Code : 9457 | Dispatch : 8-11-2021

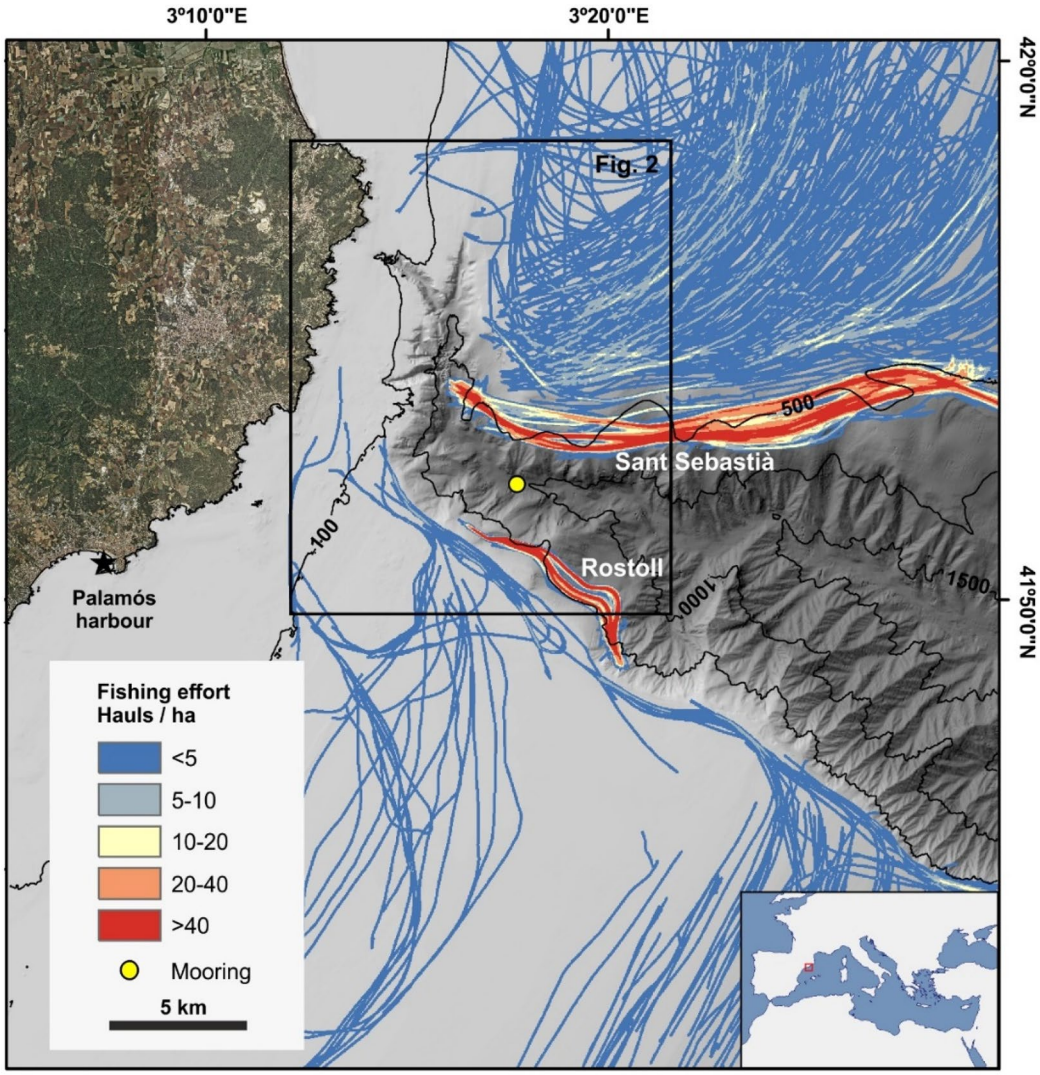

Fig. 1 Bathymetric map of the Palamós Canyon, showing the location of the mooring line in the canyon axis (yellow dot) and the main fishing grounds along the canyon flanks (Sant Sebastià and Rostoll). The overlying density represents an estimate of the fishing effort of otter board (OTB) vessels based on the number of hauls per hectare obtained from year 2017 Automatic Identification System (AIS) data. For interpretation of the references in color in this figure legend, the reader is referred to the web version of this article

an average of 15 km. The bottom trawl gear used in this fishery consists of two heavy otter boards, each up to 1 ton in weight, spreading ~ 100 m apart during the trawling operation and connected to the net opening by 60–200 m long sweeplines. The net measures 80–150 m in length and has a width of ~ 50 m at its ballasted mouth (Palanques et al. 2006a; Martín et al. 2014a). A recent fishery management established a two-month trawling closure from early-January to early-March since 2013 to allow the recruitment of juveniles and avoid the risk of overexploitation of the fishing stock (Bjørkan et al. 2020). In 2017, this seasonal trawling closure occurred from January 5 to March 8 (BOE 2017).

Materials and methods

Moored instruments

During the oceanographic cruise ABIDES-1, onboard the R/V *García del Cid*, a mooring line was deployed in the axis of the Palamós Canyon at 929 m depth (41° 52.329′ N;

Journal : Large 11001 | Article No : 9457 | Pages : 22 | MS Code : 9457 | Dispatch : 8-11-2021

3º 7.660′ E), at a slightly deeper location than the maximum working depth of the local trawling fleet (~ 800 m) (Fig. 1). One of the main concerns when deploying instruments in a trawled submarine canyon is the risk of losing data and expensive instrumental as a result of a collision with fishing gear. During this study, the position and deployment depth of the mooring was chosen in agreement with the Palamós fishermen guild in order to avoid interfering with their bottom trawling activities, and still be able to carry out our experimental observations in the canyon. The deployment was programmed from February 7 to early June, 2017, which covered a trawling closure period (February) and the continuation of the regular trawling season in the fishing grounds of the canyon (March-June). Unfortunately, the instruments recorded good data during 60 days until April 7, when the mooring line was displaced by a longline fishing vessel from a neighboring fishing harbor. Nevertheless, the recorded period allowed to capture the transition between the fishing closure and the trawling season and to address the scientific goals pursued in this study.

Autonomous hydrographic profiler

The mooring line was equipped with an autonomous hydrographic profiler (Aqualog) programmed to perform two up- and down-casts per day (at 2 a.m. and 2 p.m.), at a relative speed of 0.25 m s^{-1}, from ~ 150 to 738 m water depth (parking position). Therefore, the upper ~ 150 m and the lower ~ 200 m of the water column at the mooring location were not monitored. Unfortunately, the Aqualog did not profile the entire water column at certain time spans during the study period (i.e., February 7–27), presumably caused by the tilting of the mooring line due to strong currents, which prevented the carrier from progressing deeper and completing the hydrographic profiles.

The profiler was equipped with a SeaBird 19 plus CTD probe configured to collect temperature, salinity and pressure at 4 Hz (i.e., 4 scans per second). The profiler was also equipped with a SeaPoint turbidity sensor, programmed to measure water turbidity in Formazin Turbidity Units (FTU) by detecting scattered light from suspended particles at 0–25 FTU range, at 1 Hz (i.e., 1 scan per second).

Near-bottom instrumentation

The lower portion of the mooring line was also equipped with a single point Nortek Aquadopp current meter coupled with a SeaBird SBE-37 placed at 6 m above the bottom (mab) at 923 m depth that provided data at 5-min sampling interval. Closer to the bottom (at 5 mab), the mooring line also sustained an AQUA-logger 210TY equipped with a SeaPoint turbidity sensor that measured at 1-min sampling interval. The logger was set to operate in autogain mode, allowing to measure turbidity readings up to 2000 FTU.

CTD transect

After the mooring recovery, on June 7, 2017, a ship-based hydrographic transect was conducted in the study area onboard the R/V *García del Cid*. The transect consisted in 15 vertical stations across the canyon head, collected using a SeaBird 911 CTD probe coupled with a SeaPoint turbidity sensor (see location in Fig. 2).

Data analysis

Suspended sediment concentration

FTU readings from the CTD probes and moored instruments were converted into suspended sediment concentration (SSC) units using a regression equation obtained from a laboratory calibration. It was carried out by deploying eight different AQUA-logger 210TY SeaPoint turbidity sensors in an experimental tank, in which suspended particulate matter, using bottom sediments that were previously collected at the

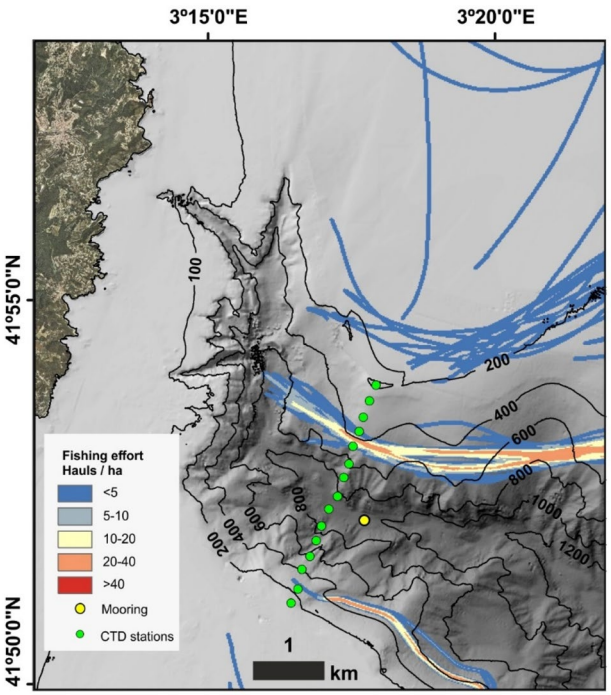

Fig. 2 Bathymetric map of the Palamós canyon head showing the fishing effort between March 9 and April 7, 2017 (trawling season). The yellow dot depicts the location of the mooring line, while the green dots indicate the position of the hydrographic transect conducted in June 7, 2017. For interpretation of the references in color in this figure legend, the reader is referred to the web version of this article

Journal : Large 11001 | Article No : 9457 | Pages : 22 | MS Code : 9457 | Dispatch : 8-11-2021

study site, was introduced incrementally. With continuous stirring, water samples were taken at given FTU readings and filtered through pre-weighed Nucleopore membranes to obtain SSC values, yielding the following linear regression (Fig. 3):

$$SSC\left(\text{mg}\cdot L^{-1}\right) = 1.14\cdot FTU - 0.37\ \left(r^2 = 0.99\right)$$

Net particulate standing crop

The SSC profiles obtained by the Aqualog were used to compute the Net Particulate Standing Crop (NPSC, mg cm^{-2}) by calculating the excess over the value of the clear water minimum and integrating the SSC excess over the height of the profiling range:

$$NPSC = \frac{1}{h}\int_0^h SSC(z)dz$$

where h stands for the depth of the considered water column (in m) and SSC (z) represents the estimated SSC (in mg L^{-1}) (see details in Karageorgis and Anagnostou 2003; Arjona-Camas et al. 2019).

As the profiler did not reach the same depths during the trawling closure and the trawling period, two distinct approaches were considered. In the first one, the NPSC was calculated for the 150–400 m depth interval, where data was recorded throughout the deployment period. In the second, the NPSC was computed only for the time-period when the profiler recorded data along most of the working depth range (150–738 m depth).

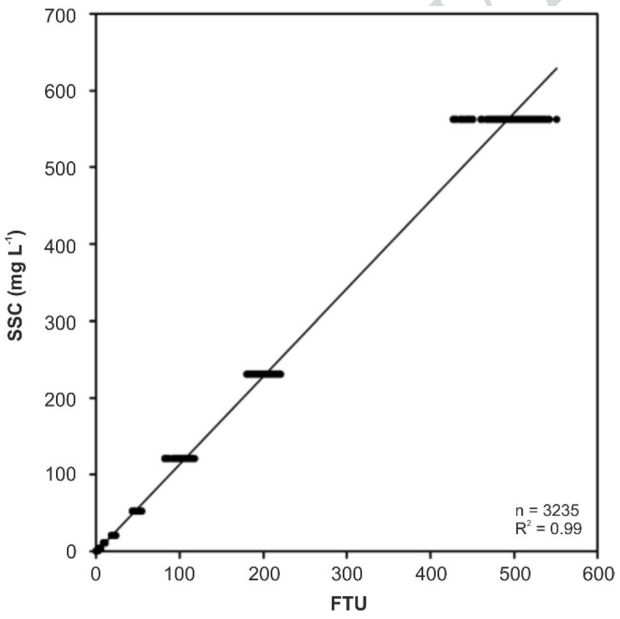

Fig. 3 Relation between the turbidity signal (FTU) and the measured suspended sediment concentration (SSC, mg L^{-1}) for the eight turbidity sensors used in this laboratory calibration

Sediment fluxes

Near-bottom currents and SSC data were used to calculate instantaneous suspended sediment fluxes, as well as time-integrated cumulative suspended sediment transport at each timestep (i), following:

$$Flux_i = V_i \times C_i = current_i \times SSC_i$$

where current speed_i, in m s^{-1}, multiplied by SSC, in mg L^{-1}, yielded to instantaneous suspended sediment flux in g m^{-2} s^{-1}.

Then, the time integrated cumulative suspended sediment transport (in kg m^{-2}) can be calculated following:

$$Cumulative\ transport = \sum_{i=1}^{N} Flux_i \times \Delta t = Sum\ of\ flux_i\ x\ time\ step$$

where the timestep was 5 min (or 300 s), corresponding to the measuring interval of the near-bottom current meter placed at 923 m depth. This multiplied by the instantaneous suspended sediment flux yielded to the time-integrated cumulative suspended sediment transport.

An intermediary computation prior to calculating sediment flux and cumulative transport is needed to estimate the current components with respect to geographical coordinates by applying an angle Θ of rotation. In our study, to obtain the along- and across-canyon components at the mooring location, the North and East current components were rotated 70 degrees counterclockwise based on the canyon axis orientation.

For the along-canyon component up-canyon fluxes are positive, whereas for the down-canyon fluxes are negative. For the across-canyon component NE orientation fluxes are positive, whereas SW fluxes are negative. The integration of the instantaneous suspended sediment fluxes for the duration of the study period yields the cumulative across- and along-canyon suspended sediment transports.

Long time series have an uncertainty associated to errors on the measurement of the different variables, which deserve to be calculated to complete sediment flux and time-integrated cumulative transport calculations. These uncertainties are derived from measurements of particle concentration derived from turbidity, as well as the propagation error along the time series. Hence, for any measure on a time series, we have an uncertainty on both along- and across-canyon current components (σ_v), an uncertainty on suspended sediment concentration (σ_c), and an uncertainty on suspended sediment fluxes (σ_F) and time-integrated cumulative transport (σ^2_{NF}). Estimated parameters' uncertainties derived from the measurement errors corresponding to each independent

Journal : Large 11001 | Article No : 9457 | Pages : 22 | MS Code : 9457 | Dispatch : 8-11-2021

time series are shown in Table 1. The uncertainty (or error propagation) in suspended sediment fluxes, for each time step, can be calculated following:

$$\sigma_F^2 = \left(\frac{\partial F}{\partial Speed}\right)^2 \times \sigma_{Speed}^2 + \left(\frac{\partial F}{\partial Dir}\right)^2 \times \sigma_{Dir}^2 + \left(\frac{\partial F}{\partial Turb}\right)^2 \times \sigma_{Turb}^2$$

$$\begin{aligned}\sigma_F^2 = {} & ([A \times Turb] \times cos(90 - Dir + \theta))^2 \times \sigma_{Speed}^2 \\ & + (-Speed \times [A \times Turb] \times sin(90 - Dir + \theta))^2 \times \sigma_{Dir}^2 \\ & + \left(A \times \left[Speed \times cos(90 - Dir + \theta)\right]\right)^2 \times \sigma_{Turb}^2\end{aligned}$$

The uncertainty associated to time-integrated cumulative transport (NF) is calculated following:

$$\sigma_{NF}^2 = \Delta t^2 \times \sum_{i=1}^{N} \sigma_{Flux_i}^2$$

Assessment of fishing effort

The activity of bottom trawlers around the Palamós Canyon operating in the fishing grounds of Sant Sebastià (northern canyon flank) and Rostoll (southern canyon flank) (Fig. 1) was obtained from ShipLocus®, the main module of the Spanish Ports Authority to exploit maritime traffic data for management and research purposes (Puertos del Estado 2017), through the use of Automatic Identification System (AIS) tracking. Vessels with AIS provide their position omni-directionally at intervals that can vary from 2 s to 3 min to nearby AIS-bearing ships, as well as to coastal stations and satellites, enabling the monitoring of fine-scale vessel behaviors and movement patterns (Natale et al. 2015).

The spatial fishing effort was estimated using AIS data from year 2017, which included the study period, and consisted in static data of fishing vessels (vessel name, call sign identifier, IMO number, dimensions) and their dynamic data (vessel position, speed over ground, course over ground and heading). Since the total volume of AIS dataset exceeded computational dataset management capacities, the dataset was reduced to the first entry per minute of each vessel. This resulted in a smaller and homogeneous dataset for the study period. Vessels equipped with otter trawl boards (OTB) were extracted by cross-checking the AIS dataset with data from the Community Fishing Fleet Register (European Commission Fisheries and Maritime Affairs 2014). AIS data were then filtered according by speed to infer whether an AIS message corresponded to fishing activity, using similar criteria to those used in previous studies (e.g., Natale et al. 2015; Oberle et al. 2016a; Paradis et al. 2021). It assumes that bottom trawler speed follows a bimodal distribution corresponding to navigating (high speed) and trawling (low speed) conditions. Trawling speed was finally obtained as the mean of the first gaussian distribution ± 2 standard deviations (95 % of the distribution) of the OTB vessel speeds. This interval corresponds to speeds between 0.8 and 3.9 knots. However, simply filtering according to this trawling speed may lead to false-positives, when a trawler is navigating or drifting at a specified trawling speeds, and false-negatives, when a trawler is hauling at anomalous speeds for a few minutes due to piloting reasons (i.e., when trawling down-slope the vessel needs to reduce its speed to keep the gear on the seafloor). Hence, a minimum length of 10 min per haul was assumed to correct for false-positives, whereas anomalous speeds that lasted less than 5 min were considered to correct for false-negatives. Hauls per vessel were then defined as consecutive entries that met these trawling criteria for at least 100 min.

Finally, bottom trawling effort was obtained from the total number of hauls within one hectare (100 × 100), assuming an average trawling-door spread of 100 m. These units are a good indicator of the times that a trawler tows an area and can be used as a proxy of their capacity to resuspend bottom sediments (Ragnarsson and Steingrimsson 2003; Martín et al. 2014b). Trawling effort was finally represented and plotted using ArcGIS© 10.4 software for the entire monitoring period (Fig. 1), and for the trawling closure (spanning from February 7 to March 8) and for the trawling season (spanning from March 9 until the end of the study period on April 7) (Fig. 2).

Table 1 Estimated parameters' uncertainties derived from the measurement errors to each independent time series. The variance of the variables as well as constant parameters are shown. "A" corresponds to the constant that multiplies FTU values to yield SSCs, while Θ corresponds to the angle of rotation applied to obtain along- and across-canyon currents. In this case, $\Theta = 70º$, with respect to the North and East components, is applied in the equations for uncertainty calculations

Variable	Variance/constant	Value
Current speed	σ_{Speed}	± 0.005 m s^{-1}
Current direction	σ_{Dir}	$\pm 5º$
Turbidity	σ_{Turb}	± 2.7 FTU
Constant of turbidity	A	1.14
Angle of rotation (counter-clockwise)	Θ	70º

Ancillary data

The daily discharges of the Ter and the Daró rivers, located slightly northwards of the Palamós Canyon, were supplied by the Agència Catalana de l'Aigua (Catalan Government Water Agency), and have been used to assess the riverine sediment supplies during the study period. This data is available online via ACA's website (http://aca-web.gencat.cat/sdim21/seleccioXarxes.do).

Wave conditions during the study period were provided by the REDEXT network of deep-water oceanographic buoys of the Spanish Ports Authority (http://www.puertos.es/es-es/oceanografia/Paginas/portus.aspx) and recorded hourly by the Cap de Begur buoy, located offshore on the northern continental slope region next to Palamós Canyon, over the 1200 m isobath (41° 55.2′ N; 3° 39.0′ E).

Results

Activity of OTB vessels

The fishing grounds of the Palamós canyon were exploited by 34 OTB vessels, most of which from the Palamós harbor, but occasionally from Blanes and Roses harbors (located southwards and northwards, respectively, and not shown in Fig. 1).

Time-series observations on OTB vessel positions, based on fishing effort, revealed no trawling activity occurred around the mooring site during the trawling closure at the flanks of the canyon (not shown), while during the trawling season, the fishing effort increased on both canyon flanks (Fig. 2). In the Rostoll fishing ground section located closer to the mooring and CTD transect, bottom trawling occurred at relatively shallow depths ranging from 250 to 450 m, at a predominating frequency of 5 hauls per hectare. The fishing effort in the Rostoll fishing ground increased seawards, reaching 10–30 hauls per hectare at 500–600 m depth. At the Sant Sebastià fishing ground, the predominating frequency in the canyon wall next to the mooring and the CTD transect was 20–40 hauls per hectare between 400 and 800 m depth (Fig. 2). The number of daily hauls was computed at both fishing grounds during the monitored trawling season, being generally higher in Sant Sebastià than in Rostoll, and accounting for a total of 74 hauls against 31 hauls, respectively (Fig. 4).

More scattered trawling activity was also observed on the upper continental slope at depths < 200 m (Fig. 2). This fishing effort was estimated to be less than 5 hauls per hectare during the monitored trawling season. The number of hauls computed at these depths was considerably smaller in comparison to those computed at the depths of the canyon flanks' fishing grounds and accounted for a total of 18 hauls for the monitored trawling season (Fig. 4).

Forcing conditions

During the monitoring period, several storms, defined as sustained significant wave heights (Hs) greater than 2 m for more than 6 h (Mendoza and Jiménez 2009), were recorded during the monitoring in early February, and early- and late-March, the majority of them caused by strong northern winds and with Hs > 3 m (Fig. 5a). These events were generally dry storms (Guillén et al. 2006) that did not lead to significant increases in Ter and Daró River discharges (Fig. 5b).

Four major storms (Hs > 4 m) were recorded during the monitoring period. A strong northern storm occurred in early February with maximum Hs of 4.9 m, which lasted more than 15 h (Fig. 5a). A unique strong eastern storm with maximum Hs of 4.7 m at the peak of the storm that lasted from February 12 to February 16 (Fig. 5a) caused a torrential Ter River discharge that reached 30.6 $m^3\ s^{-1}$ on February 15, concurrent with a small increase of 6.0 $m^3\ s^{-1}$ at the Daró River (Fig. 5b). A stronger northern storm with a maximum Hs of 5.1 m occurred on March 4 that lasted for

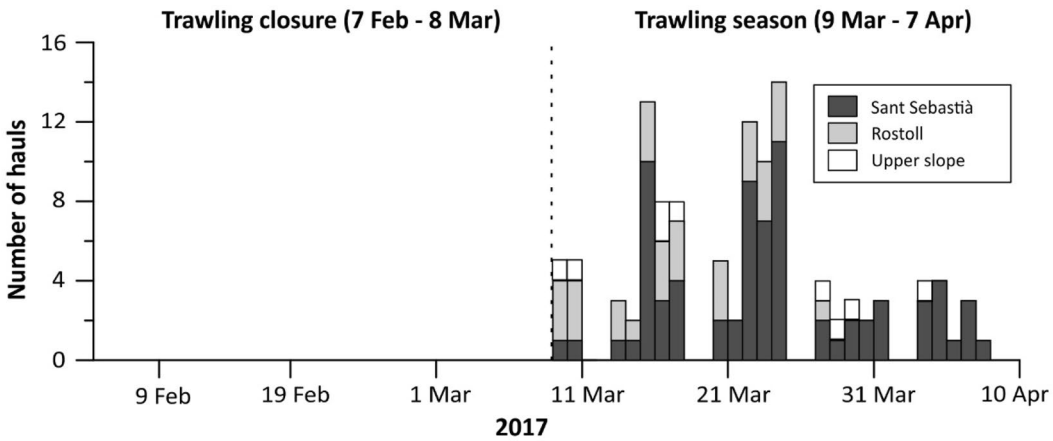

Fig. 4 Daily hauls in the Sant Sebastià and Rostoll fishing grounds, and in the upper slope region during the monitoring period. The dashed line separates the trawling closure from the trawling season

Journal : Large 11001 | Article No : 9457 | Pages : 22 | MS Code : 9457 | Dispatch : 8-11-2021

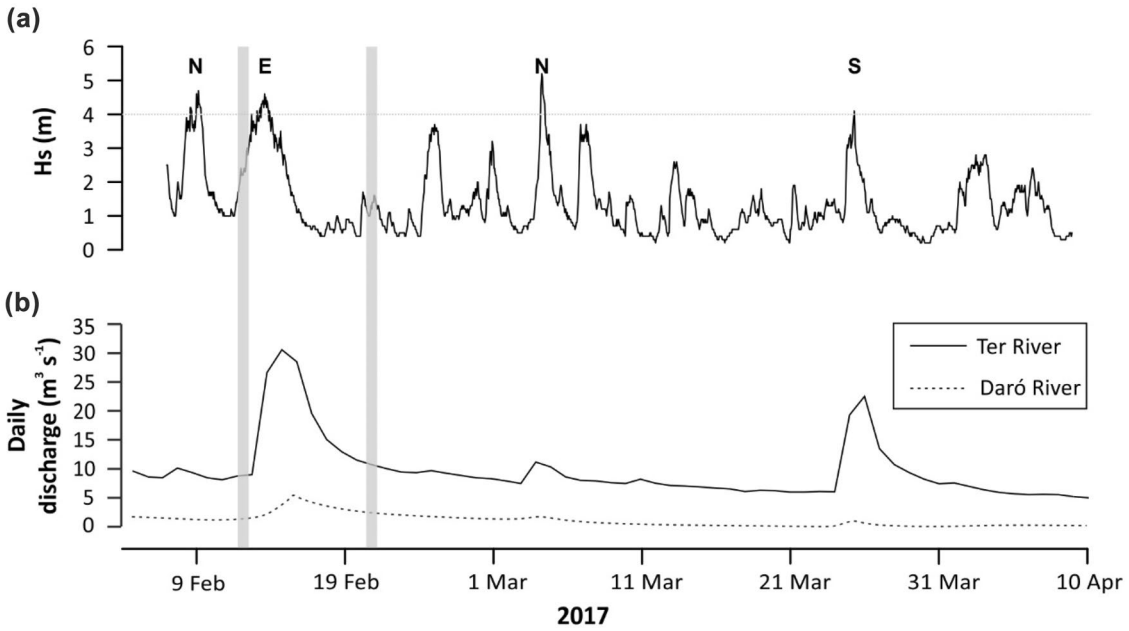

Fig. 5 Temporal evolution of the **a** significant wave height (*Hs*, m) measured at the Cap de Begur buoy and **b** the Ter and the Daró river discharges ($m^3\ s^{-1}$) during the monitoring period. Major storms, with Hs > 4, are indicated with an N (northern storms), E (eastern storms) or an S (southern storms) according to their origin. The occurrence of dense shelf water cascading (DSWC) events is indicated by a grey vertical bar

two days (Fig. 5a) and led to a Ter River discharge of 11.1 $m^3\ s^{-1}$ and a Daró River discharge of 2.2 $m^3\ s^{-1}$ (Fig. 5b). At the end of the study period, a strong southern storm with maximum Hs of 4.1 m occurred on March 25 (Fig. 5a), which lead to a Ter River discharge of 19.4 $m^3\ s^{-1}$ and a Daró River discharge of 1.5 $m^3\ s^{-1}$ (Fig. 5b).

Time series observations

Identification of water masses

Compiled data of all hydrographic profiles during the monitoring period revealed distinct changes in temperature and salinity throughout the water column that are ascribed to the different water masses in the study area (Fig. 6).

The old Atlantic Water (oAW) occupied the shallowest water column (150–300 m) during most of the recording period (Figs. 6 and 7). Below oAW, the temperature and salinity time series, as well as the *Θ*-*S* diagram, showed the more saline Levantine Intermediate Water (LIW), mainly centered at 500–600 m water depth (Figs. 6 and 7). The Western Mediterranean Deep Water (WMDW) was generally observed at the deepest part of the hydrographic profiles, exhibiting its characteristic temperature and salinity values (Figs. 6 and 7). In addition to these water masses, the seasonal Western Intermediate Water (WIW, *Θ* = 12.9–13.2 ºC; *S* = 38.1–38.3) and two pulses of Dense Shelf Water (DSW), displaying temperature minima reaching < 12.6 ºC along with salinity values < 38.2,

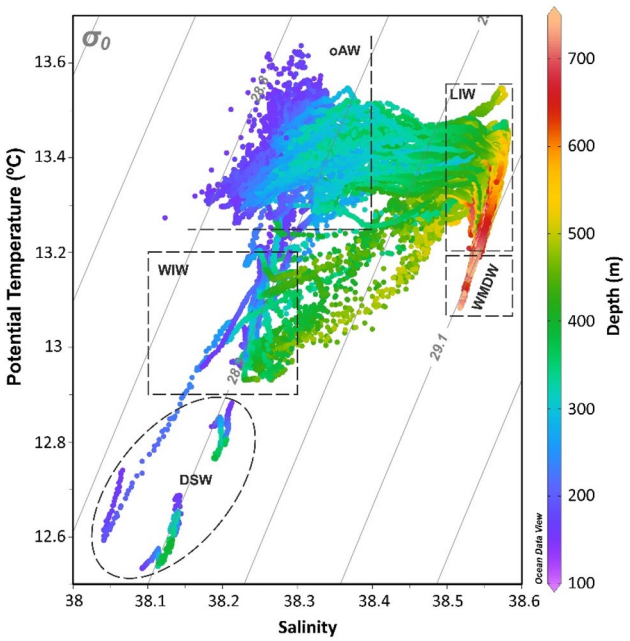

Fig. 6 General *Θ*-*S* diagram for all the hydrographic casts acquired by the autonomous hydrographic profiler (Aqualog) during the monitoring period identifying the different water masses in the study area: oAW (old Atlantic Water), WIW (Western Intermediate Water), DSW (Dense Shelf Water), LIW (Levantine Intermediate Water), WMDW (Western Mediterranean Deep Water). For interpretation of the references in color in this figure legend, the reader is referred to the web version of this article

Journal : Large 11001 | Article No : 9457 | Pages : 22 | MS Code : 9457 | Dispatch : 8-11-2021

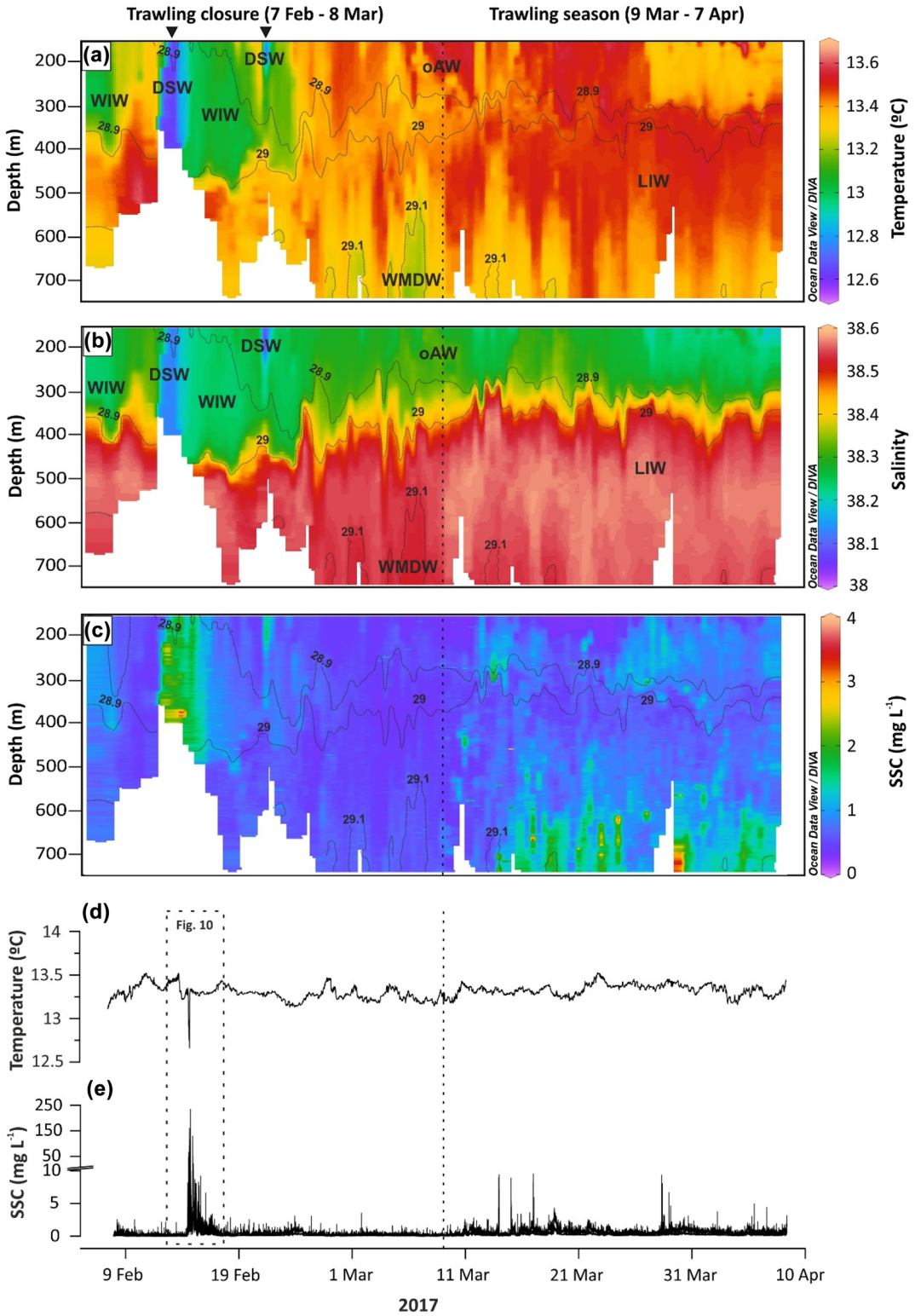

Fig. 7 Time series of **a** temperature (ºC) **b** salinity, and **c** suspended sediment concentration (SSC, mg L^{-1}) measured by the autonomous hydrographic profiler (Aqualog), as well as **d** temperature (ºC) and **e** SSC measured by the near-bottom instrumentation during the monitoring period. Panels a and b show the different water masses being present in the study area: oAW (old Atlantic Water), WIW (Western Intermediate Water), DSW (Dense Shelf Water), LIW (Levantine Intermediate Water), WMDW (Western Mediterranean Deep Water). The occurrence of two dense shelf water cascading (DSWC) events is indicated by a black triangle. Blank spaces represent incomplete profiles. The dashed line separates the trawling closure from the trawling season. For interpretation of the references in color in this figure legend, the reader is referred to the web version of this article

Journal : Large 11001 | Article No : 9457 | Pages : 22 | MS Code : 9457 | Dispatch : 8-11-2021

were observed at the beginning of the recording period (Figs. 6 and 7). Particularly, the presence of DSW and WIW over the Palamós Canyon occurred from February 7 to February 24, the latter mainly ranging from 150 to ~400 m depth (Fig. 7a, b).

Evolution of water column suspended sediment concentration (SSC)

The vertical particulate matter distribution showed increasing SSC (up to 1 mg L^{-1}) that lasted for the first two days of the monitoring period, in agreement with the presence of WIW (Fig. 7c). Immediately afterwards, the water turbidity decreased and maintained values < 0.8 mg L^{-1} in the profiled water column for 6 days, when water turbidity increased to between 1.1 and 3.8 mg L^{-1} from February 13 to February 15 coinciding with the first DSW pulse into the canyon (Fig. 7a–c) (see the first black triangle). This DSWC event was noted by a sharp decrease in temperature (~0.5 ºC) and salinity (~0.2) values (Fig. 7a, b). This first pulse of DSW was detected all along the entire profiling range recorded at that time. However, it was only observed reaching depths between 370 and 400 m in the hydrographic profiles recorded by the Aqualog, without being able to capture its deeper limit in these profiles (Fig. 7a-c). This DSW pulse reached the canyon axis, as observed by the temperature and turbidity values recorded close to the bottom by the near-bottom instrumentation, presenting near-bottom temperatures of ~12.6 ºC (Fig. 7d) and maximum SSC of ~234 mg L^{-1} (Fig. 7e). Afterwards, water turbidity maintained relatively high SSCs along the hydrographic profiles for three days associated with the presence of WIW, ranging from 0.4 to 1.1 mg L^{-1} down to depths of ~500 m (Fig. 7c). On February 21, the shallowest part of the hydrographic profiles recorded a new decrease in temperature and salinity values, and an increase of SSC of 2.2 mg L^{-1}, coinciding with the arrival of the second pulse of DSW into the canyon (Fig. 7a-c). However, it only lasted for a few hours and descended to maximum water depths of 200 m (see the second black triangle), without displacing the WIW found underneath (Fig. 7a, b). After this event, and until February 24, the vertical particulate matter distribution still showed events of moderate SSC elevation in the water column that ranged between 0.3 and 0.9 mg L^{-1} from the uppermost part of the hydrographic profiles to maximum water depths of 500 m (Fig. 7c). From February 24 to the end of the study period, the WIW was absent and recorded temperature and salinity values that corresponded to the more general hydrographic structure of the northwestern Mediterranean, with the presence of surface oAW, the core of LIW at mid-waters and centered between 500 and 600 m and the WMDW occupying the deeper part of the profiled water column (Fig. 7a, b). During this period, the vertical distribution of particulate matter showed no periods of significant SSC increase in the profiled water column until the beginning of the trawling season on March 9 (Fig. 7c).

During the trawling season, several SSC increases were recorded at intermediate waters (from 150 to 300 m depth), reaching up to 2.5 mg L^{-1} and at the lower part (> 500 m depth) of the profiled water column (Fig. 7c). A relative clear water minimum was recorded between 300 and 500 m water depth. The maximum SSC was recorded on March 30 at ~718 m depth, reaching up to 3.8 mg L^{-1} (Fig. 7c). Near-bottom time series (923 m depth) of temperature and turbidity values remained constant during most of the time, displaying temperature values ranging from 13.2 to 13.6 ºC (Fig. 7d) and SSC < 1.5 mg L^{-1} (Fig. 7e). Punctual increases in SSC between 5 and 10 mg L^{-1} were recorded during the trawling season (Fig. 7e), although such increases showed no relation with temperature fluctuations.

The NPSC for the upper part of the profiled water column peaked at ~40.7 mg cm^{-2} and 23.3 mg cm^{-2} during the two DSW pulses, respectively (see black triangles in Fig. 8a), and decreased to baseline NPSC values (~10 mg cm^{-2}) at the end of the closure season. The NPSC values increased again in the trawling season, when almost a double-fold increase in the NPSC (~20 mg cm^{-2}) was observed (Fig. 8a). In the second approach, considering the entire profiling range, the NPSC varied between 8.3 and 20.8 mg cm^{-2} during the end of the closure season, whereas it was doubled and even quadrupled during the trawling period, reaching maximum values of 50.1 mg cm^{-2} (Fig. 8b).

Near-bottom currents

During most of the recording period, near-bottom currents followed the canyon axis (Fig. 9a, b). Current speeds varied between 0.05 and 0.25 m s^{-1} during most of the monitoring in both along- and across-canyon directions (Fig. 9c, d), although periodic reversals in the current direction mainly oriented up- and down-canyon were observed (Fig. 9c).

This general current pattern was altered between February 14 and February 15, during the first DSW pulse, when near-bottom currents and SSC changed drastically (Figs. 9 and 10). During the first stages of this event, temperature experimented a slight increase of 0.2 ºC (Fig. 10a), concurrent with an increase of the down-canyon current velocity up to 0.2 m s^{-1} (Fig. 10b) but slightly oriented towards the NE sector (Fig. 10c), while turbidity progressively increased up to 75 mg L^{-1} (Fig. 10d). A sharp decrease in near-bottom temperature (~0.5 ºC) reaching down to 12.6 ºC (Fig. 10a) was recorded afterwards and, simultaneously, currents reached speeds of 0.3 m s^{-1} with dominant down-canyon direction but oriented towards the SW (Fig. 10b, c), while near-bottom turbidity increased up to 160.1 mg L^{-1} (Fig. 10d). Three hours later, the temperature increased to 13.3 ºC (Fig. 10a), which was

Journal : Large 11001 | Article No : 9457 | Pages : 22 | MS Code : 9457 | Dispatch : 8-11-2021

concurrent with a maximum peak in current speed up to 0.6 m s^{-1} directed up-canyon (Fig. 10c). When this current reversal occurred, a sharp increase in turbidity was observed, reaching maximum SSC of ~234 mg L^{-1} (Fig. 10d). Near-bottom currents maintained the up-canyon flow direction for almost 5 h (Fig. 10b), and turbidity values gradually decreased to 4 mg L^{-1} (Fig. 10d). Afterwards, the near-bottom current flow reversed following the down-canyon direction (Fig. 10b) and slightly towards the SW (Fig. 10c). Another current reversal of up to 0.3 m s^{-1} was detected up-canyon (Fig. 10b), while another concurrent important turbidity peak of 96 mg L^{-1} was recorded (Fig. 10d). Towards the end of this event, the current speed and turbidity decreased to baseline values (Fig. 10b–d).

Near-bottom suspended sediment fluxes and cumulative transport

During most of the trawling closure, instantaneous along-canyon near-bottom suspended sediment fluxes fluctuated between 0.02 and 0.1 g m^{-2} s^{-1} (Fig. 11a) and between 0.01 and 0.06 g m^{-2} s^{-1} in the across-canyon direction (Fig. 11b). However, during the first DSWC pulse, there was an increase in both along- and across-canyon suspended sediment fluxes. In the along-canyon direction, suspended sediment flux increased up to 19 g m^{-2} s^{-1} down-canyon, but the more important suspended sediment flux was registered up-canyon, reaching values of 44 g m^{-2} s^{-1} (Fig. 11a). In the across-canyon direction, suspended sediment flux increased up to 8.8 g m^{-2} s^{-1} towards the NE, although the maximum suspended sediment flux was registered towards the SW reaching up to 35 g m^{-2} s^{-1} (Fig. 11b). The cumulative transport after this event was up-canyon (Fig. 11c) and towards the SW (Fig. 11d), reaching values of 50 kg m^{-2} and 80 kg m^{-2}, respectively.

During the trawling season, near-bottom instantaneous along-canyon suspended sediment flux ranged from 0.1 to 0.7 g m^{-2} s^{-1} and was predominantly in the up-canyon direction, and across-canyon suspended sediment flux reached maximum values of 1.4 g m^{-2} s^{-1} mainly towards the SW (i.e., coming from the northern flank) (Fig. 11a, b). Therefore, throughout the trawling season, the resultant cumulative suspended sediment transport was in the up-canyon direction and from the northern canyon flank (towards the SW) in the across-canyon component, reaching 40 kg m^{-2} and 20 kg m^{-2}, respectively (Fig. 11c, d).

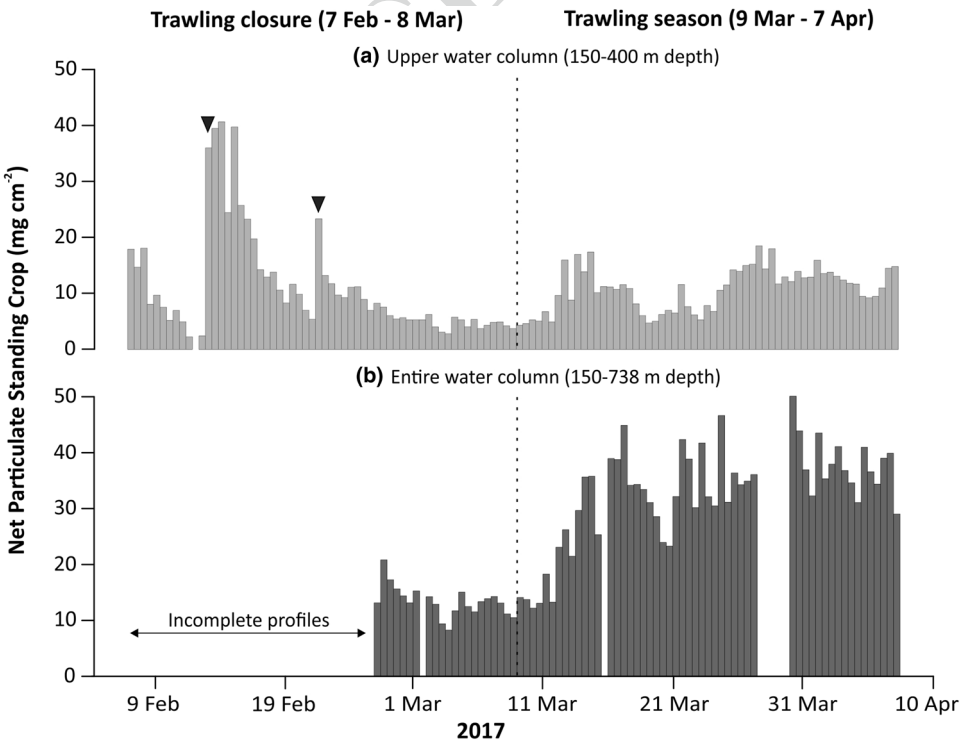

Fig. 8 Net Particulate Standing Crop for **a** the upper water column (150–400 m depth) and for **b** water depths between 150 to 738 m depth during the monitoring period. The occurrence of two dense shelf water cascading (DSWC) events is indicated by a black triangle. The dashed line separates the trawling closure from the trawling season

Journal : Large 11001 | Article No : 9457 | Pages : 22 | MS Code : 9457 | Dispatch : 8-11-2021

CTD transect

The hydrographic data obtained by the June 7, 2017 high-resolution CTD transect across the Palamós canyon head from the surface down to 925 m water depth revealed distinct changes in temperature and salinity throughout the water column (Fig. 12). In the first 50 m of water column, waters with distinctly low salinities (38.0-38.2) and high temperatures (15–19 ºC) were observed (Fig. 12a, b), most probably corresponding to the influence of the seasonal thermocline. The signature of the oAW, characterized by temperatures > 13 ºC (Fig. 12a) and salinity values ranging from 38.0 to 38.4 (Fig. 12b), was found underneath, reaching water depths down to 200 m in the northern canyon flank and ~ 300 m in the southern canyon flank. Below (down to ~ 800 m water depth), the temperature and salinity along the transect showed the more saline LIW core, which displayed a salinity maximum (S > 38.5) centered ~ 500 m water depth (Fig. 12a, b). The deepest part of the water column was occupied by the WMDW that exhibited temperature minima of 13 ºC and salinity values of 38.5 (Fig. 12a, b).

SSC distribution across the studied canyon section showed a surface clear water layer down to ~ 100 m water depth and a continuous INL with concentrations ~ 0.5 mg L^{-1} extending over the entire canyon width in the water parcel occupied by the oAW (Fig. 12c). Within the canyon confinement, the central part of the water column mainly corresponded to the upper levels of the LIW core and was characterized by low SSC, whereas near-bottom waters in both canyon flanks and close to the canyon axis displayed higher SSC. Over the southern canyon wall, there was a detachment of a thin BNL mainly centered at ~ 300 m depth, reaching SSC up to 3 mg L^{-1} (Fig. 12c, station #2). This detachment extended ~ 450 m horizontally

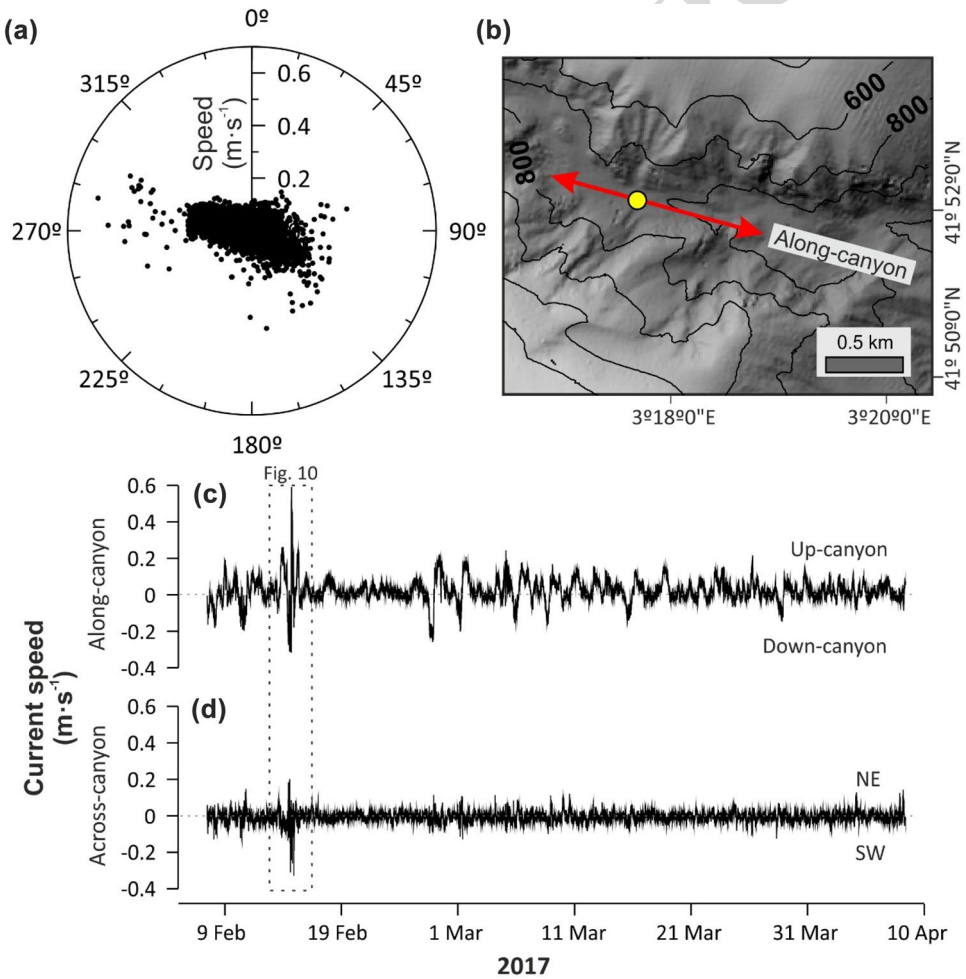

Fig. 9 Near-bottom currents during the monitoring period. **a** Polar plot of current speed and direction showing the preferential current orientation. **b** Close-up of the bathymetry at the mooring location (yellow dot) and the canyon axis orientation used to rotate the current velocity components (red arrow). Panels **c** and **d** correspond to the time series of along-canyon current velocity and across-canyon current velocity components, respectively

Journal : Large 11001 | Article No : 9457 | Pages : 22 | MS Code : 9457 | Dispatch : 8-11-2021

towards the canyon interior as an INL, which was observed in station #3 at the same water depth, but with SSC values of 0.5 mg L^{-1}. On the northern canyon wall, a well-developed BNL displaying SSCs up to 1.5 mg L^{-1} was observed at ~ 450 m water depth (Fig. 12c, station #11), which evolved towards the canyon interior and to a less concentrated and thicker BNL, with SSC ~ 1 mg L^{-1} extending from 550 to 700 m depth (Fig. 12c, station #10). The lower part of the profiled water column over the canyon axis (stations #5 to #9) showed SSC > 0.5 mg L^{-1} that corresponded to scattered and isolated INLs showing poor lateral continuity among consecutive hydrographic casts (Fig. 12c).

Discussion

Natural-induced water turbidity and suspended sediment transport

The earlier studies using moored instrumentation demonstrated that river floods and storms enhanced particle fluxes inside submarine canyons and on the continental slope (Monaco et al. 1990; Puig and Palanques 1998b), and for a long time, these processes were considered the major contemporary mechanisms able to transport sediments from shallow water environments to deeper environments. Recent studies conducted in the NW Mediterranean also recognize

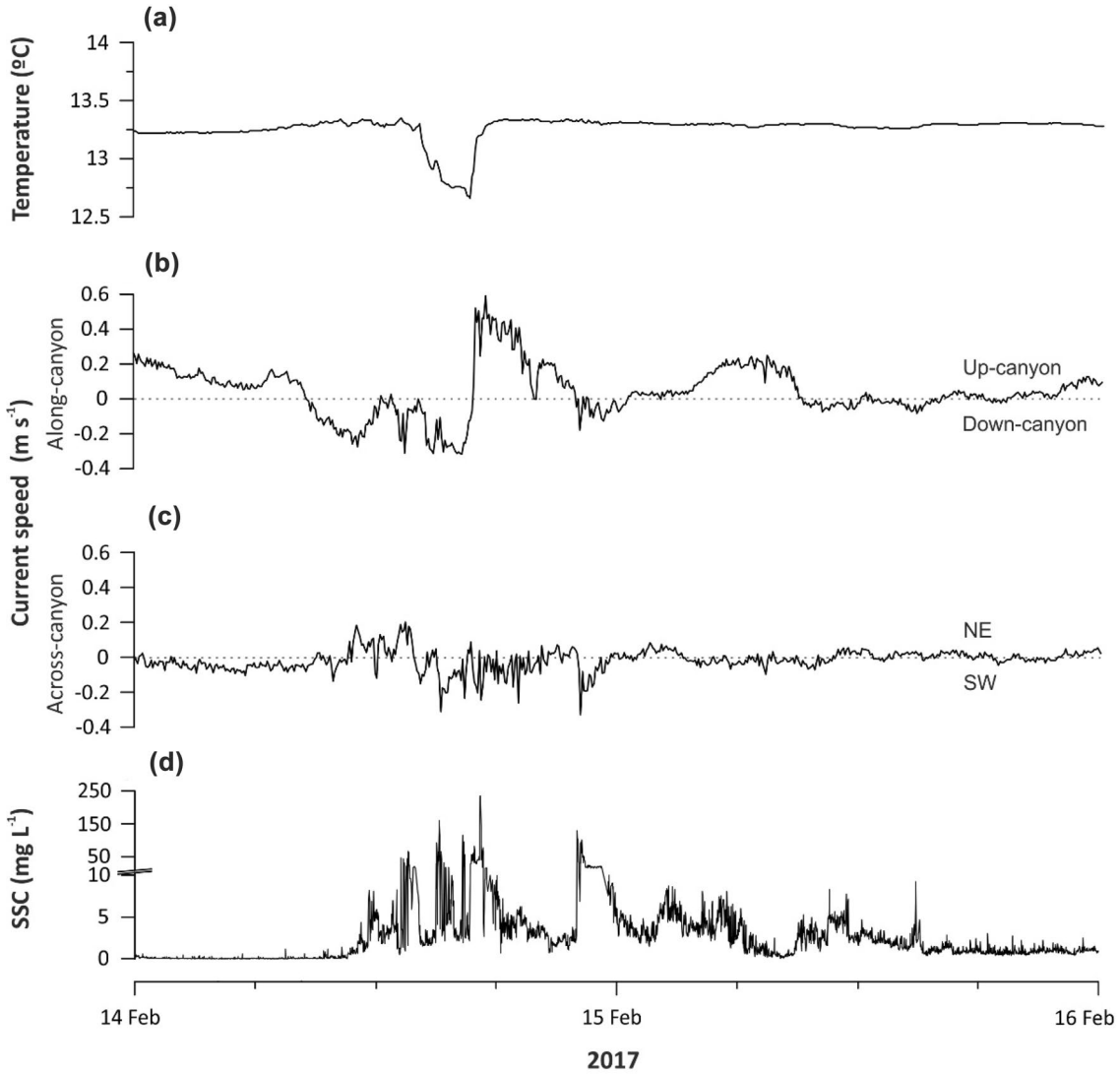

Fig. 10 Time series of near-bottom **a** temperature (ºC), **b** along-canyon current velocity (m s^{-1}), **c** across-canyon current velocity (m s^{-1}), and **d** suspended sediment concentration (SSC, mg L^{-1}) measured during the first DSWC event

Journal : Large 11001 | Article No : 9457 | Pages : 22 | MS Code : 9457 | Dispatch : 8-11-2021

the importance of the formation of dense shelf waters and their subsequent downslope cascading, exporting sediment particles towards deep-sea regions (Canals et al. 2006; Palanques et al. 2006a). DSWC events occur frequently, preferentially during early winter, after a period of several months without significant storms during which the continental shelf can be covered by easily resuspendable sediment from nearby rivers.

In the Palamós Canyon, Ribó et al. (2011) reported for the first time the presence of DSWC events related to eastern storms. In this investigation, priority was given to the deployment of near-bottom instruments at the canyon head, on the assumption that most of the suspended sediment transport and water turbidity increases were coming from the shelf and relatively confined near the canyon seafloor. The results presented in this new study contribute to refine the sediment dynamics associated to DSWC events in the Palamós Canyon providing additional information throughout the water column, as well as near the bottom at a deeper canyon axis location (Figs. 7, 8, 9, 10 and 11). During the present study, the first DSWC event was enhanced by a major eastern storm that occurred between February 12 and February 16, which also led to a torrential water discharge from the Ter River. The eastern storm was most probably responsible for the expulsion of dense coastal waters on the shelf upstream of the canyon, which alongside with the ephemerally sediment deposited on the shelf by the Ter River, generated high downslope and down-canyon sediment transport into Palamós Canyon. The DSW signal was detected along the profiled water column from 150 to 377 m depth and also

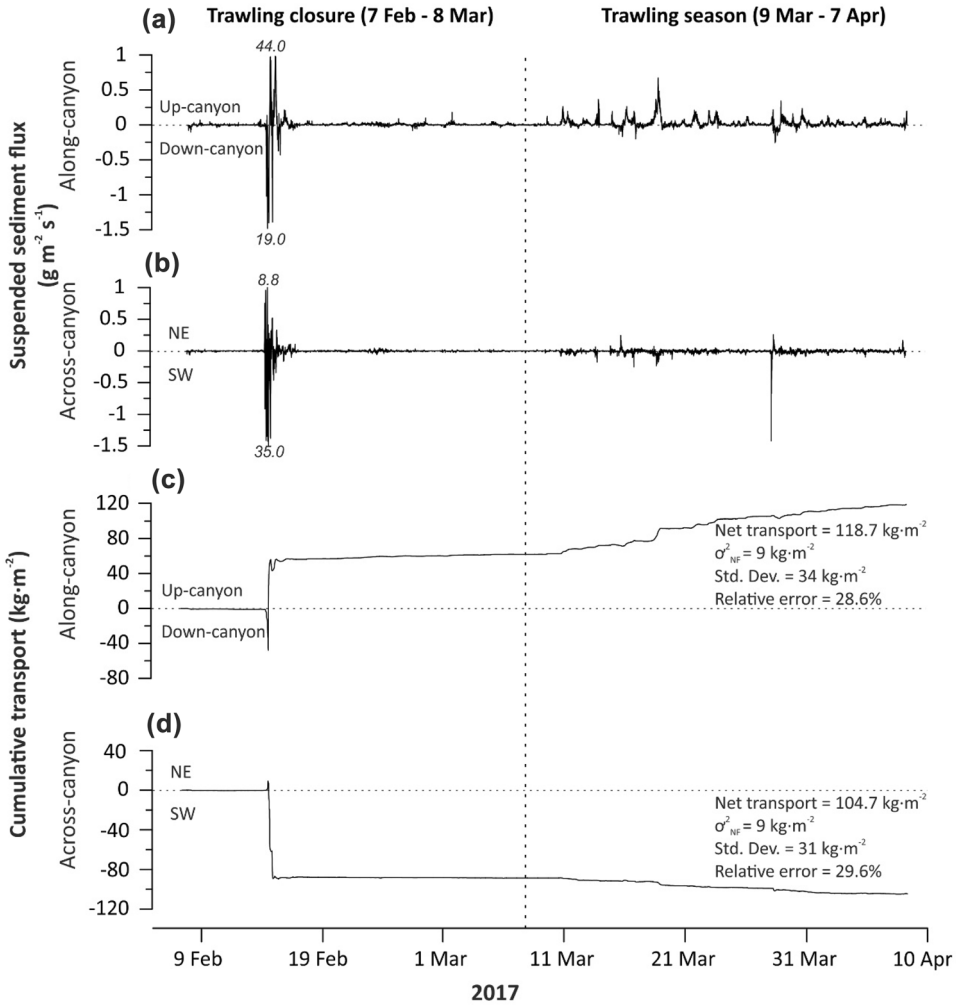

Fig. 11 **a** Instantaneous along-canyon suspended sediment flux (g m^{-2} s^{-1}), **b** instantaneous across-canyon suspended sediment flux (g m^{-2} s^{-1}), **c** along-canyon cumulative transport (kg m^{-2}) and **d** across-canyon cumulative transport (kg m^{-2}) at the mooring site during the monitoring period. Maximum sediment fluxes reached during DSWC events are indicated in italics. The dashed line separates the trawling closure from the trawling season. Inset on panels **c** and **d** provides the time-integrated cumulative transport (net transport) for the along- and across-canyon components and their uncertainty (σ^2_{NF}), the standard deviation and the relative error derived from these calculations for the entire monitoring period

Journal : Large 11001 | Article No : 9457 | Pages : 22 | MS Code : 9457 | Dispatch : 8-11-2021

near the bottom at 923 m depth (Fig. 7), which suggests an increase of turbidity throughout the entire water column. Although relatively high SSC increases were recorded at intermediate water depths (> 3.5 mg L^{-1}) (Fig. 7c), very strong SSC increases (> 200 mg L^{-1}) occurred near the bottom (Fig. 7e). This indicates that the cascade of DSW during this event caused a rapid advection of cold and turbid waters down to the deepest part of the surveyed water column, presumably transporting easily erodible sediment particles on their way as they moved down-canyon, generating high near-bottom suspended sediment fluxes (Fig. 11a, b; Table 2). Previously recorded DSWC events in Palamós Canyon by Ribó et al. (2011) were specific for the canyon head (325 m depth) and accounted for lower down-canyon current velocities (> 0.4 m s^{-1} versus 0.6 m s^{-1}) and lower SSC peaks (~ 6 mg L^{-1} versus > 200 mg L^{-1}) than in the canyon axis. However, DSWC events of similar magnitude to that observed during the present study have been

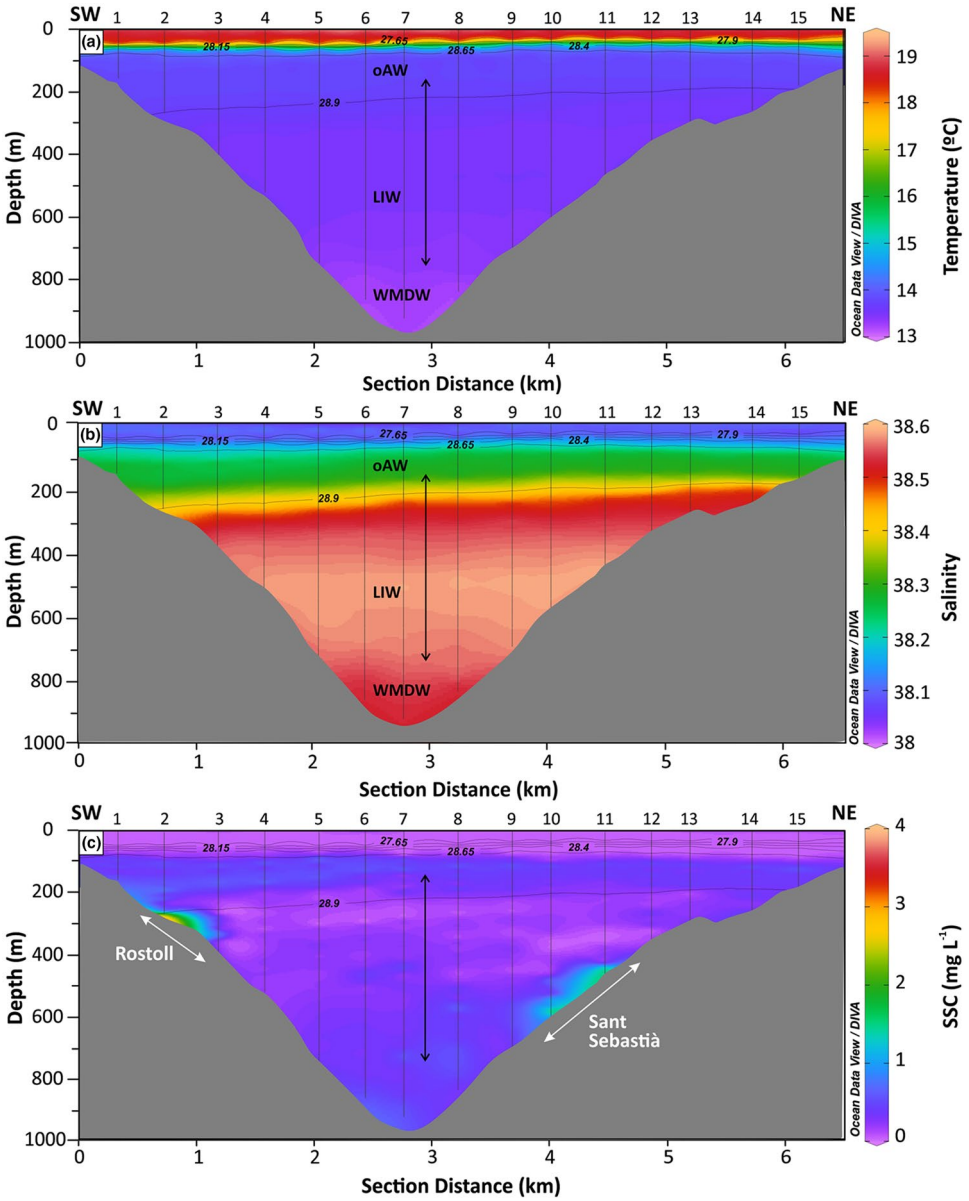

Fig. 12 CTD transect conducted in June 7, 2017 across the Palamós Canyon showing the distribution of **a** potential temperature (ºC), **b** salinity, with the different water masses present in the study area (see Fig. 5 for details), and **c** suspended sediment concentration (SSC, mg L^{-1}). The black arrow indicates the working depth range of the autonomous hydrographic profiler (Aqualog) and the white arrows indicate the bathymetric range occupied by the Sant Sebastià and Rostoll fishing grounds extracted from the AIS spatial distribution at the location where the CTD transect was conducted (see location in Fig. 2). For interpretation of the references in color in this figure legend, the reader is referred to the web version of this article

Journal : Large 11001 | Article No : 9457 | Pages : 22 | MS Code : 9457 | Dispatch : 8-11-2021

recorded in the Cap de Creus Canyon, where near-bottom SSC > 170 mg L^{-1} and currents of ~ 0.6 m s^{-1} were registered (Ribó et al. 2011).

During the first stages of the major DSWC event recorded during the study, the near-bottom suspended sediment fluxes were mainly directed down-canyon and towards the SW (Fig. 11a, b), suggesting the arrival of a non-channeled cascade coming predominantly from the northern canyon flank. As the dominant eastern field veered to south-westerlies (not shown) and the storm ceased (Fig. 5b), currents inside the canyon reversed from down-canyon to up-canyon, peaking up to 0.6 m s^{-1} (Fig. 10b), and the DSW turbid plume was retained within the canyon's interior, increasing near-bottom SSC up to ~ 234 mg L^{-1} (Fig. 10d), generating an abrupt peak in near-bottom suspended sediment flux of 44 g m^{-2} s^{-1} directed up-canyon (Fig. 11a). This sudden change in current flow, due to the compensation of the isopycnals, has been previously described as the reversal (relaxation) phase of cascading/downwelling events (Ulses et al. 2008b), and described in detail in the Cap de Creus Canyon during a similar storm event in winter 2011 (Martín et al. 2013). The second DSW pulse detected on February 21 was not associated to any storm event nor a flashflood river discharge (Fig. 5), and in contrast to the first DSW pulse, it was shorter and only reached about 200 m depth (Fig. 7). This event generated lower SSC at the upper part of the hydrographic profiles, and no signal was recorded in the near-bottom instrumentation (Fig. 7). This mild and shallow DSW pulse was therefore smaller in magnitude and resembled those recorded at similar depths (~ 300 m depth) in this submarine canyon by Ribó et al. (2011).

During the trawling closure period, the presence of the WIW was detected at the hydrographic profiles reaching maximum water depths of ~ 400 m, alongside with relatively high SSC values in the profiled water column (Fig. 7a–c). The WIW observed during the study period could have been formed earlier during the winter season by DSWC events affecting the upper slope of the GoL (Lapouyade and Durrieu de Madron 2001; Dufau-Julliand et al. 2004; Durrieu de Madron et al. 2005a). This seasonal water mass could have then been advected southwards towards the Palamós Canyon, following the general circulation, and carrying an increased SSC signature. These high turbidity values, alongside with the increased SSC associated with the two DSW pulses, were also translated into higher NPSC during this period (Fig. 8a). Towards the end of the trawling closure period, the presence of waters generated by cooling and densification during winter (WIW and DSW) was no longer detected along the hydrographic profiles, and water turbidity decreased to almost baseline SSCs and NPSC in the upper water column, reaching the lowest values in the entire record (Figs. 7 and 8a).

Trawling-induced water turbidity and sediment transport

Considering the absence of major storm or flooding events during the trawling season (Fig. 5) and the position of OTB vessels and number of daily hauls (Figs. 2 and 4), we can infer that the occurrence of frequent events of increased water turbidity within the Palamós Canyon (Fig. 7c) was induced by the passage of OTB vessels along the canyon flanks.

Throughout the monitored trawling season, the more intense fishing activity was particularly detected at depths between 250 and 600 m at the southern canyon wall (Rostoll fishing ground), and between 400 and 800 m depth at the northern canyon wall (Sant Sebastià fishing ground) (Fig. 2). Based on the relative depths at which the trawling activities occur on each flank next to the mooring location, the shallower INLs (250–350 m water depth) observed in the hydrographic profiles and the CTD transect most probably correspond to resuspended sediment detached from the Rostoll fishing ground, whereas most of the SSC increases detected below 500 m depth could correspond to resuspension from the Sant Sebastià fishing ground (Figs. 7c and 12c). These well-developed INLs and BNLs detected at depths > 500 m are in agreement with previous observations reported by Martín et al. (2014a). In their study, a hydrographic transect conducted across the Sant Sebastià fishing ground revealed the presence of enhanced INLs and BNLs coinciding with the depth range exploited by otter trawlers. The higher number of hauls carried out at this fishing ground in contrast with the lower number of hauls

Table 2 Near-bottom instantaneous suspended sediment (SS) fluxes (g m^{-2} s^{-1}) and cumulative transport (T m^{-2}) calculated for the along- and across-canyon components during the trawling closure, which includes the DSWC period, and the trawling season. For the along-canyon component up-canyon flux values and cumulative transport are positive, whereas for the down-canyon flux they are negative. For the across-canyon component NE orientation flux values are positive, whereas for the SW orientation they are negative

	Instantaneous SS flux		Cumulative transport	
	Along-canyon	Across-canyon	Along-canyon	Across-canyon
Trawling closure	0.02–0.1	0.01–0.06	+ 0.05	− 0.08
DSWC period (max.)	+ 44	− 35		
Trawling season	0.1–0.7	1.4	+ 0.04	− 0.02

occurring at the Rostoll fishing ground (Fig. 4) suggest that most of the increases in water turbidity during the trawling season were generated in the northern canyon wall. Moreover, the Sant Sebastià fishing ground is closer to the canyon axis (~ 1.5 km) than the Rostoll fishing ground (~ 2.5 km), which would favor that most of SSC increases reaching the mooring location were detached from the northern canyon wall as nepheloid layers. Over this period, near-bottom suspended sediment fluxes presented a dominant direction towards the SW (Fig. 11b; Table 2), following the main flow of the geostrophic circulation in this margin, which also suggests that most the resuspended sediment came from the northern flank. Nonetheless, the time-integrated near-bottom cumulative transport over the trawling period showed a persistently up-canyon direction (Fig. 11c; Table 2). This fact seems to confirm previous time series observations within the Palamós Canyon, revealing the presence of a residual up-canyon flux superimposed to the periodical (i.e. inertial) up- and down-canyon flow oscillations along the canyon axis (Martín et al. 2006, 2007). This has important implications for the redistribution and final fate of bottom trawling resuspended sediments in the canyon, as sediment transported down-slope from the canyon flanks' fishing grounds would be retained by the up-canyon residual flow and rapidly deposited along the canyon axis, without being exported further down-canyon towards greater depths. This continuous up-canyon cumulative transport (Fig. 11c) may also explain the increase of sediment accumulation rates in Palamós Canyon (Martín et al. 2008; Puig et al. 2015), a phenomenon observed in other trawled submarine canyons of this margin (Paradis et al. 2017, 2018a, b), leading to the formation of canyon axes' anthropogenic depocenters next to trawling grounds.

The quasi-permanent presence of INLs and near-BNLs near the fishing grounds in the Palamós Canyon during the monitored trawling season (Fig. 7) resembles the nepheloid structure linked to the trawling activities at the fishing grounds of the Foix Canyon (Arjona-Camas et al. 2019). Both submarine canyons are deeply incised in the Catalan continental margin, at a relatively close distance from the coast and are affected differently by the corresponding bottom trawling fleets that operate on them. Trawling activities at the Foix Canyon take place along the canyon axis at 600–800 m depth, and mainly over the upper slope next to the canyon (200–500 m depth) (Lleonart 1990), from where resuspended particles are advected along-margin by ambient currents and cross over the canyon via nepheloid layers (Arjona-Camas et al. 2019). In contrast, trawling activities at the Palamós Canyon are not carried out along its axis, and occur mainly at the canyon flanks, with minimal activity on the northern upper slope (Figs. 2 and 4). Nevertheless, the few hauls carried out at the upper slope of the Palamós Canyon could have contributed to feed the particulate matter detachments observed between 90 and 200 m depth during the CTD transect conducted on June 7 (Fig. 12c), which generated an INL too shallow to be recorded by the moored instruments. The pycnocline between the oAW and the LIW (Fig. 12a, b) could have favored the retention of suspended particles at this depth range, which are advected towards the southwest by the geostrophic circulation, above the profiling range of the moored instruments (Fig. 7). Nevertheless, despite the different locations where trawling activities take place at the Foix and the Palamós submarine canyons, the nepheloid structure developed in both canyons is remarkably similar (see Fig. 6 in Arjona-Camas et al. 2019).

Overall, these new data from the Palamós Canyon supports the hypothesis that resuspension induced by bottom trawling activities can play a significant role in increasing SSC in the water column and generating INLs and BNLs at certain depths based on the locations of the fishing grounds. No other submarine canyon has been studied as intensively as the Palamós Canyon regarding the effects of bottom trawling on the sediment dynamics but given that canyons are very often targeted by demersal fisheries, it is likely that similar impacts have occurred and are occurring in other submarine canyons elsewhere. Similar enhanced trawling-induced nepheloid layers such as those reported in the present study at the Palamós Canyon and at the Foix Canyon by Arjona-Camas et al. (2019), have been reported in Whittard Canyon (NE Atlantic) (Wilson et al. 2015b; Daly et al. 2018). As discussed by Wilson et al. (2015b), although the trawling activity was not always adjacent to where these enhanced nepheloid layers were observed, the canyon would have likely transported the material down to deeper regions. However, due to limited dataset consisting in discrete CTD casts, these authors were not able to conclude the frequency of these events, nor their temporal evolution during the active trawling period at the Whittard Canyon (Wilson et al. 2015b).

Comparison between water turbidity during the trawling closure and the trawling season

Remarkable aspects during the trawling closure in February 2017 were the high SSC increases related to the two DSWC events in the canyon (Fig. 7), and the relatively high SSC values at the upper levels of the water column associated with the presence of WIW (Figs. 6 and 7). This generated high NPSC values computed for the upper levels of the profiled water column (Fig. 8a). By the end of the trawling closure period, water turbidity, as well as computed NPSC, decreased to baseline values (Figs. 7 and 8a), coinciding with the disappearance of the seasonal WIW and the subsequent reestablishment of the more general hydrographic structure of this region (Figs. 6 and 7a and b). As

Journal : Large 11001 | Article No : 9457 | Pages : 22 | MS Code : 9457 | Dispatch : 8-11-2021

it has been previously stated, the formation of WIW over the GoL is directly affected by strong atmospheric events (Duffau-Julliand et al. 2004; Juza et al. 2019), being especially intense between late January to early March. However, changes in these atmospheric forcing and/or inflowing of AW and water properties including changes in LIW, can affect its horizontal advection and mixing with surrounding waters (Juza et al. 2019) and, subsequently, control its presence within the Palamós Canyon. These multiple factors could explain the rapid disappearance of the WIW from the hydrographic profiles by the end of the trawling closure season (Fig. 7a, b).

During the trawling season, almost all increases in water turbidity were associated with the trawling activities in the study area. This was translated in higher NPSC during the trawling season, which were almost two times those calculated at the end of the trawling closure (Fig. 8a). This was not only observed in the upper water column NPSC water column inventories, which allowed us to compare both periods, but also in the entire profiled water column (Fig. 8b). The higher values calculated for the trawling season indicate that trawling can more than double the suspended sediment load in the water column, which is in agreement with suspended sediment inventories previously documented in other trawling grounds, both in shallow and deep-water environments (Palanques et al. 2001, 2014; Arjona-Camas et al. 2019). Suspended sediment concentrations in the water column did not vary significantly when the trawling fleet was not operating on weekends and holidays at the flanks of the canyon. These results contrast with previous observations from a canyon tributary next to the Sant Sebastià fishing ground, which documented the occurrence of frequent events of high turbidity (i.e., sediment gravity flows) during working days and working hours of the local trawling fleet (Palanques et al. 2006a; Puig et al. 2012; Martín et al. 2014a). Additionally, this data showed that these events occurred once or twice a day when the trawling fleet went offshore and when it headed back to port (Martín et al. 2014a). However, in the present study the near-bottom time series collected at 923 m depth in the canyon axis did not record such periodic sediment gravity flows events (Figs. 7 and 10), as the instruments of the mooring were not receiving channeled trawled resuspended sediment through any canyon tributary. Instead, they received the less dense sediment particles that were scattered from the trawling grounds and remained in suspension after the passage of the sediment gravity flows. Once particles were detached in the water column, they remained in suspension for long periods of time, contributing to feed quasi-permanent INLs and BNLs, where SSC was higher. Because of this, these increases of SSC did not show differences between working days and weekends.

Conclusions

The data recorded in this monitoring study show different turbidity and sediment transport patterns between the trawling closure period and the trawling season at the Palamós Canyon.

During the trawling closure period, natural increases in water turbidity and near-bottom suspended sediment fluxes occurred mainly during DSWC events. These observations provided further insight of the sediment transport associated with this oceanographic process in Palamós Canyon and showed evidence, for the first time, of the presence of DSWC reaching > 900 m depth in the canyon axis. During the trawling season, increases in water turbidity linked to trawling activities occurred regularly and were recorded mainly concentrated at depths where the Sant Sebastià and the Rostoll fishing grounds are located. Bottom trawling introduced sediment into the water column that more than doubled the suspended sediment background values recorded during calm sea conditions of the trawling closure, in absence of dense shelf waters within the canyon. Near-bottom instantaneous suspended sediment fluxes caused by the passage of OTB vessels were some orders of magnitude smaller than those generated by DSWC events. However, the chronic trawling activities for at least 30 days over the same fishing ground are capable of producing similar cumulative suspended sediment transport to that generated by a major DSWC event.

The main difference between natural and trawling-induced mechanisms is that natural turbidity and suspended sediment transport occurs sporadically, whereas trawling-induced water turbidity and transport is periodic and constant. Taking into account that bottom trawling is practiced on a daily basis throughout the year at the flanks of Palamós Canyon, with the exception of the 60-day seasonal trawling closure, weekends and holidays, much higher suspended sediment transport would be expected for a complete trawling season. Results from this study provide further insight on how bottom trawling activities are able to overcome natural processes as the main mechanism of sediment resuspension, capable of changing the natural patterns of particulate matter dispersion and accumulation in submarine canyon environments.

The capacity of bottom trawling to produce similar accumulated impacts to those resulting from sudden and sporadic natural high-energy events points out the necessity of addressing the effect of anthropogenic activities in studies of sediment dynamics in deep-sea environments where fishing activities are practiced.

Further mooring data in this and other submarine canyons, along with data on the composition of the sediment resuspended by both natural and trawling-induced mechanisms would provide additional data on the biogeochemical

Journal : Large 11001 | Article No : 9457 | Pages : 22 | MS Code : 9457 | Dispatch : 8-11-2021

and ecological consequences derived from this human activity.

Acknowledgements The authors are very grateful to the captain, crew and scientists involved in R/V *García del Cid* cruises, and to the UTM technicians and the Instrumental Service for their guidance and assistance. The authors wish to thank the Secretaría General de Pesca (SGP) for providing the 2004 Espace Project bathymetry and the Spanish Ports Authority for the access to AIS data. This work has been supported by the ABIDES (CTM2015-65142) Spanish Project and by the autonomous government of Catalonia grants 2017 SGR 863 and 2017 SGR 1241, as well as by the TrawledSeas Project receiving funding from the European Union's Horizon 2020 Research and Innovation programme under a MSCA grant agreement (No. 867471). M. Arjona-Camas is supported by a predoctoral FPI grant from the Spanish Ministry of Economy, Industry and Competitiveness.

Author contributions MAC: methodology, software, visualization, datacuration, formal analysis, writing. PP: conceptualization, funding acquisition, reviewing and editing, supervision. AP: funding acquisition, reviewing and editing, supervision. RD: software, visualization. MW: formal analysis. SP: methodology, software, data curation. ME: methodology, formal analysis, visualization.

References

Allen SE, Durrieu de Madron X (2009) A review of the role of submarine canyons in deep-ocean exchange with the shelf. Ocean Sci 5(4):607

Amblas D, Canals M, Urgeles R, Lastras G, Liquete C, Hughes-Clarke JE, Casamor JL, Calafat AM (2006) Morphogenetic mesoscale analysis of the northeastern Iberian margin, NW Mediterranean Basin. Mar Geol 234(1–4):3–20

Arjona-Camas M, Puig P, Palanques A, Emelianov M, Durán R (2019) Evidence of trawling-induced resuspension events in the generation of nepheloid layers in the Foix submarine canyon (NW Mediterranean). J Mar Syst 196:86–96

Bjørkan M, Company JB, Gorelli G, Sardà F, Massaguer C (2020) When fishemen take charge: the development of a management plan for the red shrimp fishery in Mediterranean Sea (NE Spain). Springer, Cham, pp 159–178

BOE (2017) Resolución de 26 de enero de 2017, de la Secretaría General de Pesca, por la que se fija, para 2017, el periodo de veda establecido en la Orden AAA/923/2013, de 16 de mayo, por la que se regula la pesca de gamba rosada (Aristeus antennatus) con arte de arrastre de fondo en determinadas zonas marítimas próximas a Palamós

Bonnin J, Heussner S, Calafat A, Fabres J, Palanques A, Durrieu de Madron X, Canals M, Puig P, Avril J, Delsaut N (2008) Comparison of horizontal and downward particle fluxes across canyons of the Gulf of Lions (NW Mediterranean): meteorological and hydrodynamical forcing. Cont Shelf Res 28(15):1957–1970

Cacchione DA, Pratson LF, Ogston AS (2002) The shaping of continental slopes by internal tides. Science 296(5568):724–727

Canals M, Puig P, Durrieu de Madron X, Heussner S, Palanques A, Fabres J (2006) Flushing and reshaping submarine canyons by dense shelf water cascading. Nature 444(7117):354–357

Canals M, Company JB, Martín D, Sanchez-Vidal A, Ramirez-Llodra E (2013) Integrated study of Mediterranean deep canyons. Novel results and future challenges. Prog Oceanogr 118:1–27

Churchill JH (1989) The effect of commercial trawling on sediment resuspension and transport over the Middle Atlantic Bight continental shelf. Cont Shelf Res 9(9):841–865

Daly E, Johnson MP, Wilson AM, Gerritsen HD, Kiriakoulakis K, Allcock AL, White M (2018) Bottom trawling at Whittard Canyon: evidence for seabed modification, trawl plumes and food source heterogeneity. Progr Oceanogr 169:227–240

Dufau-Julliand C, Marsaleix P, Petrenko A, Dekeyser I (2004) Three-dimensional modeling of the Gulf of Lion's hydrodynamics (northwest Mediterranean) during January 1999 (MOOGLI3 experiment) and late winter 1999: western Mediterranean Intermediate Water's (WIW's) formation and its cascading over the shelf break. J Geophys Res 109(C1):1002

Durrieu de Madron, X, Zervakis V, Theocharis A, Georgopoulos D (2005a) Comments on ''Cascades of dense water around the world ocean''. Prog Oceanogr 64(1):83–90

Durrieu de Madron X, Ferré B, Le Corre G, Grenz C, Conan P, Pujo-Pay M, Buscail R, Bodiot O (2005b) Trawling-induced resuspension and dispersal of muddy sediments and dissolved elements in the Gulf of Lion (NW Mediterranean). Cont Shelf Res 25:2387–2409

Durrieu de Madron, X, Houpert L, Puig P, Sanchez-Vidal A, Testor P, Bosse A, Estournel C, Somot S, Bourrin F, Bouin MN, Beauverger M, Beguery L, Calafat A, Canals M, Coppola L, Dausse D, D'Ortenzio F, Font J, Heussner S, Kunesch S, Lefevre D, Le Goff H, Martín J, Mortier L, Palanques A, Raimbault P (2013) Interaction of dense shelf water cascading and open-sea convection in the Northwestern Mediterranean during winter 2012. Geophys Res Lett 40:1379–1385

European Commission Fisheries & Maritime Affairs (2014) Fleet register on the net. http://ec.europa.eu/fisheries/fleet/index.cfm. Accessed 1 Apr 2019

Ferré B, de Madron D, Estournel X, Ulses C, Le Corre C, G (2008) Impacto f natural (waves and currents) and anthropogenic (trawl) resuspension on the export of particulate matter to the open ocean: application to the Gulf of Lion (NW Mediterranean). Cont Shelf Res 28(15):2071–2091

Font J, Salat J, Tintoré J (1988) Permanent features of the circulation in the Catalan Sea. Ocenol Acta 9:51–57

Font J, Puig P, Salat J, Palanques A, Emelianov M (2007) Sequence of hydrographic changes in the NW Mediterranean deep water due to the exceptional winter of 2005. Sci Mar 71:339–346

García R, Van Oevelen D, Soetaert K, Thomsen L, De Stigter HC, Epping E (2008) Deposition rates, mixing intensity and organic content in two contrasting submarine canyons. Prog Oceanogr 76(2):192–215

Gardner WD (1989) Baltimore canyon as a modern conduit of sediment to the deep sea. Deep-Sea Res 36:323–358

Guillén J, Bourrin F, Palanques A, Durrieu de Madron XD, Puig P, Buscail R (2006) Sediment dynamics during wet and dry storm events on the Têt inner shelf (SW Gulf of Lions). Mar Geol 234:129–142

Harris PT, Whiteway T (2011) Global distribution of large submarine canyons: geomorphic differences between active and passive continental margins. Mar Geol 285:69–86

Jordi A, Orfila A, Basterretxea G, Tintoré J (2005) Shelf-slope exchanges by frontal variability in a steep submarine canyon. Prog Oceanogr 6:120–141

Juza M, Escudier R, Vargas-Yáñez M, Mourre B, Heslop E, Allen J, Tintoré J (2019) Characterization of changes in western intermediate water properties enabled by an innovative geometry-based detection approach. J Mar Sys 191:1–12

Karageorgis AP, Anagnostou CL (2003) Seasonal variation in the distribution of suspended particulate matter in the northwest Aegean Sea. J Geophys Res Oceans 108(C8):3274

Krost P, Bernhard M, Werner F, Hukriede W (1990) Otter-trawl tracks in Kiel Bay (Western Baltic) mapped by side-scan sonar. Meeresforsch 32(4):344–353

Kunze E, Rosenfeld LK, Carter GS, Gregg MC (2002) Internal waves in Monterey submarine canyon. J Phys Oceanogr 32(6):1890–1913

Lapouyade A, Durrieu de Madron X (2001) Seasonal variability of the advective transport of particulate matter and organic carbon in the Gulf of Lion (NW Mediterranean). Oceanol Acta 24:295–312

Lastras G, Canals M, Amblas D, Lavoie C, Church I, De Mol B, Duran R, Calafat AM, Hughes-Clarke JE, Smith CJ, Heussner S, "Euroléon" cruise shipboard party (2011) Understanding sediment dynamics in two large submarine valleys from seafloor data: Blanes and La Fonera canyons, northwestern Mediterranean Sea. Mar Geol 280(1–4):20–39

Liquete C, Canals M, Ludwig W, Arnau P (2009) Sediment discharge of the rivers of Catalonia, NE Spain, and the influence of human impacts. J Hydrol 366(1–4):76–88

Lleonart J (1990) La pesquería de Cataluña y Valencia: descripción global y planteamiento de bases para su seguimiento. (Informe final. EEC DG XP/-CSIC, 2)

Martín J, Palanques A, Puig P (2006) Composition and variability of downward particulate matter fluxes in Palamós submarine canyon (NW Mediterranean). J Mar Sys 60:75–97

Martín J, Palanques A, Puig P (2007) Near-bottom horizontal transfer of particulate matter in the Palamós submarine canyon (NW Mediterranean). J Mar Res 65(2):193–218

Martín J, Puig P, Palanques A, Masqué P, García-Orellana J (2008) Effect of commercial trawling on the deep sedimentation in a Mediterranean submarine canyon. Mar Geol 252(3–4):150–155

Martín J, Durrieu de Madron X, Puig P, Bourrin F, Palanques A, Houpert L, Higueras M, Sanchez-Vidal A, Calafat AM, Canals M, Heussner S, Delsaut N, Sotin C (2013) Sediment transport along the Cap de Creus canyon flank during a mild, wet winter. Biogeosciences 10(5):3221–3239

Martín J, Puig P, Palanques A, Ribo M (2014a) Trawling-induced daily sediment resuspension in the flank of a Mediterranean submarine canyon. Deep-Sea Res II Top Stud Oceanogr 104:174–183

Martín J, Puig P, Masqué P, Palanques A, Sánchez-Gómez A (2014b) Impact of bottom trawling on deep-sea sediment properties along the flanks of a submarine canyon. PLoS One 9(8):e104536

Masó M, Tintoré J (1991) Variability of the shelf water off the northeast Spanish coast. J Mar Sys 1(4):441–450

Mendoza ET, Jiménez AA (2009) Vulnerability assessment to coastal storms at a regional scale. In: Coastal engineering 2008, vol 5, pp 4154–4166

Mengual B, Cayocca F, Le Hir P, Draye R, Laffargue P, Vincent B, Garlan T (2016) Influence of bottom trawling on sediment resuspension in the 'Grande-Vasière' area (Bay of Biscay, France). Ocean Dyn 66(9):1181–1207

Millot C (1990) The Gulf of Lions' hydrodynamics. Cont Shelf Res 10(9–11):885–894

Millot C (1999) Circulation in the Western Mediterranean Sea. J Mar Sys 20:423–442

Monaco A, Biscaye PE, Soyer J, Pocklington R, Heussner S (1990) Particle fluxes and ecosystem response on a continental margin: the 1985–1988 Mediterranean ECOMARGE experiment. Cont Shelf Res 10:809–839

Natale F, Gibin M, Alessandrini A, Vespe M, Paulrud A (2015) Mapping fishing effort through AIS Data. PloS One 10(6):e0130746

Oberle FKJ, Storlazzi CD, Hanebuth TJJ (2016) What a drag: quantifying the global impact of chronic bottom trawling on continental shelf sediment. J Mar Syst 159:109–119

O'Neill FG, Summerbell K (2011) The mobilisation of sediment by demersal otter trawls. Mar Pollut Bull 62(5):1088–1097

Palanques A, Guillén J, Puig P (2001) Impact of bottom trawling on water turbidity and muddy sediment of an unfished Impact of bottom trawling continental shelf. Limnol Oceanogr 46:1100–1110

Palanques A, García-Ladona E, Gomis D, Martín J, Marcos M, Pascual A, Puig P, Gili JM, Emelianov M, Monserrat S, Guillén J, Tintoré J, Segura M, Jordi A, Ruiz S, Basterretxea G, Font J, Blasco D, Pagès F (2005) General patterns of circulation, sediment fluxes and ecology of the Palamós (La Fonera) submarine canyon, northwestern Mediterranean. Prog Oceanogr 66(2–4):89–119

Palanques A, Martín J, Puig P, Guillén J, Company JB, Sardà F (2006a) Evidence of sediment gravity flows induced by trawling in the Palamós (Fonera) submarine canyon (northwestern Mediterranean). Deep-Sea Res Part I Oceanogr Res Pap 53(2):201–214

Palanques A, Durrieu de Madron X, Puig P, Fabres J, Guillén J, Calafat A, Canals M, Bonnin J (2006b) Suspended sediment fluxes and transport processes in the Gulf of Lions submarine canyons: the role of storms and dense shelf water cascading. Mar Geol 234(1–4):43–61

Palanques A, Guillén J, Puig P, Durrieu de Madron X (2008) Storm-driven shelf-to-canyon suspended sediment transport at the southwestern Gulf of Lions. Cont Shelf Res 28(15):1947–1956

Palanques A, Puig P, Durrieu de Madron X, Sanchez-Vidal A, Pasqual C, Martín J, Calafat A, Heussner S, Canals M (2012) Sediment transport to the deep canyons and open-slope of the western Gulf of Lions during the 2006 intense cascading and open-sea convection period. Prog Oceanogr 106:1–15

Palanques A, Puig P, Guillén J, Demestre M, Martín J (2014) Effects of bottom trawling on the Ebro continental shelf sedimentary system (NW Mediterranean). Cont Shelf Res 72:83–98

Palanques A, Puig P (2018) Particle fluxes induced by benthic storms during the 2012 dense shelf water cascading and open sea convection period in the northwestern Mediterranean basin. Mar Geol 406:119–131

Paradis S, Puig P, Masqué P, Juan-Díaz X, Martín J, Palanques A (2017) Bottom trawling along submarine canyons impacts deep sedimentary regimes. Sci Rep 7:43332

Paradis S, Puig P, Sánchez-Vidal A, Masqué P, García-Orellana J, Calafat A, Canals M (2018a) Spatial distribution of sedimentation-rate increases in Blanes canyon caused by technification of bottom trawling fleet. Prog Oceanogr 169:241–252

Paradis S, Masqué P, Puig P, Juan-Díaz X, Gorelli G, Palanques A (2018b) Enhancement of sedimentation rates in the Foix canyon after the renewal of trawling fleets in the early XXI st century. Deep-Sea Res I Oceanogr Res Pap 132:51–59

Paradis S, Goñi M, Masqué P, Durán R, Arjona-Camas M, Palanques A, Puig P (2021) Persistence of biogeochemical alterations of deep-sea sediments by bottom trawling. Geophys Res Lett 48:e2020GL091279

Paull CK, Ussler W, Greene HG, Keaten R, Mitts P, Barry J (2003) Caught in the act: the 20 December 2001 gravity flow event in Monterey canyon. Geo-Mar Lett 22(4):227–232

Payo-Payo M, Jacinto RS, Lastras G, Rabineau M, Puig P, Martín J, Canals M, Sultan N (2017) Numerical modeling of bottom trawling-induced sediment transport and accumulation in La Fonera submarine canyon, northwestern Mediterranean Sea. Mar Geol 386:107–125

Pilskaln CH, Churchill JH, Mayer LM (1998) Resuspension of sediment by bottom trawling in the Gulf of Maine and sediment potential geochemical consequences. Conserv Biol 12(6):1223–1229

Piper DJW, Normark WR (2009) Processes that initiate turbidity currents and their influence on turbidites: a marine geology perspective. J Sediment Res 79(6):347–362

Pomar L, Morsili M, Hallock P, Bádenas B (2012) Internal waves, an under-explored source of turbulence events in the sedimentary record. Earth Sci Rev 111:56–81

Porter M, Inall ME, Hopkins J, Palmer MR, Dale AC, Barth JA, Mahaffey C, Smeed DA (2016) Glider observations of enhanced deep water upwelling at a shelf break canyon: a mechanism for cross-slope carbon and nutrient. J Geophys Res Oceans 121:7575–7588

Puertos del Estado, ShipLocus (2017). https://shiplocus.puertos.es/. Accessed 1 Jan 2018

Puig P, Palanques A (1998b) Temporal variability and composition of settling particle fluxes on the Barcelona continental margin (Northwestern Mediterranean). J Mar Res 56:639–654

Puig P, Ogston AS, Mullenbach BL, Nittrouer CA, Sternberg RW (2003) Shelf-to-canyon sediment-transport processes on the Eel continental margin (northern California). Mar Geol 193(1–2):129–149

Puig P, Ogston AS, Mullenbach BL, Nittrouer CA, Parsons JD, Sternberg RW (2004a) Storm-induced sediment gravity flows at the head of the Eel submarine canyon, northern California margin. J Geophys Res 109(C3):C03019

Puig P, Palanques A, Guillén J, Khatab E, M (2004b) Role of internal waves in the generation of nepheloid layers on the northwestern Alboran slope: implications for continental margin shaping. J Geophys Res-Oceans 109:C9

Puig P, Palanques A, Orange DL, Lastras G, Canals M (2008) Dense shelf water cascades and sedimentary furrow formation in the Cap de Creus canyon, northwestern Mediterranean Sea. Cont Shelf Res 28(15):2017–2030

Puig P, Canals M, Martín J, Amblas D, Lastras G, Palanques A, Calafat A (2012) Ploughing the deep-sea floor. Nature 489(7415):286

Puig P, Palanques A, Martín J (2014) Contemporary sediment-transport processes in submarine canyons. Annu Rev Mar Sci 6:53–77

Puig P, Martín J, Masqué P, Palanques A (2015) Increasing sediment accumulation rates in La Fonera (Palamós) submarine canyon axis and their relationship with bottom trawling activities. Geophys Res Lett 42:8106–8113

Ragnarsson S, Steingrímsson SA (2003) Spatial distribution of otter trawl effort on Icelandic waters: comparison of measures of effort and implications for benthic community effects of trawling activities. ICES J Mar Sci 60(6):1200–1215

Ribó M, Puig P, Palanques A, Lo Iacono C (2011) Dense shelf water cascades in the Cap de Creus and Palamós submarine canyons during winter 2007 and 2008. Mar Geol 284:175–188

Salat J, Cruzado A (1981) Water masses in the Western Mediterranean Sea: Catalan Sea and adjacent waters. Rap Proc CIESM 27(6):6

Salat J, García MA, Cruzado A, Palanques A, Arín L, Gomis D, Guillén J, de León A, Puigdefàbregas J, Sospedra J, Velásquez ZR (2002) Seasonal changes of water mass structure and shelf slope exchanges at the Ebro shelf (NW Mediterranean). Cont Shelf Res 22:327–348

Serra J (1981) Els canyons submarins del marge Català. Treb Inst Cat Hist Nat 9:53–57

Shepard FP (1972) Submarine canyons. Earth Sci Rev 8(1):1–12

Shepard FP, Dill RF (1966) Submarine canyos and other sea valleys. Rand McNally, USA

Smith C, Rumohr H, Karakassis I, Papadopoulou KN (2003) Analysing the impact of bottom trawls on sedimentary seabeds with sediment profile imagery. J Exp Mar Biol Ecol 285:479–496

Ulses C, Estournel C, Durrieu de Madron X, Palanques A (2008a) Suspended sediment transport in the Gulf of Lions (NW Mediterranean): impact of extreme storms and floods. Cont Shelf Res 28(15):2048–2070

Ulses C, Estournel C, Bonnin J, Durrieu de Madron X, Marsaleix P (2008b) Impact of storms and dense water cascading on shelf-slope exchanges in the Gulf of Lion (NW Mediterranean). J Geophys Res 113:C02010

Völker D, Scholz F, Geersen J (2011) Analysis of submarine landsliding in the rupture area of the 27 February 2010 Maule earthquake, Central Chile. Mar Geol 288:79–89

Wilson AM, Kiriakoulakis K, Raine R, Gerritsen HD, Blackbird S, Allcock AL, White M (2015b) Anthropogenic influence on sediment transport in the Whittard Canyon, NE Atlantic. Mar Pollut Bull 101(1):320–329

Xu JP, Noble MA, Rosenfeld LK (2004) In-situ measurements of velocity structure within turbidity currents. Geophys Res Lett 31(9):L09311